


Summer 2016

Investigating Taphonomic Changes of Deposits and Modeling of the 2010 Earthquake and Tsunami in South-Central Chile

Alexandra Carranco Ruiz

Central Washington University, ruiza@cwu.edu

Follow this and additional works at: <https://digitalcommons.cwu.edu/etd>

 Part of the [Geology Commons](#), [Geomorphology Commons](#), [Sedimentology Commons](#), and the [Tectonics and Structure Commons](#)

Recommended Citation

Ruiz, Alexandra Carranco, "Investigating Taphonomic Changes of Deposits and Modeling of the 2010 Earthquake and Tsunami in South-Central Chile" (2016). *All Master's Theses*. 451.

<https://digitalcommons.cwu.edu/etd/451>

This Thesis is brought to you for free and open access by the Master's Theses at ScholarWorks@CWU. It has been accepted for inclusion in All Master's Theses by an authorized administrator of ScholarWorks@CWU. For more information, please contact pingfu@cwu.edu.

INVESTIGATING TAPHONOMIC CHANGES OF DEPOSITS AND MODELING OF
THE 2010 EARTHQUAKE AND TSUNAMI IN SOUTH-CENTRAL CHILE

A Thesis

Presented to

The Graduate Faculty

Central Washington University

In Partial Fulfillment

of the Requirements for the Degree

Master of Science

Geological Sciences

by

Alexandra Carranco Ruiz

July 2016

CENTRAL WASHINGTON UNIVERSITY

Graduate Studies

We hereby approve the thesis of

Alexandra Carranco Ruiz

Candidate for the degree of Master of Science

APPROVED FOR THE GRADUATE FACULTY

Dr. Lisa Ely, Committee Chair

Dr. Breanyn MacInnes

Dr. Walter Szeliga

Dean of Graduate Studies

ABSTRACT

INVESTIGATING TAPHONOMIC CHANGES OF DEPOSITS AND MODELING OF THE 2010 EARTHQUAKE AND TSUNAMI IN SOUTH-CENTRAL CHILE

by

Alexandra Carranco Ruiz

July 2016

South-central Chile has an extensive written catalog of historic earthquakes and tsunamis, but such records can be subject to inconsistencies. Dated tsunami deposits are more objective data that provide hard evidence of past tsunamis. The inland extent of deposits from past tsunamis (paleodeposits) can be used in tsunami modeling to reveal characteristics of the source earthquake, but these deposits may have undergone taphonomic processes since initial deposition. Therefore, to determine how tsunami deposits change during burial and preservation and the potential limitations of using paleodeposits in modeling, I investigated the modern 2010 M_w 8.8 Maule earthquake and tsunami as a detailed case study. I used GeoClaw numerical modeling to compare simulated tsunamis from published co-seismic slip distributions of the earthquake with observations from post-tsunami surveys and modified these distributions to determine the most important tsunami-forming characteristics of the earthquake. To investigate taphonomic changes of the deposits, in 2015 I resurveyed the 2010 deposits where they had been previously described and related these findings to modeling results.

The majority of simulated results of the 2010 tsunami underestimated the observed field data, with the most successful simulation created by a published slip distribution that matched observations at 5 of the 6 study sites. My most successful modified slip distribution did not improve this match (4/6 sites), and had an earthquake magnitude that was too large. The errors in modeling derived from using coarse resolution bathymetry and topography were likely the main reason for under-performing simulations, although a combination of other error sources could also play a role.

The tsunami deposits at all study sites were altered by taphonomic processes since 2010, but were still recognizable, indicating moderate preservation. Changes in the deposit inland extent from 2010 - 2015 at two sites ranged from -6% to +24%. Deposit thickness was better preserved than the internal structures, therefore most deposits will likely be preserved in the long-term. Combined, the results of my modeling and sediment studies indicate that GeoClaw modeling based on preserved paleotsunami deposits could provide useful estimates of tsunami-generating earthquake characteristics in south-central Chile, provided better resolution bathymetry and topography are available.

ACKNOWLEDGMENTS

I would like to thank my advisors, Lisa and Bre, for all of their help on this project that led me to my degree — their guidance, encouragement, patience, writing edits, and funding were all tremendously appreciated. It was an unforgettable learning experience academically and personally and I wouldn't have been able to learn as much as I did without them.

I would also like to thank my family, especially my mom and dad, for their support and encouragement, for coming out to my graduation, and always being there when I needed them. Thanks for always pushing me! Thanks to my boyfriend Jonathan, for coming to visit me and for always being there to listen and being supportive while I was away from home. Also, thanks to my fellow classmates — the late nights in Lind, Hebler, and the Science building were worth it in the end!

I'd also like to thank my third committee member, Walter, all the field assistants in Chile, the tsunami research group at the USGS in Santa Cruz, and Catherine Petroff from the Fritz et al. (2011) group. Your willingness to provide writing edits, data, and deposit samples made the many aspects of this research project possible.

TABLE OF CONTENTS

Chapter	Page
I	INTRODUCTION 1
	Objectives..... 3
	General Geologic Setting 6
	2010 Earthquake..... 8
	2010 Earthquake Slip Models 9
	2010 Tsunami and Post-Tsunami Surveys 12
	Tsunami Deposition 16
II	METHODS 19
	Tsunami Modeling Methods: GeoClaw Introduction 19
	Model Input Data: Bathymetry and Topography 19
	Model Input Data: Co-Seismic Slip Distributions 20
	Comparison of Simulated Results to Observed Data 22
	“Best-Fit” Models 25
	Tsunami Deposit Field Methods 30
	Lab Methods – Tsunami Deposits..... 32
III	TSUNAMI MODELING RESULTS AND DISCUSSION 33
	Site Results..... 33
	Sources of Error in Modeling..... 42
	Discussion of Site-Specific Results 46
	Published Slip Distributions, Percent Match Results..... 49
	Discussion of the Published Slip Distribution Results in Recreating the 2010 Tsunami 51
	Best-Fit Model Results: Method 1 53
	Best-Fit Model Results: Method 2 56
	Discussion of Modifying Pre-Existing Earthquakes to Improve Overall Match with Field Observations: Methods 1 and 2 59
	Implications of Modeling..... 61
IV	TSUNAMI DEPOSIT RESULTS AND DISCUSSION 65
	La Trinchera Deposit Results..... 65
	La Trinchera Deposit Discussion 73
	Constitución Deposit Results 76
	Constitución Deposit Discussion 79

TABLE OF CONTENTS (Continued)

Chapter	Page
Coliumo Deposit Results	81
Coliumo Deposit Discussion.....	84
Tubul Deposit Results	86
Tubul Deposit Discussion	87
Quidico Deposit Results.....	88
Quidico Deposit Discussion	92
Tirúa Deposit Results	94
Tirúa Deposit Discussion	102
Sources of Error in Deposit Studies	106
Implications for Tsunami Deposit Taphonomy	107
V CONCLUSIONS	112
Future Studies in Paleotsunami Modeling	116
REFERENCES	119
APPENDIXES	132
Appendix A—Post-Tsunami Survey Data	132
Appendix B—Tsunami Deposit Data	139
Appendix C—GeoClaw Tsunami Simulation Results	144
Appendix D—Slip Distribution Parameters.....	145

LIST OF TABLES

Table		Page
1	Percent differences between observed volume or flow depth measurements and simulated results, and overall percent match, from published slip distributions and the control simulation at each study site	34
2	Percent differences between observed volume or flow depth measurements and simulated results, and overall percent match, from Method 1 slip distribution simulations at each study site	34
3	Percent differences between observed volume or flow depth measurements and simulated results, and overall percent match, from Method 2 slip distribution simulations at each study site	35
4	Distances and percent change between tsunami deposit limit traced in 2010, 2012, or 2013 to the tsunami deposit limit traced in 2015	66
5	Distances between the 2010 tsunami inundation limit and the 2015 tsunami deposit limit.....	66
6	Thicknesses and percent change of tsunami deposits	72
7	Summary of geomorphic setting, current preservation, and long-term preservation potential of the resurveyed 2010 deposits at each study site	108

LIST OF FIGURES

Figure		Page
1	The Entirety of Chile	2
2	Map of the 2010 rupture area.....	4
3	Slip distributions input to GeoClaw.....	10
4	Post-tsunami survey modified from Fritz et al. (2011).....	14
5	Definitions of terms	16
6	The subfault grid used to create slip distributions for method 1 and method 2, modified from Fujii and Satake (2013).....	27
7	Diagram to illustrate how method 1 was used to create the <i>Method 1</i> modified slip distribution.....	28
8	La Trinchera South location map.....	35
9	La Trinchera South elevation transect modified from Morton et al. (2011).....	36
10	Constitución location map	37
11	Constitución elevation transect modified from Morton et al. (2011)	38
12	Coliumo location map.....	39
13	Tubul location map	41
14	Tirúa location map	42
15	Map of observed water volumes and flow depths compared to GeoClaw simulated volumes and flow depths at each study site	50
16	Slip distributions generated based on method 1 and resulting seafloor deformation patterns calculated in GeoClaw using the Okada (1985) equations	54
17	Map of observed water volumes and flow depths compared to GeoClaw simulated volumes and flow depths at each study site	55

LIST OF FIGURES (Continued)

Figure		Page
18	Slip distributions based on Method 2 and resulting seafloor deformation deformation patterns calculated in GeoClaw using the Okada (1985) equations	57
19	Map of observed water volumes and flow depths compared to GeoClaw simulated volumes and flow depths at each study site	58
20	Normalized grain-size distributions drawn to depth scale from La Trinchera South, Pit LAT1 sampled in 2010 by Morton et al. (2011) and Pit 38 sampled in 2015	67
21	Normalized grain-size distributions drawn to depth scale from La Trinchera South, Pit LAT3 sampled in 2010 by Morton et al. (2011) and Pit 39 sampled in 2015	68
22	Normalized grain-size distributions drawn to depth scale from La Trinchera South, Pit LAT4 sampled in 2010 by Morton et al. (2011) and Pit 40 sampled in 2015	69
23	Normalized grain-size distributions drawn to depth scale from Constitución, Pit CON2 sampled in 2010 by Morton et al. (2011) and Pit 384 sampled in 2015	78
24	Quidico location map	89
25	Normalized grain-size distributions drawn to depth scale from Quidico, Pit Q9 sampled in 2013 by Hong et al. (2016) and Pit 58 sampled in 2015	90
26	Normalized grain-size distributions drawn to depth scale from Tirúa, Pit 13-1 sampled in 2012 by Ely et al. (2014) and Pit 69 sampled in 2015	97
27	Normalized grain-size distributions drawn to depth scale from Tirúa, Pit 13-3 sampled in 2012 by Ely et al. (2014) and Pit 70 sampled in 2015	98
28	Normalized grain-size distributions drawn to depth scale from Tirúa, Pit 13-11 sampled in 2012 by Ely et al. (2014) and Pit 73 sampled in 2015	99

CHAPTER I

INTRODUCTION

A long-term goal of paleotsunami studies is to predict paleoearthquake parameters from tsunami deposited sand sheets that are found on land. For many modern tsunamis, post-tsunami surveys to measure water inundation, run up, flow depth and/or deposit locations are standard. However, similar detailed measurements typically do not exist for paleotsunamis. In rare cases, written descriptions of paleotsunami water inundation may exist, or modern surveys of wracklines from older events may be possible if the area is remote and undisturbed (see Griswold, 2015). The most reliable evidence preserved in the geologic record is the tsunami sediment deposit, where the maximum elevation or inland extent of the preserved deposit can represent a minimum limit of the distance a paleotsunami traveled over land.

South-central Chile (Figure 1a.) presents an excellent opportunity to conduct a case study of paleotsunami deposits because this area has a long catalog of historic earthquakes and tsunamis described in written records, including descriptions of earthquake shaking, infrastructure damage, tsunamis, and coastal land-level changes (Lomnitz, 2004; Cisternas et al., 2005; Udías et al., 2012). Most data prior to the M_w 9.5 May 22, 1960 earthquake are limited to eyewitness written accounts from Chileans and Spanish conquistadors, or estimations from modern studies (i.e. fault rupture locations as shown in Figure 1b.). Because written evidence can be subject to human inconsistencies, paleoearthquake and paleotsunami evidence in the form of preserved and dated tsunami deposits provide more objective hard evidence that can supplement written accounts.

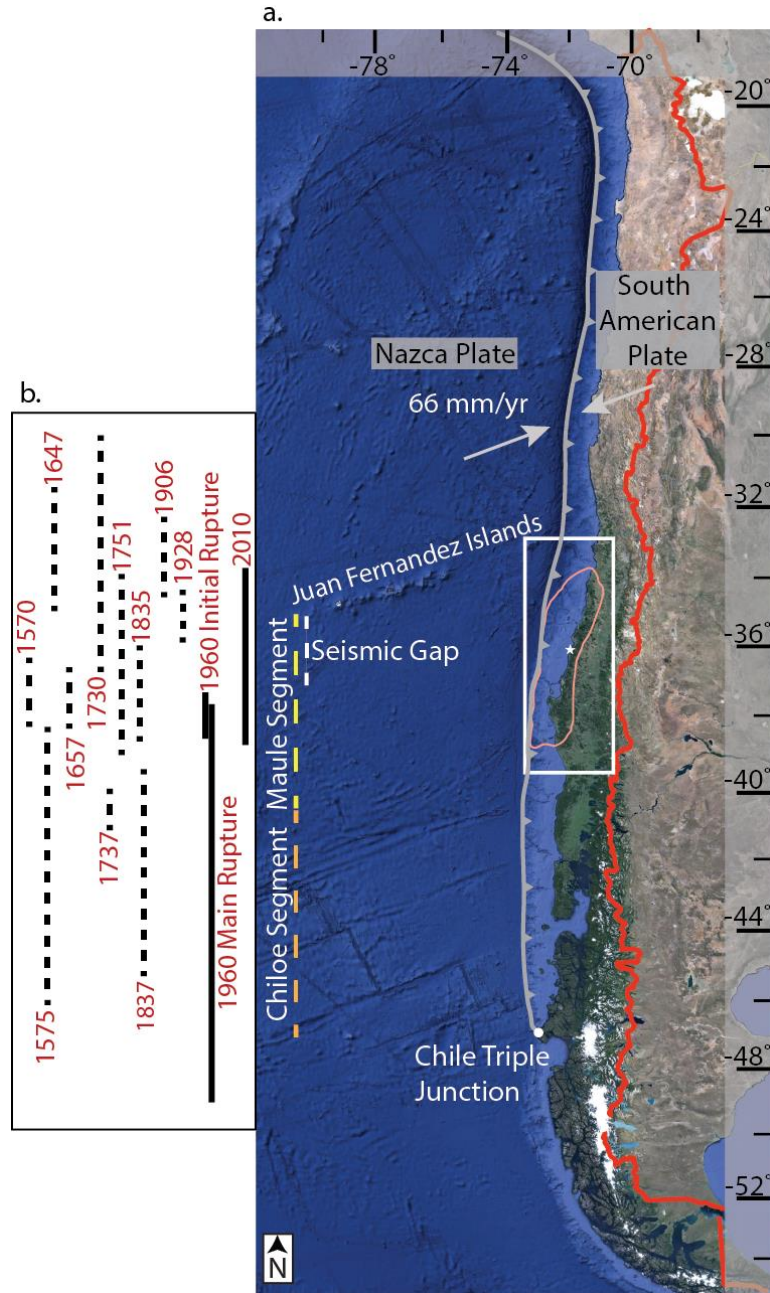


Figure 1: a.) The entirety of Chile (interior boundary outlined in red). White box contains all of my study areas and orange oval is the 2010 rupture area from Moreno et al. (2012) (shown in more detail in Figure 2). Major tectonic and oceanic features are labeled, as well as the Maule and Chiloe tectonic segments and the Concepción-Constitución seismic gap. Subduction zone boundary is outlined in grey. b.) Historic earthquake rupture extent along-strike of the subduction zone, modified from Moreno et al. (2012), Udías et al. (2012), and Hong et al. (2016). Dates are in A.D. and dashed lines are estimated locations. Image from Google Earth.

The 2010 Maule earthquake and tsunami in south-central Chile is the most recent and best-documented in the area, with published and unpublished datasets of inundation limits¹, run ups², flow depths³, and deposit descriptions from post-tsunami surveys as well as earthquake fault slip parameters from published co-seismic slip models. These modern datasets provide an opportunity to conduct a detailed study of the 2010 earthquake, tsunami, and tsunami deposits that can be used as a well-constrained analog to compare with paleotsunamis in future studies.

Objectives

This study of the 2010 Chile earthquake, tsunami, and tsunami deposits consists of two primary objectives. The first is to model the 2010 earthquake using published earthquake slip distributions to simulate tsunami flow depth and inundation at five sites in south-central Chile—La Trinchera, Constitución, Coliumo, Tubul, and Tirúa (Figure 2). In order to ultimately simulate paleotsunamis and paleoearthquakes in the region, the 2010 earthquake and tsunami should be shown to be effectively modeled and any potential limitations identified. I aim to achieve this objective by comparing simulated tsunami flow depths and inundation to 1) published post-tsunami survey observations, and 2) inundation locations based on our own and previously published field surveys of deposits from the 2010 tsunami. A comparison with post-tsunami survey observations

¹ Inundation limit: the maximum horizontal distance water traveled inland from the shoreline.

² Run up: the vertical height from sea level to the inundation limit.

³ Flow depth: the height of the tsunami water above ground level at any point within the inundation limit.

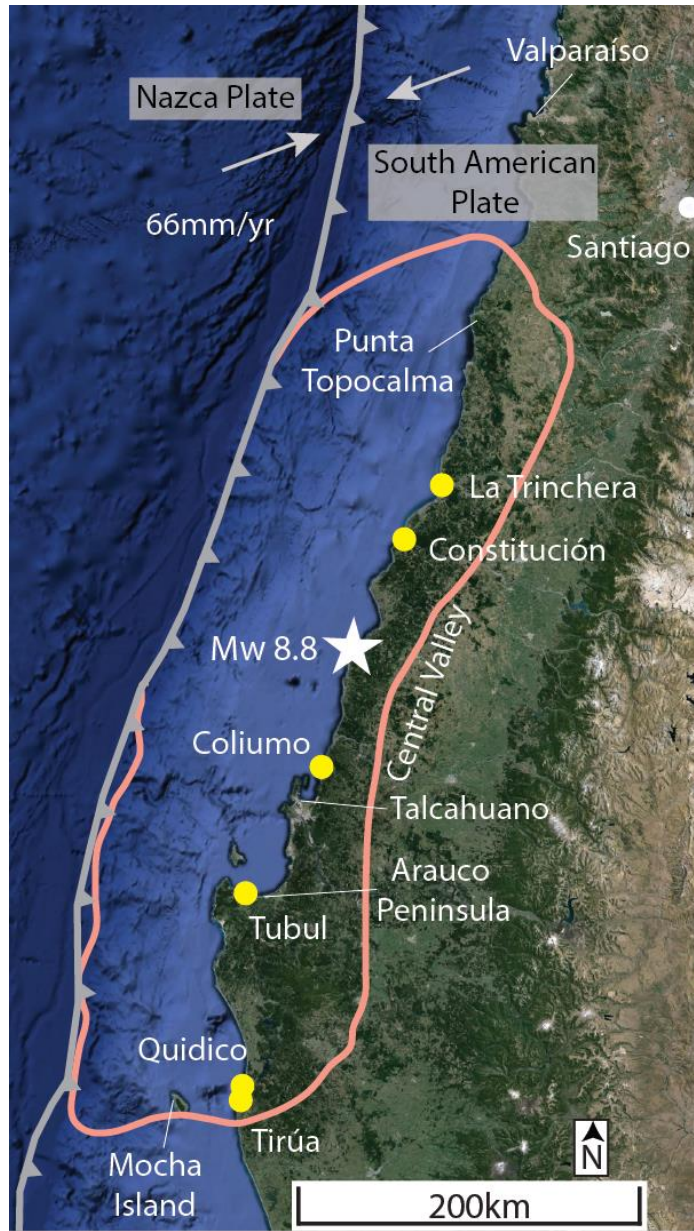


Figure 2: Map of the 2010 rupture area outlined in orange (from Moreno et al., 2012) with my tsunami-deposit field study sites as yellow circles. The 2010 earthquake epicenter location is indicated by the white star. Locations referred to in the text are also labeled. Image from Google Earth.

elucidates characteristics of the earthquake that were most important for tsunami generation, while a comparison with tsunami deposits reveals the minimum earthquake magnitude needed to produce the observed tsunami deposits, which is an important analysis for using tsunami deposits to interpret paleoearthquakes.

Published co-seismic source models can accurately resolve the amount of slip on the rupture interface, but locations of slip can vary among models, especially ones that use different input datasets (Yue et al., 2014). Most published co-seismic slip models use geodetic and teleseismic data, which may not fully represent aspects of seafloor displacement that is relevant to creating the tsunami (see also Lorito et al., 2011). Because of this, I modified published slip distributions by increasing and reducing slip to determine whether alterations in this parameter would create a better match between observations of the tsunami and the results of tsunami modeling.

My second objective is to compare the 2010 Chile tsunami deposits in south-central Chile initially described and measured in 2010 at La Trinchera, Constitución, and Coliumo, 2012 at Tirúa and Tubul, and 2013 at Quidico, with observations from revisiting the same sites in 2015. To ultimately use paleotsunamis to estimate parameters of the paleoearthquake, it is also important to consider that the sedimentary characteristics of deposits may change during burial and preservation, especially within the first few years (Nichol and Kench, 2008; Szczuciński, 2012). For example, deposit inland extent and overall thickness can be reduced or increased, and the deposit itself can be covered by soil and/or vegetation, disturbed by bioturbation, modified by human contact, or lose sedimentary structures. Over time, with some or all of these processes at

work, the deposit could become difficult to distinguish stratigraphically. For these reasons, it is important to understand tsunami deposit taphonomy in order to correctly assess paleodeposits and apply them to learning more about their paleotsunami and paleoearthquake sources. Ultimately, my combined research objectives from the 2010 event can be used as a case study to apply to paleoearthquakes where tsunami deposits are the most reliable records available.

General Geologic Setting

The central and south-central coast of Chile lies above a continental margin where the Nazca plate subducts slightly obliquely beneath the South American plate at a rate of 66 mm/yr (Figure 1; Angermann et al., 1999). South-central Chile is bounded by the Maule and Chiloe tectonic segments, which border the oceanic features of the Juan Fernandez islands and the Chile Triple Junction/Rise (Figure 1). The age of the seafloor decreases from 36 Ma at the northernmost area of the Maule segment to 5 Ma at southernmost area of the Chiloe segment (Figure 1; Melnick and Echtler, 2006).

Significant strain accumulation along the offshore subduction zone results in megathrust earthquakes, defined as great ($M_w > 8$) earthquakes on the subduction zone interface, with a recurrence interval of one earthquake per 100-200 years or shorter on any given segment of the Chilean margin (Moreno et al., 2010; Ely et al., 2014). The average historic recurrence interval based on written records falls within this range at ~one per 128 years. Longer average intervals have been interpreted for some segments based on stratigraphic evidence (Cisternas et al., 2005; Garrett et al., 2014). Subduction

zone earthquakes can generate a tsunami through the transfer of large-scale elastic deformation to potential energy within the water column (Shanmugam, 2012). A tsunami is a shallow-water wave created by a sudden vertical displacement of a body of water that by definition has a wavelength many times longer than the water depth (Shanmugam, 2012).

In addition to the recent 2010 (M_w 8.8) earthquake and tsunami, central and southern Chile have a long history of paleoearthquakes from written records and paleotsunamis from geologic records of tsunami deposits. Most data prior to the 1960 earthquake (Figure 1b.) are limited to eyewitness written accounts from Chileans or Spanish conquistadors (see also Lomnitz, 2004; Cisternas et al., 2005; Udías et al., 2012) or estimations from modern studies (see also Barrientos and Ward, 1990; Fujii and Satake, 2013). Though helpful, written records— including descriptions of earthquake shaking and duration, tsunamis, coastal uplift, and infrastructure damage— can be inaccurate due to human error, bias, lost records, inconsistencies between records, etc. (Cisternas et al., 2005). Historical earthquake rupture estimations (Figure 1b.) in the region of the 2010 earthquake include: 1570 (M 8), 1575 (M 7-7.5), 1647 (M ~8), 1657 (M \leq 8), 1730 (M 8.5-9), 1751 (M 8.5), 1835 (M 8-8.5), 1906 (M 8.6 Richter scale), 1928 (M 8.4 Richter scale) and 1960 (M_w 9.5) (all earthquake names are dates in A.D.; Hong et al., 2016; Moreno et al., 2012; Udías et al., 2012; Melnick et al., 2009; Lomnitz, 2004). Tsunami deposits have also been found at multiple coastal sites from earthquakes in 1575, 1835, 1751, 1960, and others prior to the written record (Nentwig et al., 2015; Cisternas et al., 2005; Ely et al., 2014; Hong et al., 2016).

2010 Earthquake

The February 27, 2010 M_w 8.8 earthquake (06:34:14 UTC; 35.909° S, 72.733° W epicenter, 35 km depth (Moreno et al., 2010), M_o 1.86×10^{22} Nm (Yue et al., 2014)) and tsunami was destructive to human life and property. The earthquake collapsed or destroyed more than 810,000 buildings (Saito et al., 2010). As such, the majority of the 521 deaths were attributed to the earthquake, although 124 deaths were due to the tsunami and were concentrated in the coastal regions closest to the epicenter, at the Juan Fernandez islands, -33.6°S, and at Mocha Island, ~ -38°S (Figure 2; Fritz et al., 2011). The Pacific Tsunami Warning Center issued warnings five minutes after the earthquake, but because the tsunami arrived within 30 minutes at many locations, official evacuations were not yet in place (Fritz et al., 2011).

The earthquake ruptured ~500 km of the subduction zone (Figure 1; Figure 2), including the Concepción-Constitución seismic gap where the last great earthquakes occurred in 1835 in the south-central portion and 1928 on the north-central portion of the rupture area (Figure 1b.; Moreno et al., 2012). Additionally, the 2010 rupture overlapped with the southern portion of the 1906 earthquake and the northern portion of the 1960 earthquake, the largest ever recorded (Figure 1b.; Kanamori, 1977; Barrientos and Ward, 1990). Estimates of maximum slip during the 2010 earthquake varies but could have been as high as 22 m (Fujii and Satake, 2013). From GPS measurements, uplift occurred all along the coast, reaching 1.8 m at the Arauco Peninsula (~ -37 °S; Figure 2), the land point closest to the trench. Between Punta Topocalma (~ -34°S) and Tirúa (~ -38.3°S), co-seismic uplift of the shoreline ranged from $0.15 \text{ m} \pm 0.1 \text{ m}$ to $2.5 \text{ m} \pm 0.6 \text{ m}$ as estimated

by exposed bleached algae (Figure 2; Vargas et al., 2011). Subsidence occurred mainly in the central valley, although up to 0.06 m of subsidence was measured at the coast 15 km south of Constitución (Figure 2; Vigny et al., 2011).

2010 Earthquake Slip Models

Seventeen research groups published co-seismic fault models of the 2010 slip distribution using some combination of GPS, teleseismic waves, InSAR, tsunami waveforms, and land-level change data (Delouis et al., 2010; Hayes, 2010; Lay et al., 2010; Moreno et al., 2010; Shao et al., 2010; Sladen, 2010; Tong et al., 2010; Lorito et al., 2011; Pollitz et al., 2011; Pulido et al., 2011; Vigny et al., 2011; Koper et al., 2012; Moreno et al., 2012; Bedford and Moreno, 2013; Fujii and Satake, 2013; Lin et al., 2013; Yue et al., 2014). The primary differences among the co-seismic slip distributions are the locations and depth of the maximum slip. Of the published distributions, I chose eight to simulate the resulting tsunami inundation; each is summarized in Figure 3. The reasoning behind the distributions I chose is discussed in Chapter II, *Model Input Data: Co-Seismic Slip Distributions*. Of these slip distributions, four used GPS (Delouis et al., 2010; Lorito et al., 2011; Vigny et al., 2011; Yue et al., 2014), three used InSAR (Delouis et al., 2010; Lorito et al., 2011; Vigny et al., 2011; Yue et al., 2014); five used teleseismic records (Delouis et al., 2010; Yue et al., 2014; Hayes, 2010; Shao et al., 2010; Sladen, 2010), three used coastal land-leveling change markers (Vigny et al., 2011; Lorito et al., 2011; Fujii and Satake 2013), and three used tsunami data (Lorito et al., 2011; Fujii and Satake 2013; Yue et al., 2014). The southernmost extent of the three preliminary (earliest) slip

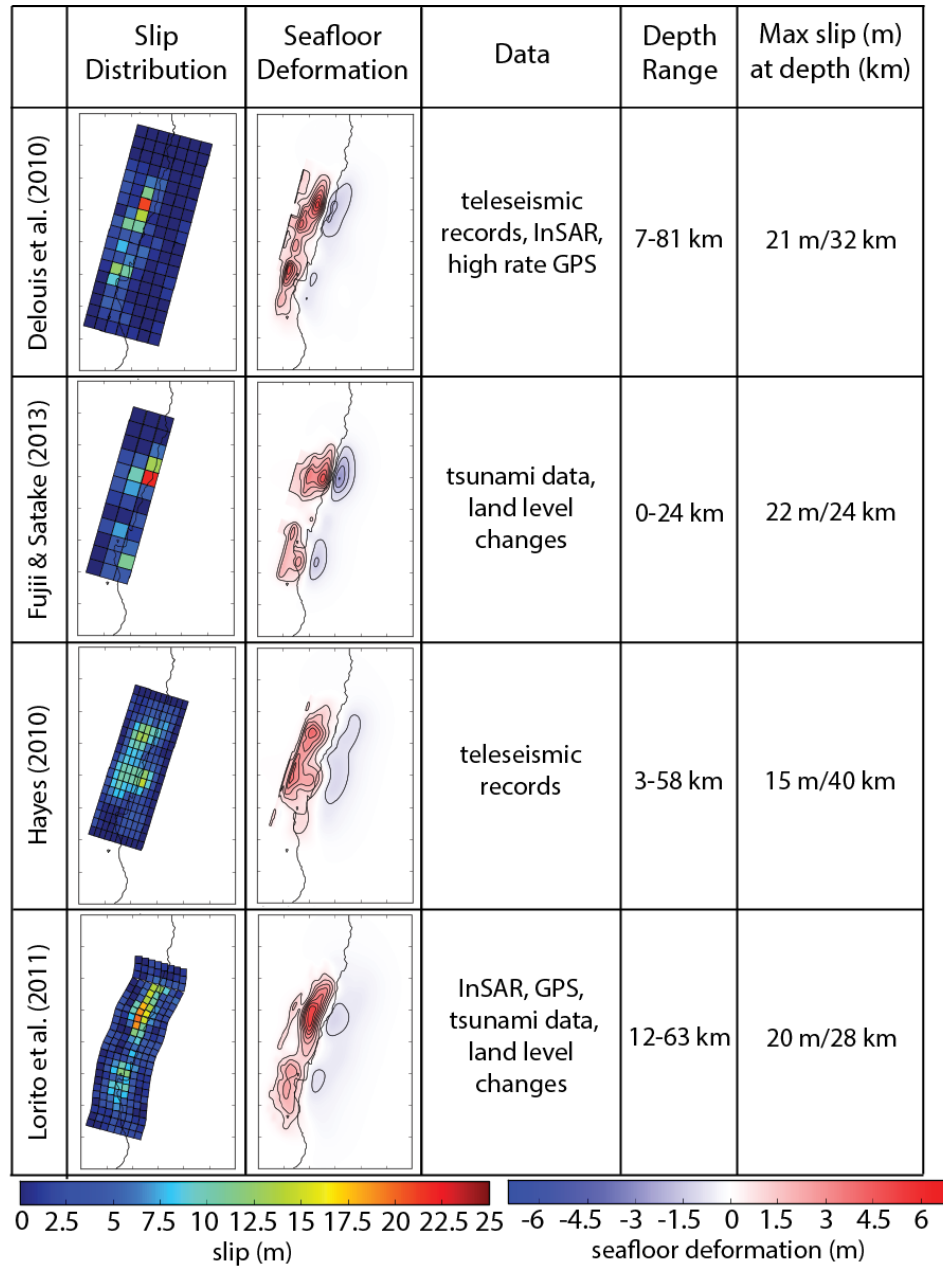


Figure 3: Slip distributions input to GeoClaw and seafloor deformation patterns calculated in GeoClaw from the inputs (listed by author). The datasets used the Okada (1985) formulation to create the slip distribution and additional notes on slip characteristics and depth are noted. Each slip distribution and seafloor deformation figure covers -32° to -40° S latitude and -75° to -69° W longitude. The shoreline is drawn in black. Figure 3 continues on next page.

distributions from Hayes (2010), Shao et al. (2010) and Sladen (2010), as well as Fujii and Satake (2013), do not extend as far as Tirúa, a coastal site where significant run up was measured (Fritz et al., 2010). All other published distributions extend south of this location. Also, maximum slip in all preliminary distributions is generally smaller than all other distributions. All distributions except Shao et al. (2010) have one large major patch that resolves the most slip to the north above $\sim -35.5^{\circ}\text{S}$ (Figure 3). Below -35.5°S the locations of slip are more variable between the distributions. Five have an additional smaller, minor patch that resolves less slip than the major patch (Delouis et al., 2010; Fujii and Satake, 2013; Lorito et al., 2011; Sladen, 2010; Yue et al., 2014), and three have an additional major patch (Figure 3; Hayes, 2010; Shao et al., 2010; Vigny et al., 2011). These southern slip patches could be located either near the trench (Vigny et al., 2011, Yue et al., 2014) or closer to the coast (Sladen, 2010; Shao et al., 2010; Lorito et al., 2011; Fujii and Satake, 2013; Delouis et al., 2010; Hayes, 2010).

2010 Tsunami and Post-Tsunami Surveys

In the near field, tide gauges in Talcahuano ($\sim -36.7^{\circ}\text{S}$) and Valparaíso ($\sim -33^{\circ}\text{S}$) (Figure 2 for location) recorded two large tsunami waves, with the maximum wave arriving after the first wave. In Talcahuano, the first wave had an amplitude of 2.3 m and a long period of 30 min, and the second tsunami wave exceeded 2.9 m amplitude but the tide gauge record stopped after the third recorded wave at 110 minutes (Fujii and Satake, 2013). In Valparaíso, the first wave had an amplitude of 1.6 m but the largest wave of 2.3 m amplitude was recorded about 2 hours later (Fujii and Satake, 2013).

Throughout the tsunami-inundated area, eyewitnesses reported one to four main waves, and at most locations the first wave arrived within 30 minutes of the earthquake (Annunziato et al., 2010; Fritz et al., 2011; Morton et al., 2010). Tsunami run up measured by post-tsunami surveys peaked at Constitución at 26.2 m and 29 m and decreased to the north with run up typically between 5 m and 10 m until Valparaíso, then uniformly below 5 m (Figure 4; Annunziato et al., 2010; Fritz et al., 2011). To the south, between Constitución and Punta Morguilla (~ -38°S; Figure 2), run up was variable between 5 m and 15 m. South of Punta Morguilla, run up was mostly below 5 m with the exception of Tirúa and Mocha Island (-38.3°S), where run up was 20 m and 23 m respectively (Figure 4; Fritz et al., 2010).

In the far field, tide gauges recorded the tsunami around the Pacific (herein reported as half of the maximum wave height, minus normal tide), including: 1.79 m at Hive Oa Island, Marquesas islands, French Polynesia; and 1.14 m in Severo-Kurilsk, Paramushir Island, Russia (NGDC/WDS, 2015). The highest tide gauge measurement in California was 91 cm in Santa Barbara (Wilson et al., 2013) and a GPS buoy in southwest Japan recorded up to 20 cm (Kato et al., 2011).

Many research groups conducted post-tsunami surveys within three months of the tsunami, including Koshimura et al. (2010), Annunziato et al. (2010), Fritz et al. (2011), and Morton et al. (2011). The Koshimura et al. (2010) survey collected data within the 2010 subduction zone rupture area but did not include data from my study sites so it was not used in my study. Annunziato et al. (2010), Fritz et al. (2011), and Morton et al. (2011) selected sites to the north and south of the epicenter where they predicted good

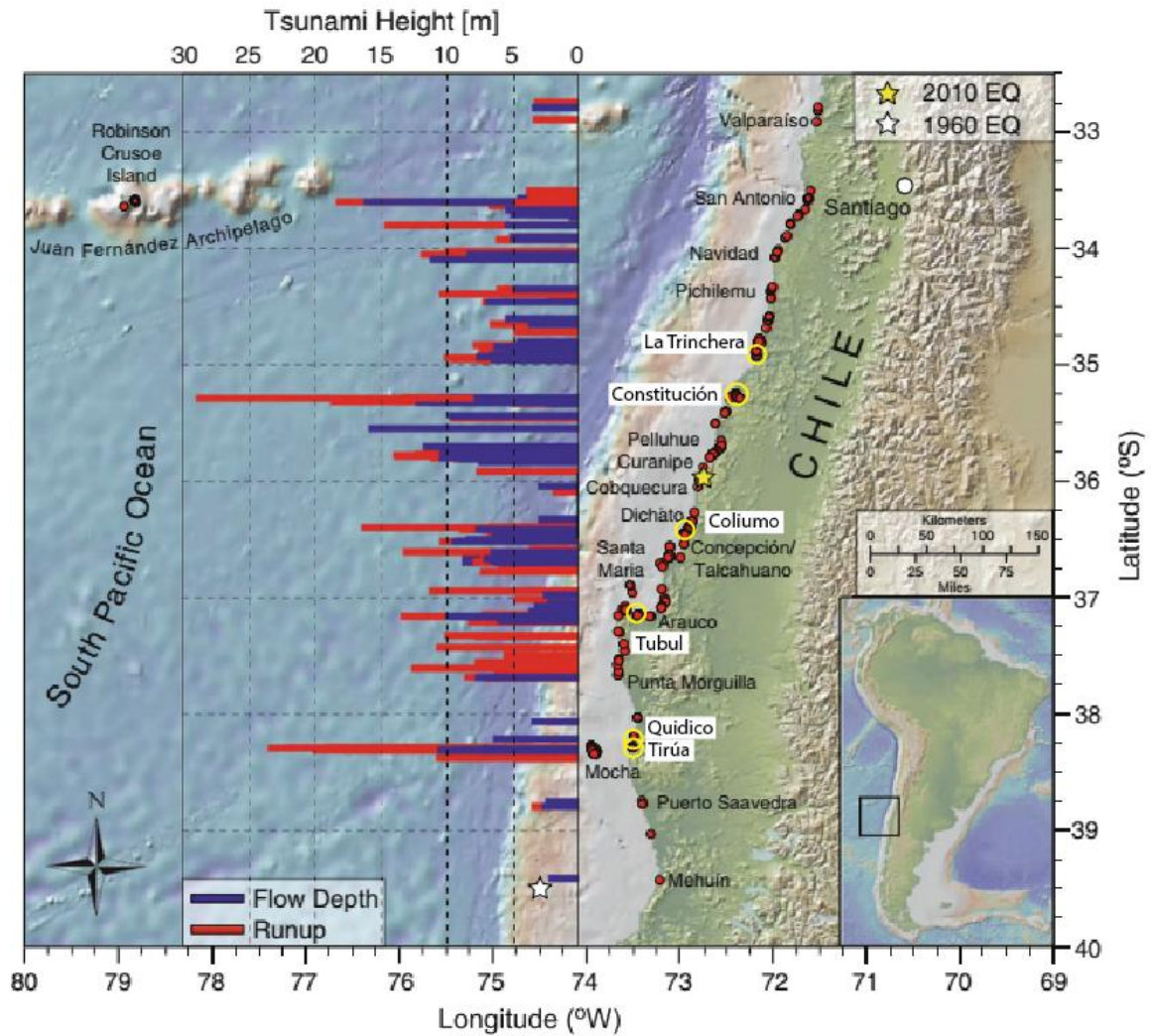


Figure 4: Post-tsunami survey modified from Fritz et al. (2011) displaying flow depth and run up measurements along the coast of south-central Chile. My six study sites are highlighted by yellow circles.

preservation of the tsunami deposit and watermarks. From March 27–30, 2010, Annunziato et al. (2010) took run up and inundation measurements, conducted eyewitness interviews, noted evidence of uplift, and photographed the damage at a number of locations that spanned 250 km of the coast from Licanten to Arauco (-34.9 to -36.5°S). Fritz et al. (2011) measured tsunami run up, inundation, flow depth, and wave-

induced deposition or erosion, assessed structural damage, and conducted eyewitness interviews from March 7–24 and May 21–22, 2010 over 800 km of the coast from Quintero to Mehuín (-32.7 to -39.4°S), as well as Santa María Island (-37.0 °S), the Juan Fernández islands (-33.6°S), Rapa Nui (-27.0°S), and Mocha Island (Figure 4). Morton et al. (2011) surveyed along a 200 km section of the coast from La Trinchera to Talcahuano (-35.1 to -36.7°S) from April 24–May 2, 2010 and measured flow depths, flow directions, vertical erosion, deposit thickness, and maximum clast sizes at each study site, topographic profiles and inundation at four sites, and flow direction histories at two sites. All three teams agreed that the tsunami run up elevations and morphological impacts were highly variable as a result of variations in tsunami wave heights, offshore bathymetry, shoreline orientations, and topography (Annunziato et al., 2010; Fritz et al., 2011; Morton et al., 2010).

In addition to the post-tsunami surveys, which focused on collecting tsunami data, field surveys have continued to study the 2010 deposit and possible paleodeposits that are preserved in the lower stratigraphy. The tsunami was both erosive and depositional: it stripped vegetation, created vertical scarps and V-shaped scours, and deposited sand sheets that are currently preserved in the sedimentary record (Morton et al., 2011). The tsunami inundation limit and 2010 deposits along Tirúa river floodplain were mapped in detail by Ely et. al (2014), and paleodeposits from three historical tsunamis (1960, 1751, 1575) were also found in lower stratigraphy. Hong et al. (2016) investigated the 2010 deposit and lower stratigraphy in detail at the Quidico river floodplain within an abandoned meander channel and discovered three paleotsunami deposits from historical

tsunamis (1960, 1835, 1751 or 1730) and a fourth that was dated to precede the historical written records.

Tsunami Deposition

When studying paleotsunamis, the paleodeposit inland limit represents the minimum tsunami inundation limit. This is because the areal extent of a tsunami deposit is smaller than the extent of tsunami water inundation (Shi et al., 1995; Yoshii et al., 2013). Sedimentologically, tsunami inundation of the land is typically divided into three zones: 1) a zone of erosion from the shore inland, interpreted to be where the wave is accelerating, 2) a broad zone of sediment deposition where the wave is neither strongly accelerating nor decelerating and 3) a narrow zone where neither erosion nor deposition occurs near the limit of inundation (Figure 5; Jaffe and Gelfenbuam, 2007).

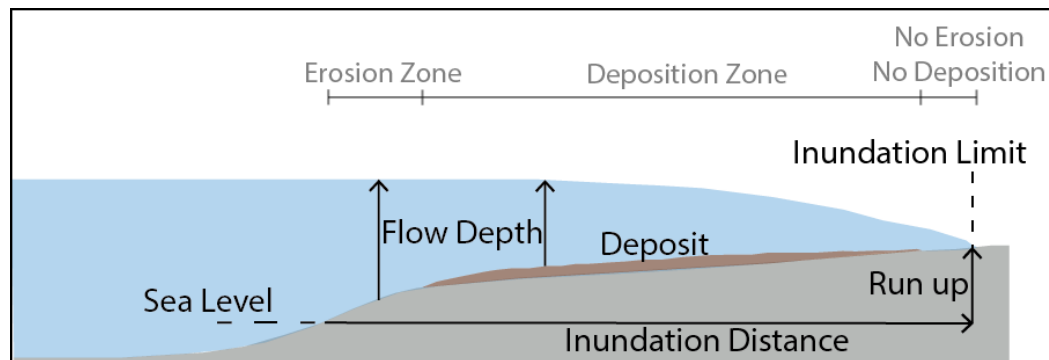


Figure 5: Definitions of terms and how they are measured in the field relative to sea level. The deposit, colored brown, does not extend over the full flooded area and defines three zones within the water inundation: the erosional zone, depositional zone and zone of neither erosion nor deposition. Figure modified from Jaffe and Gelfenbuam (2007).

The difference between the inland limit of sediment deposition and the water inundation limit is dependent on many factors, and can vary widely. For example, the 2006 Kuril Islands tsunami deposit distance was on average 95% of tsunami inundation and the maximum elevation of deposits was on average 90% of the run up elevation (MacInnes et al., 2009). In the case of the multiple-kilometer long inundation distance in the 2011 Tohoku-Oki tsunami on the Sendai Plain, when the inundation distance was less than 2.5 km, the deposit limit was over 90% of the inundation distance (Abe et al., 2012). However, when the inundation distance was more than 2.5 km, the tsunami sand limit decreased to 57-76% of the inundation extent (Abe et al., 2012). This was also seen in other locations of the Sendai Plain, where the sand deposit distance was 2.8 km (62%) of the inundation, with a mud layer that continued to the 4.5 km-water inundation limit (Goto et al., 2011). Using marine geochemical markers may be useful for detecting the tsunami inundation limit further inland than the sand deposit limit, and has the possibility of being applied to paleotsunamis and paleodeposits. Chagué-Goff et al. (2012) increased the tsunami inundation limit at the Sendai Plain measured by Goto et al. (2011) to 4.65 km inland, which decreased the extent of the sand deposit to 60% of the tsunami inundation limit and the mud deposit to 95% of the tsunami inundation distance.

A tsunami deposit can change after initial deposition, during burial, and preservation, especially within the first few years (Nichol and Kench, 2008; Szczuciński, 2012). Bioturbation from sediment mixing by roots, rodents, or insects can alter or erase internal sedimentary structures (Spiske et al., 2013) The deposit can also be altered or completely destroyed by humans, agriculture, or grazing animals (Szczuciński, 2012;

Spiske et al., 2013; Bahlburg and Spiske, 2015). Szczuciński (2012) also observed the fast recovery of overlying vegetation and soil after 4.5 years, which protected the deposits from heavy rains and erosion. On the other hand, the soil and organic accumulation can cause thin tsunami deposits to become unrecognizable (Szczuciński, 2012; Spiske et al., 2013). Sediment can also be added or removed from the deposit, such as silt or fine sand, which is easily transported by wind or rain (Szczuciński, 2012; Spiske et al., 2013; Bahlburg and Spiske, 2015). Coarse grained tsunami deposits have a higher preservation potential than finer grained deposits (McAdoo et al., 2008; Bahlburg and Spiske, 2015). Mud can easily be transported, but can also be hard to erode when dry due to the cohesion of mud particles (Spiske et al., 2013). As seen in Szczuciński (2012), thicker tsunami deposits (10 cm or greater) have a greater preservation potential than the thinner deposits.

The tsunami deposit extent can be reduced or extended over time due to the post-depositional changes as described. For instance, the 2004 Indian Ocean tsunami deposit limit was found to be near the tsunami inundation limit when initially described in 2005 as well as in 2008 on the coast of the Andaman Sea in southwestern Thailand (Goto et al., 2012). In slightly different survey areas also on the coast of the Andaman Sea, the tsunami deposits were almost within the entire water inundation area in 2005 but in areas where the tsunami was highest, only about 50% of the water inundation area was represented by the extent of tsunami deposits in 2009 (Szczuciński, 2012).

CHAPTER II

METHODS

Tsunami Modeling Methods: GeoClaw Introduction

To model the 2010 tsunami, I used GeoClaw, an open-source software available at <http://www.clawpack.org/geoclaw> that formulates the two-dimensional shallow-water wave equations (LeVeque et al., 2011). GeoClaw uses adaptive mesh refinement, which increases the modeling resolution near the tsunami wave as it travels across bathymetry and inundates topography. GeoClaw can report simulation results using synthetic tide gauges or fixed grid monitoring. I primarily used fixed grid monitoring to record the maximum flow depth, bathymetry/topography, wave arrival time, and other values that occur on a square grid of a resolution and area that can be defined. GeoClaw requires two types of input data: the bathymetry of the ocean and coastal regions combined with the topography onshore, and the motion of the seafloor to initiate the tsunami (LeVeque et al., 2011).

Model Input Data: Bathymetry and Topography

Using GeoClaw requires data to specify the bathymetry of the ocean and coastal regions, and the topography onshore of the inundated regions. I used the General Bathymetric Chart of the Oceans (GEBCO) 2014 30-second resolution raster seamless topography and bathymetry dataset (Intergovernmental Oceanographic Commission et al., 2014) to provide the bathymetric/topographic input files for La Trinchera, Constitución, Tubul, and the entire modeling space including the earthquake rupture area.

At Coliumo and Tirúa I improved the resolution of the GEBCO dataset by combining it using ArcGIS with bathymetric ship track points provided by the Servicio Hidrográfico y Oceanográfico de la Armada de Chile (SHOA) and the Shuttle Radar Topography Mission (SRTM) 2014 1-arc second data (U.S. Geological Survey, 2014) for topography. GEBCO bathymetry was used to fill in areas not covered by SHOA or where points were sparse. I removed anomalous points from the GEBCO dataset to ensure that all SRTM topography values were above sea level and all bathymetry values were below sea level. Where SHOA was used for bathymetry, a gap of no bathymetry points existed between the SHOA ship tracks and SRTM topography. All points were converted to an interpolated seamless raster that included topography and bathymetry in ArcGIS. The final Coliumo raster resolution was 10 seconds and Tirúa resolution was 4 seconds.

Model Input Data: Co-Seismic Slip Distributions

GeoClaw also requires input data to calculate the motion of the seafloor to initiate the tsunami. Out of 17 possible published slip distributions, I chose eight that exemplified different slip distribution patterns, were arranged in rectangular coordinates, and whose data were easily accessible (Figure 3). I chose Vigny et al. (2011) because it was a distribution with two major slip patches and Lorito et al. (2011) because it only had one major slip patch. The solution by Delouis et al. (2010) indicated moderately deep slip. Yue et al. (2014) resolved shallow slip that extended to the trench. Fujii and Satake (2013) represented a solution using large 50 km by 50 km square subfaults rather than the higher resolution of the others. I chose to model Sladen (2010), Shao et al. (2010), and

Hayes (2010) because they were the initial slip distributions to be released and the data were easily accessible.

In addition to the eight published distributions, I created a control earthquake of uniform slip along the entire rupture area. The top center location of the fault plane was taken from Fujii and Satake (2013) because the fault plane parameters most closely represented an average among the other slip distribution areas mentioned above. Slip was calculated for this control scenario to be 5 m using the seismic moment (M_o) equation:

$$M_o = \text{fault length} \times \text{fault width} \times \text{slip} \times \text{rigidity}$$

where $M_o = 1.8 \times 10^{22}$ Nm from the USGS Centroid Moment Solution (U.S. Geological Survey, 2011), rigidity = 4.0×10^{10} N/m², fault length = 600 km, and fault width = 150 km.

These slip distributions were arranged in subfault format, a rectangular grid defining the subduction zone, where each of the subfaults was assigned a value for latitude and longitude in decimal degrees, dip in degrees, slip in meters, width in kilometers, length in kilometers, rake in degrees, and depth in meters, for use as a GeoClaw input file. Latitude and longitude point locations were specified as either top center or hypocenter. Because Vigny et al. (2011) and Fujii and Satake (2013) latitude and longitude locations were in the southwestern corner of subfaults, I used the spherical trigonometry Haversine formulation to calculate the coordinates of the top center. Any time component of a published slip distribution was ignored for this study and only the cumulative slip at each subfault was used. To convert slip distribution parameters of each

subfault into instantaneous seafloor deformation patterns, GeoClaw uses the standard Okada (1985) equations of deformation of a homogenous half-space.

Comparison of Simulated Results to Observed Data

Published post-tsunami survey data from Morton et al. (2011) and Fritz et al. (2011) first required re-organization to be used for direct comparisons with GeoClaw simulations. Published and unpublished data provided by Morton et al. (2011) included multiple observations of flow depth for the same latitude/longitude coordinates. For my comparison, I used either the one flow depth value within a group of values that was included in the publication, or the average of all values if none were published for those coordinates. I used unpublished elevation data provided by Fritz et al. (2011) to change published flow depth values from being measured above sea level to being measured above land.

I condensed post-tsunami field data of run up, flow depth, and inundation from Fritz et al. (2011), Morton et al. (2011), and Annunziato et al. (2010) due to a large number of measurements within one grid cell of my simulations results. I combined field data points located within the bounds of the same 0.0027777° by 0.0027777° highest-resolution simulated grid cell to create a new representative observation of run up, inundation and/or flow depth value for that coordinate. I used the median value to combine three or more values within a cell, and the average value to combine two values within a cell. Because post-tsunami survey data at La Trinchera were clustered in two different areas, I renamed these areas La Trinchera North and La Trinchera South. Refer

to Appendix Table A1 for the original post-tsunami survey datasets from Fritz et al. (2011), Morton et al. (2011), and Annunziato et al. (2010) and Appendix Table A2 for the final condensed dataset of all tsunami flow depth, run up, and inundation measurements used in this study.

The observed maximum inland run up and inundation measurements were not the best data to compare to simulated results because of the low-resolution bathymetry and topography of the modeling space. Therefore, I only considered flow depth and water volume to compare the amount of water above the ground surface. When comparing the bathymetry and topography calculated by GeoClaw to the bathymetry and topography in my input file, the two values did not always match and a solution could not be easily found to fix the offset. This was a problem because the nearshore bathymetry and topography can have a first-order effect on run up (Pan et al., 2010), and if the elevation is inaccurate, it can also misrepresent the elevation of the maximum inundation distance. Although using volume of inundated water rather than flow depth or run up is not a typical approach to comparing observed to simulated results in tsunami modeling, volume based on flow depth helps solve errors associated with low resolution bathymetry and topography because volume depends less on elevation.

I used either the total volume of inundated water or individual flow depth values based on the number of data points at each study site. Constitución, Coliumo, and Tirúa had significantly more flow depth values, which allowed for the volume to be calculated. I calculated the total volume by using flow depth, inundation, and run up measurements from Fritz et al. (2011), Morton et al. (2011), Annunziato et al. (2010), and historical

imagery to trace a polygon of the inundation limit in Google Earth. At Tirúa, I supplemented with the inundation limit map from the maximum extent of visible tsunami debris in Ely et al. (2014). I imported the traced polygons into ArcGIS and used the flow depth measurements within the polygon to create an interpolated raster surface of flow depth in ASCII format to import into Microsoft Excel. I used Excel to calculate the volume of each raster square, and then summed all raster squares to get total volume. La Trinchera North, La Trinchera South, and Tubul each had two flow depth data points or less, so I compared the individual flow depth values. I made a one-to-one comparison if one flow depth value was available or averaged two flow depth measurements.

To determine the simulated volume or flow depth, I imported GeoClaw's output fixed-grid tables of maximum water depth into ArcGIS to create rasters with cell size of 0.0027777° . I set the fixed-grid cell locations to include all data points of post-tsunami field survey measurements from Morton et al. (2011), Fritz et al. (2011), Annunziato et al. (2010), and tsunami deposit locations from 2010, 2012, 2013 and 2015 field surveys. At Constitución, Coliumo, and Tirúa, I calculated the total volume of simulated water that lay within the same area as my Google Earth inundation polygon of the post-tsunami data using ArcGIS. At La Trinchera North, La Trinchera South, and Tubul, I used the single flow depth value (or the average of two cell values) of the cell(s) that contained the post-tsunami survey measurement(s). This allowed for a one-to-one comparison between observed and simulated results.

I then determined the success of a simulation producing the field observations by calculating the *percent difference* between the two using the equation:

$$\% \text{ Difference} = [(\text{simulated value} - \text{observed value}) / (\text{observed value})] \times 100$$

When comparing volumes, I first took the cube root of both the simulated and observed volume, then applied the percent difference formula above. I determined a percent difference of $\pm 35\%$ or better is considered acceptable when comparing observed results and simulated results. I chose $\pm 35\%$ because a worse percent difference significantly reduces the number of field sites with an acceptable percent difference. To determine the percentage of field sites that had a percent difference better than $\pm 35\%$ I used the *percent match*:

$$\% \text{ Match} = [(n \text{ sites better than } \pm 35\% \text{ difference}) / (n \text{ sites})] \times 100$$

where n sites are the six sites for this study. The percent match is the main value I used to determine the overall success of a source slip distribution at producing observed results. The “best-fit” models were those with the highest percent match with the observations.

“Best Fit” Models

To determine which earthquake parameters were important for creating the observed 2010 tsunami, I made slip distributions that were a combination of the parameters that created the best percent difference at each study site (La Trinchera, Constitución, Coliumo, and Tirúa). The goal was to alter the slip distribution to better match observed post-tsunami survey data, which would reveal the earthquake parameters

important to creating the tsunami. The processes of creating these improved slip distributions are called "method 1" and "method 2".

To create one simplified fault plane solution that best represented the 2010 earthquake rupture area, I used the original fault parameters of length, width, dip, rake, depth and the top center subfault latitude and longitude locations from the Fujii and Satake (2013) slip distribution (Figure 6). I removed the original northernmost row of the Fujii and Satake (2013) rupture plane grid because the slip amount in each subfault were close to 0 m, so I did not consider it to be significant. I added a new row below the original southernmost row to extend past Tirúa because the majority of the published co-seismic slip distributions also extended past Tirúa. I separated the rectangular grid into five sections, labeled using different colors in Figure 6 based on their position offshore of my field sites (La Trinchera, Constitución, Coliumo, Tubul, and Tirúa) to set consistent boundaries of modifying slip during each model run.

I employed two methods for generating new slip distributions; the idea behind both methods were to take the amount of slip simulated by the published slip distributions and control that created the best percent difference at each field site and apply it to the new modified grid. One method was not meant to be superior to the other. These methods were a way to create and test a greater number of different distributions in hopes that one could be a very good fit between observed and simulated data. For method 1 I created six new slip distributions and in method 2 I created five new slip distributions.

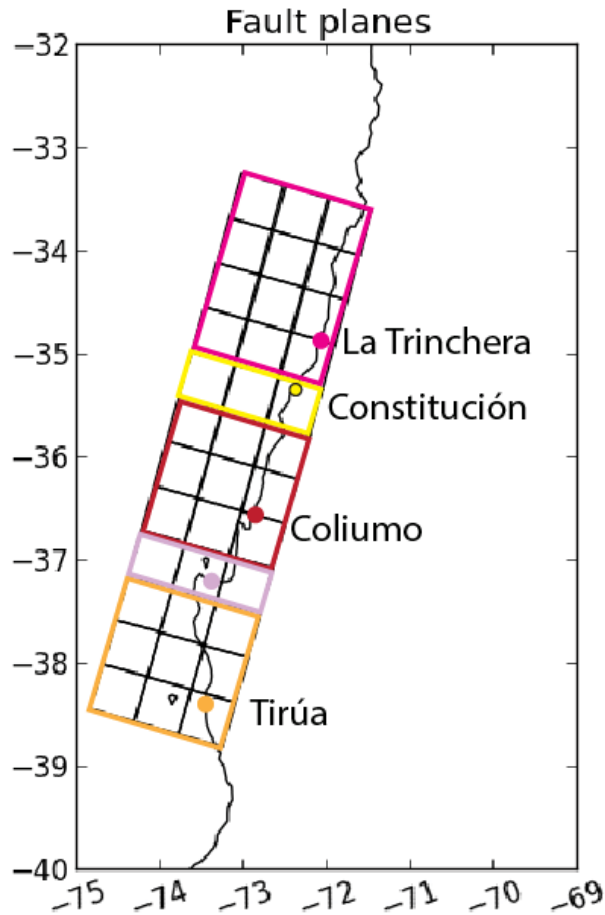


Figure 6: The subfault grid used to create slip distributions for method 1 and method 2, modified from Fujii and Satake (2013). Modeling-related field site locations are indicated with colored circles, which correspond to the boundary of those subfaults assigned to each adjacent study site.

Using method 1, I only considered the percent differences (not the percent matches) between observed and simulated results that were created by all of the published slip distributions and control scenario and gave equal consideration to all. See Figure 7 for a visual example. I started by identifying the simulation with the lowest percent difference at each study site; that published distribution was considered to be the best simulation for that particular site. Next, I overlaid the subfaults of the published slip

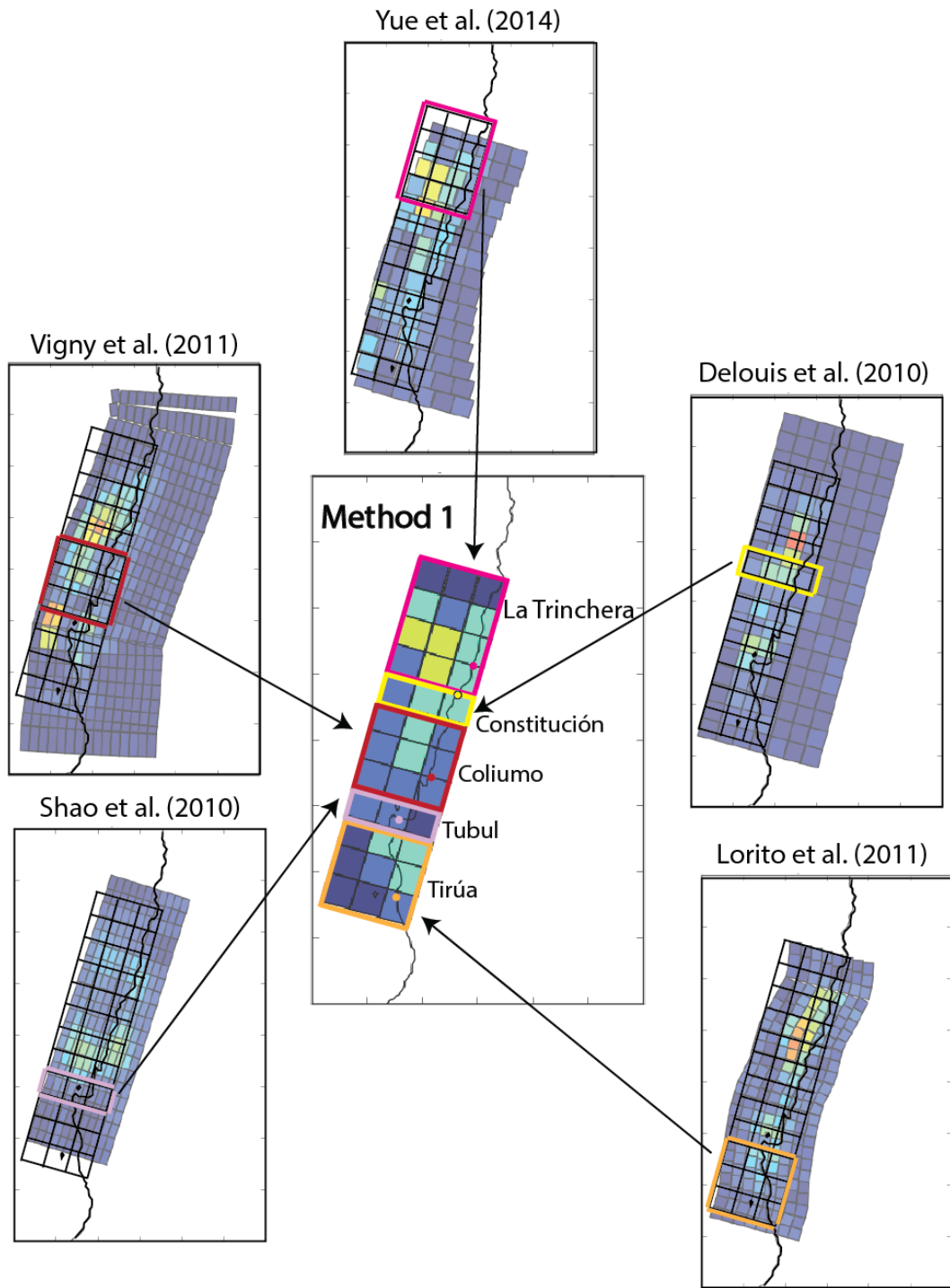


Figure 7: Diagram to illustrate how method 1 was used to create the *Method 1* modified slip distribution. The black modified subfault grid (Figure 5) overlays the published slip distribution that resulted in the best percent difference ($\pm 35\%$ or better) at each labeled study area. The colored boxes and arrow indicate the section of slip used from each published slip distribution.

distributions over my new modified subfault grid (Figure 7) using Google Earth. Where the new subfaults I separated into five sections (Figure 6) overlapped the best-fit slip distribution for that site, I assigned the published slip value to the new subfaults in 5 m increments and repeated these steps for each study area section to create the slip distribution labeled *Method 1* (slip distributions used in tsunami simulations will now be indicated in italics). I later modified the *Method 1* slip distribution to cover a range of possible slip values at each subfault: I increased slip 2.5 m and 5 m in every subfault (*Method 1 Increase 2.5 m* and *Method 1 Increase 5 m*) and decreased slip 2.5 m and 5 m in every subfault (*Method 1 Decrease 2.5 m* and *Method 1 Decrease 5 m*). Finally, using these five new slip distributions, I repeated the same steps as in method 1 but only considered the five new distribution results in the pool of possible best-fit solutions to make the *Composite* slip distribution.

Method 2 was similar to method 1, except I only considered the most successful published distributions. I first looked at the percent matches of the published slip distributions and the control and selected the top three highest percent matches, ignoring the others. I then repeated the same steps as in method 1, beginning with identifying the lowest percent difference at each study site. This created the *Method 2* distribution which I then modified to cover a range of possible slip values at each subfault: I increased slip both 2.5 m and 5 m in each subfault (*Method 2 Increase 2.5 m* and *Method 2 Increase 5 m*), increased slip 5 m to the shallowest subfaults and increase slip 2.5 m to all other subfaults (*Method 2 Increase 5 m & 2.5 m*), and increase slip 5 m only to the shallowest subfaults (*Method 2 Increase 5 m shallow*).

Tsunami Deposit Field Methods

I conducted fieldwork in Chile from January 13–23, 2015 to compare the tsunami deposits with the same deposits measured a few weeks after the 2010 tsunami from previous post-tsunami studies by Morton et al. (2011), in 2012 from Ely et al. (2014) and Ely's unpublished field notes, and in 2013 from Hong et al. (2016) and Hong's unpublished field notes. While in the field, I visited the coastal areas of La Trinchera, Constitución, Coliumo, Quidico, Tirúa, and Tubul (Figure 2), because both deposit data and tsunami water measurements were available for these six locations. I visited each study site for one day, with the exception of Coliumo for two days.

At each study site I described, sampled, and surveyed the 2010 tsunami deposits at previously described deposit locations to compare changes in sedimentary characteristics and determine changes in the maximum inland extent between 2010, 2012, or 2013 and 2015. I dug pits at the exact locations of pits described in previous studies (within handheld GPS error) as well as other locations within or near previously measured inundation limits. I measured deposit thickness, took photographs, and recorded visual observations of grading, sedimentary structures, lower and upper contacts, incipient soil development, and overlying organic material. I collected samples at each pit either as one bulk sample of the entire deposit or multiple sub-samples if there were noticeable changes in grain-size within the deposit. Samples of the pre-existing surface below the 2010 deposit were also collected if I observed a sharp contact. Refer to Appendix Table B1 for data collected on tsunami deposits. Measurements of horizontal distance and elevations (not corrected to sea level) of the 2010 tsunami deposits were

recorded by other members of the research team in the field at Coliumo and Tirúa using a surveying level and stadia rod. A portable tide gauge was used to measure mean sea level at both locations. Benchmarks were also measured while surveying, including a benchmark on a bridge at Tirúa that was also used in Ely et al. (2014). Because I compared tsunami simulation results to flow depth and volume rather than run up, these data were not used in my study.

Because there is currently no preferred grading system used to evaluate the preservation potential of paleotsunami deposits, I looked to other studies to use similar terminology. To remain consistent while examining the preservation of tsunami deposits at each study site location as a whole, I adopted a method created by Szczuciński (2012), which was also later adopted by Goto et al. (2012), to rank the current state of preservation for each study site as a whole: *good preservation* was when the revisited tsunami deposit pits were preserved in terms of thickness and also internal sedimentary structures; *moderate preservation* was when the revisited deposit pits existed but were altered in many ways, including internally; and *low preservation* was when there were generally no tsunami deposits left or they were very difficult to recognize.

The criteria I considered to determine long-term preservation potential of tsunami deposits at each study site were a combination of the current state of preservation (low, moderate or good), geomorphic environment (open beach, coastal plain, or river floodplain/valley), and land use (agricultural, animal grazing, easily accessible beach, etc.). Determining the long-term preservation is not as straightforward as determining the current preservation. For instance, two different coastal plain study sites that currently

display moderate preservation could have entirely different long-term preservation potential because of the differences in land use. For this reason, long-term preservation at each study site is either *likely* or *not likely*.

Lab Methods - Tsunami Deposits

I analyzed the tsunami sediments and soils to determine grain-size distributions using a Mastersizer 2000 laser particle-size analyzer and CAMSIZER particle-shape and size analyzer. Refer to Appendix Table B2 for grain-size values of all samples. Prior to analysis, I removed large roots by hand and picked out any small roots that could be seen by the naked eye with tweezers. I did not use other methods of preparing the sample, such as washing the sample in bleach or hydrogen peroxide, because the addition of water or other chemicals could result in the removal or dissolution of organic clays. I compared normalized grain-size distribution curves of tsunami deposits of the first sample at a deposit pit (collected by others in 2010/2012/2013) and the second sample (my sample from 2015). The grain-size distributions were graphed using Microsoft Excel. The different sampling methods between the first sample and the second sample proved a challenge to make samples from the same pit comparable. Of the samples I compared, Morton et al. (2011) did not follow a consistent sampling method for every deposit, Ely et al. (2014) and Hong et al. (2016) appeared to have taken samples based on visible grain-size differences. I accounted for this by measuring tsunami deposit thickness from bottom (contact with underlying surface, labeled as 0 cm) to top (current ground surface, labeled as the deposit total thickness) for both the first sample and second sample.

CHAPTER III
TSUNAMI MODELING RESULTS AND DISCUSSION

Site Results

La Trinchera

Post-tsunami surveys measured two observations at La Trinchera North. The flow depth observation of 4.5 m (Fritz et al., 2011) is what I used as the observed value for comparison to simulated values because I only used flow depths in my comparison methodology. The other observation was a run up measurement of 7.6 m, which provided a location for the inundation limit at 230 m inland. No tsunami deposits were described at this location in 2015 or prior. Nearly all simulations from published slip distributions underestimated tsunami flow depth at La Trinchera, except the tsunami from *Yue et al. (2014)* with a flow depth of 4.8 m, a +7% difference (Table 1). Out of all simulations ran in this study, only one-fifth resulted in a percent difference of $\pm 35\%$ or better (Tables 1-3) and none of the simulations I tested reached the limit of inundation. Tsunamis from the *Sladen (2010)*, *Shao et al. (2010)*, and the *Control* slip distributions did not inundate past the shoreline.

The geomorphology of La Trinchera South can be described as an open beach to the east and a low lying coastal plain to the west, both which have post-tsunami data measured by Morton et al. (2011) that I resurveyed (Figure 8; Figure 9). These two settings are separated by a high road. Post-tsunami surveys at La Trinchera South measured three tsunami observations, two of which were flow depths that I averaged to create a single observed value of 5.1 m to use to compare to simulated values. The third

was an inundation point from Morton et al. (2011) that marked the maximum water inundation at 790 m \pm 10 m inland in the coastal plain area (Figure 8; Figure 9).

Table 1: Percent differences between observed volume or flow depth measurements and simulated results, and overall percent match, from published slip distributions and the control simulation at each study site. Numbers are in percent; negative values indicate that simulated results were smaller than observed values. Flow depth and volume results at each study site for the three highest percent matches can be found on Figure 15; the remaining can be found in Appendix Table C1. Percent differences better than \pm 35% are highlighted in bold.

Location	Control	Delouis et al. (2010)	Fujii & Satake (2013)	Hayes (2010)	Lorito et al. (2011)	Shao et al. (2010)	Sladen (2010)	Vigny et al. (2011)	Yue et al. (2014)
La Trincher North	-100	-53	-77	-98	-71	-100	-100	-82	+7
La Trincher South	-93	-66	-82	-89	-74	-89	-87	-91	-15
Constitución	+5	+2	-16	-15	+9	-51	-41	-51	-6
Coliumo	-53	-33	-29	-42	-23	-43	-52	-23	-35
Tubul	-78	-25	-68	-17	-35	+1	-98	-30	+3
Tirúa	-54	-54	-45	-64	-37	-63	-67	-63	-51
Overall % Match	17	50	33	33	50	17	0	33	83

Table 2: Percent differences between observed volume or flow depth measurements and simulated results, and overall percent match, from *Method 1* slip distribution simulations at each study site. Numbers are in percent; negative values indicate that simulated results were smaller than observed values. Flow depth and volume results at each study site can be found on Figure 17. Percent differences better than \pm 35% are highlighted in bold.

Location	Method 1	Increase 5 m	Increase 2.5 m	Reduce 5 m	Reduce 2.5 m	Composite
La Trincher North	-51	-33	-42	-72	-61	-34
La Trincher South	-65	-40	-53	-87	-76	-44
Constitución	-10	+5	-2	-29	-19	+2
Coliumo	-31	-30	-31	-36	-34	-23
Tubul	+120	+187	+163	-23	+52	+278
Tirúa	-37	-23	-34	-57	-48	-11
Overall % Match	33	67	50	33	33	67

Table 3: Percent differences between observed volume or flow depth measurements and simulated results, and overall percent match, from *Method 2* slip distribution simulations at each study site. Numbers are in percent; negative values indicate that simulated results were smaller than observed values. Flow depth and volume results at each study site can be found on Figure 19. Percent differences better than $\pm 35\%$ are highlighted in bold.

Location	Method 2	Increase 5 m	Increase 2.5 m	Increase 5 m & 2.5 m	Increase 5 m shallow
La Trinchera North	-50	-32	-41	-50	-67
La Trinchera South	-64	-39	-52	-64	-86
Constitución	-5	+10	+3	+2	-6
Coliumo	-35	-32	-34	-35	-34
Tubul	-69	-46	-64	-54	-58
Tirúa	-34	-18	-29	-29	-37
Overall % Match	50	67	50	50	33

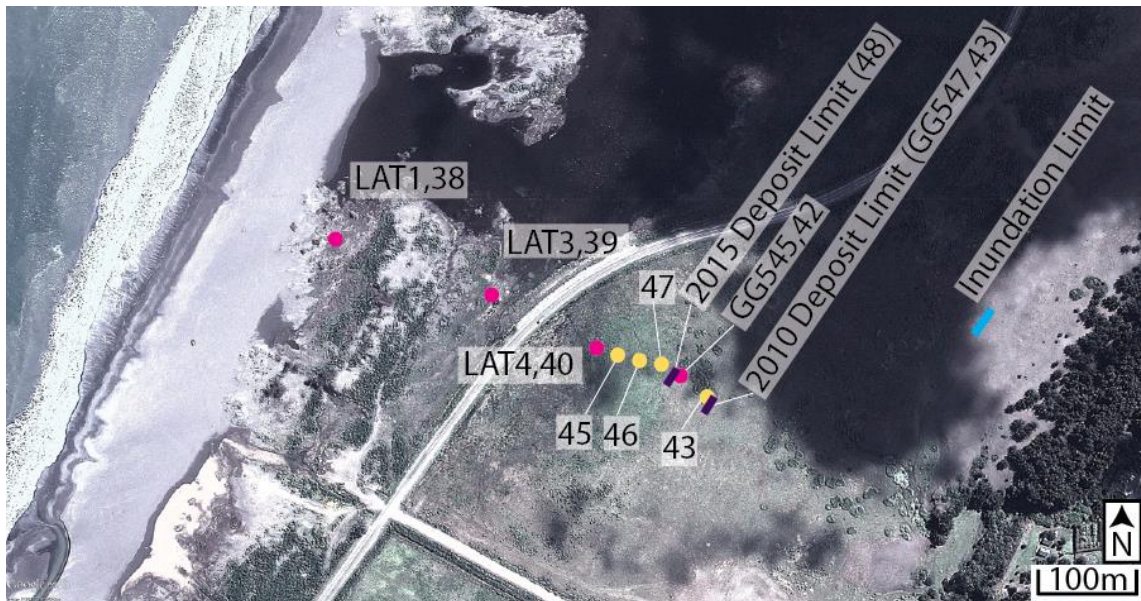


Figure 8: La Trinchera South location map. See Figure 2 for location. Tsunami deposit pit names are labeled as “2010 name, 2015 name”; descriptions can be found in Appendix Table B1. Pits re-visited in 2015 from Morton et al. (2011) are marked by pink circles and additional pits described in 2015 are marked by yellow circles. Tsunami deposits that define deposition limits are marked by purple rectangles with the pit name in parenthesis. Inundation limit in blue was measured by Morton et al. (2011) in 2010. Image from Google Earth.

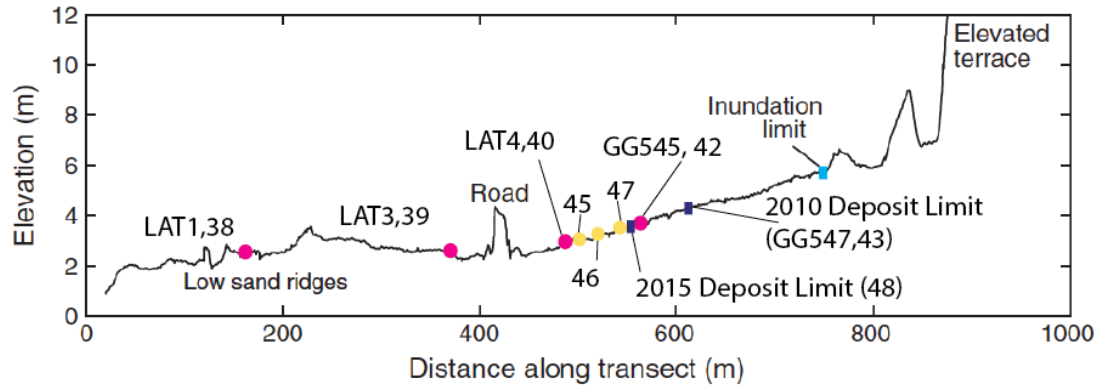


Figure 9: La Trincheras South elevation transect modified from Morton et al. (2011) to include tsunami deposit locations. See Figure 8 for color/symbol descriptions.

All simulations underestimated the tsunami flow depth, with the best match, *Yue et al. (2014)*, being the only simulation with a percent difference of $\pm 35\%$ or better, at 4.3 m (-15%; Table 1). The smallest simulated flow depth was 0.36 m from the *Control* simulation (Appendix Table C1). Like La Trincheras North, none of the simulations reached either the limit of inundation or the deposit maximum inland extent (Figure 8; Figure 9).

Constitución

The geomorphology at Constitución is both a river floodplain (Figure 10a.) and an open beach (Figure 10b.; Figure 11) where post-tsunami survey data were collected. The river floodplain extends significantly more inland and contains one run up value in Fritz et al. (2011) of 5.1 m that marked the maximum inland extent of the tsunami at a distance of 8,500 m \pm 100 m (Figure 10a.). The open beach contains the re-surveyed tsunami deposits and a local inundation limit initially described by Morton et al. (2011) (Figure

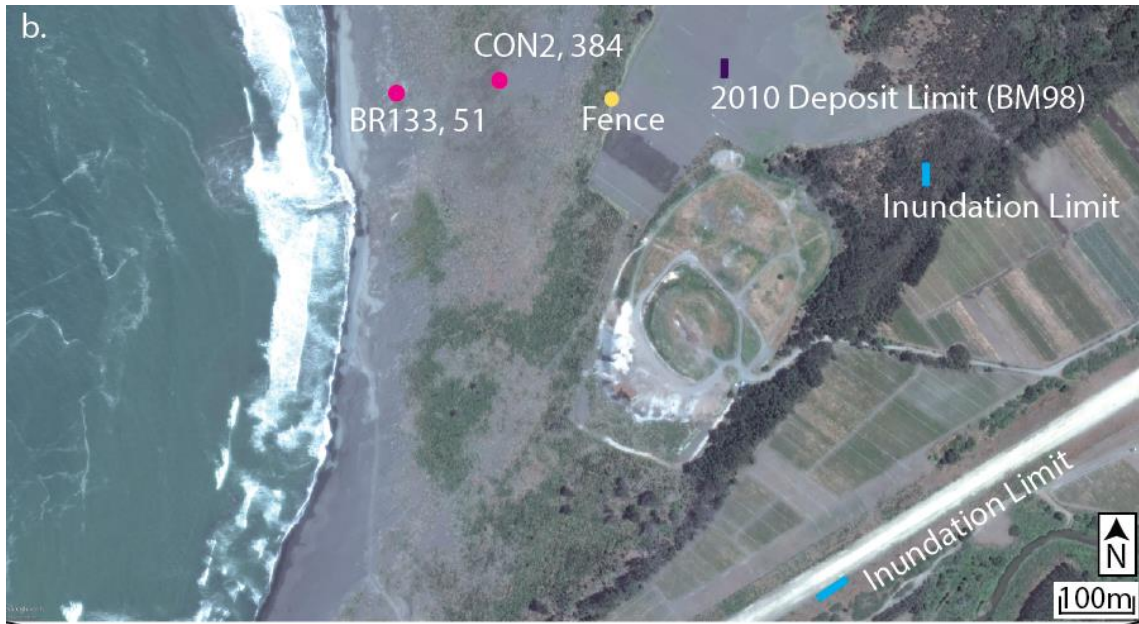


Figure 10: a.) Constitución location map. Inundation limit in blue was measured by Fritz et al. (2011) in 2010. See Figure 2 for location. b.) Tsunami deposit pit names are labeled as “2010 name, 2015 name”; descriptions can be found in Appendix Table B1. Pits revisited in 2015 from Morton et al. (2011) are marked by pink circles and an additional location visited in 2015 is marked by a yellow circle. The tsunami deposit that defines the deposition limit is marked by a purple rectangle with the pit name in parenthesis. Inundation limit in blue was measured by Morton et al. (2011) in 2010. Images from Google Earth.

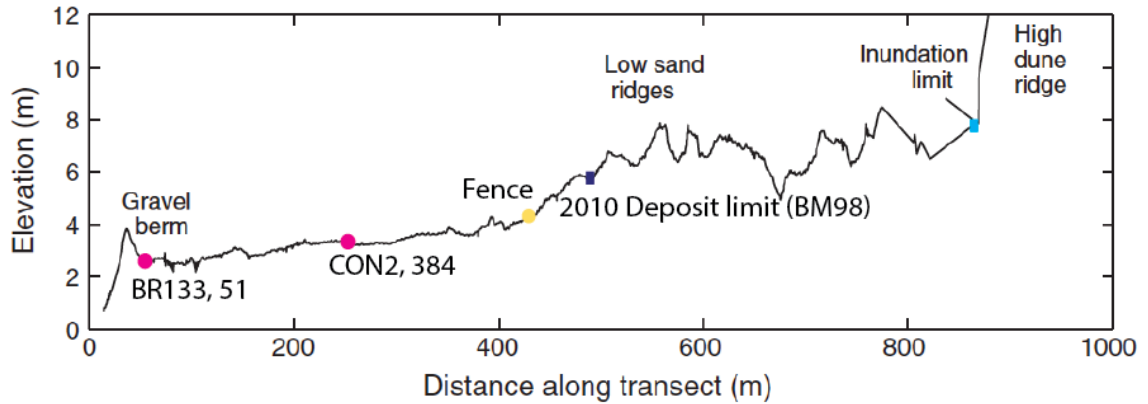


Figure 11: Constitución elevation transect modified from Morton et al. (2011) to include tsunami deposit locations described in Figure 10. See Figure 10 for color/symbol descriptions.

10b.; Figure 11). Constitución post-tsunami surveys include a significant number of data points, which I condensed to 33 to use in my modeling, the largest number of all field sites. Eighteen points measured flow depth and ranged from 0.65 m to 7.9 m. I used these points to calculate the total volume of water that inundated the area at around 3.5×10^7 m³. I did not include the 8-km-inland inundation value in my volume calculation because there were no flow depth values beyond 2,300 m \pm 100 m to interpolate a volume at this distance, although I did extend my volume to $\sim 3,000$ m \pm 100 m inland.

Nearly half of the simulations underestimated my calculated water volume, although 85% resulted in a percent difference of $\pm 35\%$ or better, which is the greatest number of well-performing simulations of all the sites (Tables 1-3). None of the simulations I tested reached the $\sim 3,000$ -m inland limit of inundation that I used to calculate the total volume, and the actual inundation limit of 8,500 m \pm 100 m (Figure 10a.) was severely underestimated. Only one simulation, *Method 2 Increase 5 m*, reached the 2010 tsunami deposit limit (Pit BM 98; Figure 10b.).

Coliumo

Post-tsunami surveys collected a large number of data points in the river valley of Coliumo (Figure 12), which I condensed to 15 to use in my models. Eleven were flow depth measurements that ranged from 2.5 m to 6 m and the remaining were either run up or inundation values. I calculated the total volume of water that came on shore as $4.8 \times 10^6 \text{ m}^3$ using the inundation limit measured by Morton et al. (2011) of $1,600 \text{ m} \pm 200 \text{ m}$ (Figure 12) and the flow depths within the river valley.



Figure 12: Coliumo location map. See Figure 2 for location. Tsunami deposit pit names are labeled as “2010 name, 2015 name”; descriptions can be found in Appendix Table B1. Pits re-visited in 2015 from Morton et al. (2011) are marked by pink circles and additional pits described in 2015 are marked by yellow circles. The tsunami deposit that defines the deposition limit is marked by a purple rectangle with the pit name in parenthesis. Inundation limit in blue was measured by Morton et al. (2011) in 2010. Image from Google Earth.

All of the simulations underestimated observations, although three-fourths resulted in a percent difference of $\pm 35\%$ or better (Tables 1-3). With the exception of one-fourth of all simulations, all simulated volumes were very similar, with a volume of 1.30 to $1.74 \times 10^6 \text{ m}^3$. None of the simulations I tested reached the limit of inundation or the deposit maximum inland extent (Figure 12).

Tubul

The geomorphology of Tubul contains both a coastal plain and river floodplain where post-tsunami survey data were collected (Figure 13). Fritz et al. (2011) made seven post-tsunami survey measurements at Tubul; two of which were flow depth points, which averaged to 2.2 m as the observed value for comparison to simulated values. A run up measurement along the floodplain, farther inland of the coastal plain, was used as the inundation limit of $1,700 \text{ m} \pm 100 \text{ m}$ (Figure 13). Out of all simulations, only 35% resulted in a percent difference of $\pm 35\%$ or better (Tables 1-3). Unusual for other sites, one-third of the simulations overestimated the tsunami flow depth, including the *Method 1 Composite* simulation, which produced a large flow depth of 8.3 m, 6 m higher than observed (a percent difference of +278%; Table 2). All simulations reached the tsunami deposit Pit 83 in the coastal plain area that I resurveyed in 2015, although none reached the limit of water inundation (Figure 13).



Figure 13: Tubul location map. See Figure 2 for location. Tsunami deposit pit name is labeled as “2012 name, 2015 name”; description can be found in Appendix Table B1. The pit re-visited in 2015 described in unpublished field notes from 2012 by L. Ely, pers. comm. (2015) is marked by a pink circle. Image from Google Earth.

Tirúa

Fritz et al. (2011) made nine post-tsunami survey measurements at the river floodplain of Tirúa (Figure 14), four of which were flow depth points that ranged from 1.2 m to 5 m. The maximum tsunami inundation was not available from the post-tsunami survey, but an inundation map based on the maximum extent of visible tsunami debris in Ely et al. (2014) showed maximum inundation at $2,170 \text{ m} \pm 10 \text{ m}$, past the extent of Figure 14 and a local inundation limit labeled in Figure 14. I calculated total water volume at $5.7 \times 10^6 \text{ m}^3$ as the observed value for comparison to simulated values.

All of the simulations underestimated observations and only 35% resulted in a percent difference of $\pm 35\%$ or better (Tables 1-3). None of the simulations I tested

reached the limits of inundation or the deposit maximum inland extent (Figure 14), and many severely underestimated these observations.

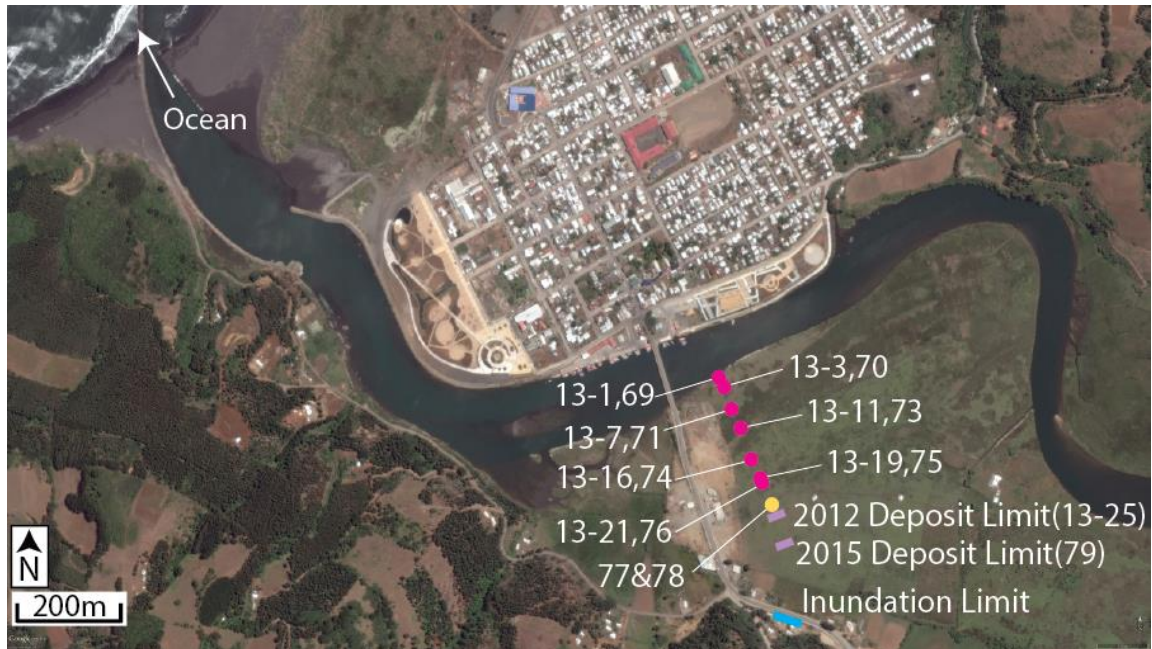


Figure 14: Tirúa location map. See Figure 2 for location. Tsunami deposit pit names are labeled as “2012 name, 2015 name”; descriptions can be found in Appendix Table B1. Pits re-visited in 2015 from Ely et al. (2014) are marked by pink circles and additional pits described in 2015 are marked by yellow circles. Pit 77 and Pit 78 are two separate deposits but are both located within one circle label. Tsunami deposits that define the deposition limits are marked by purple rectangles with the pit name in parenthesis. Inundation limit in blue was measured by Ely et al. (2014) in 2012. Image from Google Earth.

Sources of Error in Modeling

Sources of error in my tsunami modeling include: low-resolution bathymetry and topography, mathematical approximations used in GeoClaw, the location of my modified subfault grid, and my manipulation of post-tsunami field datasets. Most important for my final results, the bathymetry and topography used in my simulations likely played a major

role in the general underestimation of simulated results, especially the inundation. La Trinchera, Constitución, and Tubul had 30-second resolution bathymetry and topography, Coliumo had 10-second, and Tirúa had 4-second, all of which were in the range of hundreds of meters per grid cell. While resolution finer than 10 minutes is sufficient to model wave propagation in the open ocean, in coastal areas, such as where the wave inundates the land, it may be necessary to have a resolution of tens of meters or less (LeVeque et al., 2011), much finer than what was available for Chile. Because of the low-resolution bathymetry, my results focus on comparing simulated and observed flow depth and volume, but I mention inundation results as well.

High-resolution bathymetry is necessary to simulate the details of wave behavior and accurate tsunami heights during inundation (MacInnes et al., 2013). Nearshore bathymetry and detailed local bathymetric structures can have a first-order effect on the run up (Pan et al., 2010). If the nearshore bathymetry is misrepresented in the modeling space, the important coastal effects such as wave refraction, diffraction, and shoaling that are known to amplify wave height and current velocity will most likely be lost (Pan et al., 2010). The GEBCO and SRTM datasets I used are widely-used datasets, however, the focus of GEBCO is the deep ocean, the quality and coverage of data is highly variable, and does not include detailed bathymetry for the shallow shelf (Intergovernmental Oceanographic Commission et al., 2014). Errors from the bathymetric ship track dataset provided by SHOA are not known. I merged SHOA data with GEBCO and SRTM to improve resolution, but errors can occur when merging multiple datasets of bathymetry and topography from different sources, especially at the shoreline when topography

points overlap with bathymetry. I corrected errors I encountered in a few locations but some may still exist.

As with any numerical modeling program, complex processes in GeoClaw are simplified based on many mathematical approximations. For example, the conversion from slip to seafloor deformation using the Okada (1985) equations assumes a flat seafloor and homogenous elastic material of each subfault. It also assumes vertical instantaneous slip only, when in reality the subduction zone rupture propagated and released most of its energy in the first 90 seconds of the total 172-second rupture event (Yamazaki and Cheung, 2011). I used a generic Manning coefficient of 0.025 for the bathymetry and topography surface commonly used for tsunami modeling (LeVeque et al., 2011), which assumes unchanging friction. Because the run up and inundation distance are affected by the roughness of the ground surface (LeVeque et al., 2011), modifying this parameter to a lower value could improve the inundation. As another example, shelf resonance and edge waves can create a larger tsunami than what is expected from co-seismic slip alone. My tsunami simulation results via synthetic tide gauges at a number of my study sites do detect a larger wave after the initial wave, indicating GeoClaw can model edge waves, but they may not be captured well. Numerical tsunami modeling of the 2010 tsunami by Yamazaki and Cheung (2011) indicated that wave energy was trapped and amplified over the wide continental shelf and slope, resulting in shelf resonance. This created edge waves, where waves were refracted into multiple directions when the tsunami wave shoaled, which intensified and prolonged the tsunami on the coast in some areas, especially around the bay of Concepción near

Talcahuano (Figure 2). When such characteristics are poorly approximated in numerical modeling, especially with lower resolution bathymetry, this will often lead to underestimated inundation results.

The location and uniform parameters (except slip amount) of my method 1 and 2 grid modified from Fujii & Satake (2013) may have introduced additional errors in its simplification. Other published slip distributions extended much deeper down-dip of the trench, and most used variable parameters to define the fault surface (dip, strike, rake, etc.). For instance, adjusting the dip parameters to create a shallower dipping fault can create a longer wavelength tsunami and steeper dipping faults can shorten the wavelength and can enhance the near-field tsunami (Melnick et al., 2012). Adjusting the dip angle within a reasonable amount may have created a smaller error between my observed and simulated comparisons.

Finally, my manipulation of the post-tsunami observation datasets could have introduced error by potentially misrepresenting the observed values to compare to simulated values. For each model grid cell I had to use my own interpretation when averaging flow depth/run up data points, which are based on a finite and often small number of data points and do not necessarily report a true average for the location. Additionally, a significant issue in immediate post-tsunami survey data is the human bias towards recording only the maximum run up/inundation and recording the water marks that are the easiest to measure (Dominey-Howes et al., 2012). This could have made my calculated volumes and averaged flow depths too large and would cause the simulations to appear to underestimate the tsunami. Lastly, calculating volume of water from

observations at Constitución, Coliumo, and Tirúa required creating an interpolated raster surface from a polygon inundation area I traced based on a variety of datasets, which are largely based on my own interpretation. This could cause the observed volumes to be either too large or too small and create simulations that appear to underestimate or overestimate the tsunami

Discussion of Site-Specific Results

The success of tsunami simulations at each site varies significantly, but overall, modeling to flow depth and volume was more successful than modeling to tsunami inundation and deposits. This is largely due to the low bathymetry and topography resolution, which is discussed briefly here as well as in the previous *Sources of Error in Modeling* section.

Modeling to Inundation and Deposit Limits

At every study site, no simulation reached the water inundation limit. The most severely underestimated sites for inundation occurred when the simulated tsunami had to inundate through the river floodplain, such as at Constitución (Figure 10a.), Tubul (Figure 13), and Tirúa (Figure 14) or the alluvial valley at Coliumo (Figure 12). I attribute this to the poor resolution bathymetry and topography, which did not represent the complex morphology of the rivers.

In contrast, all simulations reached the tsunami deposit at Tubul, which is located in the area of that resembles a coastal plain rather than the river floodplain (Figure 13).

One simulation reached the 2010 deposit limit at Constitución, which was not directly on the river floodplain but on an open beach where Morton et al. (2011) conducted their post tsunami survey (Figure 10b.). La Trinchera also displays an open beach geomorphology, but the simulation did not inundate to the deposits (Figure 8). In general, the bathymetry and topography did not represent these areas well either, but slightly better than the river floodplains and alluvial valley.

Modeling to Volume and Flow Depth

Observed volumes were best simulated at Constitución, where 85% of simulations had percent differences better than $\pm 35\%$ (Tables 1-3). This was unexpected, because the tsunami inundation was also the most underestimated at this location. However, this site had the greatest number of post-tsunami field data to interpolate a calculated volume, which may have contributed to a more accurate interpolated volume compared to other sites. At Constitución the inundation distance of my calculated volume was also much shorter and closer to the shoreline than the true inundation distance (Figure 10a.) similarly suggesting open coastlines are represented better than river floodplains in coarse resolution bathymetry and topography datasets.

Relative to all other results, volumes were also well simulated at Coliumo with 75% of the percent differences better than $\pm 35\%$ (Tables 1-3). Similar to Constitución, this is slightly unexpected since inundation was also poorly matched at this location and simulations did not inundate much farther than the river mouth. Again, this suggests that

the coarse resolution bathymetry and topography did not represent the river valley well, but could at least represent the mouth of the river better.

At Tirúa, the observed volumes were simulated poorly in all simulations, with only 35% of the simulations at each site resulting in percent differences better than $\pm 35\%$ (Tables 1-3). However, the percent differences that were worse than $\pm 35\%$ did not exceed -64%, so the bad matches were not extreme. In terms of inundation, this site is more complex in geomorphology than the area I modeled to in Constitución, and is more inland than Coliumo, and was therefore likely not represented well in the model.

Where I compared flow depths rather than volume, the overall success of the models was quantitatively lower. At La Trinchera North, one-fifth of the percent differences were acceptable, while at La Trinchera South, only one was acceptable (Tables 1-3). The large negative percent differences (up to -100%) from the published distributions improved when I created the modified distributions, but most percent differences were still larger than the acceptable limit of $\pm 35\%$. While the geomorphology of La Trinchera North and South are less complex, it reveals that it may be more difficult to get a good match between one flow depth point, as opposed to an interpolated volume of many flow depths of an entire area when the bathymetry and topography are low.

At Tubul, only 35% of the simulated flow depths were acceptable (Tables 1-3). Similar to La Trinchera North and South, it may also be difficult to get a good match from one flow depth point as opposed to an interpolated volume of many flow depth points. The worst percent difference at Tubul (+278%) was seen when Coliumo and Tirúa (the study sites that bound Tubul to the north and south) needed a larger tsunami for the

best percent differences out of all simulations (-23% and -11% respectively; Table 3). The best match at Tubul was +3% from *Yue et al. (2014)*, but occurred when Coliumo had a -35% difference and Tirúa did not reach an acceptable percent difference (Table 1). In this case, poor results at Tubul were necessary for better percent differences at Coliumo and Tirúa.

Published Slip Distributions, Percent Match Results

I determined the success of a simulation at a study site by calculating the percent difference between the simulated and observed values; if the percent difference is $\pm 35\%$ or better, it is a “match”. The percent match is the percentage of study sites (out of six) that had a percent difference of $\pm 35\%$ or better. Of all eight published slip distributions and the control, the simulations based on *Yue et al. (2014)*, *Delouis et al. (2010)*, and *Lorito et al. (2011)* produced the highest percent matches to the six sites’ observations, at 83%, 50%, and 50% respectively (Figure 15; Table 1), based on the number of percent differences at $\pm 35\%$ or better. At Tirúa, none of the percent differences were better than $\pm 35\%$ (Table 1). The best percent difference was -37% based on *Lorito et al. (2011)* (Table 1), so I considered this the best simulation for this location. The simulation based on *Sladen (2010)* resulted in the lowest percent match of 0%, where results from all six sites were worse than a $\pm 35\%$ percent difference (Figure 15; Table 1) and it did not inundate past the shoreline at La Trinchera North. Volume and flow depth values for all simulations are included in Appendix Table C1. Refer to Appendix Tables D1-D9 for the slip distribution parameters of the control earthquake and all published earthquakes.

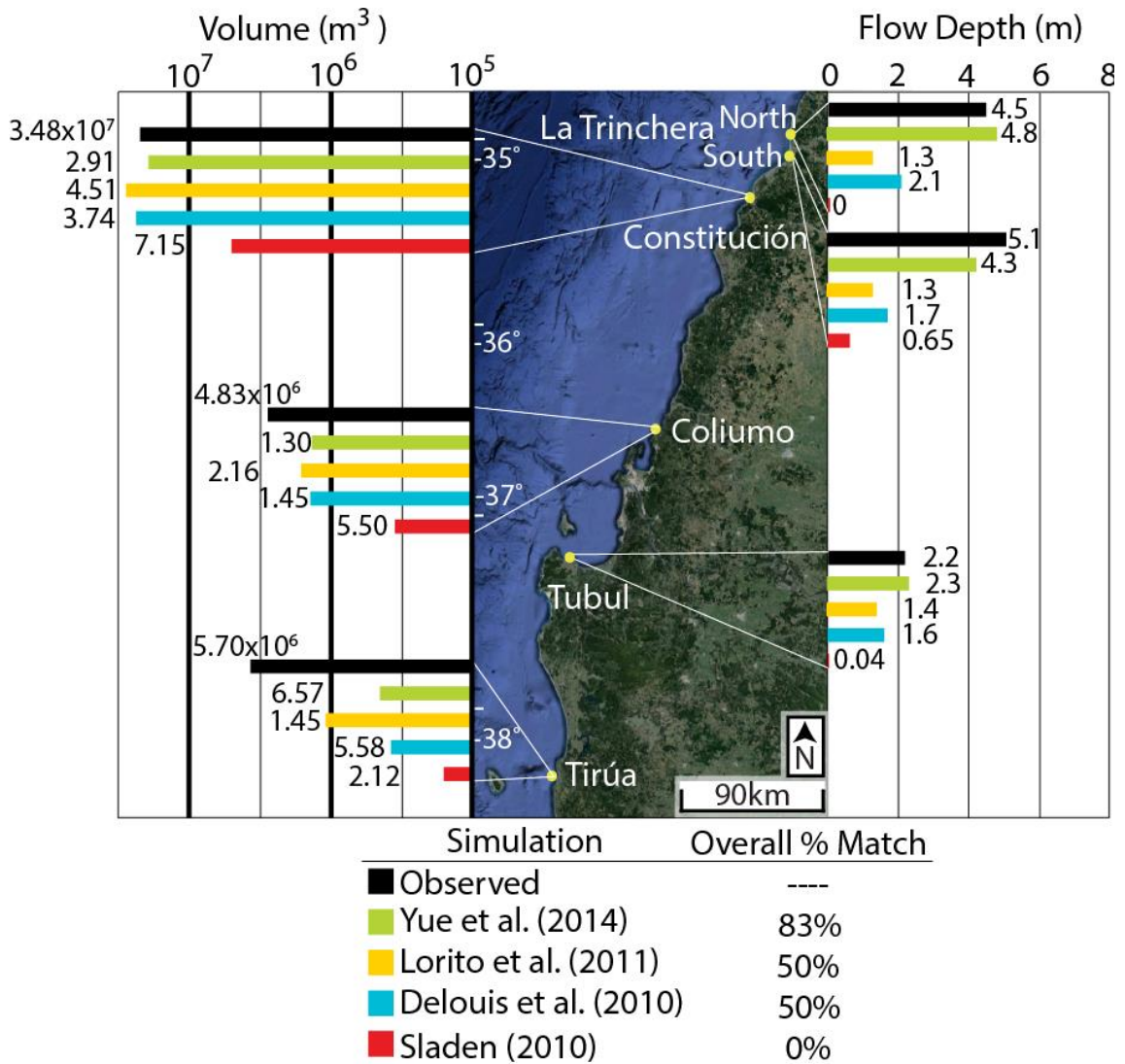


Figure 15: Map of observed water volumes and flow depths compared to GeoClaw simulated volumes and flow depths at each study site. Only the three published slip distributions that resulted in the highest percent matches and the lowest percent match are shown. Additional model run results of published and control distributions are in Appendix Table C1. Image from Google Earth.

Discussion of the Published Slip Distribution Results in Recreating the 2010 Tsunami

Percent matches between simulated volume or flow depth and field measurements were not high except for *Yue et al. (2014)* (Figure 15). The overwhelming majority of simulated tsunami water volumes and flow depths were underestimated when compared to the observed values, with very few sites overestimated (Appendix Table C1). However, the moment magnitudes of the published earthquakes are all very close to the accepted M_w 8.8 value (Moreno et al., 2010), except Sladen (2010) with a M_w 8.61. This suggests that the total amount of slip for each distribution, except Sladen (2010), was likely well resolved.

The three slip distributions that created the overall highest percent matches each have a major and minor slip patch, resolve the majority of slip offshore, and extend south of Tirúa. The seafloor deformation from *Yue et al. (2014)* is greater and distributed along the trench, with the exception of a few areas (Figure 3). *Delouis et al. (2010)* and *Lorito et al. (2011)* have less deformation at the trench because there is less slip (Figure 3), which may explain the lower percent matches in comparison to *Yue et al. (2014)*.

I expected that slip distributions that included tsunami data as input parameters would create the best-fitting simulated tsunami. However, based on my three best-fit models above, a variety of input data types rather than just tsunami data appeared to be more important. Of the three solutions that included tsunami data, *Yue et al. (2014)* and *Lorito et al. (2011)* created the highest percent matches, but the other, *Fujii & Satake (2013)*, had a low percent match at 33%. The simulation based on *Delouis et al. (2010)*

did not include tsunami data. The importance of a variety of input data types was also seen in Sladen (2010) slip distribution as it resulted in the lowest percent match of 0%. Sladen (2010) only used teleseismic p-waves to create the distribution, which resolved a low maximum slip of ~8 m and a rupture area that did not extend south to Tirúa (Figure 3).

Slip distribution inversions use different datasets to resolve slip during an earthquake, many of which have predictable biases. For instance, using teleseismic and geodetic data to invert co-seismic slip distributions tends to not resolve shallow slip near the trench well (Yue et al., 2014). However, joint inversion of both high rate GPS and teleseismic datasets together can improve resolution of near trench slip (Yue and Lay, 2013; Yue et al., 2014). Tsunami data can also resolve slip at the trench, but comparisons of tsunami data used by Yue et al. (2014), Lorito et al. (2011), and Fujii and Satake (2013) show the importance of the type of tsunami data, such as Deep-ocean Assessment and Reporting of Tsunami (DART) buoys or coastal tide gauges, and accurate propagation corrections (Yue et al., 2014). Lorito et al. (2011) used mostly tide gauge data which is not as sensitive to slip near the trench compared to DART data (Yue et al., 2014). Fujii and Satake (2013) used the same DART data as Yue et al. (2014) as well as regional tide gauge observations but with different inversion methods that did not use a velocity correction. Yue et al. (2014) also combined DART data with teleseismic and high rate GPS, to improve near trench slip. Even though Delouis et al. (2010) did not include tsunami data, its simulation produced comparable results to Lorito et al. (2011), which I interpret as indicating teleseismic and high rate GPS data together may be just as

effective as the tsunami data that Lorito et al. (2011) included at capturing the sensitive tsunami-forming properties of the earthquake rupture.

Best-Fit Model Results: Method 1

In the absence of higher-resolution datasets, more accurate bathymetry, or account for shelf resonance and edge waves, modifying the slip distributions could produce lower percent differences and better percent matches. Using method 1, as illustrated in Figure 7, I determined the published slip distribution that was the best simulation for each individual study site: *Yue et al. (2014)* at La Trinchera, *Delouis et al. (2010)* at Constitución, *Vigny et al. (2011)* at Coliumo, *Shao et al. (2010)* at Tubul, and *Lorito et al. (2011)* at Tirúa. I then assigned the published slip values, in 5 m increments, to the new modified subfault grids adjacent to each study site section (Figure 7) to create the *Method 1* slip distribution (Figure 16). Refer to Appendix Table D10 for the resulting slip distribution parameters of the *Method 1* M_w 8.86 earthquake. The resulting simulation produced an overall percent match of 33% and underestimated the tsunami at all locations (Figure 17; Table 2).

To increase the percent match above 33%, I then modified the *Method 1* slip distribution to create four additional distributions by increasing slip 2.5 m and 5 m in every subfault and decreasing slip 2.5 m and 5 m in every subfault. Refer to Appendix Tables D11-D14 for the resulting slip distribution parameters of the *Method 1 Increase 2.5 m*, *Method 1 Increase 5 m*, *Method 1 Reduce 2.5 m* and *Method 1 Reduce 5 m* earthquakes (Figure 16). The percent matches of these four additional distributions were

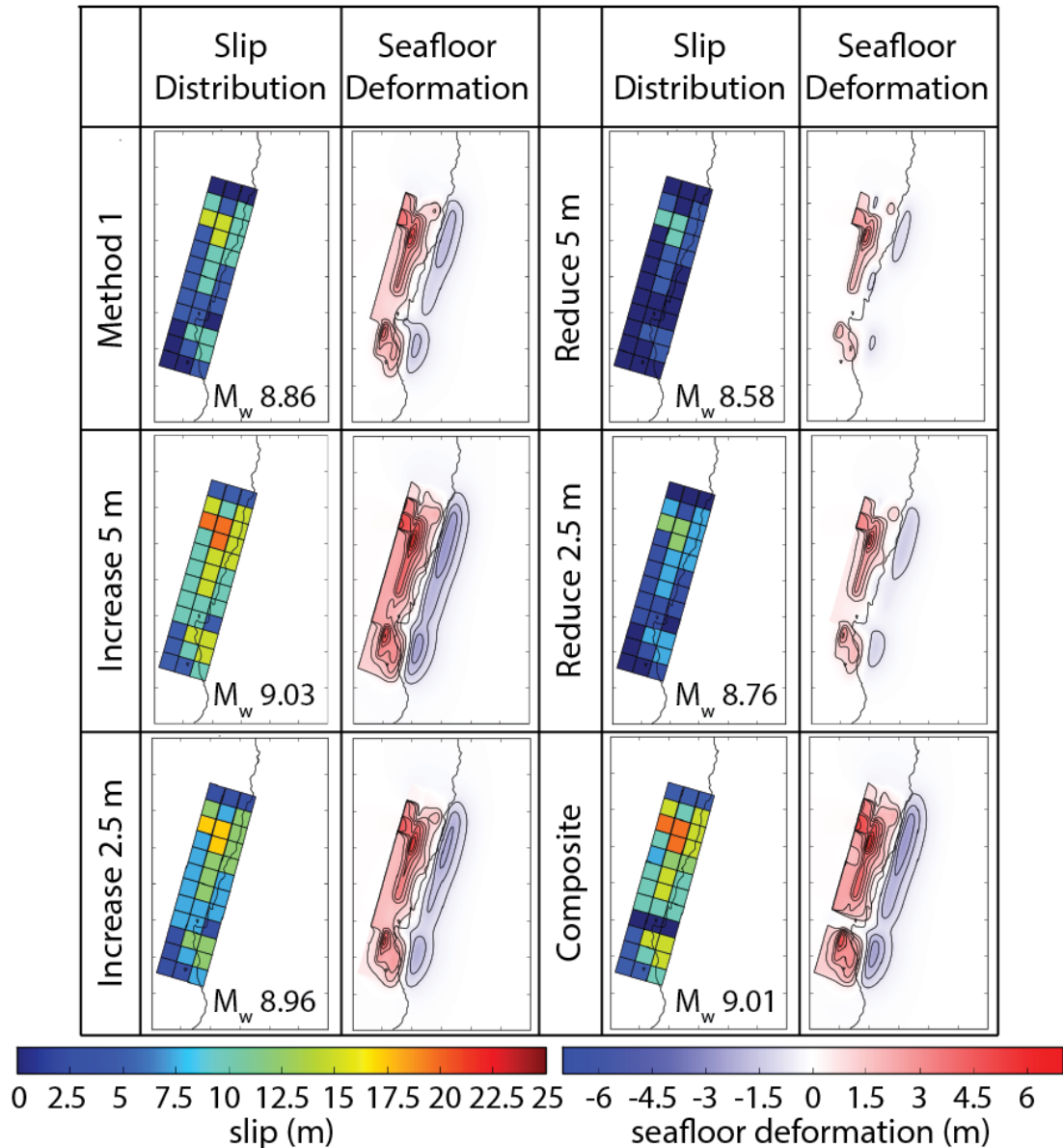


Figure 16: Slip distributions generated based on method 1 and resulting seafloor deformation patterns calculated in GeoClaw using the Okada (1985) equations. “Increase/Reduce” refer to amount of slip (meters) increased or reduced in each subfault from the *Method 1* slip distribution (upper left). Each slip distribution and seafloor deformation figure covers -32° to -40° S latitude and -75° to -69° W longitude. The shoreline is drawn in black; land is to the east of the line.

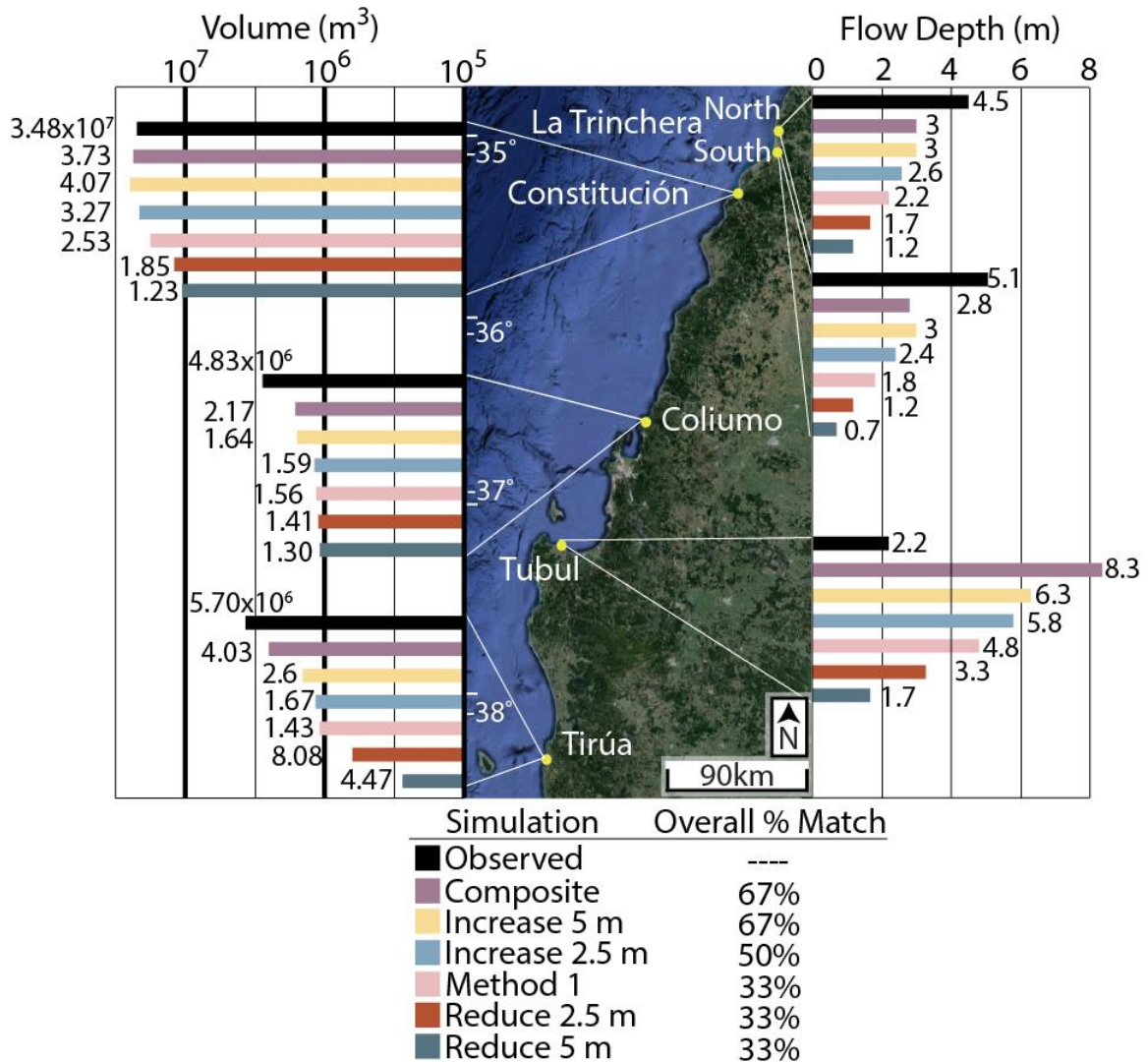


Figure 17: Map of observed water volumes and flow depths compared to GeoClaw simulated volumes and flow depths at each study site. All simulations using method 1 are included. Image from Google Earth.

not as successful as anticipated; *Method 1 Increase 5 m* was the best match at 67% (Table 2; Figure 17), with an earthquake magnitude of M_w 9.03. *Method 1 Increase 2.5 m* was a lower percent match of 50% (Table 2; Figure 17) and magnitude of M_w 8.96. *Method 1 Reduce 5 m* and *Method 1 Reduce 2.5 m* were both a 33% match (Table 2; Figure 17) and magnitude of M_w 8.58 and M_w 8.76 respectively.

Finally, to attempt to increase the percent match above 67%, I then re-determined the source models that were the best simulations for each individual site of all the new method 1 slip distributions: *Method 1 Increase 5 m* at La Trinchera, Coliumo, and Tirúa, *Method 1 Increase 2.5 m* at Constitución, and *Method 1 Reduce 5 m* at Tubul. I then assigned slip, in 5 m increments, to the new modified subfault grids adjacent to each study site as before (see Figure 7 as an example) to create the *Method 1 Composite* slip distribution (Figure 16). Refer to Appendix Table D15 for the resulting slip distribution parameters of the *Method 1 Composite* M_w 9.01 earthquake. The resulting percent match did not improve, with a percent match of 67% (Table 2; Figure 17).

Best-Fit Model Results: Method 2

Method 2 was not superior to method 1, but was a way to test more distributions to improve the fit between simulated tsunamis and field observations. In method 2 I determined the top three source models that were the best simulations overall based on the percent match: *Yue et al. (2014)*, *Lorito et al. (2011)* and *Delouis et al. (2010)* rather than the best model at each individual site. With only these three distributions, I then determined the best fit model at each site: *Yue et al. (2014)* at La Trinchera and Tubul, *Delouis et al. (2010)* at Constitución, and *Lorito et al. (2011)* at Coliumo and Tirúa. I then assigned the published slip, in 5 m increments, to the same modified subfault grid adjacent to each study site as in method 1 (see Figure 7 as an example) to create the *Method 2* slip distribution. Refer to Appendix Table D16 for the resulting slip distribution parameters of the M_w 8.86 *Method 2* earthquake (Figure 18). The simulation based on the

Method 2 slip distribution produced an overall percent match of 50% and underestimated the tsunami at all locations (Table 3; Figure 19).

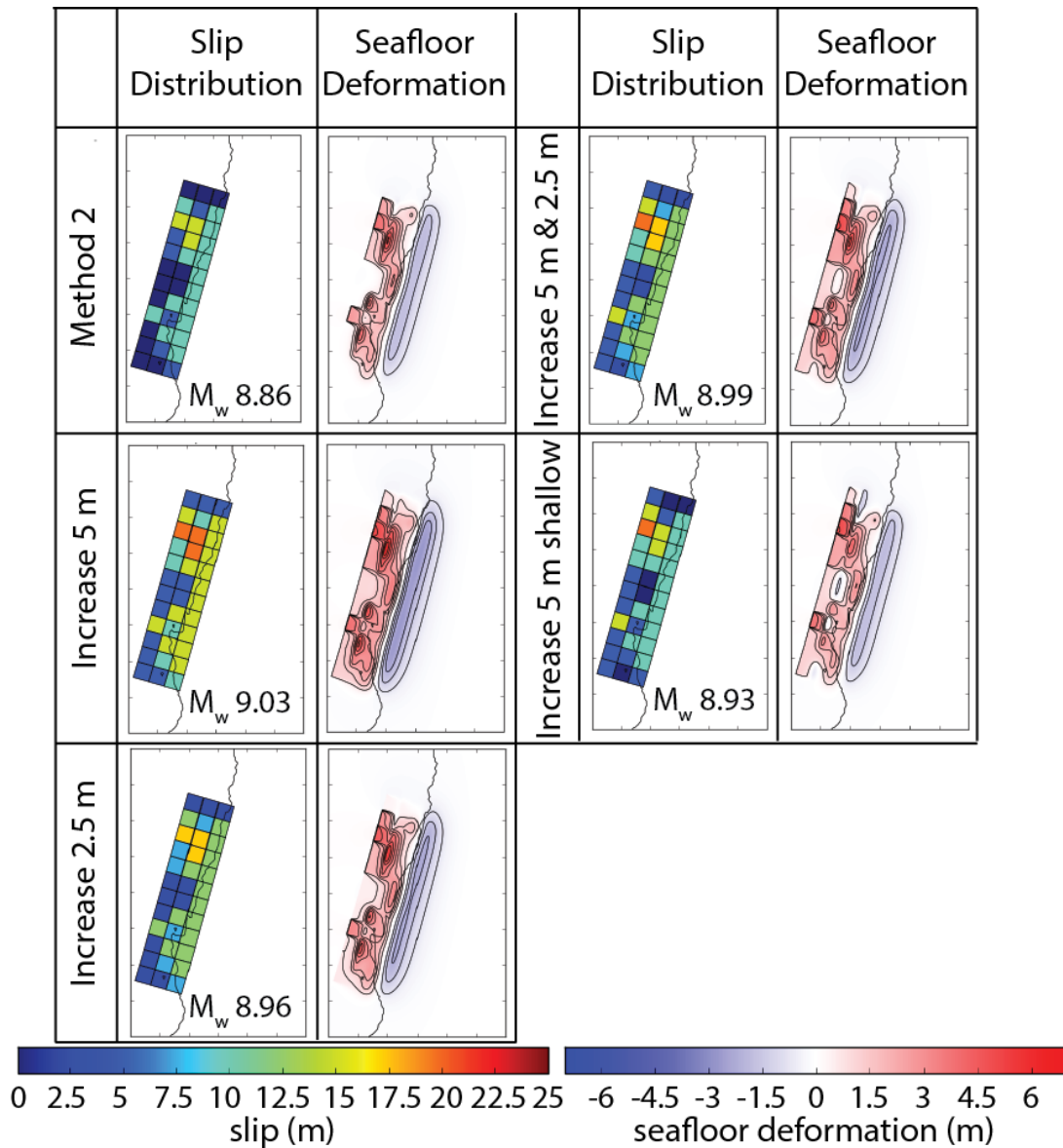


Figure 18: Slip distributions based on Method 2 and resulting seafloor deformation patterns calculated in GeoClaw using the Okada (1985) equations. “Increase” refers to the slip (meters) increased on each subfault from the *Method 2* slip distribution (upper left). At *Increase 5 m shallow*, 5 m of slip was only added to the shallowest subfaults and at *Increase 5 m & 2.5 m*, 5 m of slip was added to the shallowest subfaults and 2.5 m was added to all other subfaults. Each slip distribution and seafloor deformation figure covers -32° to -40° S latitude and -75° to -69° W longitude. The shoreline is drawn in black; land is to the east of the line.

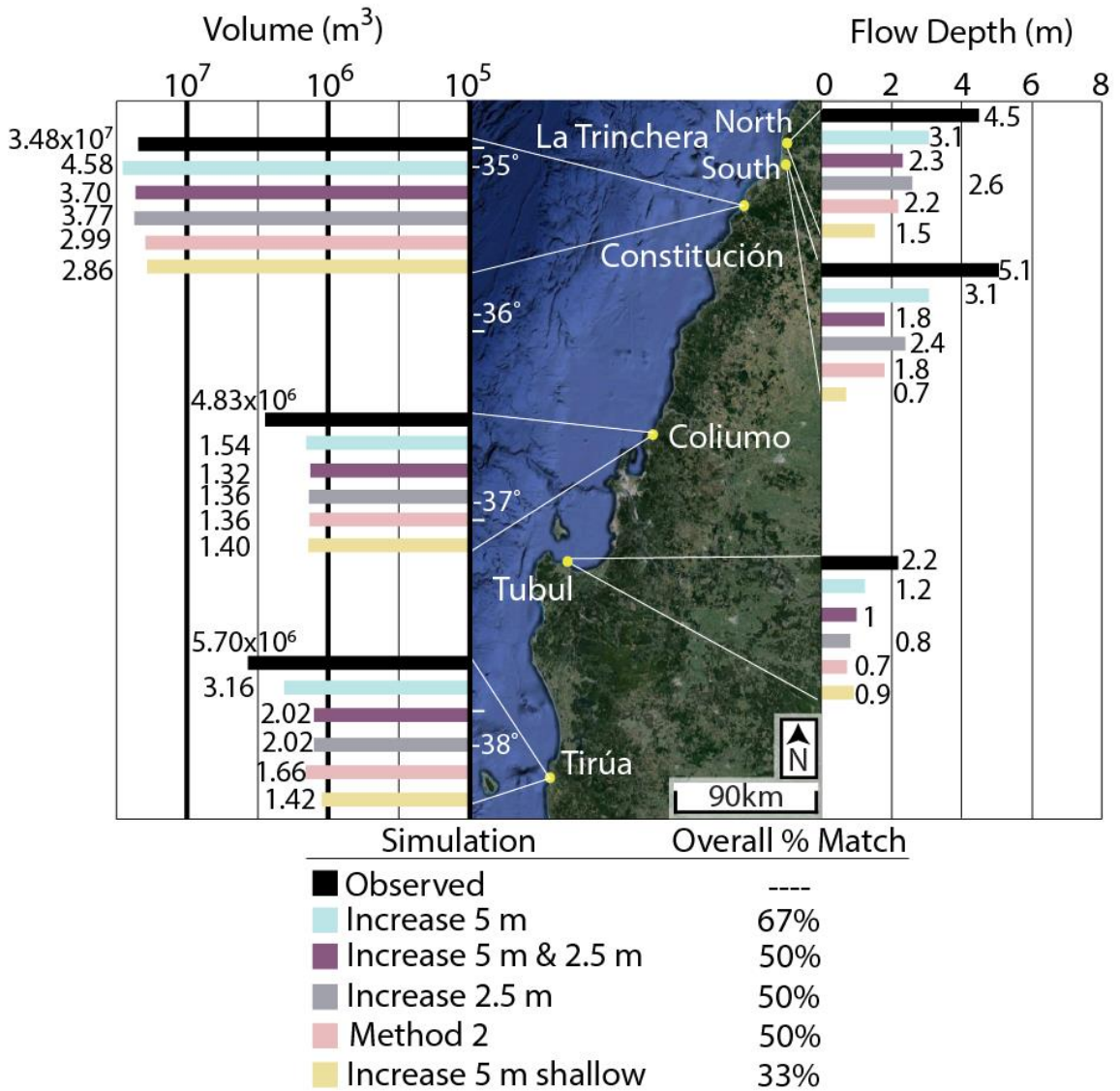


Figure 19: Map of observed water volumes and flow depths compared to GeoClaw simulated volumes and flow depths at each study site. All simulations using Method 2 are included. Image from Google Earth.

To increase the percent match above 50%, I then modified the *Method 2* source model to create four additional distributions by increasing slip 2.5 m and 5 m in every subfault, increasing slip 5 m in the shallow subfaults and 2.5 m everywhere else, and 5 m only to the shallow subfaults. Refer to Appendix Tables D17-D20 for the resulting slip distribution parameters of the *Method 2 Increase 2.5 m*, *Method 2 Increase 5 m*, *Method 2 Increase 5 m & 2.5 m* and *Method 2 Increase 5 m shallow* earthquakes (Figure 18). The best match of 67% was based from *Method 2 Increase 5 m* (Table 3; Figure 19) with an earthquake magnitude of M_w 9.03. At Constitución, all simulations except *Method 2 Increase 5 m shallow* slightly overestimated the tsunami (Figure 19). At all other locations, the tsunami was underestimated. Simulations based on *Method 2 Increase 2.5 m*, *Method 2 Increase 5 m & 2.5 m*, and *Method 2 Increase 5 m shallow* had percent matches of 50%, 50%, and 33%, (Table 3; Figure 19) and magnitudes M_w 8.96, 8.99, and 8.93 respectively.

Discussion of Modifying Pre-Existing Earthquakes to Improve Overall Match with Field Observations: Methods 1 and 2

Because most published slip distribution models produced tsunamis that underestimated the simulated tsunami flow depth, water volume, and inundation, I predicted that increasing the amount of slip in the source models would result in greater seafloor deformation and create an overall larger tsunami. The four models (*Method 1 Increase 5 m*, and *Method 1 Composite*, *Method 2 Increase 5 m*), with the highest overall percent matches of the modified distributions, all at 67%, support this idea because they

resolve more slip than other solutions. However, these had a lower percent match than the 83% from *Yue et al. (2014)*. Also, the resulting magnitudes were too high compared to the well-accepted M_w 8.8 (Moreno et al., 2010) of the earthquake: M_w 9.03 for *Method 1 Increase 5 m* and *Method 2 Increase 5m*, and M_w 9.01 for *Method 1 Composite*. Conversely, when slip was reduced 5 m and 2.5 m at *Method 1 Reduce 5 m* and *Method 1 Reduce 2.5 m*, the percent match is too low, both at 33%. Of the two, *Method 1 Reduce 5 m* had a too low magnitude of M_w 8.58.

Because this method did not improve the match-magnitude ratio, two source models from method 2, *Method 2 Increase 5m & 2.5m* and *Method 2 Increase 5m shallow*, were solutions that increased shallow seafloor deformation without significantly increasing the magnitude. This method creates “tsunami earthquakes”, where slip is focused on the shallowest area closest to the trench, which can create a larger tsunami (Geist and Dmowska, 1999). However, of the simulation results from the “tsunami earthquake”-style source model that I created, *Method 2 Increase 5 m shallow* had a magnitude that is too large (M_w 8.93) and resulted in a lower percent match of 33%. The simulated flow depths and volumes of *Method 2 Increase 5 m & 2.5 m* were consistently, but not significantly, larger than *Method 2 Increase 5 m shallow* at all sites (Figure 19), which is expected. *Method 2 Increase 5 m & 2.5 m* had a percent match of 50%, but an earthquake magnitude that is too large (M_w 8.99). When the two tsunami earthquakes simulations are compared to the original *Method 2* simulation, the results were variable rather than the expected larger simulated tsunami from the tsunami earthquakes (Figure 19). *Method 2 Increase 5 m & 2.5 m* was larger than *Method 2* at all locations except

Coliumo, and at La Trinchera South, where the flow depths were the same (Figure 19). *Method 2 Increase 5m shallow* was only larger than *Method 2* at Coliumo and Tubul. Despite the many tested slip distributions of different earthquake scenarios, simulating both an overall percent match greater than 83% by *Yue et al. (2014)* and an earthquake magnitude close to the well-accepted M_w 8.8 was not possible.

Implications of Modeling

Tsunami-Forming Parameters

Yue et al. (2014) resulted in the highest percent match of 83% among all distributions (Tables 1-3). *Method 1 Increase 5 m*, *Method 1 Composite*, and *Method 2 Increase 5 m* were the next best, all with a percent match of 67% (Tables 1-3). Comparing all four of these distributions, *Yue et al. (2014)* simulated La Trinchera North, La Trinchera South, and Tubul the best (Table 1; Figure 15) and *Method 1 Composite* simulated Constitución, Coliumo, and Tirúa the best (Table 2; Figure 17). Because both *Yue et al. (2014)* and *Method 1 Composite* resulted in the best simulations for half of the sites, these two distributions are the focus for revealing the tsunami-forming parameters. Slip and seafloor deformation of all the *Method 1* (Figure 16) and *Method 2* (Figure 18) earthquakes in the La Trinchera and Constitución sections were identical, while *Yue et al. (2014)* with higher-resolution subfaults differs by having a much narrower band of uplift directly at the trench from -34°S to -35.5°S (Figure 3). Both *Yue et al. (2014)* and *Method 1 Composite* had a concentrated patch of uplift at -35 °S (Figure 3; Figure 16). This patch abruptly ends in *Yue et al. (2014)* and in *Method 1 Composite* the uplift decreased, but

remained as a uniform band along strike until -36.5°S . This narrow band of uplift in *Method 1 Composite* (Figure 16) likely contributed to the slight overestimation of the volume and better match at Constitución. The better match at Coliumo by *Method 1 Composite* was because uplift to the north of Coliumo had a greater effect at increasing the wave at Coliumo than perpendicularly adjacent uplift because this study site was a northward facing bay blocked from the open ocean by cliffs directly to the west. Similarly, this may be the cause of the very high percent difference of +278% at Tubul by *Method 1 Composite*, which was also north facing. *Yue et al. (2014)* had the best match at Tubul, which was likely due to less uplift to the north of that site (Figure 3), despite the area of no slip and uplift directly adjacent to Tubul at -37°S (Figure 16) in the larger simulated tsunami *Method 1 Composite* scenario. At Tirúa, the *Method 1 Composite* distribution resulted in the best percent difference because there was generally more slip and uplift from -37.5°S to -38.5°S (Figure 16) than in *Yue et al. (2014)* (Figure 3). *Yue et al. (2014)* had a narrow concentrated band of slip and uplift at the trench at -38°S , but it significantly decreased landward and deformation was patchier than *Method 1 Composite*.

Large Earthquake Magnitude Yet an Underestimation of the Tsunami

Many of the method 1 and 2 source models I created had a magnitude that was too large compared to the accepted value, they underestimated the observed values of the tsunami, and were therefore not an improvement in overall percent match from the 83% match of *Yue et al (2014)*. My attempt to create “tsunami earthquakes”, *Method 2*

Increase 5m & 2.5m and *Method 2 Increase 5 m shallow*, where slip was focused in the shallowest depths at the trench (Figure 18), also did not produce a better fit (Figure 19) but this is not entirely surprising since no previous studies state this event was a “tsunami earthquake”. As such, I expect that *Yue et al. (2014)* and my method 1 and 2 slip distributions were missing important tsunami-forming features that existed during the 2010 event. For example, splay faulting is a source of seafloor deformation that is difficult to detect in seismic studies and is considered to enhance tsunami generation (Lieser et al., 2014). Evidence of splay faulting from the 2010 rupture has been documented for this event (Melnick et al., 2012; Moreno et al., 2012; Lieser et al., 2014) and may not have been entirely accounted for in the published slip models. However, I also attribute some of my underestimated results to the poor resolution bathymetry and topography or missing or approximated components of tsunami generation and propagation in GeoClaw, such as the instantaneous slip or edge waves, discussed in the *Source of Error* section above. The exact effect each error had on my simulations is difficult to quantify, but when combined, could have a significant effect.

No published studies have previously compared simulated tsunami results to on-land observations of the 2010 Chile earthquake and tsunami. The closest is from Yamazaki and Cheung (2011), who modeled tsunami spectral energy in the shallow ocean and validated their results with flow depth and run up values from Fritz et al. (2011). Yamazaki and Cheung (2011) concluded that their modeled spectral energy corresponds well with the observed flow depth and run up values on land. Yamazaki and Cheung (2011) used a different tsunami modeling code, NEOWAVE, which builds upon

the Okada (1985) equations with a vertical velocity term that allows for modeling based from time histories of seafloor deformation a more accurate near-field wave (Yamazaki and Cheung, 2011). Their finest bathymetry and topography resolution was 30-seconds, which is very coarse, so I attribute their improved results to accurately accounting for rupture/seafloor deformation times and shelf resonance which creates edge waves.

CHAPTER IV

TSUNAMI DEPOSIT RESULTS AND DISCUSSION

La Trinchera Deposit Results

In 2015 at La Trinchera (Figure 2), I dug nine total pits (Figure 8), five of which are located in the same location (within GPS error) as tsunami deposits described nine weeks after the 2010 tsunami by Morton et al. (2011). I recorded deposit latitude and longitude locations, thicknesses, and descriptions at all nine pits (Appendix Table B1). I sampled tsunami deposits (with subsamples based on visible changes in grain-size) at five pits, measured grain size distributions at three pits, and sampled underlying soils at four pits. I estimated tsunami deposit elevations from a topographic transect in Morton et al. (2011) (Figure 9). I also estimated horizontal distances from sea level by measuring the distance inland from an estimated swash zone using Google Earth. The local tsunami inundation limit (Figure 8; Figure 9) was measured by Morton et al. (2011).

Maximum Inland Extent:

Deposit GG547 was the deposition limit measured by Morton et al. (2011) in 2010 (Figure 8). Using Google Earth, I estimated a distance of 612 m \pm 10 m from that point location to the visual swash zone. Pit 48 was the farthest inland deposit I traced in 2015 and was measured using a laser range finder to be 133 m from the top of the road in the field (Figure 9). From Morton et al. (2011)'s topographic transect (Figure 9), I estimated the distance from the swash zone to the top of the road to be 416 \pm 16 m. The exact top of the road location was not specified in the field, thus the width of the road

adds error. As a result, the maximum inland distance of the deposit traced in 2015 was 549 m \pm 16 m. Therefore, the deposit extent changed by -6% to -14 % between 2010 and 2015 (Table 4; negative percent change values here and hereafter indicate the deposit/maximum inland extent was reduced). Morton et al. (2011) marked the local inundation to be 790 m \pm 16 m inland (Figure 8); a difference of 241 m \pm 16m (Table 5).

Table 4: Distances and percent change between the tsunami deposit limit traced in 2010, 2012, or 2013 to the tsunami deposit limit traced in 2015.

Location	Pit ID (2010-2013/2015)	2010-2013 Distance (m)	2015 Distance (m)	Percent Change (%)
La Trinchera South	GG547/48	612 \pm 10	549 \pm 16	-6 to -14
Constitución	BM98/ ---	490 \pm 10	---	---
Coliumo	BM 49/ ---	1696 \pm 100	---	---
Tirúa	13-25/79	284 \pm 10	329 \pm 10	+9 to +24

Table 5: Distances between the 2010 tsunami inundation limit and the 2015 tsunami deposit limit.

Location	Pit ID (2015)	Inundation limit (m)	2015 Distance (m)
La Trinchera South	48	790 \pm 10	549 \pm 16
Tirúa	79	463 \pm 10	329 \pm 10

Grain-size:

At La Trinchera, I compared normalized grain-size distributions of three deposits collected in 2015 (Pit 38, Pit 39, Pit 40) to normalized distributions from deposits collected in 2010 (Pit LAT1, Pit LAT3, Pit LAT4) by Morton et al. (2011) (Figure 20; Figure 21; Figure 22).

La Trinchera

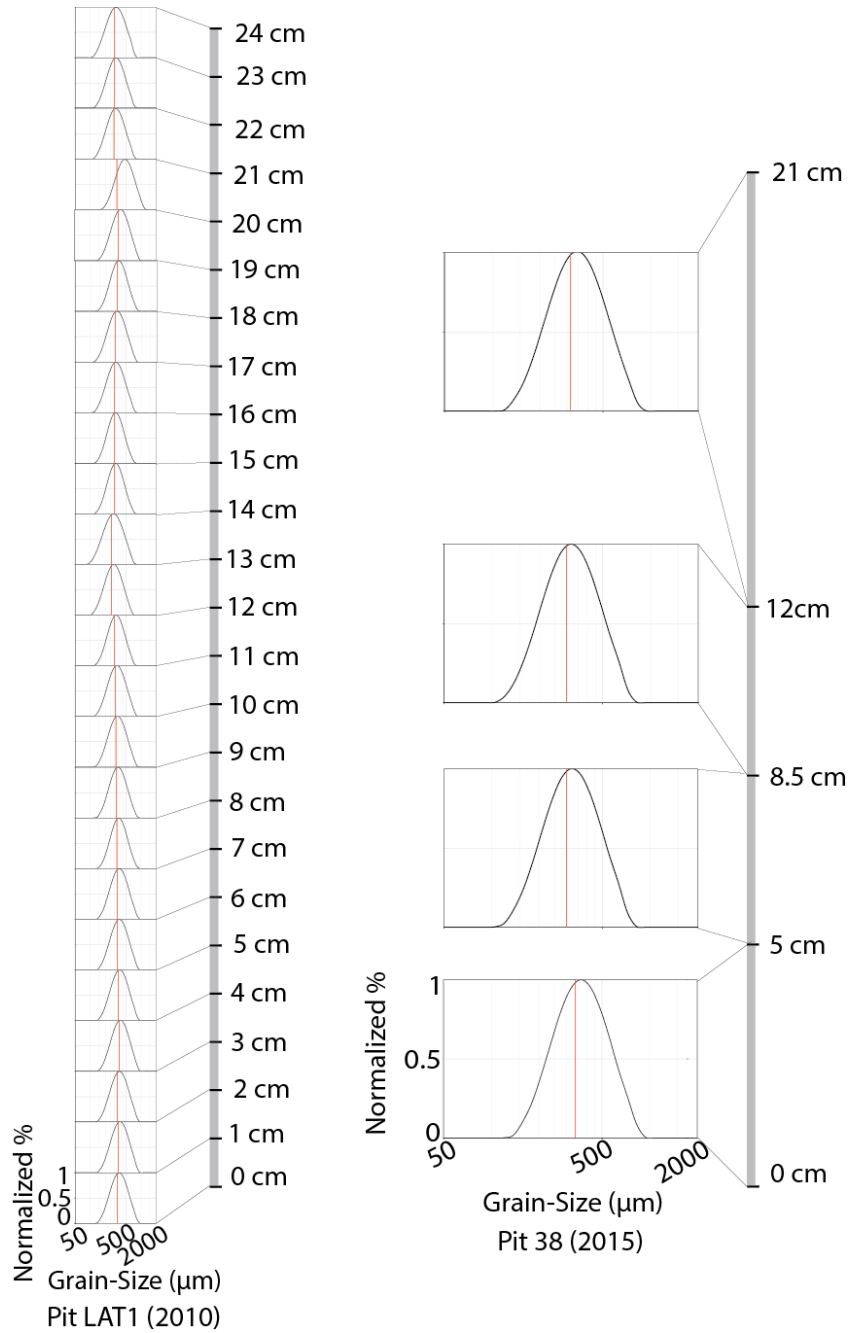


Figure 20: Normalized grain-size distributions drawn to depth scale from La Trinchera South, Pit LAT1 sampled in 2010 by Morton et al. (2011) and Pit 38 sampled in 2015. Red line within each distribution marks the average grain size (50th percentile). The base of the 2010 tsunami deposit (directly above contact with pre-existing soil) is labeled as “0 cm”. The uppermost depth label indicates top of the deposit and total deposit thickness. Centimeter labels denote the boundaries between every subsample. Refer to Figure 8 for pit location.

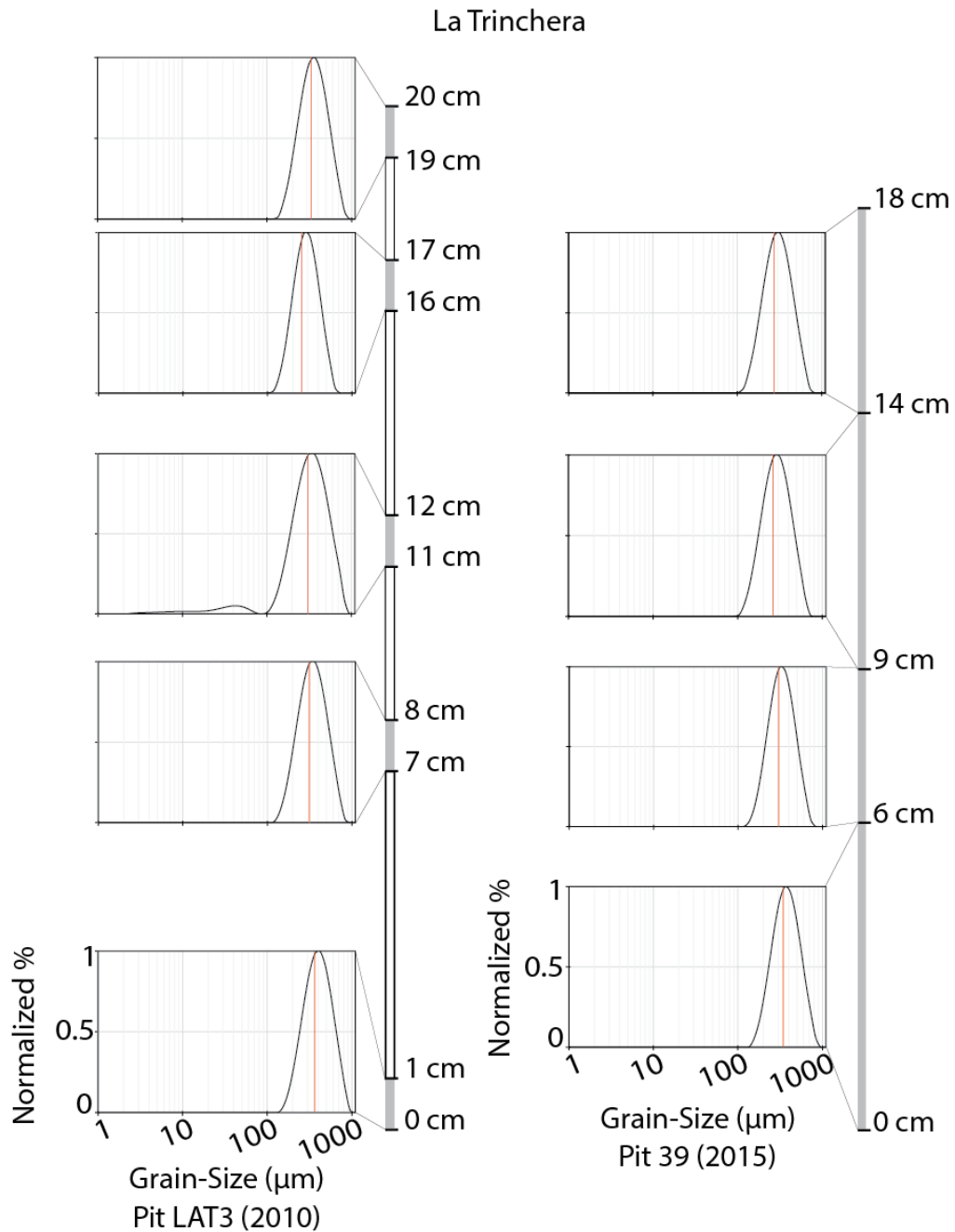


Figure 21: Normalized grain-size distributions drawn to depth scale from La Trincherera South, Pit LAT3 sampled in 2010 by Morton et al. (2011) and Pit 39 sampled in 2015. Red line within each distribution marks the average grain size (50th percentile). The base of the 2010 tsunami deposit (directly above contact with pre-existing soil) is labeled as “0 cm”. The uppermost depth label indicates top of the deposit and total deposit thickness. Centimeter labels denote the boundaries between every subsample. Grey bars indicate the depth range of subsample; white indicates no sample taken. Refer to Figure 8 for pit location.

La Trinchera

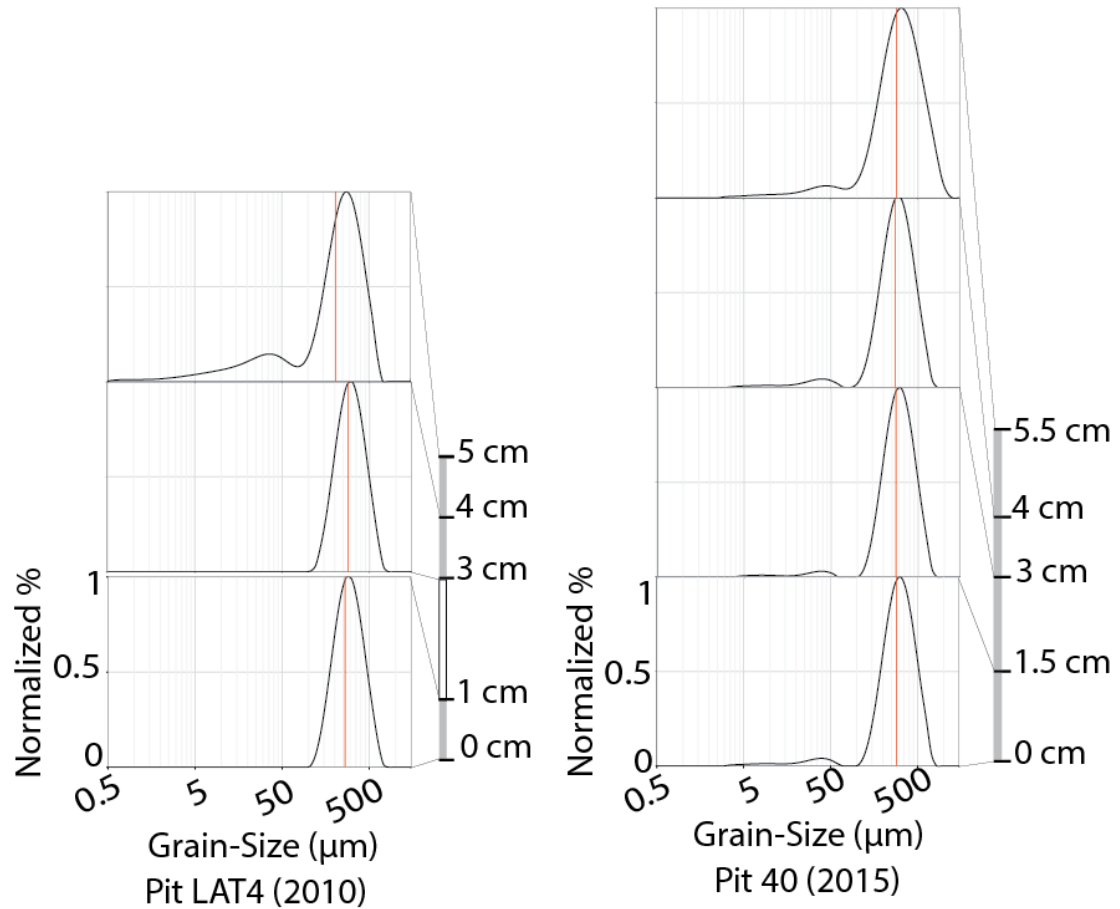


Figure 22: Normalized grain-size distributions drawn to depth scale from La Trinchera South, Pit LAT4 sampled in 2010 by Morton et al. (2011) and Pit 40 sampled in 2015. Red line within each distribution marks the average grain size (50th percentile). The base of the 2010 tsunami deposit (directly above contact with pre-existing soil) is labeled as “0 cm”. The uppermost depth label indicates top of the deposit and total deposit thickness. Centimeter labels denote the boundaries between every subsample. Grey bars indicated the depth range of subsample; white indicates no sample taken. Refer to Figure 8 for pit location.

At Pit LAT1, Morton et al. (2011) subsampled every 1 cm throughout the 24-cm deposit and I collected four larger subsamples of Pit 38 in the 21-cm deposit based on visible changes in grain-size in the field (Figure 20). In all subsamples of Pit LAT1 and

Pit 38 the average grain size was medium sand and with a symmetrical or near symmetrical skew (Appendix Table B2).

At Pit LAT3, Morton et al. (2011) took five 1-cm subsamples at various depths in the 20-cm deposit and I collected four larger subsamples of Pit 39 in the 18-cm deposit (Figure 21). All subsamples of Pit LAT3 and Pit 39 were medium sand with a symmetrical or near symmetrical skew except at Pit LAT3 subsample 11-12 cm, which was negatively skewed (Appendix Table B2). This subsample also contained a finer tail that was not present in other samples at either pit.

At Pit LAT4, Morton et al. (2011) took three 1-cm subsamples in the 5-cm deposit except 1-3 cm, while I collected four subsamples in the 5.5-cm deposit (Figure 22). Pit 40 contained a fine tail throughout and the entire deposit average grain size was medium sand. All subsamples of Pit 40 were negatively skewed except subsample 1.5-3 cm, which was symmetrical (Appendix Table B2). Pit LAT4 0-4 cm average grain size was medium sand with near symmetrical and symmetrical skew (Appendix Table B2). The uppermost subsample Pit LAT4 4-5 cm contained a fine tail and average grain size was fine sand with a strongly negatively skew. Pit LAT 4 was overall normally graded from medium to fine sand (Figure 22).

Thickness:

Morton et al. (2011) measured the 2010 deposit thicknesses but did not provide deposit descriptions. Table 6 summarizes measured thicknesses and the percent change of thicknesses from 2010 to 2015 at the five sites where both they and I measured at the

same location. Overall, percent changes in deposit thickness at La Trincherera range from -12.5 to +10%.

Pit 38 (2015) was 21-cm thick and extended to the surface; it was not covered by vegetation but had roots throughout the upper 9 cm. Pit LAT 1 was 24-cm thick in 2010, therefore the deposit decreased 3 cm (-12.5%) in thickness.

Pit 39 (2015) was 18-cm thick and contained non-decomposed organic material in the upper 1 cm of the deposit and a root zone in the uppermost 3 cm. Pit LAT3 was 20-cm thick in 2010. The deposit decreased 2 cm (-10%) in thickness.

Pit 40 (2015) was 5.5-cm thick with a layer of soil and organic material in the uppermost 1.5 cm of the deposit. The soil layer contained a few sandy patches and thin roots were throughout the deposit. Pit LAT4 (2010) was measured to be 5 cm in thickness. Between 2010 and 2015, the deposit increased 0.5 cm (+10%).

Pit GG545 and Pit GG547 were recorded in 2010 as being <1 cm in thickness and were measurable in 2015 (Pit 42 and Pit 43) but were difficult to distinguish. Pit 43, which was very close to the 2010 deposition limit, was not considered a distinguishable deposit because it would not have been easily recognizable without prior measurements from Morton et al. (2011). However, it is important to note that the sand from the tsunami was interpreted to be still present in 2015 by field researchers. Percent change should not be calculated for pits with thicknesses less than 1 cm because at sub-millimeter resolution, human measurement errors could be a significant part of any calculated change.

Table 6: Thicknesses and percent change of tsunami deposits. Data from 2010 was measured by Morton et al. (2011) at La Trinchera South, Coliumo, and Constitución; from 2012 in unpublished field notes by L. Ely, pers. comm. (2015) at Tubul and Ely et al. (2014) at Tirúa; and from 2013 by Hong et al. (2016) at Quidico compared to my measurements in 2015. Refer to Figure 8, 10, 12, 13, 14, and 24 for pit locations.

Site	Pit ID (2010-2013/2015)	2010-2013 Thickness (cm)	2015 Thickness (cm)	Percent Change (%)
La Trinchera South	LAT1/38	24	21	-12.5
La Trinchera South	LAT3/39	20	18	-10
La Trinchera South	LAT4/40	5	5.5	+10
La Trinchera South	GG545/42	<1	0.9	--
La Trinchera South	GG547/43	<1	0.3	--
Constitución	BM133/51	3	2-4	-33 to +33
Constitución	CON2/384	76	62±2	-15 to -21
Coliumo	BM53/385	6	0	-100
Coliumo	BM29/52	2	2-3	0 to +50
Coliumo	COL1/389	2	11	+450
Coliumo	GG452/84	12	12-14	0 to +17
Coliumo	COL3/85	12	5.5-8.5	-29 to -54
Coliumo	COL7/390	12	9	-25
Tubul	T1/83	2-3	6	+100 to +200
Quidico	Q16/68	3	6-13	+100 to +333
Quidico	Q15/67	0.1	0	-100
Quidico	Q6/61	2	5-6	+150 to +200
Quidico	Q8/59	5	2-3.5	-30 to -60
Quidico	Q9/58	5	9	+80
Tirúa	13-1/69	12	10	-17
Tirúa	13-3/70	25	27-30	+8 to +20
Tirúa	13-7/71	12	11	-8
Tirúa	13-11/73	6	4.5-6.5	-25 to +8
Tirúa	13-16/74	12	6.5	-46
Tirúa	13-19/75	1	1	0
Tirúa	13-21/76	9	6.5	-28

La Trincheras Deposit Discussion

Grain Size

Overall, differences in grain size are present in two of the three locations: Pit LAT3/Pit 39 and Pit LAT4/Pit 40. The third location, Pit LAT1/ Pit 38, did not show change- all grain-size distributions in 2010 and 2015 were bell-shaped curves with no fine/coarse tails and average grain size of medium sand.

Pit LAT3/Pit 39 remained relatively similar between 2010 and 2015 except subsample LAT3 11-12 cm from 2010 (Figure 21). While this subsample contains a fine-grained component that was not present in any other subsamples of Pit LAT3 and Pit 39, I interpret it and the corresponding lack of a similar sand in 2015 as insignificant. Pit LAT3 11-12 cm was negatively skewed indicating the coarser fraction was still more prominent and all samples from both pits were dominantly medium sand. The 2015 overlapping subsample of Pit 39 9-14 cm is not comparable because the 2010 LAT3 11-12 cm sample only represents a thin interval that could have easily been sampled in a finer grained sand pocket in 2010.

In 2010, the samples collected from Pit LAT4 displayed normal grading, which was no longer present in 2015 Pit 40 (Figure 22). Based on previous studies of tsunami deposit taphonomy, I interpret the loss of grading as likely caused by bioturbation in the form of sediment mixing from the fine roots throughout the deposit. Spiske et al. (2013) defines bioturbation as causing a loss of internal structures from sediment mixing, which negatively affects deposit preservation. Szczuciński (2012) and Yawsangratt et al. (2012) also found this when the 2004 Indian Ocean tsunami deposits were resurveyed about five

years after the event. Pit 40 displayed a fine-grained portion throughout the entire deposit and that was only measured in the uppermost subsample 4-5 cm in 2010 Pit LAT4.

However, at Pit 40, all subsamples were negatively skewed (except the interval 1.5-3 cm which was symmetrical). Because Pit 40 total thickness only increased 0.5 cm, I consider it less likely that the fine tail present in all 5.5 cm in 2015 was solely from soil formation adding finer-grained material, and more likely that it was due to a combination of soil-forming processes and bioturbation which also erased the normal grading, because the lowest part of the 5.5-cm deposit was affected equally as the upper.

Preservation Potential

La Trinchera can be described as an open beach to the west with low sand ridges seaward and a gently sloping coastal plain that increases elevation landward, to the east. The two areas are separated by a road (Figure 8; Figure 9). The inundation limit and deposition limit are both to the east, on the sloping coastal plain.

In La Trinchera, the preservation of the tsunami deposits between 2010 and 2015 was moderate, since deposits were easily recognizable and only changed in thickness by an insignificant amount, but the internal structures were altered (see section above). The percent change in deposit inland extent between 2010 and 2015 is low, with only a decrease in the inland limit between -6 to -14%. Additionally, tsunami deposit thicknesses decreased only -10 to -12.5% from 2010 to 2015 on the western (seaward) side of the road (Pit 38 and Pit 39) and increased +10% on the eastern (landward) side (Pit 40). I interpret the change as insignificant because it is likely due to a local variation

in the deposit, which is around a few centimeters in thickness. This local variation could be due to the local undulation of the underlying surface, and is a similar thickness variation to what was observed by Goto et al. (2012) when they resurveyed the 2004 Indian Ocean tsunami deposits four years later at pits located less than 10 m apart in an area that was flat, with minor undulations of up to several tens of centimeters.

In evaluating the total area, the potential for preservation in the future is higher on the eastern (inland) side than the western (seaward) side of the road in the study area. Deposits on the eastern side of the road are more likely to be preserved because they are farther inland from the open beach/coast and the elevated road can block the surface from strong on-shore winds, decreasing the likelihood of erosion. This is similar to what is seen when a tsunami deposit is behind a back dune, as described in a review of tsunami deposits on the arid coasts of Peru by Spiske et al. (2013). Also, the eastern area is less likely to be frequented by humans or wildlife since it is a roadside location behind a fence that is difficult to cross while the western area contains a crude parking lot for visitors to the beach.

Deposits in La Trinchera also showed signs of overlying soil development and the addition of organic material (Pit 39 and Pit 40), which can help stabilize and protect the deposit from erosion of the uppermost section (see also Szczuciński, 2012). However, the organic material that can protect the deposit from erosion can also contribute to the loss of internal structures from root bioturbation, such as seen with Pit LAT4/ Pit 40. Szczuciński (2012) also observed this with the 2004 Indian Ocean deposits, where the fast recovery of vegetation after 4.5 years protected the deposits from heavy rains and

erosion; however, the root systems caused mixing of sediment and altered the sedimentary structures.

Constitución Deposit Results

In 2015 at Constitución (Figure 2), I dug two total pits (Figure 10; Figure 11) that were in the same location (within GPS error) as tsunami deposits described nine weeks after the tsunami by Morton et al. (2011). I recorded deposit latitude/longitude locations, thicknesses, and descriptions at the two pits (Appendix Table B1). I sampled tsunami deposits at the two pits (with subsamples based on visible changes in grain size) but did not sample underlying soil. Out of the two 2010/2015 deposit sets, I measured grain-size distributions at one (Pit CON2/Pit 384) because the 2010 Pit BR133 sample was not available. Because I did not measure tsunami deposit elevations and horizontal distances in the field, I estimated elevations from a topographic transect in Morton et al. (2011) (Figure 11). I also estimated horizontal distances by measuring inland from an estimated swash zone using Google Earth because they did not label the 2010 deposits on the topographic transect, and the accompanying site map was not drawn to scale.

Maximum Inland Extent:

The tsunami deposition limit (Pit BM98) was traced by Morton et al. (2011) in 2010 (Figure 10; Figure 11). Using Google Earth, I measured the inland distance of Pit BM98 to be 490 m \pm 10 m. In 2015, a fence surrounding a commercial tree plantation (Figure 10; Figure 11) could not be crossed to reach other tsunami deposits that were

farther inland, including Pit BM98. Because tsunami deposits beyond this fence were not investigated, I could not compare the 2010 and 2015 deposition limits.

Grain-size:

At Constitución, I compared normalized grain-size distributions at Pit 384 (2015) to Pit CON2 (2010) collected by Morton et al. (2011) (Figure 23). In the 76-cm thick CON2 deposit, Morton et al. (2011) took 1-cm subsamples at 5-cm increments, totaling 8 subsamples. I collected 5 subsamples throughout the 62-cm Pit 384 deposit based on visible changes in grain size in the field. Pit CON 2 was normally graded with an average grain size of coarse sand in the lower majority of the deposit (subsample 5-6 cm to subsample 55-56 cm) and medium sand in the remaining upper portion. All subsamples skew were near symmetrical or symmetrical (Appendix Table B2). Pit 384 was slightly normally graded, changing from coarse sand in lower subsamples (6-45 cm) to medium sand in the upper subsamples (45-62 cm), although the lowermost subsample (0-6 cm) was also medium sand (Figure 23; Appendix Table B2). All subsamples skew were near symmetrical (Appendix Table B2).

Thickness:

At Constitución, Morton et al. (2011) measured the 2010 deposit thicknesses but did not provide deposit descriptions. Table 6 summarizes the measured thicknesses and percent change from 2010 to 2015. Overall, changes in deposit thickness at this location ranged from -33 to +33%.

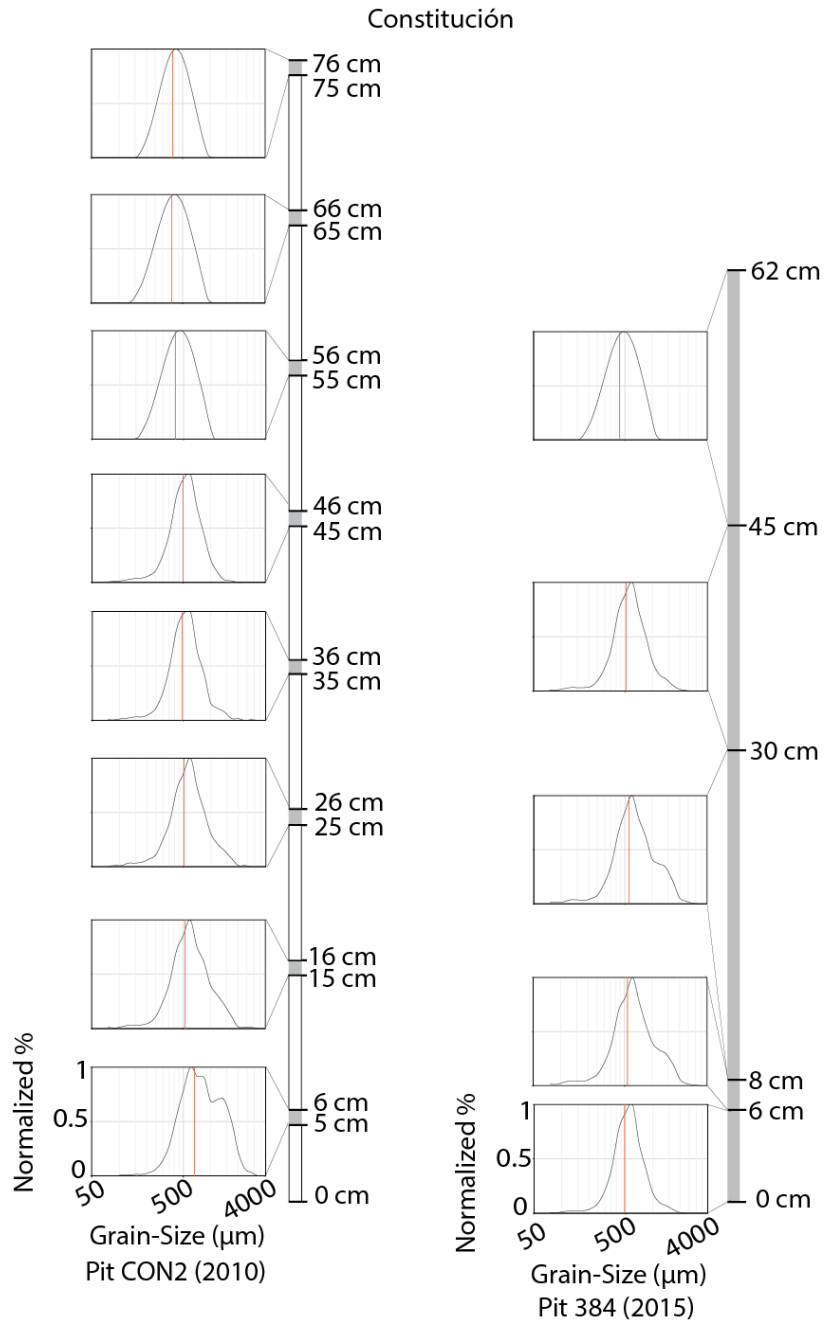


Figure 23: Normalized grain-size distributions drawn to depth scale from Constitución, Pit CON2 sampled in 2010 by Morton et al. (2011) and Pit 384 sampled in 2015. Red line within each distribution marks the average grain size (50th percentile). The base of the 2010 tsunami deposit (directly above contact with pre-existing soil) is labeled as “0 cm”. The uppermost depth label indicates top of the deposit and total deposit thickness. Centimeter labels denote the boundaries between every subsample; grey bars indicated the depth range of subsample; white indicates no sample taken. Refer to Figure 10 for pit location.

The Pit 51 (2015) deposit was not covered with soil or an organic mat and was between 2 and 4 cm thick. Pit BM133 measured in 2010 was 3-cm thick (Table 6), which resulted in a possible decrease or increase in deposit thickness of 1 cm (a -33 to +33% change).

Pit 384 (2015) was covered by succulent-like vegetation with thick roots that penetrated into the top of the deposit. Morton et al. (2011) noted cobbles and complex sedimentary structures in some deposits at this location, but I observed only slight parallel laminations in Pit 384. I measured Pit 384 to be 62 cm with a 2-cm error (due to the loosely consolidated upper surface which may have removed or added sediment while digging the pit), which is a thickness decrease of 14 cm to 16 cm from the Pit CON2 thickness of 76 cm (a -15 to -21% change).

Constitución Deposit Discussion

Grain-Size

Overall, the tsunami deposit at the one comparable location remained relatively similar between 2010 (Pit CON2) and 2015 (Pit 384), considering the significant thickness decrease of 14 cm and different sampling methods. Both deposits displayed normal grading with near symmetrical to symmetrical skew and no fine or coarse tails. The only noticeable change was the lowest interval 0-6 cm of Pit 384, which was finer in 2015 suggesting that coarse sediments were “lost” over time. Such a change could be caused by an error in sampling where underlying surface is also collected in the sample.

Preservation Potential

The geomorphic environment that contained the tsunami deposits I compared at Constitución are on a narrow open beach. The tsunami deposition limit beyond the fence is where low sand ridges were located in 2010, but was later a tree plantation in 2015. The inundation limit extends beyond the sand ridges until the high dune ridge (Figure 10; Figure 11). Currently in Constitución, I interpret the preservation potential of the tsunami deposits over time as moderate, but an argument could also be made for good preservation in isolated locations. The deposits I investigated in excavation were easily recognizable and some internal structures were still preserved, however, the thickness loss at Pit CON2 is still a large volume of sediment despite a lower percent change compared to deposits at some other study sites.

The significant decrease in thickness of 14 cm at Pit CON2/Pit 384 is likely due to wind processes acting on the sandy open beach environment where the opportunity for soil or organic accumulation to protect the deposit from erosion was low (see also Spiske et al., 2013). Tsunami run up measured by post-tsunami surveys was highest at this location (Annunziato et al., 2010; Fritz et al., 2011), significantly eroding the planted forest of eucalyptus and pine trees in the first 300 m inland from the shoreline, and depositing a thick sand sheet beyond this erosional zone (Morton et al., 2011). This left an exposed sandy surface where eolian ripples were already reworking the surface in April 2010 (Morton et al., 2011). The area was starting to recover at the beginning of 2015 with patches of succulent vegetation, although the deposit surface was likely

exposed for a longer period of time than my other sites with fast recolonization, which could have enabled enhanced erosion and redeposition of deposit material.

An argument can also be made that the preservation potential at Constitución is good, because the deposits were so thick, ultimately erosion may not be able to remove the entire deposit and it could remain a recognizable feature (see also Spiske et al., 2013). If the parallel laminations and normal grading at Pit 384 (2015) are maintained in the long term, it can be distinguished from the underlying beach sand, which might lack these features.

However, considering the Constitución environment, it is unlikely the tsunami deposit will be well preserved in the future across its entire extent. This location is an easily accessible open beach, and the growth of the neighboring tree plantation, as seen in 2015, may ultimately result in destroyed deposits due to human activity in the long term. Such was the case for tracing the maximum extent at this location—the farthest inland deposits were located behind a fence, and I expect much of the deposit has been plowed and mixed with soil by the tree plantation.

Coliumo Deposit Results

In 2015 at Coliumo (Figure 2), I dug 11 total pits (Figure 12), six of which are located in the same location (within GPS error) as tsunami deposits described eight weeks after the 2010 tsunami by Morton et al. (2011). Additional information on the five pits can be found in Appendix Table B1. I recorded deposit latitude/longitude locations, thicknesses, and descriptions at all 11 pits (Appendix Table B1). I sampled tsunami

deposits (with subsamples based on visible changes in grain-size) at seven pits, and sampled underlying soils at two pits. In 2015, elevations of tsunami deposits were measured with a surveying level and stadia rod relative to mean sea level, which was measured using a portable tide gauge. Horizontal distances from the mouth of the river to the tsunami deposit were estimated using the Google Earth ruler tool.

Maximum Inland Extent:

The tsunami deposition limit (Pit BM29) was traced by Morton et al. (2011) in 2010 (Figure 12). Using Google Earth, the distance (drawn as a straight line) from the mouth of the river to the point of Pit BM49 was $1,696 \text{ m} \pm 100 \text{ m}$ inland. While this may underestimate the distance the tsunami wave traveled through the curved valley, it makes inland distance comparisons to any other tsunami deposits or post-tsunami survey data within Coliumo more consistent. In 2015, when re-visiting locations described by Morton et al. (2011), Pit Col7/ Pit 390 was the farthest inland deposit that I could revisit (Figure 12). While it is possible that deposits exist farther inland, they would be difficult to reach and could be blocked by fences and overly-friendly horses. For this reason, a maximum inland extent comparison between 2010 and 2015 cannot be made.

Grainsize:

Grain-size distributions were not measured for tsunami deposits I collected in 2015 because tsunami deposit samples collected in 2010 were not available.

Thickness:

At Coliumo, Morton et al. (2011) measured the 2010 deposit thicknesses but did not provide deposit descriptions. Pit BM53, Pit BM29, and Pit COL7 were all noted by Morton et al. (2011) to be variable in thickness, but the variability was not specified. I used the single number they provided when calculating the percent change, but it must be noted there is error that is not entirely accounted for. Table 6 summarizes the measured thicknesses and percent change from 2010 to 2015. Overall, percent change between 2010 and 2015 is large, from -100% to +450%.

The location of the 6-cm thick deposit Pit BM53 (2010) was soil in 2015. As a result, the deposit at Pit 385 (2015) had a thickness of 0 cm, which was a -100% change (Table 6).

Pit 52 (2015) did not have a noticeable soil or organic layer above the tsunami deposit. I measured Pit 52 to be variable in thickness from 2-3 cm and Pit BM29 (2010) was 2 cm, indicating the deposit either remained the same or increased in thickness by 1 cm. This is a range of percent changes between 0 to +50%.

Pit 389 (2015) had a 2-cm organic mat above the 11-cm thick tsunami sand. The corresponding Pit COL1 (2010) was originally 2 cm, meaning there was an additional 9 cm of material that was added, assuming the organic mat I measured was not present in 2010. This results in a significant percent change of +450%.

Pit 84 (2015) was slightly downslope of Pit GG452 because high vegetation covered the exact location. Pit 84 developed a 1.5-cm organic mat above the sand and parallel lamination was present despite the thin roots that extended throughout the

deposit. I measured Pit 84 to be variable in thickness between 12 and 14 cm and Pit GG452 was 12 cm in 2010, which means the deposit either remained the same thickness or increased 2 cm, a change between 0 and +17%.

Pit 85 (2015) was also not in the exact location as Pit COL3 (2010) due to the exact deposit location being altered by a newly built fence. Pit 85 had an undulatory contact with underlying soil and the uppermost surface was also uneven and included a surficial 1-cm thick organic layer. I measured Pit 85 to be variable in thickness between 5.5 cm and 8.5 cm. Pit COL3 was 12 cm, indicating a decrease in thickness between 3.5-6.5 cm (a -29% to -54% change).

Pit 390 (2015) included a 1.5-cm thick organics detritus and mud layer above the tsunami sand and an uneven contact with the underlying soil that appears to be a hoof print (likely from the many local grazing cows). I measured the total thickness of Pit 390 to be 9 cm and Pit COL7 (2010) was 12 cm, a decrease of 3 cm (-25%).

Coliumo Deposit Discussion

Preservation Potential

The geomorphic environment of Coliumo is a U-shaped river valley, with a wide floodplain-like valley middle bounded by sloping edges (Figure 12). Currently in Coliumo, the preservation potential is moderate as the deposits displayed evidence of alteration since 2010. The deposits that experienced the most alteration (Pit BM53, Pit BM29, and Pit COL1) are all located in relatively close proximity to the shoreline and the road and are in an easily accessible agricultural area. Because these deposits are not

protected by a by a taller landform such as dunes or a high road like at La Trinchera, the deposits are more likely to experience greater change either from windblown erosion when the thickness decreases, and/or human and animal disturbance since it is an easily accessible area as seen with Pit BM53/ Pit 385 which was completely removed in 2015. Significant deposit thickness increases also occurred, such as with Pit COL1/ Pit 389, which increased +450%. This could be from human disturbance, specifically plowing, or animal disturbance, which both have been shown to rework the deposit internal structure (see also Szczuciński, 2012). I believe the reworking may have caused an error in interpretation of the contact with underlying lower soil, due to the significant increase of 9 cm. Pit BM29/ Pit 52 percent change ranged between 0 and +50%. While +50% is a large percent change, the absolute value was only 1 cm, which could be within the range of thickness measured by Morton et al. (2011) in 2010.

Deposit thickness changes indicate that the margins of a valley are better sites of preservation in valleys where humans are modifying the landscape, even if minor disturbances such as animal grazing still occur. The deposits with greater total thickness (Pit GG452, Pit COL3, Pit COL7) in 2010 had lower percent changes in thickness when re-measured in 2015, but still displayed other changes such as overlying organic material and roots. These deposits were all located on the eastern side of the valley margin, where the ground begins to slope up. This contrasts with the deposits in the center of the valley, Pit BM53, Pit BM29, and Pit COL1, which all had a smaller total thickness in 2010 and had greater percent changes in 2015. The deposits in the center of the valley are more susceptible to change because they are much thinner. Morton et al. (2011) noted that

while the deposit thicknesses were variable in Coliumo, the thickest deposits (~10-20 cm) were found where vegetation was high and dense, as well as along the sloping valley margins where flow depths decreased and flow decelerated. My observations support this.

Tubul Deposit Results

In 2015 at Tubul (Figure 2), I dug one pit (Figure 13) which was located near the location (within GPS error) of an excavation into a 2010 tsunami deposit described in unpublished field notes from 2012 by L. Ely, pers. comm. (2015), one year and 11 months after the tsunami. At that site, I recorded latitude/longitude location and the deposit thickness and a description. I collected subsamples based on visible changes in grain-size but did not collect a sample of underlying soil (Appendix Table B1).

Maximum Inland Extent:

The maximum inland extent of tsunami deposits at Tubul was not traced in 2012 or 2015. Using Google Earth, I estimated the distance of Pit T1/ Pit 83 was 338 m \pm 10 m from an estimated shoreline, but this site was not located at the maximum inland extent of the deposit (Figure 13).

Grainsize:

Tsunami deposit grain-size distributions were not measured because samples of the tsunami deposit described in 2012 was not available.

Thickness:

Pit 83 (2015) was a few meters next to Pit T1 (2010) because the original location was heavily trampled by cows. The deposit in Pit 83 was a total of 6-cm thick with thin roots throughout and a 1.5 to 2.5-cm thick layer of grass detritus in the uppermost section. The deposit visually appeared to be a grey very fine silt with little sand, above a sharp boundary with the brown underlying soil. Pit T1 was originally described to be a fine sand that overlaid a sandy silt soil and a variable in thickness of 2-3 cm. This is an increase in thickness between 3 and 4 cm and a range of percent changes between +100 to +200%.

Tubul Deposit Discussion

Preservation Potential

The geomorphic setting of Tubul is both a coastal plain (where the resurveyed tsunami deposit is located) and on the larger scale, a river floodplain where the maximum inundation limit is marked (Figure 13). The preservation of the deposit in Tubul is challenging with only one excavation to compare, however based on this site, it is currently moderate. The tsunami deposit was still detectable in 2015, but, as evidenced by the original site of Pit T1 being heavily trampled by cows, anthropogenic-related modification is ongoing. The effect of heavy trampling is deposit reworking, decreasing the potential for future preservation. Visually the deposit contained more silt in 2015, which, like in La Trinchera and Coliumo above, could have been due to bioturbation and sediment mixing from the roots throughout the deposit (see also Szczuciński, 2012;

Yawsangratt et al., 2012; Spiske et al., 2013). The thick organic mat is favorable for preservation and can protect from erosion (see also Szczuciński, 2012).

Quidico Deposit Results

In 2015 at Quidico (Figure 2), I dug five pits located in the same location (within GPS error) as tsunami deposits described in 2013 by Hong et al. (2016), two years and 11 months after the tsunami (Figure 24). I recorded excavation latitude/longitude locations and deposit thicknesses and descriptions at all nine pits (Appendix Table B1). I sampled tsunami deposits (with subsamples based on visible changes in grain size) at seven pits, sampled one underlying soil, and measured grain-size distributions at one pit. Tsunami deposit elevations relative to sea level were not measured in 2013 or 2015. Horizontal distances between the tsunami deposits were measured using a laser range finder.

Maximum inland extent

At Quidico, I traced the maximum inland extent of tsunami deposits in 2015 on two transects (not the entire river valley), starting at the riverbank edge (Figure 24). Pit 63 (2015) was one of the farthest inland visible deposits I traced, 30 m from Pit 61 (2015). Pit 66 (2015) was 12.5 m inland from Pit Q9 (2013). The maximum inland extent of tsunami deposits was not traced by Hong et al. (2016) in 2013 at these two transect locations, so a percent change could not be determined.



Figure 24: Quidico location map. See Figure 2 for location. Tsunami deposit pit names are labeled as “2013 name, 2015 name”; descriptions can be found in Appendix Table B1. Pits revisited from Hong et al. (2016) are marked by pink circles and additional pits described are marked by yellow circles. Tsunami deposits that define the local deposition limits are marked by purple rectangles with pit name in parenthesis. Image from Google Earth.

Grain size

At Quidico, I compared normalized grain-size distributions at one location: Pit 58 collected in 2015 and Pit Q9 collected by Hong et al. (2016) in 2013 (Figure 25). At Pit Q9, Hong et al. (2016) collected two 1-cm subsamples for the uppermost section of the

5-cm deposit and I took two subsamples of the entire 9-cm deposit. At Pit Q9 and Pit 58, the average grain size was fine sand throughout and all subsamples' skew was near symmetrical (Appendix B2). Pit 58 grain-size distributions also contained a fine tail (Figure 25).

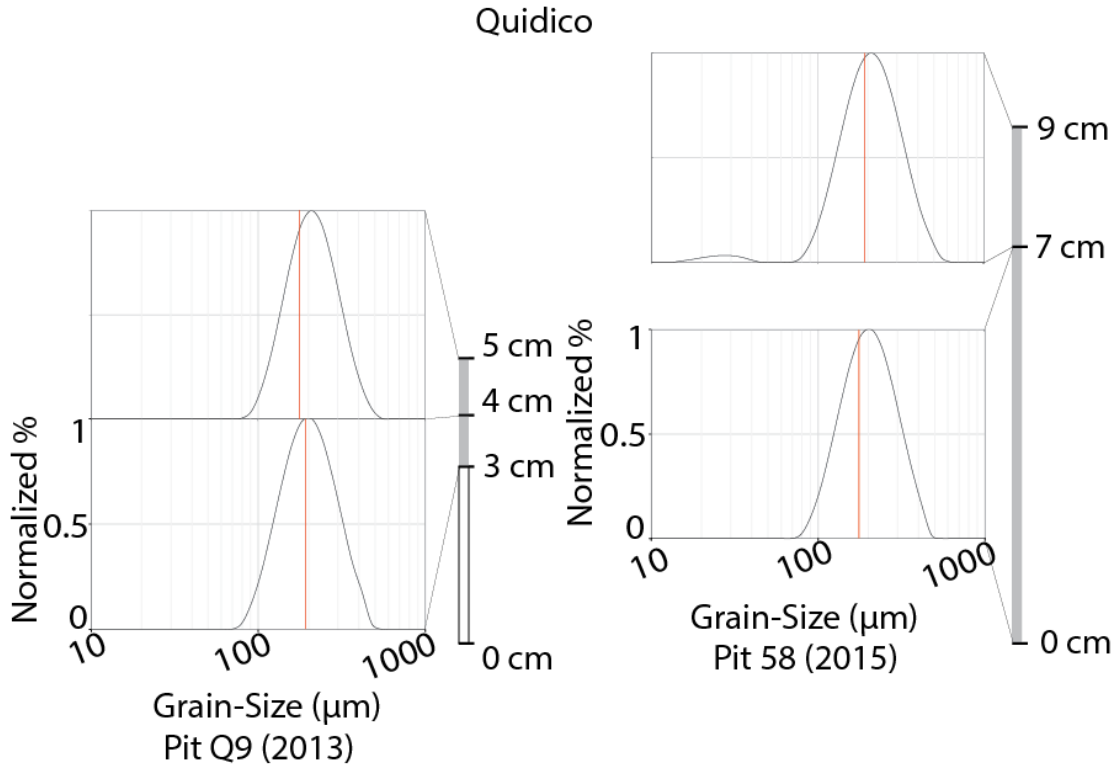


Figure 25: Normalized grain-size distributions drawn to depth scale from Quidico, Pit Q9 sampled in 2013 by Hong et al. (2016) and Pit 58 sampled in 2015. Red line within each distribution marks the average grain size (50th percentile). The base of the 2010 tsunami deposit (directly above contact with pre-existing soil) is labeled as “0 cm”. The uppermost depth label indicates top of the deposit and total deposit thickness. Centimeter labels denote the boundaries between every subsample. Grey bars indicated the depth range of subsample; white indicates no sample taken. Refer to Figure 24 for pit location.

Thickness

At Quidico, Hong et al. (2016) measured 2010 deposit thicknesses, and descriptions from 2013 were available for most deposits. Table 6 summarizes the

measured thicknesses and percent change from 2013 to 2015. At this location, percent changes range between -100% and +333%.

Pit Q16 (2013) was 3-cm thick and was described to be loosely-consolidated grey sand with large roots from reeds in the uppermost 1 cm. The lower 2 cm was mixed with lenses of loose and compact silty sand or sand, but still had a sharp contact with the underlying soil. Pit 68 (2015) was covered with a dry organic mat about 2-cm thick. The tsunami sand was loosely consolidated and visibly appeared to be mixed with the underlying soil below. This made the contact with the underlying soil difficult to distinguish and resulted in a significant variation in thickness of 6-13 cm. As such, the thickness of the deposit at this site could have increased between 3 and 10 cm (+100% to +333%).

Pit Q15 (2013) was a surface dusting of the tsunami sand 0.1-cm thick, and was not visible in 2015. Percent change was therefore -100%.

Pit 61 (2015) sand was loosely consolidated and had thick and thin roots throughout the deposit that began to extend to the underlying soil and create small sand pockets in the soil, but the contact was still well defined. I measured Pit 61 to be variable in thickness between 5 and 6 cm and Pit Q6 (2013) was 2-cm thick, resulting in a thickness increase of 3-4 cm (+150% to +200%).

Above Pit 59 (2015) was a thin green mat-like ground cover vegetation. A tan colored visibly finer layer in the uppermost 2.5 cm of the deposit as well as roots within the uppermost 2 cm was also present. The lower portion of Pit 59 was a coarser grey and white sand that visually appeared to mix with the underlying soil. Pit Q8 (2013) was only

described as grey and white colored sand and did not contain the features such as overlying vegetation, a tan-colored finer layer, or roots that were seen in Pit 59. I measured Pit 59 to be variable in thickness between 2 and 3.5 cm and Pit Q8 was 5-cm thick, resulting in a thickness decrease between 1.5 and 3 cm (-30% to -60%; Table 6).

Pit Q9 (2013) was visible at the riverbank, but my descriptions of Pit 58 (2015) were from an excavation 2-m inland of the riverbank. Pit 58 contained many thin roots throughout the uppermost 7 cm, and the remaining lower 2 cm were more loosely consolidated and lacked roots. A thin detritus grass layer mixed with green grass lay above the deposit, but was not thick enough to measure. The boundary with the underlying soil was sharp, but the soil visually appeared to be mixing in with the tsunami deposit. Pit Q9 was described in 2013 to be 5 cm thick and a relatively clean sand without the features seen in Pit 58 such as roots and overlying detritus. Since Pit 58 was 9 cm thick, this was an increase of 4 cm (+80%; Table 6).

Quidico Deposit Discussion

Grain-Size

Pit Q9 (2013) and Pit 58 (2015) grain-size distributions remained relatively similar (Figure 25), except that Pit 58's uppermost subsample of 7-9 cm gained finer sediments by 2015. This addition is slight because the entirety of the deposit was still symmetrically skewed, indicating neither fine nor coarse material dominated. The finer tail of Pit 58 subsample 7-9 cm could be due to the thin detritus layer, which marks the

beginning of soil development. The detritus layer was friable, and could have easily been collected during sampling along with the sand deposit.

Preservation Potential

The geomorphic setting of Quidico is a flat and low lying river floodplain, and my compared tsunami deposits were mostly located within an abandoned meander channel. A few cows were seen grazing the general floodplain area, but their presence did not appear to alter the deposits. Currently in Quidico, the preservation potential is moderate because the deposits were still recognizable, but showed changes between 2013 and 2015. Internal structures were not analyzed as closely since only one 2013/2015 set of deposits were available and neither contained recognizable structures. The percent changes of tsunami deposit thickness at Quidico were the largest of all sites in this study, which is significant because the amount of time between the deposit descriptions was the shortest (2013 to 2015). Excluding Pit Q8/ Pit 59, deposits changed by 80% or more (mainly increases in thickness). However, Pit Q15/ Pit 57 which changed by -100% at the riverbank was initially a surface dusting (0.1 cm) of sand in 2013 and was unlikely to be preserved and should be considered an exception. Pit Q16/ Pit 68, also on the riverbank, with a percent change of +100% to +300%, was in at a site that is frequently flooded and can accumulate silty overbank deposits (Hong et al., 2016). The increase in thickness at Pit Q6/ Pit 61 is difficult to explain, since the deposit did not display significant soil or organic material in the uppermost section to add to the deposit and it still had a distinguishable lower contact with the soil. This was also the case with Pit Q9/ Pit 58

(increase of +80%) that had no signs of significant soil or organic material at the top, and even though the underlying soil appeared to be mixing with the tsunami deposit, it still displayed a distinguishable contact. The change may have been due to the deposit being sampled 2 m away from its original location in 2013.

Hong et al. (2016) identified four additional paleotsunami deposits in the stratigraphy of an abandoned meander and along the riverbank, which proves that tsunami deposits can be preserved in the long term, despite the rapid changes seen in the 2010 deposit after only 2 years. The transects include all of my compared 2010 deposits except one (Pit Q16/Pit 68; Figure 24) and four dated paleotsunami deposits (1960, 1835, 1751 or 1730, and one deposit predating the tsunami record). While tsunami deposits were identified in the riverbank exposure, they are separated by sandy silt overbank deposits, which could make the contacts more difficult to distinguish. Deposits in the meander were more prominent because they were separated by silty peat, which is attributed to the depositional environment of the abandoned meander setting— an area that is infrequently flooded, lacks fluvial overbank deposits, and is a lower energy wetland environment ideal for preserving the deposits (Hong et al., 2016). Because of this depositional setting, this site displays good deposit preservation potential for the future.

Tirúa Deposit Results

In 2015 at Tirúa (Figure 2), I dug 10 pits (Figure 14), seven of which were located in the same location (within GPS error) as tsunami deposits described in 2012 one year and 11 months after the tsunami in Ely et al. (2014) and in unpublished field notes from

2012 (L. Ely, pers. comm., 2015). I recorded latitude/longitude locations, deposit thicknesses, and descriptions at all seven pits (Appendix Table B1). I sampled tsunami deposits (with subsamples based on visible changes in grain size) at six pits, and sampled underlying soils at two pits. In 2015, elevations and horizontal distances of tsunami deposits (relative to mean sea level) were measured from the riverbank with a surveying level, stadia rod, and portable tide gauge. I used Google Earth to measure the 2012 deposit limit south of the riverbank (Figure 14) for comparison to the deposit limit I traced in 2015.

Maximum Inland Extent

The tsunami deposition limit (Pit 13-25) in 2012 was traced by Ely et al. (2014), which I measured using Google Earth to be $284 \text{ m} \pm 10 \text{ m}$ inland from the edge of the riverbank at Pit 13-1/ Pit 69 (Figure 14). In 2015, when re-visiting locations described by Ely et al. (2014), Pit 79 was the deposit limit. Using the same measurement methods as the 2012 deposit limit, I measured Pit 79 to be $329 \text{ m} \pm 10 \text{ m}$. From these two sites, the range of possible percent change in deposit extent is from +9% to +24% (Table 4). When comparing the inland distance of Pit 79 (2015) to the local tsunami inundation limit of $463 \pm 10 \text{ m}$ defined by Ely et al. (2014) in 2010, it was a difference of $134 \text{ m} \pm 10 \text{ m}$ (Table 5).

Grain-size

At Tirúa, I compared normalized grain-size distributions of three deposits collected in 2015 (Pit 69, Pit 70, Pit 73) to normalized distributions from deposits collected in 2012 (Pit 13-1, Pit 13-3, Pit 13-11) by Ely et al. (2014) (Figure 26; Figure 27; Figure 28). At Pit 69 (Figure 26) and Pit 70 (Figure 27), the uppermost grain-size distributions were measured with both a Mastersizer (distributions labeled “a.” in Figures 26 and 27) and CAMSIZER (distributions labeled “b.” in Figures 26 and 27). Prior to Mastersizer analysis, I removed sand grains greater than 1 mm with a sieve.

At Pit 13-1 (2012), Ely et al. (2014) collected two subsamples in the 12-cm deposit and at Pit 69 (2015) I collected three subsamples in the 10-cm deposit (Figure 26). Pit 13-1 average grain size changed from medium sand in the lower subsample 0-8 cm to fine sand in the uppermost 8-12 cm, indicating normal grading. Both subsamples were positively skewed (Appendix Table B2). Pit 69 subsample 7-10 cm Mastersizer measurement was able to measure a fine-grained portion smaller than 75 μ m that the CAMSIZER distribution could not detect (Figure 26). Pit 69 average grain size was medium sand throughout all subsamples (Appendix Table B2). The lowermost 0-7cm was strongly positive skewed. Subsample 7-10 cm Mastersizer distribution indicated a near symmetrical skew while the CAMSIZER distribution of the same subsample measured a positive skew.

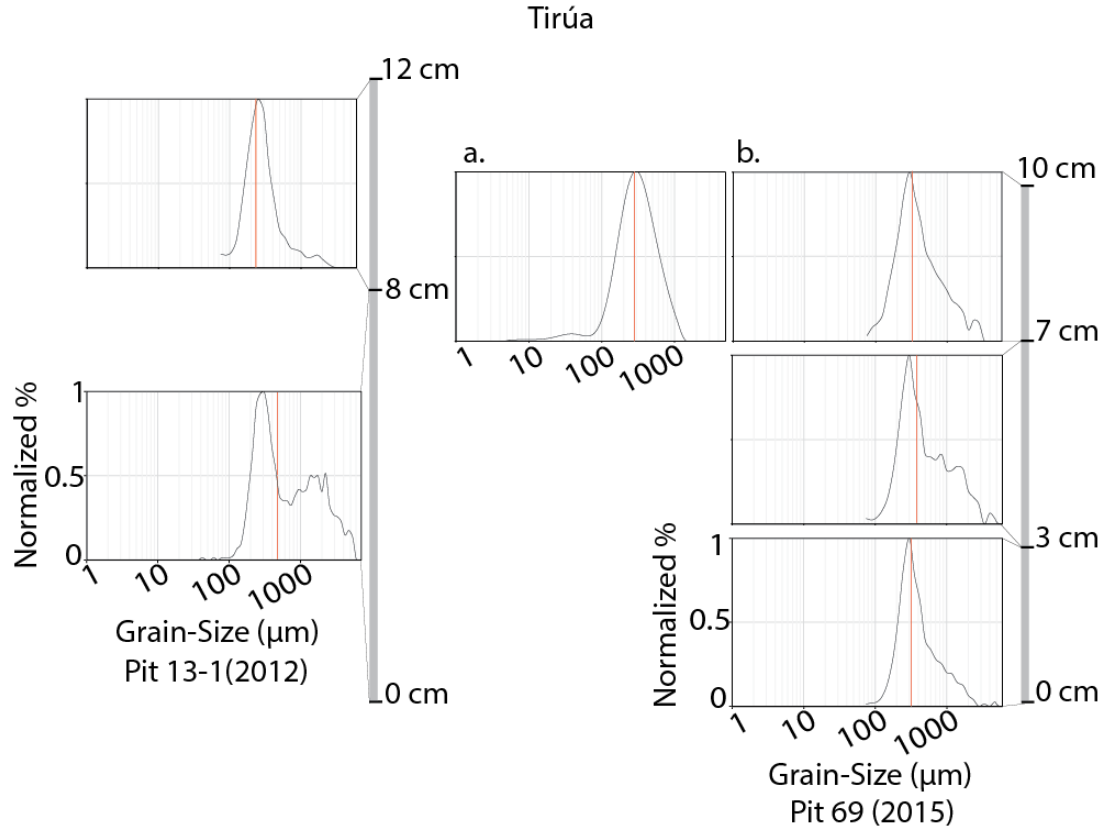


Figure 26: Normalized grain-size distributions drawn to depth scale from Tirúa, Pit 13-1 sampled in 2012 by Ely et al. (2014) and Pit 69 sampled in 2015. Red line within each distribution marks the average grain size (50th percentile). The base of the 2010 tsunami deposit (directly above contact with pre-existing soil) is labeled as “0 cm”. The uppermost depth label indicates top of the deposit and total deposit thickness. Centimeter labels denote the boundaries between every subsample. Grain-size distributions labeled “a.” were measured using the Mastersizer and “b.” using the CAMSIZER. Refer to Figure 14 for pit locations.

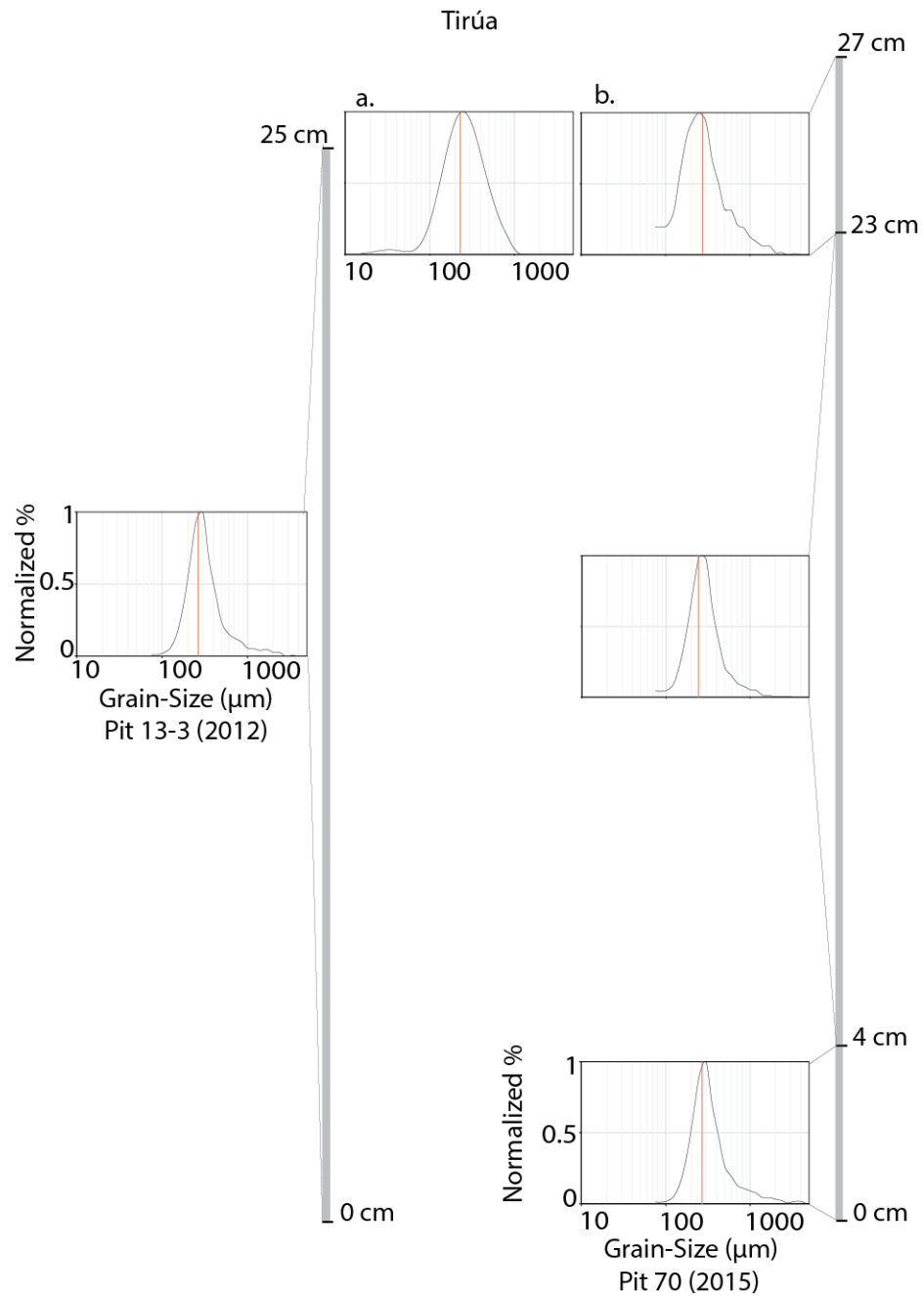


Figure 27: Normalized grain-size distributions drawn to depth scale from Tirúa, Pit 13-3 sampled in 2012 by Ely et al. (2014) and Pit 70 sampled in 2015. Red line within each distribution marks the average grain size (50th percentile). The base of the 2010 tsunami deposit (directly above contact with pre-existing soil) is labeled as “0 cm”. The uppermost depth label indicates top of the deposit and total deposit thickness. Centimeter labels denote the boundaries between every subsample. Grain-size distributions labeled “a.” were measured using the Mastersizer and “b.” using the CAMSIZER. Refer to Figure 14 for pit locations.

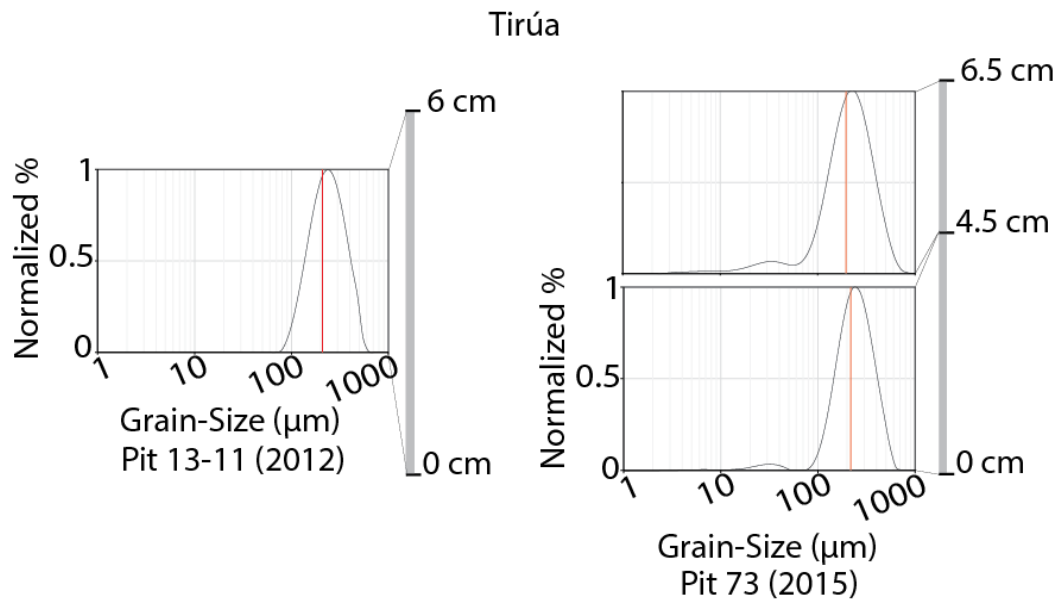


Figure 28: Normalized grain-size distributions drawn to depth scale from Tirúa, Pit 13-11 sampled in 2012 by Ely et al. (2014) and Pit 73 sampled in 2015. Red line within each distribution marks the average grain size (50th percentile). The base of the 2010 tsunami deposit (directly above contact with pre-existing soil) is labeled as “0 cm”. The uppermost depth label indicates top of the deposit and total deposit thickness. Centimeter labels denote the boundaries between every subsample. Refer to Figure 14 for pit locations.

At Pit 13-3 (2012), Ely et al. (2014) collected one bulk sample of the 25-cm thick deposit and at Pit 70 (2015) I took three subsamples of the 27-cm thick deposit (Figure 27). Pit 13-3 average grain size was medium sand and positively skewed. The Pit 70 subsample 23-27 cm Mastersizer measurement was able to measure a fine-grained tail (not present in Pit 13-3) smaller than 75 μm that the CAMSIZER could not detect (Figure 27). The two measurement methods still resulted in the same average grain size of fine sand and positive skew (Appendix Table B2). Pit 70 average grain-sizes display normal grading from medium sand in the lowermost 0-4 cm subsample to fine sand in all

remaining subsamples from 4-27 cm. Each subsample of Pit 70 is also positively skewed (Appendix Table B2).

At Pit 13-11 (2012), Ely et al. (2014) collected one bulk sample in the 6-cm deposit and at Pit 73 (2015) I took two subsamples in the 6.5-cm deposit (Figure 28). Pit 13-11 average grain size was fine sand with a near symmetrical skew (Appendix Table B2). Pit 73 average grain size was also fine sand throughout, but the lowermost subsample 0-4.5 cm skew was nearly symmetrical while the upper portion of the deposit was negatively skewed. Pit 73 also has finer grained tails throughout the deposit which is not present in Pit 13-11.

Thickness

At Tirúa, Ely et al. (2014) measured the 2010 deposit thicknesses and provided descriptions of the deposits. Table 6 summarizes the measured thicknesses and percent change from 2012 to 2015. At this location, percent changes of thickness at individual sites ranged between -46% and +20%.

Pit 69 (2015) was 10-cm thick and had a sandy soil layer in the uppermost 3 cm with thick roots at the surface and thin roots throughout the deposit. Pit 69 contact with the underlying soil was sharp, but visually displayed some sand mixing. Pit 13-1 (2012) was 2-cm thick and not described to have a sandy soil layer and roots. Percent change in thickness between 2012 and 2015 was -17%.

Pit 70 (2015) sand was loosely consolidated with many thick and thin roots throughout and did not have overlying soil or organic accumulation. The deposit also had

a sharp but undulatory contact with underlying soil. These characteristics were not described in Pit 13-3 (2012). I measured Pit 70 to be variable in thickness between 27 and 30 cm, and Pit 13-3 was 25-cm thick, resulting in a change between +8% and +20%.

Pit 71 (2015) was a 11-cm thick deposit that contained thick roots in the uppermost portion, a thick organic mat in the uppermost 3-4.5 cm, and thin roots throughout the deposit. Pit 13-7 (2012) was 12-cm thick with a silt cap in the uppermost 5 mm. Percent change was -8%.

Pit 73 (2015) contained detritus mat in the upper 1.5-2 cm of the deposit with both thin and thick roots throughout the deposit. Pit 13-11 (2012) contained new vegetation growth at the surface and 3-mm silt cap above sand. I measured Pit 73 to be variable in thickness between 4.5 and 6.5 cm and Pit 13-11 was measured to be 6 cm, creating the possibility that the deposit at this site gained 0.5 cm or lost 1.5 cm (+8% to -25%) in thickness.

Pit 74 (2015) contained a tan, finer grained 1-cm thick band (bounded by grey sand) in the upper 2-3 cm of the deposit and did not have an organic mat. Pit 13-16 (2012) was similarly described as having a 1-cm laminated sit cap at the uppermost section of the deposit. Pit 13-16 was initially described in 2012 as 12-cm thick and Pit 74 was 6.5-cm thick (a -46% change).

Pit 75 (2105) contained a very thin organic layer above the deposit and both Pit 75 and Pit 13-19 (2012) grain size was described as silty. Pit 75 remained the same thickness as Pit 13-19 (1-cm thick).

Pit 76 (2105) was 6.5-cm thick silty sand deposit with an organic detritus and a thin silt layer (not laminated) in the upper 2 cm. Pit 13-21 (2012) was 9-cm thick and described to have a laminated silt layer in the uppermost 3 cm of the sand deposit. Pit 76 was measured to be 6.5 cm and Pit 13-21 was 9 cm (-28% change).

Tirúa Deposit Discussion

Grain Size

Pit 13-1/Pit 69 lost coarse grained material in the lowermost section and gained fine material in the uppermost section between 2012 and 2015. In the lowermost section, the 2015 Pit 69 slightly lost coarse-grained material compared to the earlier 2012 Pit 13-1 (Figure 26, Pit 13-1 subsample 0-8 cm vs. Pit 69 subsamples 0-3 cm and 3-7 cm). I expect this is either a result of mixing of the underlying finer-grained soil with the tsunami deposit that I also visually observed, or a slight error in sampling in 2015 where soil could have contaminated the lowermost samples. In the uppermost section, the 2015 Pit 69 7-10 cm subsample is finer grained than Pit 13-1 subsample 8-12 cm (Figure 26) and corresponds with the sandy soil layer in the uppermost 3 cm of the deposit that was visually seen in 2015 but was not described in 2012. While the percentage of finer grained material in Pit 69 subsample 7-10 cm measured using the Mastersizer is not precisely known, sediments less than 75 μm clearly exist even though they could not be detected with the CAMSIZER (Figure 26).

Pit 13-3/Pit 70 also experienced changes between 2012 and 2015, but the difference in sampling methods makes the cause unclear. Pit 13-3 (2012) and Pit 70

(2015) grain-size distributions are difficult to compare because Pit 13-3 was sampled as a bulk deposit while Pit 70 was sampled in three sections (Figure 27). Because Pit 13-3 was a bulk sample, it is impossible to tell if the deposit was normally graded. If it were, the internal structure would have been preserved since 2012 despite the abundant thick and thin roots by 2015. At my other study sites and in previous research (see also Spiske et al., 2013), roots typically cause bioturbation and sediment mixing, although exceptions are noted in tsunami deposit taphonomy studies (Szczuciński, 2012). If Pit 13-3 was not normally graded in 2012, there would need to have been a source of fine sediment addition to the upper section, and roots (which were seen) to rework the fine sand throughout the upper 23 cm but not affect the lowermost 0-4 cm which is medium sand at Pit 70 (2015). Also, even though Pit 70 did not have a visually noticeable organic layer above the deposit and appeared to be entirely sand in 2015, it still increased in thickness between 2 and 5 cm. I interpret this as due to the addition of fine windblown sand, which is easily transported (see also Spiske et al., 2013) and could explain why the upper Pit 70 23-27 cm subsample averaged fine sand and had a slight finer tail, although equally likely is an error or natural variability missed when measuring the thickness in either 2012 or 2015.

Lastly, Pit 13-11/Pit 73 also experienced grain-size changes, but these changes were slight, and were most likely caused by bioturbation. When comparing Pit 13-11 (2012) to subsamples of Pit 73 (2015), the greatest change was the addition of fine-grained sediments throughout Pit 73. This addition is slight, however, since the lower Pit 73 subsample 0-4.5 cm was skewed negatively to the coarser portion of the distribution

and the upper subsample 4.5-6.5 cm was near symmetrical, meaning there the fine grained portion of the deposit is not dominant (Figure 28). I interpret finer grains throughout the deposit in 2015 as due to the 3-mm silt cap present in 2012 being reworked by the thick and thin roots that extended throughout the deposit as described in prior studies (see also Szczuciński, 2012; Yawsangratt et al., 2012; Spiske et al., 2013) as well as in other tsunami deposits in my study areas.

Preservation Potential

The geomorphic environment of Tirúa can be described as a flat and low lying river floodplain (Figure 14). Cows were seen grazing the floodplain, but their presence did not appear to alter the deposits. Currently in Tirúa, the preservation potential is moderate because the deposits experienced changes to thickness and internal structures since initially described in 2012. However, the percent changes of tsunami deposit thickness were the lowest here compared to all other sites, which I interpret as due to the overlying silt caps described in 2012 as well as overlying organic mats and soil development observed in 2015, that act to protect the deposit from surficial processes. Because Tirúa deposits were collected in 2012, the smaller difference in 2015 compared to deposits collected in 2010 from La Trinchera, Constitución, and Coliumo was expected. However, Tirúa deposits are also less changed than Tubul and Quidico, collected in 2012 and 2013, respectively. No distinct trend exists between changes in deposit thickness and distance inland, as the percent changes were variable.

Tirúa deposits stood out from all other locations because of the presence of silt caps over the tsunami deposits before 2012, which do not seem to be preserved in 2015; their lack of preservation is why my evaluation of the preservation is moderate rather than good. By 2015, many tsunami deposits also included organic mats (4.5 cm maximum thickness at Pit 71). However, there is no clear trend as to whether the 2012 deposits with silt caps were more likely to develop soil and organic mats in 2015 than those without. There also does not seem to be a correlation between the thickness of the silt cap in 2012 and the percent change in deposit thickness. Regardless, I conclude that because of these silt caps (and organic mats), that changes in deposit thickness at Tirúa were minor. Fine-grained sediment is easily transported (Spiske et al., 2013), and if this silt cap is removed, it would likely be removed before the tsunami deposit sand would be affected by erosion. Ely et al. (2014) also identified three additional paleotsunami deposits in the stratigraphy, which verifies that the presence of tsunami deposits persists in the long-term.

The maximum inland extent of the tsunami deposit re-traced in 2015 was farther inland than the 2012 location, which is different than what is typically seen. The usual expectation from past research is that the maximum extent decreases or stays the same over time due to post-depositional changes (see also Goto et al., 2012; Szczuciński, 2012). The 2015 deposit at Pit 76 still had a sharp contact with the underlying soil at the 2012 maximum inland extent location of Pit 13-21, while farther inland tsunami deposits in 2015 (Pit 79) had an underlying soil contact with a sandy soil and was therefore not

sharp making it difficult to determine. Potentially, this extent of the deposit may have overlooked in 2012.

Sources of Error in Deposit Studies

Sources of error have been mentioned for each applicable deposit thickness and grain-size comparison in the above sections. While they are important to consider for the details of each specific tsunami deposit pit comparison, I consider these discrepancies to not be significant to the bigger picture of assessing the preservation potential for the entire study site.

One source of error I encountered in all paleotsunami resurveys is associated with revisiting a previously described tsunami deposit. Handheld GPS error is usually a few (3-4) meters, meaning the exact pit location exists within a 3-4 m radius circle. Unless evidence of the previous pit still exists on the surface, the exact location cannot be precisely pinpointed. Also, if we did find the previous pit, we did not re-dig the exact pit again, since it had already been disturbed from the previous study (see also Szczuciński, 2012). Therefore, it is always implied that the location cannot be the same. If the deposit was originally variable in characteristics and thickness over short distances, differences in location on the order of meters can lead to apparent changes in the deposit in our resurvey.

Another important error to note in our study is the different sampling methods between the first sampled deposit in 2010/2012/2013 and the second deposit in 2015. Each site's sampling strategy depended on the preference of the person collecting the

sample. When I sampled the deposits in 2015, the previous sampling methods were unknown to me. However, the difference became apparent when I compared grain-size distributions between the first sampled deposit and the second sampled deposit. Direct detailed comparisons are impossible because the depth ranges of samples were not identical. This could be because the deposit changed thickness, deposits were only partially sampled, or different sample intervals were used. As a result, I could only consider major and obvious changes, such as the presence or absence of a fine or coarse tail, changes in general skew of coarse, fine, or symmetrical/near symmetrical, and changes in grain-size classes. For future paleodeposit resurveys, this error can be partially reduced by collecting samples using the same methods with the same intervals between years, although if the total thickness of the deposits changed, residual errors of this kind are still likely.

Implications for Tsunami Deposit Taphonomy

Based on my study of tsunami deposits at the six sites, preservation of the deposit as an intact and exact representation of what was deposited during the tsunami is currently moderate at all sites and is summarized in Table 7. I predict that deposits at all sites will continue to be modified by taphonomic processes, such as soil development and/or organic cover, bioturbation from roots or animals, or from human activity (plowing, etc.), but the majority will remain recognizable in the long-term (Table 7). From what I observed over five years of change, internal structures will often be lost, the

thickness of the deposit can easily be altered, and the inland extent modified, but rarely was a deposit that was thicker than 1 cm affected to the point of disappearance.

Table 7: Summary of geomorphic settings, current preservation, and long-term preservation potential of the resurveyed 2010 tsunami deposits at each study site.

Site	Geomorphic Setting	Current Preservation	Long-Term Preservation Potential
La Trinchera South	Open beach/coastal plain	Moderate	Likely
Constitución	Open beach	Moderate	Not likely
Coliumo	U-shaped river valley	Moderate	Likely
Tubul	Coastal plain	Moderate	Not likely
Quidico	River floodplain	Moderate	Likely
Tirúa	River floodplain	Moderate	Likely

A clear sand layer (altered or not) from the 2010 deposit is very likely to be preserved in the future at all sites, with the possible exception of Tubul and maybe Constitución. The coastal plain area of Tubul has undergone heavy grazing, which can significantly alter tsunami deposit thickness and internal structure. It is likely this grazing will continue, so the deposits are not likely to remain well distinguishable in the landscape. The tsunami deposits at Constitución that have not been removed by human disturbance from the tree plantation may be preserved in the future, though the slow regrowth of overlying vegetation and open beach environment may lead to more alteration of the deposit, either decreasing or increasing the deposit thickness and removing internal structures that were preserved at one of the two revisited pits. At La Trinchera, preservation in thickness is more likely at the coastal plain to the east because it is less accessible to the public, farther landward, was covered by vegetation, and

blocked by windblown erosion from the high road. This is favorable for long-term preservation because it is in the same location as the deposition limits. Tsunami deposits in the open beach to the west of the road were preserved and have the potential to be preserved in the future, but are more exposed to the windblown erosion from the open beach environment. At Coliumo, all deposits are likely to be preserved in the future, but those on the valley slopes rather than the valley middle show the most potential for future preservation of thickness and possibly internal structures because they were initially deposited thicker and are farther removed from erosive forces such as grazing cows and agriculture. Like La Trinchera, this is favorable for long-term preservation because edges of the valley include the limit of the tsunami. It is important to note that evidence of erosion from grazing and agriculture were still present near the valley slopes, but bioturbation from such isolated events are ultimately difficult to accurately predict. Quidico is a river floodplain, with the majority of my examined deposits within an abandoned meander, which is a low energy environment less likely to be flooded and reworked by flood deposits (Hong et al., 2016). It is also significantly inland, away from the coastline and has ample overlying vegetation that can assist in preserving tsunami deposit thickness, but less so in preserving internal structures. Paleodeposits dated to be from 1960 and earlier have also been found at Quidico and were well preserved (Hong et al., 2016), which is evidence that the 2010 deposits are very likely to also be preserved in the sedimentary record. Lastly, Tirúa is a similar river floodplain environment that is far from the coastline and had ample overlying vegetation as well as a protective silt cap over some deposits. Well-preserved dated paleotsunami deposits from 1960 and earlier

have been found by Ely et al. (2014) and Nentwig et al. (2015) in the underlying stratigraphy, which indicates that the 2010 deposit is very likely to also be preserved in the future.

The evolution of the deposits at my study sites suggest that the taphonomic processes involved in burying and preserving deposits (and ultimately the preservation potential) are controlled by the geomorphology of the area as well as land use. Two of the six sites, Quidico and Tirúa, which are both river floodplains, have proved to preserve paleotsunami deposits well in the geologic record (Ely et al., 2014; Nentwig et al., 2015; Hong et al., 2016). Analysis of other studies in Chile similarly shows that preservation potential in floodplains are better than other environments. At the Rio Maullín river estuary in southern Chile, an environment similar to Quidico and Tirúa, the 1960 and 1575 tsunami deposits as well as four older tsunami deposits were found by Cisternas et al. (2005) in the stratigraphy. The 1960 deposit lower soil contact was patchy, likely being trampled by animals (Cisternas et al., 2005), but still remained preserved. In contrast, a survey of the 2010 tsunami in 2012 by Bahlburg and Spiske (2015) on a low coastal plain on Mocha Island, revealed the aerial extent of the sand was reduced by 50% mostly due to heavy rainfall, windblown erosion, and human and animal disturbance, despite the tsunami deposits being covered with vegetation by 2012. Excluding the heavy rainfall, this site is geomorphologically similar to Tubul and Constitución, which are relatively low-lying, easily accessible areas prone to disturbance by humans and/or animals.

The preservation of deposit thickness is important for models that use maximum deposit limits as observation points to compare with simulated results, while the preservation of internal structures is important for formulas that calculate flow parameters based on grain size characteristics. For a modeling program such as TsuSedMod, which calculates flow depth and flow speed based on stratigraphic changes in grain size in the tsunami deposit, the grain-size input is more sensitive than the deposit thickness parameter (Jaffe and Gelfenbuam, 2007). As seen in my grain-size comparisons, changes of the deposit since initial deposition do occur and could produce different tsunami flow results as the tsunami deposit changes over time.

The taphonomic processes in south-central Chile allow tsunami deposits to remain intact and readily distinguishable more so than preserving the internal structures. For paleotsunami studies, where the long-term goal is to predict paleoearthquake parameters based on tsunami deposits, this implies that tsunami modeling with programs such as GeoClaw, which does not factor in grain size, could provide a better paleotsunami simulation. This would also provide a source model more reflective of the paleoearthquake, which is not provided when using TsuSedMod. However, at Constitución, internal structures were still preserved, so programs such as TsuSedMod should not be entirely dismissed for calculating flow depth and flow speed, although should be used with caution for paleoevents.

CHAPTER V

CONCLUSIONS

South-central Chile contains an extensive written catalog describing paleoearthquakes and paleotsunamis as well as paleodeposits found on land. The well-documented 2010 M_w 8.8 earthquake and tsunami is the most recent event to occur in the area. This presented the opportunity to conduct a detailed study of the 2010 event and its associated tsunami deposits to determine if 1) numerical modeling of the tsunami and earthquake can be effectively matched with surveys of tsunami inundation flow depths on land and 2) to learn about the taphonomic processes the 2010 deposits experienced over time. This 2010 event and its deposits can be used as a well-constrained modern analog that can be applied to future paleotsunami studies.

In my study I modeled the 2010 south-central Chile earthquake and tsunami using GeoClaw at La Trinchera, Constitución, Coliumo, Tubul, and Tirúa. I used published slip distributions and my own modified distributions to compare post-tsunami field observations to simulated results to determine the viability of modeling in south-central Chile, and ultimately, to paleodeposits. Published co-seismic slip distributions that used techniques to resolve slip near the trench using DART buoy data and a combination of high rate GPS and teleseismic records produced the highest overall percent match of observed to simulated data. My modified earthquakes did not improve the overall percent match of 83% from the underestimated tsunami simulation by *Yue et al. (2014)* even though these earthquakes were larger than the M_w 8.8 of the actual event.

Generally, simulations of the tsunami were too small at most study sites, the greatest disparity between simulations and observations occurred at sites which only few flow depth values, compared to sites with enough flow depths where I could determine the approximate volume of water inundation. Additionally, the maximum inland limit of tsunami inundation was not reached in all simulations and the deposit limits were not reached in the large majority of simulations.

The pervasive undersized simulated tsunami in my results reveals that either the earthquake scenarios used in this study were missing important tsunami-forming features that occurred during the 2010 event or errors associated with my modeling methods were too great to accurately represent the tsunami on land. If due to the earthquake scenarios, shallow splay faulting may be a missing feature, which is known to create a larger tsunami and has been documented to occur during this event. If due to the modeling methods, the most likely cause is the coarse resolution bathymetry and topography, which did not represent the complex geomorphologies such as river floodplains and river valleys and therefore simulated the tsunami inundation distances especially poorly in these areas. Also, shelf resonance and edge waves, which is known to amplify the tsunami, may not have been well simulated by GeoClaw and could be another factor in the underestimation of the tsunami.

Modeling the 2010 tsunami to tsunami deposits that have existed in the landscape for five years required an investigation of the changes the deposits may have experienced over time. In addition to tsunami modeling, I also resurveyed the 2010 tsunami deposits in 2015 that were initially described in 2010/2012/2013 to see how tsunami deposits are

affected by taphonomic processes and determine the long-term preservation potential at each study site listed above, as well as the additional site of Quidico.

In 2015, all sites currently displayed moderate preservation, where the deposits were still present as a sand layer but were noticeably altered and most of the internal structures initially described in post-tsunami surveys were not preserved in 2015. The areas where deposits displayed overlying organic material protected the deposit, but this also added roots throughout the deposit which contributed to bioturbation by sediment mixing and the removal of internal structures in most instances. Some deposits were also bioturbated by grazing animals and a few were completely removed by human activity. Also, the tsunami deposit inland extent was observed to either decrease or increase over time, depending on the site.

The leading factors that affect the preservation in the deposit currently and in the future are the geomorphic environment and land use. The river floodplain environments, such as Quidico and Tirúa, show the best potential for future preservation; these sites also known to have paleodeposits in the underlying stratigraphy, demonstrating this environment would likely preserve the 2010 deposit into the future. At the U-shaped river valley of Coliumo, the sloped valley edges are more likely to preserve deposits in the long-term than the valley middle. At the valley edges, thicker sand sheets are deposited initially and it is less accessible to humans and grazing animals in comparison to the valley middle. The coastal plain environment of La Trinchera was low lying and protected from an open beach environment, also making it likely that the tsunami deposits will be preserved in the future. In contrast, the heavy grazing at Tubul suggests

future preservation potential is low, even though the site was also a coastal plain environment, like La Trinchera. Finally, Constitución was an open beach environment, which exposed the tsunami deposits to windblown erosion and slow regrowth of vegetation. Between the unprotected geomorphic setting and the human land use appearing to have destroyed some deposits by 2015, the deposit is less likely to be preserved in the future here.

Modeling of paleotsunamis and paleoearthquakes based on paleodeposits on land requires two aspects to be fulfilled: successful tsunami modeling and knowledge of paleodeposit taphonomy. Modeling the 2010 earthquake and tsunami to observed flow depths and volumes was possible with a reasonable disparity between the observed and simulated values, but simulating tsunami inundation to reach the deposit limits resurveyed in 2015 or the tsunami inundation limit was not successful. This first points to the necessity of higher resolution bathymetry and topography to successfully simulate water inundation to paleodeposit limits which greatly relies on the accurate elevation of the inundated coast. The 2010 tsunami deposits and the deposit inland extent were altered over the five years since initial deposition, but this change was moderate, and it is likely many of the tsunami deposits will be preserved in the sedimentary record in the future. Because the modeling results to flow depth and volume were successful, in consideration with the limitations that were discussed, and the paleodeposits are moderately preserved, GeoClaw works for this location and it is very likely that modeling to paleodeposits is entirely possible with a better bathymetry and topography dataset.

Future Studies in Paleotsunami Modeling

One of the most important factors of modeling paleotsunamis to paleodeposits found on land is the change of the paleodeposit limit over time. In my study, the 2010 tsunami deposit extents both decreased and increased over five years. However, the percent change range of -6% to +24% is not significant in the scale of tsunami modeling in GeoClaw. The extent of the deposits after five years would still generally be representative of the true deposit extent from 2010. If the tsunami deposits remain stable and do not continue to change significantly in the long-term, this could simulate a near true paleotsunami inundation limit. If the deposits continue to change in the long-term, an increase in inland extent would require a larger tsunami and would overestimate the true tsunami inundation and the tsunami hazard. A decrease in the deposit inland extent would require a smaller tsunami and would underestimate the true tsunami inundation and tsunami hazard. An overestimation or underestimation greater than the tsunami inundation limits of my studied tsunami deposits may result in a misunderstanding of the true tsunami hazard of the area.

The taphonomic processes in south-central Chile allow tsunami deposits to remain intact and readily distinguishable more so than preserving the internal structures. This implies that tsunami modeling with programs such as GeoClaw could provide a better paleotsunami simulation, provide a source model more reflective of the paleoearthquake, and a better understanding of tsunami hazards in the area. TsuSedMod in comparison, which is more sensitive to grain size than deposit thickness, could misrepresent the

paleotsunami flow depth and flow speed if the internal structures have been erased or altered over time.

For the specific case of modeling paleotsunamis in south-central Chile, I suggest that improvements need to be made in both tsunami modeling and tsunami deposit studies. As mentioned previously, higher resolution bathymetry and topography are essential for modeling tsunami inundation. Although paleotsunami studies typically result in only a few isolated sites, my work also suggests that having more sites within the estimated rupture zone is important for a comprehensive representation of the earthquake scenario that created the tsunami. Additional data could include field indicators of the paleotsunami height and distance such as wracklines if the area is remote and undisturbed, and tracing the paleodeposit limit in detail. As seen in my comparisons between simulated and observed flow depth and volumes, the sites with 1-2 flow depth measurements (La Trinchera and Tubul) had worse results than the sites with numerous flow depth measurements (Constitución, Coliumo, Tirúa) where I could calculate a total volume. Finally, a significant longitudinal distribution of sites within the estimated rupture zone is ideal. In my modified slip distributions, I removed the uppermost row of subfaults because this row extended beyond my northernmost site of La Trinchera and I did not have post-tsunami survey data to make comparisons between the simulated and observed results. In the case of the 2010 earthquake, I decided this row was insignificant. However, if this were a different paleoearthquake, the northernmost portion of the distribution may have been important. If there was not a site to compare observed to simulated values, the tsunami forming parameters could be mis-represented in that

northernmost portion. Overall, this will improve the resolution of the resulting earthquake scenario that created the tsunami. The six sites I studied should be considered a minimum for modeling paleotsunamis in south-central Chile, since paleotsunamis by definition contain less detailed datasets for one to compare simulated to observed values and less co-seismic slip distribution datasets to use as a foundation for modeling the earthquake.

While the tsunami deposit inland extent and the compared deposit pits at my study sites were only moderately altered within the first five years, it would be worthwhile to conduct another resurvey of these study areas. A resurvey, especially one targeted at specific taphonomic processes, could determine how the tsunami deposits continue to be altered in the future. While such a study could change my predicted preservation potential at a few or all of my study sites, it would give a better indication of long-term preservation of paleodeposits that have been in the landscape greater than five years, which would be more reflective of all known paleodeposits prior to the modern 2010 deposits in south-central Chile.

Paleotsunami modeling to paleodeposits in south-central Chile and elsewhere around the world not only advances the field of tsunami modeling, but can greatly improve or create new inundation maps for high-risk coastal communities. This is important in assessing the risk of future tsunami events, hazard mitigation, and community preparedness for these potentially life-threatening events.

REFERENCES

- Abe, T., Goto, K., and Sugawara, D., 2012, Relationship between the maximum extent of tsunami sand and the inundation limit of the 2011 Tohoku-oki tsunami on the Sendai Plain, Japan: *Sedimentary Geology*, v. 282, p. 142–150, doi: 10.1016/j.sedgeo.2012.05.004.
- Angermann, D., Klotz, J., and Reigber, C., 1999, Space-geodetic estimation of the Nazca-South America Euler vector: *Earth and Planetary Science Letters*, v. 171, p. 329–334, doi: 10.1016/S0012-821X(99)00173-9.
- Annunziato, A., Franchello, G., and Barberopoulou, A., 2010, 27 February 2010 Chile Tsunami Post Event Survey Mission.: European Commission Joint Research Centre Institute for the Protection and Security of the Citizen, doi: 10.2788/9732.
- Bahlburg, H., and Spiske, M., 2015, Styles of early diagenesis and the preservation potential of onshore tsunami deposits—A re-survey of Isla Mocha, Central Chile, 2years after the February 27, 2010, Maule tsunami: *Sedimentary Geology*, v. 326, p. 33–44, doi: 10.1016/j.sedgeo.2015.06.009.
- Barrientos, S.E., and Ward, S.N., 1990, The 1960 Chile earthquake: inversion for slip distribution from surface deformation: *Geophysical Journal International*, v. 103, p. 589–598, doi: 10.1111/j.1365-246X.1990.tb05673.
- Bedford, J., Moreno, M., Baez, J.C., Lange, D., Tilmann, F., Rosenau, M., Heidbach, O., Oncken, O., Bartsch, M., Rietbrock, A., Tassara, A., Bevis, M., and Vigny, C., 2013,

A high-resolution, time-variable afterslip model for the 2010 Maule Mw = 8.8, Chile megathrust earthquake: *Earth and Planetary Science Letters*, v. 383, p. 26–36, doi: 10.1016/j.epsl.2013.09.020.

Chagué-Goff, C., Andrew, A., Szczuciński, W., Goff, J., and Nishimura, Y., 2012, Geochemical signatures up to the maximum inundation of the 2011 Tohoku-oki tsunami - Implications for the 869AD Jogan and other palaeotsunamis: *Sedimentary Geology*, v. 282, p. 65–77, doi: 10.1016/j.sedgeo.2012.05.021.

Cisternas, M., Atwater, B.F., Torrejón, F., Sawai, Y., Machuca, G., Lagos, M., Eipert, A., Youlton, C., Salgado, I., Kamataki, T., Shishikura, M., Rajendran, C.P., Malik, J.K., Rizal, Y., and Husni, M., 2005, Predecessors of the giant 1960 Chile earthquake.: *Nature*, v. 437, p. 404–407, doi: 10.1038/nature03943.

Delouis, B., Nocquet, J.-M., and Vallée, M., 2010, Slip distribution of the February 27, 2010 Mw = 8.8 Maule Earthquake, central Chile, from static and high-rate GPS, InSAR, and broadband teleseismic data: *Geophysical Research Letters*, v. 37, p. L17305, doi: 10.1029/2010GL043899.

Dominey-Howes, D., Dengler, L., Dunbar, P., Kong, L., Fritz, H., Imamura, F., McAdoo, B., Satake, K., Yalciner, A., Yamamoto, M., Yulianto, E., Koshimura, S., and Borrero, J., 2012, International Tsunami Survey Team (ITST) Post-Tsunami Survey Field Guide: UNESCO-IOC, 2nd Edition.

- Ely, L.L., Cisternas, M., Wesson, R.L., and Dura, T., 2014, Five centuries of tsunamis and land-level changes in the overlapping rupture area of the 1960 and 2010 Chilean earthquakes: *Geology*, v. 42, p. 995–998, doi: 10.1130/G35830.1.
- Fritz, H.M., Petroff, C.M., Catalán, P.A., Cienfuegos, R., Winckler, P., Kalligeris, N., Weiss, R., Barrientos, S.E., Meneses, G., Valderas-Bermejo, C., Ebeling, C., Papadopoulos, A., Contreras, M., Almar, R., Dominguez, J.C., and Synolakis, C.E., 2011, Field Survey of the 27 February 2010 Chile Tsunami: *Pure and Applied Geophysics*, v. 168, p. 1989–2010, doi: 10.1007/s00024-011-0283-5.
- Fujii, Y., and Satake, K., 2013, Slip Distribution and Seismic Moment of the 2010 and 1960 Chilean Earthquakes Inferred from Tsunami Waveforms and Coastal Geodetic Data: *Pure and Applied Geophysics*, v. 170, p. 1493–1509, doi: 10.1007/s00024-012-0524-2.
- Garrett, E., Shennan, I., Woodroffe, S.A., Cisternas, M., Hocking, E.P., and Gulliver, P., 2014, Reconstructing paleoseismic deformation, 2: 1000 years of great earthquakes at Chucalén, south central Chile: *Quaternary Science Reviews*, v. 113, p. 112–122, doi: 10.1016/j.quascirev.2014.10.010.
- Geist, E.L., and Dmowska, R., 1999, Local Tsunamis and Distributed Slip at the Source: *Pure and Applied Geophysics*, v. 154, p. 485–512, doi: 10.1007/s000240050241.
- Goto, K., Chagué-Goff, C., Fujino, S., Goff, J., Jaffe, B., Nishimura, Y., Richmond, B., Sugawara, D., Szczuciński, W., Tappin, D.R., Witter, R.C., and Yulianto, E., 2011,

New insights of tsunami hazard from the 2011 Tohoku-oki event: *Marine Geology*, v. 290, p. 46–50, doi: 10.1016/j.margeo.2011.10.004.

Goto, K., Takahashi, J., and Fujino, S., 2012, Variations in the 2004 Indian Ocean tsunami deposits thickness and their preservation potential, southwestern Thailand: *Earth, Planets and Space*, v. 64, p. 923–930, doi: 10.5047/eps.2011.08.019.

Griswold, F.R., 2015 Field Observations and Modeling of the 1957 Earthquake and Tsunami on the Islands of the Four Mountains, Aleutian Islands, Alaska [Master's thesis]: Central Washington University, 91 p.

Hayes, G., 2010, Finite Fault Model Updated Result of the Feb 27, 2010 Mw 8.8 Maule, Chile Earthquake:
http://earthquake.usgs.gov/earthquakes/eqinthenews/2010/us2010tfan/finite_fault.php
p (accessed July 2016).

Hong, I., Dura, T., Ely, L.L., Horton, B.P., Nelson, A.R., Cisternas, M., Nikitina, D., and Wesson, R.L., 2016, A 600-year-long stratigraphic record of tsunamis in south-central Chile: *The Holocene*, doi: 10.1177/0959683616646191.

Intergovernmental Oceanographic Commission, 2014, The GEBCO_2014 Grid:
International Hydrographic Organization and Intergovernmental Oceanic
Commission of UNESCO.

- Jaffe, B.E., and Gelfenbuam, G., 2007, A simple model for calculating tsunami flow speed from tsunami deposits: *Sedimentary Geology*, v. 200, p. 347–361, doi: 10.1016/j.sedgeo.2007.01.013.
- Kanamori, H., 1977, The energy release in great earthquakes: *Journal of Geophysical Research*, v. 82, p. 2981–2987, doi: 10.1029/JB082i020p02981.
- Kato, T., Terada, Y., Nishimura, H., Nagai, T., and Koshimura, S., 2011, Tsunami records due to the 2010 Chile Earthquake observed by GPS buoys established along the Pacific coast of Japan: *Earth, Planets and Space*, v. 63, p. e5–e8, doi: 10.5047/eps.2011.05.001.
- Koper, K.D., Hutko, A.R., Lay, T., and Sufri, O., 2012, Imaging short-period seismic radiation from the 27 February 2010 Chile (MW 8.8) earthquake by back-projection of P, PP, and PKIKP waves: *Journal of Geophysical Research: Solid Earth*, v. 117, p. B02308, doi: 10.1029/2011JB008576.
- Koshimura, S., Matsuoka, M., Matsuyama, M., Yoshii, T., Mas, E., Jimenez, C., and Yamazaki, F., 2010, Field survey of the 2010 tsunami in Chile, in Yamazaki, F., 2010 Chile Earthquake and Tsunami Technical Report: Japan Science and Technology Agency, p. 10-26.
- Lay, T., Ammon, C.J., Kanamori, H., Koper, K.D., Sufri, O., and Hutko, A.R., 2010, Teleseismic inversion for rupture process of the 27 February 2010 Chile (Mw 8.8)

earthquake: *Geophysical Research Letters*, v. 37, p. L13301, doi:
10.1029/2010GL043379.

LeVeque, R.J., George, D.L., and Berger, M.J., 2011, Tsunami modelling with adaptively refined finite volume methods: *Acta Numerica*, v. 20, p. 211–289, doi:
10.1017/S0962492911000043.

Lieser, K., Grevemeyer, I., Lange, D., Flueh, E., Tilmann, F., and Contreras-Reyes, E., 2014, Splay fault activity revealed by aftershocks of the 2010 Mw 8.8 Maule earthquake, central Chile: *Geology*, v. 42, p. 823–826, doi: 10.1130/G35848.1.

Lin, Y.N., Sladen, A., Ortega-Culaciati, F., Simons, M., Avouac, J.-P., Fielding, E.J., Brooks, B.A., Bevis, M., Genrich, J., Rietbrock, A., Vigny, C., Smalley, R., and Socquet, A., 2013, Coseismic and postseismic slip associated with the 2010 Maule Earthquake, Chile: Characterizing the Arauco Peninsula barrier effect: *Journal of Geophysical Research: Solid Earth*, v. 118, p. 3142–3159, doi: 10.1002/jgrb.50207.

Lomnitz, C., 2004, Major Earthquakes of Chile: A Historical Survey, 1535-1960: *Seismological Research Letters*, v. 75, p. 368–378, doi: 10.1785/gssrl.75.3.368.

Lorito, S., Romano, F., Atzori, S., Tong, X., Avallone, A., McCloskey, J., Cocco, M., Boschi, E., and Piatanesi, A., 2011, Limited overlap between the seismic gap and coseismic slip of the great 2010 Chile earthquake: *Nature Geoscience*, v. 4, p. 173–177, doi: 10.1038/ngeo1073.

- MacInnes, B.T., Bourgeois, J., Pinegina, T.K., and Kravchunovskaya, E.A., 2009, Tsunami geomorphology: Erosion and deposition from the 15 November 2006 Kuril Island tsunami: *Geology*, v. 37, p. 995–998, doi: 10.1130/G30172A.1.
- MacInnes, B.T., Gusman, A.R., LeVeque, R.J., and Tanioka, Y., 2013, Comparison of Earthquake Source Models for the 2011 Tohoku Event Using Tsunami Simulations and Near-Field Observations: *Bulletin of the Seismological Society of America*, v. 103, p. 1256–1274, doi: 10.1785/0120120121.
- McAdoo, B.G., Fritz, H.M., Jackson, K.L., Kalligeris, N., Kruger, J., Bonte-Graptin, M., Moore, A.L., Rafiau, W.B., and Billix, D., 2008, Solomon Islands tsunami, one year later: *EOS* 89, 169-170.
- Melnick, D., and Echtler, H.P., 2006, Inversion of forearc basins in south-central Chile caused by rapid glacial age trench fill: *Geology*, v. 34, p. 709–712, doi: 10.1130/G22440.1.
- Melnick, D., Bookhagen, B., Strecker, M.R., and Echtler, H.P., 2009, Segmentation of megathrust rupture zones from fore-arc deformation patterns over hundreds to millions of years, Arauco peninsula, Chile: *Journal of Geophysical Research*, v. 114, p. B01407, doi: 10.1029/2008JB005788.
- Melnick, D., Moreno, M., Motagh, M., Cisternas, M., and Wesson, R.L., 2012, Splay fault slip during the Mw 8.8 2010 Maule Chile earthquake: *Geology*, v. 40, p. 251–254, doi: 10.1130/G32712.1.

Moreno, M., Rosenau, M., and Oncken, O., 2010, 2010 Maule earthquake slip correlates with pre-seismic locking of Andean subduction zone: *Nature*, v. 467, p. 198–202, doi: 10.1038/nature09349.

Moreno, M., Melnick, D., Rosenau, M., Baez, J., Klotz, J., Oncken, O., Tassara, A., Chen, J., Bataille, K., Bevis, M., Socquet, A., Bolte, J., Vigny, C., Brooks, B., Ryder, I., Grund, V., Smalley, B., Carrizo, D., Bartsch, M., and Hase, H., 2012, Toward understanding tectonic control on the Mw 8.8 2010 Maule Chile earthquake: *Earth and Planetary Science Letters*, v. 321-322, p. 152–165, doi: 10.1016/j.epsl.2012.01.006.

Morton, R.A., Gelfenbaum, G., Buckley, M.L., and Richmond, B.M., 2011, Geological effects and implications of the 2010 tsunami along the central coast of Chile: *Sedimentary Geology*, v. 242, p. 34–51, doi: 10.1016/j.sedgeo.2011.09.004.

National Geophysical Data Center / World Data Service (NGDC/WDS), 2015, Global Historical Tsunami Database. National Geophysical Data Center, NOAA, doi:10.7289/V5PN93H7 (Access date March 2015).

Nentwig, V., Tsukamoto, S., Frechen, M., and Bahlburg, H., 2015, Reconstructing the tsunami record in Tirúa, Central Chile beyond the historical record with quartz-based SAR-OSL: *Quaternary Geochronology*, v. 30, p. 299–305, doi: 10.1016/j.quageo.2015.05.020.

- Nichol, S.L., and Kench, P.S., 2008, Sedimentology and preservation potential of carbonate sand sheets deposited by the December 2004 Indian Ocean tsunami: South Baa Atoll, Maldives: *Sedimentology*, v. 55, p. 1173–1187, doi: 10.1111/j.1365-3091.2007.00941.x.
- Okada, Y., 1985, Surface deformation due to shear and tensile faults in a half-space: *Bulletin of the Seismological Society of America*, v. 75, no.4, p. 1135–1154.
- Pan, W., Wang, S., and Cai, S., 2010, Numerical simulations of the coastal effects of tsunami waves caused by the 1993 Hokkaido-Nansei-Oki earthquake: *Chinese Journal of Oceanology and Limnology*, v. 28, p. 1029–1039, doi: 10.1007/s00343-010-9041-2.
- Pollitz, F.F., Brooks, B., Tong, X., Bevis, M.G., Foster, J.H., Bürgmann, R., Smalley, R., Vigny, C., Socquet, A., Ruegg, J.-C., Campos, J., Barrientos, S., Parra, H., Soto, J.C.B., Cimbaro, S., and Blanco, M., 2011, Coseismic slip distribution of the February 27, 2010 Mw 8.8 Maule, Chile earthquake: *Geophysical Research Letters*, v. 38, p. L09309, doi: 10.1029/2011GL047065.
- Pulido, N., Yagi, Y., Kumagai, H., and Nishimura, N., 2011, Rupture process and coseismic deformations of the 27 February 2010 Maule earthquake, Chile: *Earth, Planets and Space*, v. 63, p. 955–959, doi: 10.5047/eps.2011.04.008.

Saito, T., Kono, S., and Kusunoki, K., 2010, Building Damage Investigation of the 2010 Chile Earthquake and Tsunami Disaster, in Yamazaki, F., 2010 Chile Earthquake and Tsunami Technical Report: Japan Science and Technology Agency, p. 27-31.

Shanmugam, G., 2012, Process-sedimentological challenges in distinguishing paleo-tsunami deposits: *Natural Hazards*, v. 63, p. 5–30, doi: 10.1007/s11069-011-9766-z.

Shao, G., Li, X., Liu, Q., Zhao, X., Yano, T., and Ji, C., 2010, Preliminary slip model of the Feb 27, 2010 Mw 8.9 Maule, Chile Earthquake:
http://www.geol.ucsb.edu/faculty/ji/big_earthquakes/2010/02/27/chile_2_27.html
(accessed July 2016)

Shi, S., Dawson, A. G., and Smith, D. E., 1995, Coastal sedimentation associated with the December 12th, 1992 tsunami in Flores, Indonesia, *in* *Tsunamis Their Generation, Dynamics, and Hazard: 1992–1994*: p. 525-536, Birkhäuser Basel.

Sladen, A., 2010, Preliminary Result 02/27/2010 (Mw 8.8) Chile:
http://tectonics.caltech.edu/slip_history/2010_chile/index.html (accessed July 2016)

Spiske, M., Piepenbreier, J., Benavente, C., and Bahlburg, H., 2013, Preservation potential of tsunami deposits on arid siliciclastic coasts: *Earth-Science Reviews*, v. 126, p. 58–73, doi: 10.1016/j.earscirev.2013.07.009.

- Szczuciński, W., 2012, The post-depositional changes of the onshore 2004 tsunami deposits on the Andaman Sea coast of Thailand: *Natural Hazards*, v. 60, p. 115–133, doi: 10.1007/s11069-011-9956-8.
- Udías, A., Madariaga, R., Buforn, E., Muñoz, D., and Ros, M., 2012, The large Chilean historical earthquakes of 1647, 1657, 1730, and 1751 from contemporary documents: *Bulletin of the Seismological Society of America*, v. 102, p. 1639–1653, doi: 10.1785/0120110289.
- U.S. Geological Survey, 2011, Magnitude 8.8 – OFFSHORE BIO-BIO, CHILE 2010 February 27 06:34:14 UTC:
<http://earthquake.usgs.gov/earthquakes/eqinthenews/2010/us2010tfan/us2010tfan.php> (accessed July 2015).
- U.S. Geological Survey, 2014, Earth Explorer SRTM 1 Arc-Second Global:
<http://earthexplorer.usgs.gov> (accessed April 2015).
- Vargas, G., Farías, M., Carretier, S., Tassara, A., Baize, S., and Melnick, D., 2011, Coastal uplift and tsunami effects associated to the 2010 M w 8.8 Maule earthquake in Central Chile: *Andean Geology*, v. 38, p. 219–238.
- Vigny, C., Socquet, A., Peyrat, S., Ruegg, J.-C., Metois, M., Madariaga, R., Morvan, S., Lancieri, M., Lacassin, R., Campos, J., Carrizo, D., Bejar-Pizarro, M., Barrientos, S., Armijo, R., Aranda, C., Valderas-Bermejo, M.-C., Ortega, I., Bondoux F., Baize, S., Lyon-Caen, H., Pavez, A., Vilotte, J. P., Bevis, M., Brooks, B., Smalley, R.,

Parra, H., Baez, J.-C., Blanco, M., Cimbaro, S., and Kendrick, E., 2011, The 2010 Mw 8.8 Maule Megathrust Earthquake of Central Chile, Monitored by GPS: *Science*, v. 332, p. 1417–1421, doi: 10.1126/science.1204132.

Wilson, R.I., Admire, A.R., Borrero, J.C., Dengler, L.A., Legg, M.R., Lynett, P., McCrink, T.P., Miller, K.M., Ritchie, A., Sterling, K., and Whitmore, P.M., 2013, Observations and Impacts from the 2010 Chilean and 2011 Japanese Tsunamis in California (USA): *Pure and Applied Geophysics*, v. 170, p. 1127–1147, doi: 10.1007/s00024-012-0527-z.

Yamazaki, Y., and Cheung, K.F., 2011, Shelf resonance and impact of near-field tsunami generated by the 2010 Chile earthquake: *Geophysical Research Letters*, v. 38, p. L12605, doi: 10.1029/2011GL047508.

Yawsangratt, S., Szczuciński, W., Chaimanee, N., Chatprasert, S., Majewski, W., and Lorenc, S., 2012, Evidence of probable paleotsunami deposits on Kho Khao Island, Phang Nga Province, Thailand: *Natural Hazards*, v. 63, p. 151–163, doi: 10.1007/s11069-011-9729-4.

Yoshii, T., Imamura, M., Matsuyama, M., Koshimura, S., Matsuoka, M., Mas, E., and Jimenez, C., 2013, Salinity in Soils and Tsunami Deposits in Areas Affected by the 2010 Chile and 2011 Japan Tsunamis: *Pure and Applied Geophysics*, v. 170, p. 1047–1066, doi: 10.1007/s00024-012-0530-4.

Yue, H., and Lay, T., 2013, Source rupture models for the Mw 9.0 2011 Tohoku earthquake from joint inversions of high-rate geodetic and seismic data: *Bulletin of the Seismological Society of America*, v. 103, p. 1242–1255, doi: 10.1785/0120120119.

Yue, H., Lay, T., Rivera, L., An, C., Vigny, C., Tong, X., and Báez Soto, J.C., 2014, Localized fault slip to the trench in the 2010 Maule, Chile $M_w = 8.8$ earthquake from joint inversion of high-rate GPS, teleseismic body waves, InSAR, campaign GPS, and tsunami observations: *Journal of Geophysical Research: Solid Earth*, v. 119, p. 7786–7804, doi: 10.1002/2014JB011340.

APPENDIXES

Appendix A

Post-Tsunami Survey Data

Table A1: Original post-tsunami dataset.

Location*	Latitude	Longitude	Citation [#]	ID	Flow Depth (m)	Runup (m)	Inundation (m)	Watermark**
LTN	-34.99680	-72.17820	F	285	4.50			
LTN	-34.99630	-72.17720	F	286		7.60	227.00	
LTS	-35.1073	-72.19915	M	305MB	5.13			
LTS	-35.10733	-72.19921	M	306MB	4.10			
LTS	-35.10736	-72.19927	M	307MB	4.97			
LTS	-35.10986	-72.20124	M	310MB	5.54			
LTS	-35.10967	-72.2009	M	311MB	5.45			
LTS	-35.10964	-72.20082	M	312MB	5.16			
LTS	-35.10943	-72.20079	M	313MB	3.73			
LTS	-35.10945	-72.20066	M	314MB	3.92			
CON	-35.30437	-72.39859	M	318 MB	8.04			branch
CON	-35.30408	-72.39864	M	320MB	5.54			debris
CON	-35.3038	-72.39846	M	321MB	6.89			branches
CON	-35.30441	-72.39864	M	507GG	8.63			broken branch
CON	-35.30418	-72.39867	M	508GG	5.78			broken branch
CON	-35.30407	-72.39852	M	509GG	7.48			broken branch, debris
CON	-35.30383	-72.39853	M	510GG	6.90			broken branch
CON	-35.30362	-72.39858	M	511GG	5.34			broken branch
CON	-35.30552	-72.39904	M	317MB	4.97			branch
CON	-35.30551	-72.39908	M	560GG	4.97			broken branch
CON	-35.30542	-72.39473	M	514GG	1.67			debris in tree
CON	-35.30542	-72.39469	M	515GG	1.75			debris in tree
CON	-35.30511	-72.39499	M	520GG	1.65			debris in tree
CON	-35.3091	-72.3991	M	568GG	6.06			broken branch
CON	-35.30797	-72.40065	M	325MB	5.39			debris
CON	-35.30806	-72.40059	M	326MB	6.79			branch
CON	-35.3083	-72.40092	M	327MB	5.49			debris
CON	-35.30864	-72.40112	M	328MB	7.05			debris, branches
CON	-35.32011	-72.39968	F	27	6.30		121.60	TB
CON	-35.32015	-72.39918	F	28	4.10		167.30	TB
CON	-35.32005	-72.39875	F	29		13.50	205.30	WL, BV
CON	-35.33421	-72.405035	A	66			8.61	
CON	-35.3342	-72.405090	A	67			8.50	

CON	-35.33463	-72.404870	A	68			8.39	
CON	-35.33459	-72.405019	A	69			7.39	
CON	-35.33448	-72.405279	A	70			7.07	
CON	-35.33455	-72.405464	A	71			6.66	
CON	-35.33471	-72.405566	A	72			7.06	
CON	-35.33512	-72.405142	A	73			5.95	
CON	-35.33469	-72.405549	A	74			7.00	
CON	-35.33488	-72.405606	A	75			6.70	
CON	-35.33493	-72.405863	A	76			6.39	
CON	-35.33514	-72.406483	A	77			5.98	
CON	-35.33518	-72.40386	F	45	7.00		10.90	DT, RD
CON	-35.33676	-72.40695	F	49	0.65		337.50	MO
CON	-35.33705	-72.40776	F	50		6.30	417.10	RD
CON	-35.33085	-72.40629	F	12	3.20		19.90	DT
CON	-35.33090	-72.40649	F	13	3.00		33.80	RD, SD
CON	-35.33095	-72.40678	F	14	1.20		57.90	MI
CON	-35.33052	-72.40675	F	15	2.60		51.90	DT, RD
CON	-35.33054	-72.40712	F	16	2.70		80.10	
CON	-35.33078	-72.40777	F	17	2.00		144.70	
CON	-35.33108	-72.40857	F	18	1.60		224.60	
CON	-35.33146	-72.40935	F	19	1.10		307.00	
CON	-35.33184	-72.41004	F	20	0.80		382.00	MO
CON	-35.33191	-72.41053	F	21		7.50	425.20	RD, WL, MO
CON	-35.3283	-72.40703	M	315MB	4.48			branch
CON	-35.32413	-72.408820	A	79			8.15	
CON	-35.32440	-72.40864	F	6	3.50		66.90	DT
CON	-35.32424	-72.40887	F	22	4.20		82.80	DT
CON	-35.32544	-72.40977	F	24	2.60		231.80	MO
CON	-35.32592	-72.41165	F	25	2.20		396.40	MO
CON	-35.32632	-72.41250	F	26		5.70	485.20	RD, WL, MO
CON	-35.32254	-72.40998	F	7	2.30		62.90	DT
CON	-35.32252	-72.41034	F	8	3.10		90.70	TB, RD
CON	-35.32730	-72.42080	F	241	1.33		520.00	MO
CON	-35.3259	-72.425360	A	50		26.16		
CON	-35.32623	-72.42591	F	32	7.90		89.50	TB, RD
CON	-35.32626	-72.42543	F	33		23.20	111.40	WL, RD, BV
CON	-35.32630	-72.42544	F	34		26.20	114.90	WL, RD, BV
CON	-35.32633	-72.42544	F	35		29.00	117.70	WL, RD, BV
CON	-35.32639	-72.42639	F	36		28.00	89.80	WL, RD, BV
CON	-35.32620	-72.42580	F	240		24.09	80.00	WL, RD, BV
CON	-35.32843	-72.42967	F	37		13.20	95.40	WL, RD, BV
CON	-35.33457	-72.43446	F	38		5.80	87.40	WL, RD, BV
CON	-35.35173	-72.38709	F	51	4.20		0.00	RD
CON	-35.35181	-72.38733	F	52		8.50	23.60	WL, RD, BV

CON	-35.36966	-72.34809	F	53	1.00	37.20	MO
CON	-35.37056	-72.34801	F	54		5.10 134.50	WL, RD, BV
CON	-35.35271	-72.44595	F	39		17.10 54.20	WL, RD, BV
CON	-35.35299	-72.44656	F	40		18.80 65.30	WL, RD, BV
CON	-35.35877	-72.455470	A	44		5.90	
CON	-35.35868	-72.455690	A	45		6.91	
CON	-35.35891	-72.45615	F	41	5.80	106.80	DT, RD
CON	-35.35948	-72.45605	F	42	4.10	168.20	DT, RD
CON	-35.35964	-72.45587	F	43	3.50	191.10	DT, RD
CON	-35.35989	-72.45557	F	44		11.30 227.20	WL, RD, BV
COL	-36.52980	-72.95880	F	255		8.49 53.00	WL, RD
COL	-36.53250	-72.95790	F	256	2.60		MO
COL	-36.53820	-72.95950	F	258	2.50		RD
COL	-36.556	-72.9569	M	108MB	6.27		debris
COL	-36.55602	-72.95688	M	109MB	6.02		branch, debris
COL	-36.55608	-72.95693	M	110MB	6.33		debris
COL	-36.55611	-72.957050	A	185		9.22	
COL	-36.55689	-72.9577	M	441GG	5.70		dead vegetation
COL	-36.55774	-72.9575	M	442GG	4.91		dead vegetation
COL	-36.55856	-72.95752	M	443GG	4.51		dead vegetation
COL	-36.55894	-72.95674	M	444GG	6.67		debris in tree
COL	-36.56131	-72.95789	M	448GG	5.07		plastic debris in tree
COL	-36.56142	-72.95759	M	449GG	4.94		broken branches, debris in tree
COL	-36.56232	-72.95621	M	452GG	3.54		water level
COL	-36.5621	-72.95613	M	450GG	3.94		dead vegetation
COL	-36.5602	-72.95904	M	445GG	6.16		vegetation and boat on hillside
COL	-36.56116	-72.95899	M	446GG	6.64		boat and dead grass
COL	-36.56223	-72.95999	M	453GG	5.41		dead grass
COL	-36.56117	-72.95814	M	447GG	5.88		marine vegetation in tree
COL	-36.56193	-72.96056	M	454GG	0.00		wrack line on W valley wall
COL	-36.5603	-72.959565	A	181		8.63	
COL	-36.56044	-72.959665	A	182		9.53	
COL	-36.56069	-72.959889	A	183		9.84	
COL	-36.56366	-72.9582	M	079BR	3.72		
COL	-36.56491	-72.95997	M	455GG	5.32		marine vegetation in tree
COL	-36.565	-72.96001	M	456GG	4.38		marine vegetation in tree

COL	-36.56515	-72.95926	M	457GG	4.96			marine vegetation in tree
COL	-36.565	-72.96001	M	456GG	6.47			trim line on E valley wall
COL	-36.56521	-72.95891	M	458GG	1.74			trim line on E valley wall
COL	-36.56523	-72.95865	M	459GG	0.00			trim line on E valley wall
COL	-36.56476	-72.96159	M	460GG	4.00			dead vegetation on W side of valley
COL	-36.56566	-72.96075	M	463GG	4.94			trim line on E valley wall
COL	-36.56713	-72.96043	M	471GG	4.16			trim line on E valley wall
COL	-36.57016	-72.95549	M	480GG	3.84			debris line
COL	-36.56899	-72.95801	M	474GG	4.38			marine veg in tree
COL	-36.56893	-72.95696	M	475GG	4.12			marine veg in tree
COL	-36.56898	-72.95841	M	473GG	3.98			broken branch, marine debris in tree
COL	-36.56935	-72.95936	M	476GG	3.33			trim line on W valley wall
COL	-36.56992	-72.96001	M	477GG	2.70			trim line on W valley wall
TUB	-37.22586	-73.43676	F	178		6.20	145.10	WL, RD, BV
TUB	-37.22565	-73.43697	F	179		5.90	171.20	WL, RD, BV
TUB	-37.22536	-73.43744	F	180		5.30	213.40	WL, RD, BV
TUB	-37.22441	-73.43876	F	182		5.40	384.30	WL, RD, BV
TUB	-37.22588	-73.43798	F	181	0.90		208.10	TB, BB, RD
TUB	-37.22678	-73.43808	F	183	1.50		122.50	AL, WL, RD
TUB	-37.22634	-73.43881	F	184	0.70		203.40	MI, DT
TUB	-37.22556	-73.44132	F	185		5.40	439.20	WL, RD, BV, BO
TUB	-37.23165	-73.43953	F	187	2.50		263.60	TB, BB, RD
TUB	-37.23184	-73.44007	F	188	1.20		315.50	MI, DT
TUB	-37.23145	-73.44039	F	189	1.10		333.10	MO, DT
TUB	-37.24016	-73.42801	F	162		7.20	117.70	WL, RD, BV
TUB	-37.24009	-73.42923	F	163		8.40	124.70	WL, RD, BV
TUB	-37.23109	-73.44513	F	186		4.40	39.60	WL, RD, BV
TUB	-37.23018	-73.45706	F	190	3.20		9.70	TB, BB, RD
TUB	-37.22904	-73.45708	F	191		3.20	127.70	MI, DT
QUI	-38.24410	-73.47760	F	266		6.47	233.00	WR, RD
QUI	-38.24710	-73.49090	F	267			56.00	OT

QUI	-38.24820	-73.49110	F	268		4.42	175.00	RD
TIR	-38.33466	-73.49636	F	416		13.70	178.40	WL, RD, BV
TIR	-38.33490	-73.49630	F	417		13.10	184.20	WL, RD, BV
TIR	-38.33806	-73.49810	F	415		11.00	121.10	WL, RD, BV
TIR	-38.34251	-73.50384	F	412		18.00	207.40	WL, RD, BV
TIR	-38.34149	-73.50420	F	413		17.20	72.50	WL, RD, BV
TIR	-38.34172	-73.50507	F	414		20.10	71.70	WL, RD, BV
TIR	-38.34270	-73.50140	F	280		15.91	56.00	WL, RD, BV, ER
TIR	-38.34060	-73.49860	F	269	5.00		150.00	BB
TIR	-38.34080	-73.49750	F	271	3.94		239.00	RD, WL
TIR	-38.34120	-73.49690	F	272	2.33		300.00	RD, WL
TIR	-38.34190	-73.49630	F	273	4.25		354.00	BB, RD
TIR	-38.34280	-73.49600	F	274	2.90		418.00	RD
TIR	-38.34370	-73.49510	F	275	3.04		539.00	DT
TIR	-38.34440	-73.49460	F	276	2.10		623.00	DT
TIR	-38.34400	-73.49380	F	277	0.55		652.00	MO
TIR	-38.34370	-73.49280	F	278	0.55		702.00	MO
TIR	-38.34350	-73.49240	F	279		7.88	729.00	MO
CON	-35.33593	-72.40442	F	46	2.20		107.30	RD
CON	-35.33620	-72.40599	F	48	0.95		230.90	MO
CON	-35.33581	-72.40535	F	47	1.20		158.40	MO
COL	-36.55595	-72.95855	M				147.60	
COL	-36.56397	-72.95807	M				732.69	
COL	-36.56456	-72.96179	M				997.38	
COL	-36.55957	-72.95951	M				450.80	
COL	-36.56643	-72.962235	M				1144.27	
COL	-36.56719	-72.95839	M				1087.06	
COL	-36.56986	-72.95381	M				1298.11	
COL	-36.57229	-72.95157	M				1571.17	
CON	-35.30545	-72.39417	M				756.39	
CON	-35.30366	-72.39458	M				731.17	
CON	-35.3037	-72.39656	M				549.82	
LTS	-35.10907	-72.19675	M				454.23	
LTS	-35.1092	-72.192659	M				793.74	
CON	-35.31046	-72.39559	M				731.22	

* Location: La Trinchera North (LTN), La Trinchera South (LTS), Constitución (CON), Coliumo (COL), Tubul (TUB), Quidico (QUI), Tirúa (TIR)

Citation: Fritz et al. (2011) (F), Morton et al. (2011) (M), Annunziato et al. (2010) (A)

** Watermarks from Fritz et al. (2011): wrack line (WL), algae (AL), broken branch (BB), boat (BO), brown vegetation (BV), damaged trimline (DT), mudline inside (MI), mudline outside (MO), overtopped (OT), rafted debris (RD), sediment deposit (SD), tree bark (TB)

Table A2: Condensed post-tsunami dataset.

Location	Latitude	Longitude	Citation	Flow Depth (m)	Runup (m)	Inundation (m)
La Trinchera North	-34.9968	-72.1782	Fritz et al. (2011)	4.5		102*
La Trinchera North	-34.9963	-72.1772	Fritz et al. (2011)		7.6	227
La Trinchera South	-35.107311	-72.199202	Morton et al. (2011)	4.97*		177*
La Trinchera South	-35.109648	-72.20083	Morton et al. (2011)	5.16*		159*
Constitucion	-35.305464	-72.399073	Morton et al. (2011)	5.93*		298*
Constitucion	-35.305285	-72.39479	Morton et al. (2011)	1.67*		700*
Constitucion	-35.3091	-72.3991	Morton et al. (2011)	6.09*		319*
Constitucion	-35.320108	-72.399401	Fritz et al. (2011)	5.2*		144
Constitucion	-35.32005	-72.39875	Fritz et al. (2011)		13.5	205
Constitucion	-35.33518	-72.40386	Fritz et al. (2011)	7		2313*
Constitucion	-35.33676	-72.40695	Fritz et al. (2011)	0.65		2176*
Constitucion	-35.33705	-72.40776	Fritz et al. (2011)		6.3	2152*
Constitucion	-35.330703	-72.40664	Fritz et al. (2011)	2.8*		1709*
Constitucion	-35.33146	-72.40935	Fritz et al. (2011)	1.8*		1630*
Constitucion	-35.33184	-72.41004	Fritz et al. (2011)	0.8		1554*
Constitucion	-35.33191	-72.41053	Fritz et al. (2011)		7.5*	1548*
Constitucion	-35.3283	-72.40703	Morton et al. (2011)	4.48		1479*
Constitucion	-35.324325	-72.408778	Fritz et al. (2011)	3.85*		1034*
Constitucion	-35.325708	-72.410867	Fritz et al. (2011)	2.4*		1038*
Constitucion	-35.32632	-72.4125	Fritz et al. (2011)		5.7	988*
Constitucion	-35.322525	-72.410184	Fritz et al. (2011)	2.7*		804*
Constitucion	-35.327209	-72.420132	Fritz et al. (2011)	1.33		634
Constitucion	-35.3259	-72.42536	Annunziato et al. (2010)		26.16	98*
Constitucion	-35.32623	-72.42591	Fritz et al. (2011)	7.9		90
Constitucion	-35.32843	-72.42967	Fritz et al. (2011)		13.2	95
Constitucion	-35.33457	-72.43446	Fritz et al. (2011)		5.8	87
Constitucion	-35.35173	-72.38709	Fritz et al. (2011)	4.2		4644*
Constitucion	-35.35181	-72.38733	Fritz et al. (2011)		8.5	4628*
Constitucion	-35.36966	-72.34809	Fritz et al. (2011)	1		8102*
Constitucion	-35.37056	-72.34801	Fritz et al. (2011)		5.1	8189*
Constitucion	-35.352831	-72.446292	Fritz et al. (2011)		17.95*	60
Constitucion	-35.359378	-72.455866	Fritz et al. (2011)	4.1*		168
Constitucion	-35.35989	-72.45557	Fritz et al. (2011)		11.3	227
Coliumo	-36.5298	-72.9588	Fritz et al. (2011)		8.49	53
Coliumo	-36.538291	-72.959705	Fritz et al. (2011)	2.5		130
Coliumo	-36.55689	-72.9577	Morton et al. (2011)	5.98*		145*
Coliumo	-36.55894	-72.95674	Morton et al. (2011)	5.69*		244*
Coliumo	-36.5621	-72.95613	Morton et al. (2011)	4.44*		772*
Coliumo	-36.561278	-72.959289	Morton et al. (2011)	6.02*		561*
Coliumo	-72.959708	-36.560474	Morton et al. (2011)		4.76*	535*
Coliumo	-36.565095	-72.959408	Morton et al. (2011)	4.1*		909*
Coliumo	-36.56476	-72.96159	Morton et al. (2011)	4		1051*
Coliumo	-36.566447	-72.960459	Morton et al. (2011)	4.55		1080*

Coliumo	-36.5708	-72.95504	Morton et al. (2011)	0		1414*
Coliumo	-36.57016	-72.95549	Morton et al. (2011)	4.*		1334*
Coliumo	-36.569646	-72.959708	Morton et al. (2011)	3.01*		1401*
Tubul	-37.22556	-73.44132	Fritz et al. (2011)		5.4	439*
Tubul	-37.23184	-73.44007	Fritz et al. (2011)	1.2*		288*
Tubul	-37.24016	-73.42801	Fritz et al. (2011)		7.2	118
Tubul	-37.24009	-73.42923	Fritz et al. (2011)		8.4	125
Tubul	-37.23109	-73.44513	Fritz et al. (2011)		4.4	671*
Tubul	-37.23018	-73.45706	Fritz et al. (2011)	3.2		1701*
Tubul	-37.22904	-73.45708	Fritz et al. (2011)		3.2	1701*
Quidico	-38.2441	-73.4776	Fritz et al. (2011)		6.47	233
Quidico	-38.2471	-73.4909	Fritz et al. (2011)			369*
Quidico	-38.2482	-73.4911	Fritz et al. (2011)		4.42	472*
Tirua	-38.33466	-73.49636	Fritz et al. (2011)		13.7	178
Tirua	-38.3349	-73.4963	Fritz et al. (2011)		13.1	184
Tirua	-38.33806	-73.4981	Fritz et al. (2011)		11	121
Tirua	-38.342059	-73.504494	Fritz et al. (2011)		18*	73*
Tirua	-38.3427	-73.5014	Fritz et al. (2011)		15.91	304*
Tirua	-38.340773	-73.498347	Fritz et al. (2011)	5		274*
Tirua	-73.496141	-38.342306	Fritz et al. (2011)	3.35*		569*
Tirua	-38.343843	-73.493345	Fritz et al. (2011)	1.56*		885*
Tirua	-38.3435	-73.4924	Fritz et al. (2011)		7.88	955*
Constitucion	-35.33581	-72.40535	Fritz et al. (2011)	1.2*		2159*
Coliumo	-36.55595	-72.95855	Morton et al. (2011)			148
Coliumo	-36.55957	-72.95951	Morton et al. (2011)			451
Coliumo	-36.566431	-72.962235	Morton et al. (2011)			1144
Coliumo	-36.57229	-72.95157	Morton et al. (2011)			1571
Constitucion	-35.30366	-72.39458	Morton et al. (2011)			731
Constitucion	-35.3037	-72.39656	Morton et al. (2011)			550
La Trinchera (South)	-35.109203	-72.192659	Morton et al. (2011)			794
Constitucion	-35.31046	-72.39559	Morton et al. (2011)			731

* Flow Depth/Runup modified from original published dataset (Appendix Table A1). Inundation distances estimated from Google Earth.

Appendix B

Tsunami Deposit Data

Table B1: Tsunami deposit descriptions/samples/thicknesses.

Location	Date	Pit ID	Latitude	Longitude	Samples Collected	Notes
La Trinchera	1/13/15	38	-35.10816	-72.20004	38-1 (0-9cm)	Thickness total 21cm. Root zone 0-9cm. Sharp contact with soil.
					38-2 (9-12.5cm)	
					38-3 (12.5-16cm)	
					38-4 (16-21cm)	
					38-5 (21-23.5cm) soil	
La Trinchera	1/13/15	39	-35.10869	-72.19814	39-1 (0-4cm)	Thickness total 18cm. Upper 1cm organic material not decomposed. Most roots through top 2-3cm, fine roots throughout. Soil contact sharp.
					39-2 (4-9cm)	
					39-3 (9-12cm)	
					39-4 (12-18cm)	
					39-5 (18-25cm) soil	
					39-6 (27-35cm) sand	
La Trinchera	1/13/15	40	-35.10927	-72.19686	40-1 (0-1.5cm) soil	Thickness total 5.5cm. Large roots. Uppermost 1.5cm is soil. Sandy soil contact not sharp.
					40-2 (1.5-2.5cm)	
					40-3 (2.5-4cm)	
					40-4 (4-5.5cm)	
					40-5 (5.5-7cm) soil	
La Trinchera	1/13/15	42	-35.10949	-72.19604	42-1 (0-9mm)	Thickness total 9mm. Lat/Long a few meters away from GG545. Difficult to see. Deposit not consistent nearby.
					42-2 (9mm-3cm) soil	
La Trinchera	1/13/15	43	-35.10975	-72.19556	Not sampled	Thickness total 3mm. Difficult to see.
La Trinchera	1/13/15	45	-35.10933	-72.19661	Not sampled	Thickness total 5cm.
La Trinchera	1/13/15	46	-35.10938	-72.19638	46-1 46-2	No notes collected
La Trinchera	1/13/15	47	-35.10941	-72.19613	Not sampled	Variable thickness total 1-2cm.
La Trinchera	1/13/15	48	-35.10948	-72.19608	Not sampled	Thickness total 1.5cm. Upper 0.5cm organic material. 2015 deposit limit.
Constitución	1/14/15	384	-35.30426	-72.40028	384-1 (0-17cm)	1-2cm error in measurement. Sharp contact with soil. Complex sedimentary structures not easily seen/present.
					384-2 (17-32cm)	
					384-3 (32-54cm)	
					384-4 (54-56cm)	
					384-5 (56-62cm)	
Constitución	1/14/15	51	-35.30441	-72.40185	Not sampled	Deposit 2-4cm thick (variable). Very sharp, almost planar, contact with soil.
Coliumo	1/16/15	385	-36.55509	-72.95776	Not sampled	No deposit found.
Coliumo	1/16/15	387	-36.55513	-72.9576	Not sampled	Possible tsunami deposit. 14-21cm thick (variable). Upper 3cm soil. Roots throughout but thicker in upper 7cm.
Coliumo	1/16/15	52	-36.55777	-72.95697	052-1 (bulk)	Deposit 2-3cm thick (variable).
Coliumo	1/16/15	389	-36.55875	-72.95702	Not sampled	Deposit 11cm thick. Upper 2cm dry organic mat.
Coliumo	1/16/15	390	-36.57013	-72.95545	390-1 (0-1.5cm)	Upper 1.5cm dead organics/mud. Uneven contact.
					390-2 (1.5-5.5cm)	
					390-3 (5.5-9cm)	
					390-4 (12-14cm) soil	

Coliumo	1/16/15	391	-36.57005	-72.9567	Not sampled	Deposit 9cm thick. Upper 1.5-2cm (variable) dead organics. Normal grading. Roots throughout. Sharp contact with soil.
Coliumo	1/23/15	84	-36.5623	-72.95623	84-1 (0-7cm) 84-2 (7-11.5cm) 84-3 (11.5-14cm) 84-4 (14-21cm) soil	Variable thickness total 12-14cm. Upper 1.5cm dead organic layer. Normal grading and parallel laminations. Thin roots. Downslope from GG452.
Coliumo	1/23/15	85	-36.56364	-72.95819	85 (bulk)	Variable thickness total 5.5-8.5cm. Upper 1cm dead organic layer. Undulating, sharp soil contact. Normal grading. Thin roots throughout.
Coliumo	1/23/15	86	-36.55841	-72.95794	86-1 (0-4cm) 86-2 (4-7cm)	Variable thickness total 6-7cm. Upper 1cm dead organic layer. Root zone in upper 4cm. Sharp contact with soil.
Coliumo	1/23/15	56	-36.55872	-72.95842	56 (bulk)	Variable thickness total 2-3cm. Within tree roots, difficult to see. Sharp contact with soil. Uneven bottom surface. Highest sand found.
Coliumo	1/23/15	55	-36.55873	-72.95839	55 (bulk)	6cm total thickness. Upper 3cm mud cap. Contact not sharp. Uneven top and bottom surface. Plastic bag at base of deposit.
Tubul	1/21/15	83	-37.22616	-73.44051	83-1 (0-2.25cm) 83-2 (2.25-4.5cm)	6cm total thickness. Upper 1.5-2cm dead organic layer. Possible tsunami deposit.
Quidico	1/19/15	58	-38.25246	-73.49398	58-1 (0-7cm) 58-2 (7-9cm)	Root zone upper 7cm. Flat, sharp contact with soil
Quidico	1/19/15	59	-38.2524	-73.49408	59-1 (0-2.5cm) 59-2 (2.5-3.5cm)	Variable thickness total 2-3.5cm. Roots throughout. Sharp contact with soil. Normal grading.
Quidico	1/19/15	61	-38.25223	-73.4942	61-1 (0-6cm) 61-2 (soil)	Variable thickness total 5-6cm. Roots, some large, throughout. Flat, Sharp contact with soil.
Quidico	1/19/15	62	-38.25216	-73.49438	62 (bulk)	Variable thickness total 0.5-1.5cm. Roots throughout. Difficult to see and sample.
Quidico	1/19/15	63	-38.25211	-73.49453	Not sampled	Surface dusting about 0.5cm total thickness. Within layer of dead organics and roots. Difficult to see.
Quidico	1/19/15	65	-38.25256	-73.49397	65 (bulk)	Variable thickness total 3.9-4.4cm. Upper 4mm algal mat. Roots throughout. Sharp, not flat, soil contact.
Quidico	1/19/15	66	-38.25255	-73.49401	66 (bulk)	Thickness total 4cm. Upper 2cm dead organics. Roots throughout. Not a sharp soil contact, generally flat.
Quidico	1/19/15	67	-38.25168	-73.49369	Not sampled	No deposit found.
Quidico	1/19/15	68	-38.24987	-73.49157	68-1 (1-4cm) 68-2 (4-8cm)	Variable thickness total 6-13. Upper 2cm dry organics. Not a sharp, flat soil contact. Difficult to measure thickness.
Tirúa	1/20/15	69	-38.34525	-73.48961	69-1 (0-3cm) 69-2 (3-7cm) 69-3(7-10cm) 69-4 (10-13cm) soil	Upper 3cm developing soil zone. Sharp soil contact. Roots throughout, with thicker roots at the top.

Tirúa	1/20/15	70	-38.34544	-73.48947	70-1 (0-4cm) 70-2(4-23cm) 70-3 (23-27cm) 70-4 (27-32cm)	Variable thickness total 27-30cm. Sharp, undulating contact with soil. Abundant thick and thin roots throughout.
Tirúa	1/20/15	71	-38.34578	-73.48929	71 071-1 072-2	Upper 3-4.5cm dead organics mat. Total deposit thickness 11cm. Normal graded. Thin roots throughout. Cement piece found within deposit
Tirúa	1/20/15	73	-38.34614	-73.48908	73-1 (0-4.5cm) 73-2(4.5-6.5)	Variable thickness total 4.5-6.5cm. Upper 1.5-2cm dead organics mat. Sharp, undulatory soil contact. More thin than thick roots throughout. Slight visible normal grading.
Tirúa	1/20/15	74	-38.34662	-73.48885	74-1 (0-3cm) 74-2 (3-6.5cm)	Roots throughout. Normal grading. Fine (possibly soil) band from 2-3cm.
Tirúa	1/20/15	75	-38.34692	-73.48863	Not sampled	Total thickness 1cm. Very thin dried organics layer at top. Sandy soil below. Possibly sand mixed with soil.
Tirúa	1/20/15	76	-38.34702	-73.48863	Not sampled	Total thickness 6.5cm. Upper 2cm dead organics and silty. Sharp contact with soil.
Tirúa	1/20/15	77	-38.34733	-73.48837	Not sampled	Total thickness 13cm. Upper 3cm root zone, upper 6cm mixed silty zone. Difficult to determine lower contact with clean soil, soil mixed with sand.
Tirúa	1/20/15	78	-38.34737	-73.48843	Not sampled	Variable thickness total 5-7cm. Upper 1cm dead organics and fine sand. Thin roots throughout. Sandy soil contact with sand pockets.
Tirúa	1/20/15	79	-38.34795	-73.48817	79 (bulk)	Variable thickness total 3-8cm. Upper 1.5cm dead organics. Difficult to determine soil contact by sight.
Tirúa	1/20/15	80	-38.34799	-73.48812	Not sampled	no visible deposit

Table B2: Tsunami deposit grain-size distribution parameters in phi units.

Pit ID	Depth (cm)	Grain Size Percentile (phi)							Avg. Grain-Size	Skew (phi)	Skew
		5	10	16	50	84	90	95			
LAT1 0-1	23-24	2.73	2.53	2.37	1.75	1.14	1.00	0.82	m.sand	-0.02	near symmetrical
LAT1 1-2	22-23	2.63	2.45	2.30	1.74	1.18	1.05	0.88	m.sand	-0.01	near symmetrical
LAT1 2-3	21-22	2.67	2.49	2.34	1.77	1.20	1.06	0.89	m.sand	-0.01	near symmetrical
LAT1 3-4	20-21	2.50	2.31	2.16	1.57	0.99	0.85	0.68	m.sand	-0.01	near symmetrical
LAT1 4-5	19-20	2.37	2.18	2.03	1.46	0.90	0.76	0.44	m.sand	0.02	near symmetrical
LAT1 5-6	18-19	2.43	2.26	2.12	1.59	1.07	0.94	0.76	m.sand	0.00	symmetrical
LAT1 6-7	17-18	2.61	2.42	2.26	1.69	1.13	0.99	0.82	m.sand	-0.01	near symmetrical
LAT1 7-8	16-17	2.67	2.48	2.33	1.76	1.19	1.06	0.89	m.sand	-0.01	near symmetrical
LAT1 8-9	15-16	2.59	2.42	2.28	1.76	1.25	1.12	0.94	m.sand	0.00	symmetrical
LAT1 9-10	14-15	2.60	2.43	2.29	1.76	1.24	1.11	0.93	m.sand	0.00	symmetrical
LAT1 10-11	13-14	2.95	2.73	2.56	1.92	1.30	1.15	0.96	m.sand	-0.02	near symmetrical
LAT1 11-12	12-13	2.82	2.63	2.47	1.90	1.33	1.20	1.03	m.sand	-0.01	near symmetrical
LAT1 12-13	11-12	2.60	2.42	2.28	1.74	1.20	1.07	0.90	m.sand	-0.01	near symmetrical
LAT1 13-14	10-11	2.59	2.41	2.25	1.69	1.12	0.99	0.81	m.sand	-0.01	near symmetrical
LAT1 14-15	9-10	2.56	2.37	2.22	1.64	1.08	0.94	0.75	m.sand	-0.01	near symmetrical
LAT1 15-16	8-9	2.48	2.30	2.16	1.61	1.07	0.93	0.74	m.sand	-0.01	near symmetrical
LAT1 16-17	7-8	2.39	2.22	2.08	1.56	1.04	0.91	0.73	m.sand	0.00	symmetrical
LAT1 17-18	6-7	2.42	2.24	2.09	1.53	0.97	0.84	0.67	m.sand	-0.01	near symmetrical
LAT1 18-19	5-6	2.42	2.24	2.09	1.53	0.96	0.83	0.67	m.sand	-0.01	near symmetrical
LAT1 19-20	4-5	2.41	2.22	2.07	1.51	0.95	0.82	0.66	m.sand	-0.01	near symmetrical
LAT1 20-21	3-4	2.43	2.18	2.10	1.46	0.96	0.77	0.66	m.sand	-0.10	near symmetrical
LAT1 21-22	2-3	2.43	2.25	2.10	1.52	0.96	0.82	0.66	m.sand	-0.01	near symmetrical
LAT1 22-23	1-2	2.40	2.21	2.09	1.49	0.93	0.80	0.63	m.sand	-0.03	near symmetrical
LAT1 23-24	0-1	2.44	2.26	2.11	1.54	0.97	0.84	0.67	m.sand	-0.01	near symmetrical
LAT1 soil	soil	3.21	2.63	2.38	1.64	0.98	0.83	0.65	m.sand	-0.14	negative/coarse
38-1	12-21	2.59	2.40	2.24	1.65	1.07	0.92	0.73	m.sand	-0.01	near symmetrical
38-2	8.5-12	2.70	2.51	2.36	1.77	1.19	1.05	0.88	m.sand	-0.01	near symmetrical
38-3	5-8.5	2.67	2.48	2.33	1.74	1.17	1.03	0.86	m.sand	-0.01	near symmetrical
38-4	0-5	2.45	2.27	2.12	1.55	0.98	0.85	0.68	m.sand	-0.01	near symmetrical
38-5	soil	2.70	2.49	2.32	1.68	1.05	0.89	0.70	m.sand	-0.01	near symmetrical
LAT3 0-1	19-20	2.48	2.30	2.16	1.60	0.95	0.90	0.72	m.sand	0.03	near symmetrical
LAT3 3-4	16-17	2.70	2.53	2.40	1.90	1.39	1.27	1.11	m.sand	0.00	symmetrical
LAT3 8-9	11-12	4.36	2.76	2.49	1.73	1.06	0.90	0.70	m.sand	-0.25	negative/coarse
LAT3 12-13	7-8	2.57	2.38	2.23	1.66	1.09	0.96	0.77	m.sand	-0.01	near symmetrical
LAT3 19-20	0-1	2.35	2.16	2.01	1.44	0.89	0.75	0.58	m.sand	-0.02	near symmetrical
LAT3 soil	soil	3.91	2.87	2.58	1.79	1.13	0.97	0.78	m.sand	-0.22	negative/coarse
39-1	14-18	2.73	2.54	2.39	1.83	1.27	1.13	0.95	m.sand	-0.01	near symmetrical
39-2	9-14	2.81	2.62	2.47	1.90	1.33	1.20	1.02	m.sand	-0.01	near symmetrical
39-3	6-9	2.56	2.38	2.24	1.73	1.21	1.09	0.91	m.sand	-0.01	near symmetrical
39-4	0-6	2.40	2.22	2.07	1.53	0.99	0.86	0.69	m.sand	-0.01	near symmetrical
39-5	soil	4.24	3.40	2.88	1.87	1.13	0.96	0.75	m.sand	-0.26	negative/coarse
39-6	sand	2.62	2.43	2.28	1.70	1.14	1.01	0.83	m.sand	-0.02	near symmetrical
LAT4 top	4-5	6.67	5.48	4.55	2.23	1.47	1.29	1.09	f.sand	-0.55	strong negative/coarse
LAT4 1-2	3-4	2.72	2.54	2.43	1.83	1.28	1.14	0.96	m.sand	-0.02	near symmetrical
LAT4 4-5	0-1	2.79	2.60	2.45	1.89	1.33	1.19	1.01	m.sand	0.00	symmetrical

40-1	4-5.5	4.53	3.11	2.72	1.80	1.00	0.81	0.56	m.sand	-0.22	negative/coarse
40-2	3-4	3.44	2.81	2.58	1.91	1.30	1.15	0.95	m.sand	-0.14	negative/coarse
40-3	1.5-3	2.95	2.65	2.46	1.85	1.27	1.12	0.94	m.sand	-0.06	near symmetrical
40-4	0-1.5	3.96	2.71	2.49	1.83	1.23	1.09	0.90	m.sand	-0.22	negative/coarse
40-5 soil	soil	5.48	4.53	3.79	1.85	0.97	0.78	0.55	m.sand	-0.42	strong negative/coarse
CON2 5-6	75-76	2.24	2.06	1.92	1.37	0.83	0.71	0.54	m.sand	-0.02	near symmetrical
CON2 15-16	65-66	2.41	2.20	2.04	1.43	0.84	0.70	0.53	m.sand	-0.03	near symmetrical
CON2 25-26	55-56	2.22	2.03	1.86	1.26	0.69	0.55	0.38	m.sand	-0.03	near symmetrical
CON2 35-36	45-46	2.10	1.77	1.58	1.03	0.51	0.36	0.13	m.sand	-0.05	near symmetrical
CON2 45-46	35-36	2.03	1.75	1.58	1.05	0.51	0.34	0.05	m.sand	0.00	symmetrical
CON2 55-56	25-26	2.09	1.75	1.55	0.95	0.30	0.08	-0.20	c.sand	0.03	near symmetrical
CON2 65-66	15-16	1.99	1.69	1.49	0.88	0.15	-0.07	-0.33	c.sand	0.07	near symmetrical
CON2 75-76	5-6	1.65	1.39	1.20	0.50	-0.35	-0.51	-0.73	c.sand	0.06	near symmetrical
384-1	45-62	2.15	1.95	1.79	1.18	0.59	0.46	0.30	m.sand	-0.04	near symmetrical
384-2	30-45	2.02	1.70	1.51	0.96	0.36	0.18	-0.11	c.sand	0.02	near symmetrical
384-3	8-30	1.96	1.63	1.43	0.81	-0.01	-0.25	-0.47	c.sand	0.09	near symmetrical
384-4	6-8	2.11	1.72	1.50	0.85	0.05	-0.19	-0.45	c.sand	0.06	near symmetrical
384-5	0-6	1.97	1.69	1.53	1.01	0.50	0.33	0.05	m.sand	0.01	near symmetrical
Q9	1-2	3.31	3.13	2.98	2.43	1.88	1.74	1.55	f.sand	0.00	near symmetrical
Q9	0-1	3.17	2.99	2.86	2.36	1.85	1.71	1.53	f.sand	0.01	near symmetrical
58-1	7-9	3.38	3.13	2.97	2.37	1.78	1.64	1.45	f.sand	-0.03	near symmetrical
58-2	0-7	3.32	3.14	3.00	2.45	1.91	1.77	1.60	f.sand	-0.01	near symmetrical
13-1 a.	8-12	3.22	2.85	2.68	2.05	1.23	0.78	0.03	f.sand	0.20	positive/fine
13-1 b.	0-8	2.51	2.29	2.11	1.06	-0.94	-1.30	-1.72	m.sand	0.22	positive/fine
69-1 a.	7-10	3.48	3.01	2.70	1.84	0.94	0.73	0.40	m.sand	-0.02	near symmetrical
69-1 b.	7-10	3.00	2.67	2.47	1.63	0.20	-0.10	-0.73	m.sand	0.26	positive/fine
69-2	3-7	2.71	2.40	2.04	1.44	-0.24	-0.57	-1.00	m.sand	0.39	strong positive/fine
69-3	0-3	2.70	2.43	2.26	1.65	0.33	-0.02	-0.49	m.sand	0.36	strong positive/fine
13-11	0-6	3.18	2.98	2.81	2.19	1.58	1.43	1.26	f.sand	-0.02	near symmetrical
73-1	4.5-6.5	4.78	3.53	3.18	2.33	1.60	1.42	1.17	f.sand	-0.22	negative/coarse
73-2	0-4.5	3.33	3.00	2.80	2.15	1.55	1.41	1.22	f.sand	-0.07	near symmetrical
13-3	0-25	2.74	2.53	2.40	1.91	1.20	0.81	0.25	m.sand	0.25	positive/fine
70-1 b.	23-27	3.47	3.08	2.86	2.09	1.03	0.74	0.23	f.sand	0.15	positive/fine
70-1 a.	23-27	3.47	3.08	2.84	2.09	1.11	0.74	0.24	f.sand	0.14	positive/fine
70-2	4-23	2.97	2.71	2.54	2.01	1.35	1.09	0.61	f.sand	0.15	positive/fine
70-3	0-4	2.72	2.51	2.38	1.86	1.07	0.66	0.04	m.sand	0.29	positive/fine
70-4 soil	soil	5.99	5.37	4.98	3.95	3.08	2.84	2.54	vf.sand	-0.13	negative/coarse

Grain-size -- c.sand: coarse sand; m.sand: medium sand; f.sand: fine sand; vf.sand: very fine sand

Appendix C
GeoClaw Tsunami Simulation Results

Table C1: Simulated volume and flow depth model results at each site.

Model Name	La Trinchera North (4.5 m)		La Trinchera South (5.1 m)		Constitución (3.48x10 ⁷ m ³)		Coliumo (4.83x10 ⁶ m ³)		Tubul (2.2 m)		Tirúa (5.70x10 ⁶ m ³)	
	Flow Depth (m)	% Difference	Flow Depth (m)	% Difference	Volume (m ³)	% Difference	Volume (m ³)	% Difference	Flow Depth (m)	% Difference	Volume (m ³)	% Difference
Control	0.0	-100	0.36	-93	4.00E+07	+5	5.11E+05	-53	0.47	-78	5.39E+05	-54
Delouis et al. (2010)	2.1	-53	1.7	-66	3.74E+07	+2	1.45E+06	-33	1.6	-25	5.58E+05	-54
Fujii & Satake (2013)	1.0	-77	0.89	-82	2.09E+07	-16	1.74E+06	-29	0.70	-68	9.49E+05	-45
Hayes (2010)	0.07	-98	0.56	-89	2.15E+07	-15	9.39E+05	-42	1.8	-17	2.68E+05	-64
Lorito et al. (2011)	1.3	-71	1.3	-74	4.51E+07	+9	2.16E+06	-23	1.4	-35	1.45E+06	-37
Shao et al. (2010)	0.0	-100	0.58	-89	4.17E+06	-51	8.91E+05	-43	2.2	+1	2.79E+05	-63
Sladen (2010)	0.0	-100	0.65	-87	7.15E+06	-41	5.50E+05	-52	0.04	-98	2.12E+05	-67
Vigny et al. (2011)	0.83	-82	0.43	-91	4.01E+06	-51	2.22E+06	-23	1.5	-30	2.86E+05	-63
Yue et al. (2014)	4.8	+7	4.3	-15	2.91E+07	-6	1.30E+06	-35	2.3	+3	6.57E+05	-51
<u>Method 1</u>												
Method 1	2.2	-51	1.8	-65	2.53E+07	-10	1.56E+06	-31	4.8	+120	1.43E+06	-37
Increase 5m	3.0	-33	3.0	-40	4.07E+07	5	1.64E+06	-30	6.3	+187	2.60E+06	-23
Increase 2.5m	2.6	-42	2.4	-53	3.27E+07	-2	1.59E+06	-31	5.8	+163	1.67E+06	-34
Reduce 5m	1.2	-72	0.68	-87	1.23E+07	-29	1.30E+06	-36	1.7	-23	4.47E+05	-57
Reduce 2.5m	1.7	-61	1.2	-76	1.85E+07	-19	1.41E+06	-34	3.3	+52	8.08E+05	-48
Composite	3.0	-34	2.8	-44	3.73E+07	2	2.17E+06	-23	8.3	+278	4.03E+06	-11
<u>Method 2</u>												
Method 2	2.2	-50	1.8	-64	2.99E+07	-5	1.36E+06	-35	0.67	-69	1.66E+06	-34
Increase 5m	3.1	-32	3.1	-39	4.58E+07	10	1.54E+06	-32	1.2	-46	3.16E+06	-18
Increase 2.5m	2.6	-41	2.4	-52	3.77E+07	3	1.36E+06	-34	0.78	-64	2.02E+06	-29
Increase 5m & 2.5m	2.3	-50	1.8	-64	3.70E+07	2	1.32E+06	-35	1.0	-54	2.02E+06	-29
Increase 5m shallow	1.5	-67	0.73	-86	2.86E+07	-6	1.40E+06	-34	0.93	-58	1.42E+06	-37

Appendix D

Slip Distribution Parameters

Table D1: Control parameters.

Latitude	Longitude	Depth (km)	Length (km)	Width (km)	Strike	Dip	Rake	Slip (m)
-35.949025	-73.634425	0	600	150	16	14	104	5

Table D2: Delouis et al. (2010) parameters.

Latitude	Longitude	Depth (km)	Length (km)	Width (km)	Strike	Dip	Rake	Slip (m)
-39.001	-72.138	81.08	40	40	15	18	111	0.43
-38.652	-72.023	81.08	40	40	15	18	102	0.91
-38.304	-71.908	81.08	40	40	15	18	112	0.03
-37.956	-71.794	81.08	40	40	15	18	112	0.03
-37.608	-71.679	81.08	40	40	15	18	114	1.14
-37.259	-71.564	81.08	40	40	15	18	106	1.13
-36.911	-71.45	81.08	40	40	15	18	107	0.23
-36.563	-71.335	81.08	40	40	15	18	109	0.14
-36.215	-71.22	81.08	40	40	15	18	105	0.03
-35.867	-71.106	81.08	40	40	15	18	100	1.13
-35.518	-70.991	81.08	40	40	15	18	104	1.1
-35.17	-70.877	81.08	40	40	15	18	104	0.05
-34.822	-70.762	81.08	40	40	15	18	100	0.57
-34.474	-70.647	81.08	40	40	15	18	107	0.03
-34.125	-70.533	81.08	40	40	15	18	115	0.36
-33.777	-70.418	81.08	40	40	15	18	115	0.03
-33.429	-70.303	81.08	40	40	15	18	116	0.03
-33.081	-70.189	81.08	40	40	15	18	109	0.03
-38.912	-72.545	68.72	40	40	15	18	105	0.03
-38.564	-72.43	68.72	40	40	15	18	116	0.03
-38.215	-72.315	68.72	40	40	15	18	113	0.03
-37.867	-72.201	68.72	40	40	15	18	103	0.03
-37.519	-72.086	68.72	40	40	15	18	108	0.03
-37.171	-71.971	68.72	40	40	15	18	102	0.04
-36.822	-71.857	68.72	40	40	15	18	103	0.84
-36.474	-71.742	68.72	40	40	15	18	100	0.04
-36.126	-71.627	68.72	40	40	15	18	114	0.03
-35.778	-71.513	68.72	40	40	15	18	104	0.03
-35.43	-71.398	68.72	40	40	15	18	106	0.03
-35.081	-71.283	68.72	40	40	15	18	101	0.04
-34.733	-71.169	68.72	40	40	15	18	103	0.03
-34.385	-71.054	68.72	40	40	15	18	120	0.03
-34.037	-70.939	68.72	40	40	15	18	118	0.39
-33.688	-70.825	68.72	40	40	15	18	104	0.03

-33.34	-70.71	68.72	40	40	15	18	100	0.19
-32.992	-70.596	68.72	40	40	15	18	118	0.03
-38.823	-72.952	56.36	40	40	15	18	114	0.9
-38.475	-72.837	56.36	40	40	15	18	110	0.03
-38.127	-72.722	56.36	40	40	15	18	118	0.03
-37.778	-72.608	56.36	40	40	15	18	106	0.03
-37.43	-72.493	56.36	40	40	15	18	107	0.03
-37.082	-72.378	56.36	40	40	15	18	111	0.03
-36.734	-72.264	56.36	40	40	15	18	117	0.03
-36.385	-72.149	56.36	40	40	15	18	120	0.85
-36.037	-72.034	56.36	40	40	15	18	120	2.05
-35.689	-71.92	56.36	40	40	15	18	118	0.03
-35.341	-71.805	56.36	40	40	15	18	116	0.03
-34.993	-71.69	56.36	40	40	15	18	110	0.03
-34.644	-71.576	56.36	40	40	15	18	110	0.03
-34.296	-71.461	56.36	40	40	15	18	117	0.03
-33.948	-71.346	56.36	40	40	15	18	103	0.03
-33.6	-71.232	56.36	40	40	15	18	106	0.03
-33.251	-71.117	56.36	40	40	15	18	104	0.03
-32.903	-71.002	56.36	40	40	15	18	117	0.03
-38.734	-73.359	44	40	40	15	18	113	0.6
-38.386	-73.244	44	40	40	15	18	118	2.85
-38.038	-73.129	44	40	40	15	18	118	0.99
-37.69	-73.015	44	40	40	15	18	109	0.04
-37.341	-72.9	44	40	40	15	18	100	0.58
-36.993	-72.785	44	40	40	15	18	100	0.98
-36.645	-72.671	44	40	40	15	18	120	3.48
-36.297	-72.556	44	40	40	15	18	120	5.86
-35.949	-72.441	44	40	40	15	18	120	0.92
-35.6	-72.327	44	40	40	15	18	120	2.36
-35.252	-72.212	44	40	40	15	18	118	0.64
-34.904	-72.097	44	40	40	15	18	120	3.33
-34.556	-71.983	44	40	40	15	18	115	3.93
-34.207	-71.868	44	40	40	15	18	100	5.62
-33.859	-71.753	44	40	40	15	18	100	1.6
-33.511	-71.639	44	40	40	15	18	114	0.03

-33.163	-71.524	44	40	40	15	18	116	0.03
-32.815	-71.409	44	40	40	15	18	100	0.03
-38.646	-73.766	31.64	40	40	15	18	118	0.89
-38.297	-73.651	31.64	40	40	15	18	120	2.21
-37.949	-73.536	31.64	40	40	15	18	120	4.88
-37.601	-73.422	31.64	40	40	15	18	100	3.4
-37.253	-73.307	31.64	40	40	15	18	100	5.05
-36.904	-73.192	31.64	40	40	15	18	102	10.6
-36.556	-73.078	31.64	40	40	15	18	117	6.65
-36.208	-72.963	31.64	40	40	15	18	112	3.76
-35.86	-72.848	31.64	40	40	15	18	110	4.25
-35.512	-72.734	31.64	40	40	15	18	109	10.7
-35.163	-72.619	31.64	40	40	15	18	100	14.1
-34.815	-72.504	31.64	40	40	15	18	106	21.3
-34.467	-72.39	31.64	40	40	15	18	103	11.5
-34.119	-72.275	31.64	40	40	15	18	100	6.29
-33.77	-72.16	31.64	40	40	15	18	105	0.03
-33.422	-72.046	31.64	40	40	15	18	108	0.03
-33.074	-71.931	31.64	40	40	15	18	114	0.03
-32.726	-71.816	31.64	40	40	15	18	100	0.03
-38.557	-74.173	19.28	40	40	15	18	111	0.23
-38.209	-74.058	19.28	40	40	15	18	117	1.62
-37.86	-73.943	19.28	40	40	15	18	100	5.32
-37.512	-73.829	19.28	40	40	15	18	117	3.19
-37.164	-73.714	19.28	40	40	15	18	107	8.98
-36.816	-73.599	19.28	40	40	15	18	105	12.7
-36.467	-73.485	19.28	40	40	15	18	100	3.13
-36.119	-73.37	19.28	40	40	15	18	100	7.85
-35.771	-73.255	19.28	40	40	15	18	100	4.39
-35.423	-73.141	19.28	40	40	15	18	104	11.1
-35.075	-73.026	19.28	40	40	15	18	100	6.13
-34.726	-72.911	19.28	40	40	15	18	120	1.03
-34.378	-72.797	19.28	40	40	15	18	119	0.96
-34.03	-72.682	19.28	40	40	15	18	106	1.28
-33.682	-72.567	19.28	40	40	15	18	108	1.07
-33.333	-72.453	19.28	40	40	15	18	102	0.03

-32.985	-72.338	19.28	40	40	15	18	119	0.03
-32.637	-72.223	19.28	40	40	15	18	118	0.03
-38.468	-74.579	6.918	40	40	15	18	113	0.03
-38.12	-74.465	6.918	40	40	15	18	113	0.03
-37.772	-74.35	6.918	40	40	15	18	104	0.04
-37.423	-74.236	6.918	40	40	15	18	110	0.03
-37.075	-74.121	6.918	40	40	15	18	105	0.03
-36.727	-74.006	6.918	40	40	15	18	101	0.84
-36.379	-73.892	6.918	40	40	15	18	115	2.35
-36.031	-73.777	6.918	40	40	15	18	120	2.09
-35.682	-73.662	6.918	40	40	15	18	105	1.93
-35.334	-73.548	6.918	40	40	15	18	119	4.77
-34.986	-73.433	6.918	40	40	15	18	103	0.21
-34.638	-73.318	6.918	40	40	15	18	111	1.95
-34.289	-73.204	6.918	40	40	15	18	100	3.26
-33.941	-73.089	6.918	40	40	15	18	100	3.98
-33.593	-72.974	6.918	40	40	15	18	100	1.42
-33.245	-72.86	6.918	40	40	15	18	112	0.03
-32.897	-72.745	6.918	40	40	15	18	107	0.03
-32.548	-72.63	6.918	40	40	15	18	113	0.03

Table D3: Fujii and Satake (2013) parameters.

Latitude	Longitude	Depth (km)	Length (km)	Width (km)	Strike	Dip	Rake	Slip (m)
-37.7838531	-74.6215876	0	50	50	16	14	104	0
-37.3505935	-74.4701223	0	50	50	16	14	104	0
-36.9173239	-74.3186375	0	50	50	16	14	104	0
-36.4840643	-74.1671531	0	50	50	16	14	104	2.24
-36.0507947	-74.0156496	0	50	50	16	14	104	0
-35.6175351	-73.864147	0	50	50	16	14	104	1.32
-35.1842654	-73.7126256	0	50	50	16	14	104	3.94
-34.7510058	-73.5611056	0	50	50	16	14	104	4.69
-34.3177362	-73.409567	0	50	50	16	14	104	2.11
-33.8844766	-73.2580302	0	50	50	16	14	104	0
-33.4512069	-73.1064753	0	50	50	16	14	104	0
-33.0179473	-72.9549224	0	50	50	16	14	104	0
-37.908093	-74.0916354	12.1	50	50	16	14	104	4.73
-37.4748234	-73.9401629	12.1	50	50	16	14	104	4.21
-37.0415638	-73.7886908	12.1	50	50	16	14	104	4.85
-36.6082942	-73.6371992	12.1	50	50	16	14	104	7.33
-36.1750346	-73.4857082	12.1	50	50	16	14	104	0.2
-35.7417649	-73.3341982	12.1	50	50	16	14	104	1.92
-35.3085053	-73.1826893	12.1	50	50	16	14	104	7.38
-34.8752357	-73.0311617	12.1	50	50	16	14	104	10.06
-34.4419761	-72.8796356	12.1	50	50	16	14	104	5.23
-34.0087065	-72.7280912	12.1	50	50	16	14	104	0.14
-33.5754468	-72.5765486	12.1	50	50	16	14	104	0.2
-33.1421772	-72.4249979	12.1	50	50	16	14	104	0
-38.0323229	-73.5616723	24.2	50	50	16	14	104	4.65
-37.5990633	-73.4102127	24.2	50	50	16	14	104	11.18
-37.1657937	-73.2587334	24.2	50	50	16	14	104	5.79
-36.7325341	-73.1072544	24.2	50	50	16	14	104	1.36
-36.2992644	-72.9557561	24.2	50	50	16	14	104	4.38
-35.8660048	-72.8042587	24.2	50	50	16	14	104	0
-35.4327352	-72.6527424	24.2	50	50	16	14	104	5.41
-34.9994756	-72.5012272	24.2	50	50	16	14	104	22.22
-34.566216	-72.3496935	24.2	50	50	16	14	104	13.38
-34.1329463	-72.1981615	24.2	50	50	16	14	104	6.08
-33.6996867	-72.0466212	24.2	50	50	16	14	104	0
-33.2664171	-71.8950628	24.2	50	50	16	14	104	0

Table D4: Hayes (2010) parameters.

Latitude	Longitude	Depth (km)	Length (km)	Width (km)	Strike	Dip	Rake	Slip (m)
-37.679	-74.5829	2.8622	30	20	17.5	18	129.4659	5.91764
-37.4215	-74.4828	2.8622	30	20	17.5	18	117.8459	250.1644
-37.164	-74.3826	2.8622	30	20	17.5	18	120.7814	307.6412
-36.9065	-74.2824	2.8622	30	20	17.5	18	130.0279	147.5491
-36.6491	-74.1823	2.8622	30	20	17.5	18	99.48671	125.7285
-36.3916	-74.0821	2.8622	30	20	17.5	18	86.90758	259.0986
-36.1341	-73.982	2.8622	30	20	17.5	18	83.11176	288.40189
-35.8766	-73.8818	2.8622	30	20	17.5	18	83.10876	291.63391
-35.6191	-73.7816	2.8622	30	20	17.5	18	82.79553	252.60181
-35.3616	-73.6815	2.8622	30	20	17.5	18	106.2142	164.1721
-35.1042	-73.5813	2.8622	30	20	17.5	18	89.86546	64.77453
-34.8467	-73.4812	2.8622	30	20	17.5	18	120.148	11.58376
-34.5892	-73.381	2.8622	30	20	17.5	18	130.2388	14.14916
-34.3317	-73.2809	2.8622	30	20	17.5	18	99.79929	16.52921
-34.0742	-73.1807	2.8622	30	20	17.5	18	129.9377	82.93747
-33.8167	-73.0805	2.8622	30	20	17.5	18	99.08452	247.0067
-33.5593	-72.9804	2.8622	30	20	17.5	18	112.7178	149.44
-33.3018	-72.8802	2.8622	30	20	17.5	18	101.8105	8.11135
-37.7305	-74.3815	9.0426	30	20	17.5	18	128.0216	8.4379
-37.473	-74.2813	9.0426	30	20	17.5	18	89.57764	66.66985
-37.2155	-74.1812	9.0426	30	20	17.5	18	87.43345	30.20486
-36.958	-74.081	9.0426	30	20	17.5	18	94.77892	28.27766
-36.7005	-73.9809	9.0426	30	20	17.5	18	87.11237	281.6051
-36.443	-73.8807	9.0426	30	20	17.5	18	91.44271	653.35919
-36.1856	-73.7805	9.0426	30	20	17.5	18	90.70399	855.2312
-35.9281	-73.6804	9.0426	30	20	17.5	18	98.75188	857.58948
-35.6706	-73.5802	9.0426	30	20	17.5	18	96.25528	879.66589
-35.4131	-73.4801	9.0426	30	20	17.5	18	97.69676	689.27771
-35.1556	-73.3799	9.0426	30	20	17.5	18	99.47742	513.8136
-34.8981	-73.2798	9.0426	30	20	17.5	18	101.6845	500.88589
-34.6407	-73.1796	9.0426	30	20	17.5	18	85.60384	487.2988
-34.3832	-73.0794	9.0426	30	20	17.5	18	95.68392	385.80981
-34.1257	-72.9793	9.0426	30	20	17.5	18	110.2655	217.8663
-33.8682	-72.8791	9.0426	30	20	17.5	18	119.685	79.40733
-33.6107	-72.779	9.0426	30	20	17.5	18	90.35181	106.3975
-33.3532	-72.6788	9.0426	30	20	17.5	18	141.2239	5.41658

-37.7819	-74.1801	15.223	30	20	17.5	18	126.8061	1.85867
-37.5244	-74.0799	15.223	30	20	17.5	18	112.068	17.99608
-37.267	-73.9798	15.223	30	20	17.5	18	113.0278	6.28698
-37.0095	-73.8796	15.223	30	20	17.5	18	86.61698	36.8209
-36.752	-73.7795	15.223	30	20	17.5	18	117.8721	354.16989
-36.4945	-73.6793	15.223	30	20	17.5	18	121.6406	800.75928
-36.237	-73.5791	15.223	30	20	17.5	18	106.2371	976.89502
-35.9795	-73.479	15.223	30	20	17.5	18	109.9181	1061.674
-35.7221	-73.3788	15.223	30	20	17.5	18	107.7594	1018.398
-35.4646	-73.2787	15.223	30	20	17.5	18	91.36826	887.75031
-35.2071	-73.1785	15.223	30	20	17.5	18	91.42039	798.94592
-34.9496	-73.0783	15.223	30	20	17.5	18	100.4478	935.97083
-34.6921	-72.9782	15.223	30	20	17.5	18	85.47787	1091.33
-34.4347	-72.878	15.223	30	20	17.5	18	97.9896	843.68488
-34.1772	-72.7779	15.223	30	20	17.5	18	82.77827	409.55151
-33.9197	-72.6777	15.223	30	20	17.5	18	134.2637	143.62959
-33.6622	-72.5776	15.223	30	20	17.5	18	98.48377	120.699
-33.4047	-72.4774	15.223	30	20	17.5	18	120.4204	2.21355
-37.8334	-73.9787	21.403	30	20	17.5	18	126.1778	5.61497
-37.5759	-73.8785	21.403	30	20	17.5	18	138.6276	7.24198
-37.3184	-73.7784	21.403	30	20	17.5	18	115.2853	0.3239
-37.061	-73.6782	21.403	30	20	17.5	18	133.5317	34.74867
-36.8035	-73.578	21.403	30	20	17.5	18	137.6994	363.94449
-36.546	-73.4779	21.403	30	20	17.5	18	140.1117	807.65942
-36.2885	-73.3777	21.403	30	20	17.5	18	121.2362	853.39862
-36.031	-73.2776	21.403	30	20	17.5	18	129.0067	1033.8669
-35.7735	-73.1774	21.403	30	20	17.5	18	116.7185	991.26819
-35.5161	-73.0773	21.403	30	20	17.5	18	105.3471	770.44019
-35.2586	-72.9771	21.403	30	20	17.5	18	105.4579	859.27692
-35.0011	-72.8769	21.403	30	20	17.5	18	103.2319	1026.547
-34.7436	-72.7768	21.403	30	20	17.5	18	103.4418	1322.392
-34.4861	-72.6766	21.403	30	20	17.5	18	117.7504	1141.415
-34.2286	-72.5765	21.403	30	20	17.5	18	101.5667	576.69769
-33.9712	-72.4763	21.403	30	20	17.5	18	93.49589	350.79639
-33.7137	-72.3761	21.403	30	20	17.5	18	84.48014	241.59911
-33.4562	-72.276	21.403	30	20	17.5	18	139.6204	0.82856
-37.8849	-73.7773	27.584	30	20	17.5	18	130.7799	5.30474
-37.6274	-73.6771	27.584	30	20	17.5	18	139.2314	151.5611
-37.3699	-73.577	27.584	30	20	17.5	18	135.5737	142.3295

-37.1124	-73.4768	27.584	30	20	17.5	18	114.7163	47.54208
-36.8549	-73.3766	27.584	30	20	17.5	18	136.5127	182.62199
-36.5975	-73.2765	27.584	30	20	17.5	18	98.29987	354.11719
-36.34	-73.1763	27.584	30	20	17.5	18	102.9217	761.85663
-36.0825	-73.0762	27.584	30	20	17.5	18	113.0086	1041.118
-35.825	-72.976	27.584	30	20	17.5	18	108.1822	1068.875
-35.5675	-72.8758	27.584	30	20	17.5	18	114.608	742.37433
-35.31	-72.7757	27.584	30	20	17.5	18	112.2047	744.68982
-35.0526	-72.6755	27.584	30	20	17.5	18	95.3312	965.93079
-34.7951	-72.5754	27.584	30	20	17.5	18	106.2642	1333.391
-34.5376	-72.4752	27.584	30	20	17.5	18	119.8135	1236.552
-34.2801	-72.375	27.584	30	20	17.5	18	107.8542	691.79523
-34.0226	-72.2749	27.584	30	20	17.5	18	98.14899	495.91959
-33.7651	-72.1747	27.584	30	20	17.5	18	83.21251	308.17471
-33.5077	-72.0746	27.584	30	20	17.5	18	131.2081	2.81045
-37.9364	-73.5759	33.764	30	20	17.5	18	86.2551	1.43595
-37.6789	-73.4757	33.764	30	20	17.5	18	129.613	275.4556
-37.4214	-73.3755	33.764	30	20	17.5	18	133.6361	352.52081
-37.1639	-73.2754	33.764	30	20	17.5	18	124.8307	326.34369
-36.9064	-73.1752	33.764	30	20	17.5	18	105.6434	240.19479
-36.6489	-73.0751	33.764	30	20	17.5	18	93.5866	296.24661
-36.3915	-72.9749	33.764	30	20	17.5	18	103.1482	778.70569
-36.134	-72.8747	33.764	30	20	17.5	18	97.34324	1142.251
-35.8765	-72.7746	33.764	30	20	17.5	18	98.89584	1022.542
-35.619	-72.6744	33.764	30	20	17.5	18	128.4554	673.98102
-35.3615	-72.5743	33.764	30	20	17.5	18	111.5355	422.09439
-35.104	-72.4741	33.764	30	20	17.5	18	90.43279	566.18628
-34.8466	-72.374	33.764	30	20	17.5	18	102.5077	902.83893
-34.5891	-72.2738	33.764	30	20	17.5	18	98.23479	995.85779
-34.3316	-72.1736	33.764	30	20	17.5	18	83.54255	444.10681
-34.0741	-72.0735	33.764	30	20	17.5	18	90.95366	404.06119
-33.8166	-71.9733	33.764	30	20	17.5	18	84.97417	218.11481
-33.5591	-71.8732	33.764	30	20	17.5	18	135.5646	4.27308
-37.9878	-73.3745	39.944	30	20	17.5	18	101.6867	5.60655
-37.7303	-73.2743	39.944	30	20	17.5	18	117.4681	212.77699
-37.4729	-73.1741	39.944	30	20	17.5	18	103.3072	460.8248
-37.2154	-73.074	39.944	30	20	17.5	18	120.3199	523.15649
-36.9579	-72.9738	39.944	30	20	17.5	18	117.0231	356.9223
-36.7004	-72.8737	39.944	30	20	17.5	18	120.4408	370.12549

-36.4429	-72.7735	39.944	30	20	17.5	18	102.1076	844.40057
-36.1854	-72.6733	39.944	30	20	17.5	18	95.50404	1462.165
-35.928	-72.5732	39.944	30	20	17.5	18	108.0257	1261.7111
-35.6705	-72.473	39.944	30	20	17.5	18	124.9634	527.70142
-35.413	-72.3729	39.944	30	20	17.5	18	91.40468	373.24481
-35.1555	-72.2727	39.944	30	20	17.5	18	102.1091	303.31381
-34.898	-72.1725	39.944	30	20	17.5	18	115.143	702.9906
-34.6405	-72.0724	39.944	30	20	17.5	18	102.6736	911.92517
-34.3831	-71.9722	39.944	30	20	17.5	18	95.70218	663.30103
-34.1256	-71.8721	39.944	30	20	17.5	18	106.5739	575.47052
-33.8681	-71.7719	39.944	30	20	17.5	18	82.70718	274.46909
-33.6106	-71.6718	39.944	30	20	17.5	18	129.555	2.00173
-38.0393	-73.173	46.125	30	20	17.5	18	94.59487	2.65252
-37.7818	-73.0729	46.125	30	20	17.5	18	135.7031	234.2968
-37.5243	-72.9727	46.125	30	20	17.5	18	130.3899	401.85818
-37.2668	-72.8726	46.125	30	20	17.5	18	133.1926	450.85239
-37.0094	-72.7724	46.125	30	20	17.5	18	99.09406	359.3685
-36.7519	-72.6722	46.125	30	20	17.5	18	136.5498	241.7086
-36.4944	-72.5721	46.125	30	20	17.5	18	101.5861	476.14011
-36.2369	-72.4719	46.125	30	20	17.5	18	88.8748	912.84528
-35.9794	-72.3718	46.125	30	20	17.5	18	116.4047	898.31079
-35.722	-72.2716	46.125	30	20	17.5	18	142.2165	581.50159
-35.4645	-72.1715	46.125	30	20	17.5	18	118.3906	286.29761
-35.207	-72.0713	46.125	30	20	17.5	18	129.0115	157.259
-34.9495	-71.9711	46.125	30	20	17.5	18	141.7505	414.95721
-34.692	-71.871	46.125	30	20	17.5	18	107.3198	616.35999
-34.4345	-71.7708	46.125	30	20	17.5	18	119.3085	746.11011
-34.1771	-71.6707	46.125	30	20	17.5	18	123.6602	526.58942
-33.9196	-71.5705	46.125	30	20	17.5	18	82.55672	250.40289
-33.6621	-71.4703	46.125	30	20	17.5	18	114.754	1.42313
-38.0908	-72.9716	52.305	30	20	17.5	18	133.9718	2.79769
-37.8333	-72.8715	52.305	30	20	17.5	18	141.6785	231.24229
-37.5758	-72.7713	52.305	30	20	17.5	18	113.6974	304.64359
-37.3183	-72.6712	52.305	30	20	17.5	18	107.4049	365.1478
-37.0608	-72.571	52.305	30	20	17.5	18	118.0001	196.79221
-36.8034	-72.4708	52.305	30	20	17.5	18	106.483	109.2547
-36.5459	-72.3707	52.305	30	20	17.5	18	141.9411	117.6683
-36.2884	-72.2705	52.305	30	20	17.5	18	112.7818	237.22479
-36.0309	-72.1704	52.305	30	20	17.5	18	115.8728	355.6167

-35.7734	-72.0702	52.305	30	20	17.5	18	111.6662	257.8967
-35.5159	-71.97	52.305	30	20	17.5	18	94.06551	211.5295
-35.2585	-71.8699	52.305	30	20	17.5	18	92.69079	3.6425
-35.001	-71.7697	52.305	30	20	17.5	18	98.94059	74.23933
-34.7435	-71.6696	52.305	30	20	17.5	18	96.86476	288.71201
-34.486	-71.5694	52.305	30	20	17.5	18	120.3682	365.96579
-34.2285	-71.4692	52.305	30	20	17.5	18	133.6014	271.54031
-33.971	-71.3691	52.305	30	20	17.5	18	82.57005	201.3681
-33.7136	-71.2689	52.305	30	20	17.5	18	136.7124	5.90037
-38.1422	-72.7702	58.485	30	20	17.5	18	85.88792	7.55016
-37.8848	-72.6701	58.485	30	20	17.5	18	126.3063	1.96626
-37.6273	-72.5699	58.485	30	20	17.5	18	91.38926	0.60387
-37.3698	-72.4697	58.485	30	20	17.5	18	121.5443	5.62837
-37.1123	-72.3696	58.485	30	20	17.5	18	123.0498	9.06247
-36.8548	-72.2694	58.485	30	20	17.5	18	124.6193	0.87394
-36.5973	-72.1693	58.485	30	20	17.5	18	91.98961	3.38494
-36.3399	-72.0691	58.485	30	20	17.5	18	103.5942	3.33964
-36.0824	-71.9689	58.485	30	20	17.5	18	126.4125	2.0065
-35.8249	-71.8688	58.485	30	20	17.5	18	114.6953	9.01019
-35.5674	-71.7686	58.485	30	20	17.5	18	126.6657	3.98212
-35.3099	-71.6685	58.485	30	20	17.5	18	137.13	7.19575
-35.0525	-71.5683	58.485	30	20	17.5	18	115.9971	6.59061
-34.795	-71.4682	58.485	30	20	17.5	18	94.57927	7.46006
-34.5375	-71.368	58.485	30	20	17.5	18	102.8947	7.03195
-34.28	-71.2678	58.485	30	20	17.5	18	86.44215	6.49726
-34.0225	-71.1677	58.485	30	20	17.5	18	91.81796	6.85666
-33.765	-71.0675	58.485	30	20	17.5	18	90.08573	0.21374

Table D5: Lorito et al. (2011) parameters.

Latitude	Longitude	Depth (km)	Length (km)	Width (km)	Strike	Dip	Rake	Slip (m)
-38.931	-72.787	63.022	25	25	16.031	22	110	2
-38.877	-73.047	53.657	25	25	16.031	22	110	2
-38.82	-73.307	44.597	25	25	16.031	21	110	2
-38.766	-73.567	35.842	25	25	16.031	21	110	3
-38.709	-73.837	28.019	25	25	16.031	16	110	3
-38.651	-74.097	21.128	25	25	16.031	16	110	1
-38.593	-74.377	15.512	25	25	16.031	10	110	0
-38.534	-74.647	11.171	25	25	16.031	10	110	0
-38.723	-72.71	63.022	25	25	19.349	22	110	1
-38.668	-72.97	53.657	25	25	19.349	22	110	3
-38.613	-73.23	44.597	25	25	19.349	21	110	2
-38.557	-73.49	35.842	25	25	19.349	21	110	1
-38.5	-73.75	28.019	25	25	19.349	16	110	3
-38.443	-74.02	21.128	25	25	19.349	16	110	1
-38.384	-74.29	15.512	25	25	19.349	10	110	2
-38.326	-74.56	11.171	25	25	19.349	10	110	0
-38.493	-72.633	63.022	25	25	12.014	22	110	1
-38.438	-72.893	53.657	25	25	12.014	22	110	1
-38.383	-73.153	44.597	25	25	12.014	21	110	3
-38.327	-73.403	35.842	25	25	12.014	21	110	3
-38.27	-73.673	28.019	25	25	12.014	16	110	4
-38.213	-73.943	21.128	25	25	12.014	16	110	1
-38.154	-74.213	15.512	25	25	12.014	10	110	1
-38.096	-74.483	11.171	25	25	12.014	10	110	1
-38.258	-72.601	63.022	25	25	4.649	22	110	0
-38.202	-72.861	53.657	25	25	4.649	22	110	0
-38.147	-73.111	44.597	25	25	4.649	21	110	2
-38.091	-73.371	35.842	25	25	4.649	21	110	5
-38.034	-73.641	28.019	25	25	4.649	16	110	7
-37.977	-73.901	21.128	25	25	4.649	16	110	4
-37.919	-74.171	15.512	25	25	4.649	10	110	3
-37.86	-74.441	11.171	25	25	4.649	10	110	0
-38.034	-72.578	63.022	25	25	4.664	22	110	0
-37.979	-72.828	53.657	25	25	4.664	22	110	2
-37.923	-73.088	44.597	25	25	4.664	21	110	3
-37.867	-73.348	35.842	25	25	4.664	21	110	5

-37.81	-73.608	28.019	25	25	4.664	16	110	8
-37.753	-73.878	21.128	25	25	4.664	16	110	6
-37.695	-74.148	15.512	25	25	4.664	10	110	3
-37.636	-74.418	11.171	25	25	4.664	10	110	2
-37.818	-72.556	63.022	25	25	8.287	22	110	2
-37.763	-72.806	53.657	25	25	8.287	22	110	1
-37.707	-73.066	44.597	25	25	8.287	21	110	2
-37.652	-73.326	35.842	25	25	8.287	21	110	8
-37.594	-73.586	28.019	25	25	8.287	16	110	7
-37.537	-73.846	21.128	25	25	8.287	16	110	8
-37.479	-74.116	15.512	25	25	8.287	10	110	4
-37.42	-74.386	11.171	25	25	8.287	10	110	1
-37.594	-72.516	63.022	25	25	8.31	22	110	1
-37.54	-72.766	53.657	25	25	8.31	22	110	0
-37.483	-73.026	44.597	25	25	8.31	21	110	5
-37.428	-73.286	35.842	25	25	8.31	21	110	10
-37.371	-73.546	28.019	25	25	8.31	16	110	9
-37.314	-73.806	21.128	25	25	8.31	16	110	9
-37.255	-74.076	15.512	25	25	8.31	10	110	4
-37.198	-74.346	11.171	25	25	8.31	10	110	0
-37.372	-72.485	63.022	25	25	8.332	22	110	1
-37.317	-72.735	53.657	25	25	8.332	22	110	1
-37.261	-72.995	44.597	25	25	8.332	21	110	4
-37.206	-73.255	35.842	25	25	8.332	21	110	8
-37.149	-73.515	28.019	25	25	8.332	16	110	6
-37.092	-73.775	21.128	25	25	8.332	16	110	5
-37.033	-74.045	15.512	25	25	8.332	10	110	1
-36.975	-74.305	11.171	25	25	8.332	10	110	0
-37.15	-72.444	63.022	25	25	8.355	22	105	1
-37.095	-72.694	53.657	25	25	8.355	22	105	1
-37.04	-72.954	44.597	25	25	8.355	21	105	5
-36.984	-73.204	35.842	25	25	8.355	21	105	12
-36.927	-73.464	28.019	25	25	8.355	16	105	12
-36.87	-73.734	21.128	25	25	8.355	16	105	8
-36.811	-73.994	15.512	25	25	8.355	10	105	4
-36.753	-74.264	11.171	25	25	8.355	10	105	0
-36.941	-72.389	63.022	25	25	14.464	22	105	2
-36.886	-72.639	53.657	25	25	14.464	22	105	1
-36.831	-72.899	44.597	25	25	14.464	21	105	7

-36.776	-73.149	35.842	25	25	14.464	21	105	8
-36.718	-73.409	28.019	25	25	14.464	16	105	10
-36.662	-73.669	21.128	25	25	14.464	16	105	7
-36.602	-73.939	15.512	25	25	14.464	10	105	2
-36.544	-74.209	11.171	25	25	14.464	10	105	1
-36.725	-72.329	63.022	25	25	14.504	22	105	3
-36.67	-72.589	53.657	25	25	14.504	22	105	2
-36.614	-72.839	44.597	25	25	14.504	21	105	3
-36.558	-73.089	35.842	25	25	14.504	21	105	6
-36.501	-73.349	28.019	25	25	14.504	16	105	2
-36.444	-73.609	21.128	25	25	14.504	16	105	2
-36.386	-73.879	15.512	25	25	14.504	10	105	1
-36.327	-74.139	11.171	25	25	14.504	10	105	0
-36.522	-72.265	63.022	25	25	20.566	22	105	4
-36.467	-72.515	53.657	25	25	20.566	22	105	4
-36.411	-72.765	44.597	25	25	20.566	21	105	6
-36.355	-73.015	35.842	25	25	20.566	21	105	8
-36.298	-73.275	28.019	25	25	20.566	16	105	2
-36.241	-73.535	21.128	25	25	20.566	16	105	0
-36.183	-73.795	15.512	25	25	20.566	10	105	2
-36.124	-74.065	11.171	25	25	20.566	10	105	3
-36.327	-72.174	63.022	25	25	26.64	22	105	4
-36.272	-72.424	53.657	25	25	26.64	22	105	4
-36.216	-72.674	44.597	25	25	26.64	21	105	4
-36.161	-72.924	35.842	25	25	26.64	21	105	6
-36.104	-73.184	28.019	25	25	26.64	16	105	2
-36.046	-73.444	21.128	25	25	26.64	16	105	0
-35.988	-73.704	15.512	25	25	26.64	10	105	2
-35.929	-73.964	11.171	25	25	26.64	10	105	3
-36.126	-72.05	63.022	25	25	26.7	22	105	4
-36.071	-72.3	53.657	25	25	26.7	22	105	4
-36.015	-72.55	44.597	25	25	26.7	21	105	5
-35.96	-72.8	35.842	25	25	26.7	21	105	9
-35.903	-73.06	28.019	25	25	26.7	16	105	7
-35.846	-73.31	21.128	25	25	26.7	16	105	1
-35.787	-73.58	15.512	25	25	26.7	10	105	2
-35.729	-73.84	11.171	25	25	26.7	10	105	3
-35.904	-71.933	63.022	25	25	18.689	22	105	2

-35.849	-72.183	53.657	25	25	18.689	22	105	1
-35.794	-72.433	44.597	25	25	18.689	21	105	3
-35.738	-72.683	35.842	25	25	18.689	21	105	10
-35.681	-72.943	28.019	25	25	18.689	16	105	12
-35.624	-73.193	21.128	25	25	18.689	16	105	0
-35.565	-73.463	15.512	25	25	18.689	10	105	0
-35.507	-73.723	11.171	25	25	18.689	10	105	2
-35.682	-71.854	63.022	25	25	14.692	22	105	2
-35.627	-72.104	53.657	25	25	14.692	22	105	0
-35.572	-72.354	44.597	25	25	14.692	21	105	2
-35.516	-72.604	35.842	25	25	14.692	21	105	11
-35.459	-72.864	28.019	25	25	14.692	16	105	19
-35.402	-73.114	21.128	25	25	14.692	16	105	6
-35.343	-73.374	15.512	25	25	14.692	10	105	0
-35.285	-73.644	11.171	25	25	14.692	10	105	2
-35.465	-71.794	63.022	25	25	14.734	22	105	1
-35.41	-72.044	53.657	25	25	14.734	22	105	3
-35.355	-72.294	44.597	25	25	14.734	21	105	7
-35.298	-72.544	35.842	25	25	14.734	21	105	15
-35.242	-72.804	28.019	25	25	14.734	16	105	20
-35.184	-73.054	21.128	25	25	14.734	16	105	8
-35.127	-73.314	15.512	25	25	14.734	10	105	1
-35.068	-73.574	11.171	25	25	14.734	10	105	3
-35.274	-71.721	63.022	25	25	25.298	22	105	2
-35.219	-71.961	53.657	25	25	25.298	22	105	2
-35.163	-72.211	44.597	25	25	25.298	21	105	7
-35.107	-72.461	35.842	25	25	25.298	21	105	16
-35.05	-72.711	28.019	25	25	25.298	16	105	19
-34.993	-72.971	21.128	25	25	25.298	16	105	10
-34.935	-73.231	15.512	25	25	25.298	10	105	2
-34.876	-73.491	11.171	25	25	25.298	10	105	4
-35.085	-71.593	63.022	25	25	30.619	22	120	3
-35.03	-71.833	53.657	25	25	30.619	22	120	2
-34.974	-72.083	44.597	25	25	30.619	21	120	7
-34.919	-72.333	35.842	25	25	30.619	21	120	14
-34.861	-72.583	28.019	25	25	30.619	16	120	18
-34.804	-72.843	21.128	25	25	30.619	16	120	10
-34.746	-73.103	15.512	25	25	30.619	10	120	0

-34.687	-73.363	11.171	25	25	30.619	10	120	3
-34.89	-71.454	63.022	25	25	30.682	22	120	3
-34.835	-71.704	53.657	25	25	30.682	22	120	2
-34.779	-71.944	44.597	25	25	30.682	21	120	4
-34.724	-72.194	35.842	25	25	30.682	21	120	11
-34.667	-72.444	28.019	25	25	30.682	16	120	14
-34.61	-72.704	21.128	25	25	30.682	16	120	5
-34.551	-72.964	15.512	25	25	30.682	10	120	0
-34.493	-73.224	11.171	25	25	30.682	10	120	2
-34.695	-71.327	63.022	25	25	29.61	22	120	6
-34.64	-71.577	53.657	25	25	29.61	22	120	4
-34.585	-71.827	44.597	25	25	29.61	21	120	4
-34.529	-72.067	35.842	25	25	29.61	21	120	10
-34.472	-72.317	28.019	25	25	29.61	16	120	15
-34.415	-72.577	21.128	25	25	29.61	16	120	6
-34.356	-72.837	15.512	25	25	29.61	10	120	0
-34.298	-73.087	11.171	25	25	29.61	10	120	0
-34.498	-71.203	63.022	25	25	29.392	22	120	1
-34.443	-71.443	53.657	25	25	29.392	22	120	3
-34.388	-71.693	44.597	25	25	29.392	21	120	9
-34.332	-71.933	35.842	25	25	29.392	21	120	13
-34.275	-72.183	28.019	25	25	29.392	16	120	14
-34.218	-72.443	21.128	25	25	29.392	16	120	5
-34.159	-72.693	15.512	25	25	29.392	10	120	2
-34.101	-72.953	11.171	25	25	29.392	10	120	0
-34.262	-71.096	63.022	25	25	13.035	22	120	4
-34.206	-71.336	53.657	25	25	13.035	22	120	5
-34.151	-71.586	44.597	25	25	13.035	21	120	3
-34.095	-71.826	35.842	25	25	13.035	21	120	6
-34.038	-72.076	28.019	25	25	13.035	16	120	6
-33.981	-72.336	21.128	25	25	13.035	16	120	3
-33.923	-72.586	15.512	25	25	13.035	10	120	0
-33.864	-72.846	11.171	25	25	13.035	10	120	1
-34.031	-71.048	63.022	25	25	7.587	22	120	2
-33.976	-71.298	53.657	25	25	7.587	22	120	1
-33.92	-71.538	44.597	25	25	7.587	21	120	0
-33.864	-71.778	35.842	25	25	7.587	21	120	0
-33.807	-72.038	28.019	25	25	7.587	16	120	1
-33.75	-72.288	21.128	25	25	7.587	16	120	2

-33.692	-72.538	15.512	25	25	7.587	10	120	1
-33.633	-72.798	11.171	25	25	7.587	10	120	1
-33.797	-71.033	63.022	25	25	2.714	22	120	1
-33.742	-71.273	53.657	25	25	2.714	22	120	0
-33.686	-71.513	44.597	25	25	2.714	21	120	1
-33.631	-71.763	35.842	25	25	2.714	21	120	1
-33.573	-72.013	28.019	25	25	2.714	16	120	2
-33.516	-72.263	21.128	25	25	2.714	16	120	2
-33.458	-72.513	15.512	25	25	2.714	10	120	0
-33.399	-72.773	11.171	25	25	2.714	10	120	0

Table D6: Shao et al. (2010) parameters.

Latitude	Longitude	Depth (km)	Length (km)	Width (km)	Strike	Dip	Rake	Slip (cm)
-37.9048	-74.6486	5.4803	30	17	17.5	18	113.1559	15.65442
-37.6473	-74.5485	5.4803	30	17	17.5	18	97.0263	8.43307
-37.3899	-74.4483	5.4803	30	17	17.5	18	86.4164	20.28927
-37.1324	-74.3481	5.4803	30	17	17.5	18	109.9568	7.84621
-36.8749	-74.248	5.4803	30	17	17.5	18	151.6786	87.76616
-36.6174	-74.1478	5.4803	30	17	17.5	18	151.1255	255.27499
-36.3599	-74.0477	5.4803	30	17	17.5	18	140.4734	510.55621
-36.1024	-73.9475	5.4803	30	17	17.5	18	138.2031	610.17822
-35.845	-73.8474	5.4803	30	17	17.5	18	134.574	546.60938
-35.5875	-73.7472	5.4803	30	17	17.5	18	138.0864	414.7894
-35.33	-73.647	5.4803	30	17	17.5	18	142.8516	417.11691
-35.0725	-73.5469	5.4803	30	17	17.5	18	151.8874	354.8241
-34.815	-73.4467	5.4803	30	17	17.5	18	151.508	371.79321
-34.5576	-73.3466	5.4803	30	17	17.5	18	149.6509	419.61191
-34.3001	-73.2464	5.4803	30	17	17.5	18	148.9986	515.69482
-34.0426	-73.1462	5.4803	30	17	17.5	18	151.6576	566.45367
-33.7851	-73.0461	5.4803	30	17	17.5	18	147.1385	444.237
-33.5276	-72.9459	5.4803	30	17	17.5	18	148.2888	159.34731
-33.2701	-72.8458	5.4803	30	17	17.5	18	142.8863	18.42455
-33.0127	-72.7456	5.4803	30	17	17.5	18	111.6746	29.72534
-37.9486	-74.4774	10.734	30	17	17.5	18	105.9586	38.88167
-37.6911	-74.3773	10.734	30	17	17.5	18	100.1095	1.46679
-37.4336	-74.2771	10.734	30	17	17.5	18	131.7641	4.61225
-37.1761	-74.1769	10.734	30	17	17.5	18	147.0618	83.62536
-36.9187	-74.0768	10.734	30	17	17.5	18	151.7176	345.8483
-36.6612	-73.9766	10.734	30	17	17.5	18	151.4899	548.29248
-36.4037	-73.8765	10.734	30	17	17.5	18	129.4779	822.84241
-36.1462	-73.7763	10.734	30	17	17.5	18	118.1857	970.55298
-35.8887	-73.6762	10.734	30	17	17.5	18	118.732	907.92902
-35.6312	-73.576	10.734	30	17	17.5	18	126.7524	711.61719
-35.3738	-73.4758	10.734	30	17	17.5	18	126.6601	594.08948
-35.1163	-73.3757	10.734	30	17	17.5	18	136.1605	539.31519
-34.8588	-73.2755	10.734	30	17	17.5	18	145.0498	577.48523
-34.6013	-73.1754	10.734	30	17	17.5	18	146.4495	676.20312
-34.3438	-73.0752	10.734	30	17	17.5	18	140.5612	676.54559

-34.0863	-72.975	10.734	30	17	17.5	18	145.1302	717.45453
-33.8289	-72.8749	10.734	30	17	17.5	18	143.2521	535.02112
-33.5714	-72.7747	10.734	30	17	17.5	18	130.5315	242.1891
-33.3139	-72.6746	10.734	30	17	17.5	18	146.4762	88.13851
-33.0564	-72.5744	10.734	30	17	17.5	18	145.7666	17.97685
-37.9923	-74.3062	15.987	30	17	17.5	18	109.8685	109.3253
-37.7349	-74.2061	15.987	30	17	17.5	18	89.59662	136.8837
-37.4774	-74.1059	15.987	30	17	17.5	18	145.2195	94.26677
-37.2199	-74.0058	15.987	30	17	17.5	18	150.2701	124.6873
-36.9624	-73.9056	15.987	30	17	17.5	18	151.36	442.09451
-36.7049	-73.8054	15.987	30	17	17.5	18	139.2422	727.4353
-36.4474	-73.7053	15.987	30	17	17.5	18	113.6862	1015.461
-36.19	-73.6051	15.987	30	17	17.5	18	102.2745	1216.3149
-35.9325	-73.505	15.987	30	17	17.5	18	110.3935	982.5683
-35.675	-73.4048	15.987	30	17	17.5	18	135.5643	650.36218
-35.4175	-73.3046	15.987	30	17	17.5	18	121.9541	551.24298
-35.16	-73.2045	15.987	30	17	17.5	18	115.2149	610.04657
-34.9025	-73.1043	15.987	30	17	17.5	18	114.7945	604.53522
-34.6451	-73.0042	15.987	30	17	17.5	18	113.6282	736.15228
-34.3876	-72.904	15.987	30	17	17.5	18	114.9986	777.10828
-34.1301	-72.8038	15.987	30	17	17.5	18	124.1027	619.85028
-33.8726	-72.7037	15.987	30	17	17.5	18	126.577	479.51089
-33.6151	-72.6035	15.987	30	17	17.5	18	125.6709	271.08319
-33.3576	-72.5034	15.987	30	17	17.5	18	131.4485	95.68645
-33.1002	-72.4032	15.987	30	17	17.5	18	139.7958	5.84604
-38.0361	-74.135	21.24	30	17	17.5	18	114.669	160.3476
-37.7786	-74.0349	21.24	30	17	17.5	18	86.36763	143.48689
-37.5211	-73.9347	21.24	30	17	17.5	18	128.0252	131.6868
-37.2636	-73.8345	21.24	30	17	17.5	18	151.6421	81.57919
-37.0062	-73.7344	21.24	30	17	17.5	18	126.0026	393.40149
-36.7487	-73.6342	21.24	30	17	17.5	18	117.9157	854.96118
-36.4912	-73.5341	21.24	30	17	17.5	18	111.5684	1153.7011
-36.2337	-73.4339	21.24	30	17	17.5	18	102.2824	1218.0649
-35.9762	-73.3338	21.24	30	17	17.5	18	112.1439	868.22119
-35.7187	-73.2336	21.24	30	17	17.5	18	140.3578	472.18591
-35.4613	-73.1334	21.24	30	17	17.5	18	122.1105	399.9278
-35.2038	-73.0333	21.24	30	17	17.5	18	96.02011	542.21259
-34.9463	-72.9331	21.24	30	17	17.5	18	93.10575	589.9917
-34.6888	-72.833	21.24	30	17	17.5	18	88.54765	733.09192

-34.4313	-72.7328	21.24	30	17	17.5	18	86.77584	757.42432
-34.1738	-72.6326	21.24	30	17	17.5	18	87.00486	540.52039
-33.9164	-72.5325	21.24	30	17	17.5	18	88.88116	471.6907
-33.6589	-72.4323	21.24	30	17	17.5	18	91.45515	317.71909
-33.4014	-72.3322	21.24	30	17	17.5	18	102.8806	119.4387
-33.1439	-72.232	21.24	30	17	17.5	18	138.7062	10.44599
-38.0798	-73.9638	26.493	30	17	17.5	18	134.24	89.19544
-37.8224	-73.8637	26.493	30	17	17.5	18	147.1473	0.41215
-37.5649	-73.7635	26.493	30	17	17.5	18	131.9149	12.77301
-37.3074	-73.6634	26.493	30	17	17.5	18	87.03534	1.52823
-37.0499	-73.5632	26.493	30	17	17.5	18	104.83	329.26309
-36.7924	-73.463	26.493	30	17	17.5	18	106.1275	826.18481
-36.5349	-73.3629	26.493	30	17	17.5	18	114.5691	1110.476
-36.2775	-73.2627	26.493	30	17	17.5	18	113.4034	1104.3731
-36.02	-73.1626	26.493	30	17	17.5	18	122.7862	695.8598
-35.7625	-73.0624	26.493	30	17	17.5	18	148.84	430.0752
-35.505	-72.9622	26.493	30	17	17.5	18	138.1456	343.6871
-35.2475	-72.8621	26.493	30	17	17.5	18	115.2278	389.51059
-34.99	-72.7619	26.493	30	17	17.5	18	111.7842	372.4364
-34.7326	-72.6618	26.493	30	17	17.5	18	99.68571	633.06732
-34.4751	-72.5616	26.493	30	17	17.5	18	95.77733	698.77521
-34.2176	-72.4614	26.493	30	17	17.5	18	82.19093	492.16589
-33.9601	-72.3613	26.493	30	17	17.5	18	89.49805	436.13229
-33.7026	-72.2611	26.493	30	17	17.5	18	84.13276	294.94031
-33.4451	-72.161	26.493	30	17	17.5	18	86.03401	154.5127
-33.1877	-72.0608	26.493	30	17	17.5	18	120.3696	16.71979
-38.1236	-73.7926	31.747	30	17	17.5	18	150.2563	69.83429
-37.8661	-73.6925	31.747	30	17	17.5	18	108.2887	3.17627
-37.6086	-73.5923	31.747	30	17	17.5	18	99.8322	15.15678
-37.3511	-73.4922	31.747	30	17	17.5	18	134.4551	12.22941
-37.0937	-73.392	31.747	30	17	17.5	18	104.5588	199.3093
-36.8362	-73.2918	31.747	30	17	17.5	18	116.9388	551.47601
-36.5787	-73.1917	31.747	30	17	17.5	18	125.8329	878.2926
-36.3212	-73.0915	31.747	30	17	17.5	18	119.8216	978.01477
-36.0637	-72.9914	31.747	30	17	17.5	18	121.0182	701.48669
-35.8062	-72.8912	31.747	30	17	17.5	18	141.2293	383.91089
-35.5488	-72.791	31.747	30	17	17.5	18	114.3102	266.33331

-35.2913	-72.6909	31.747	30	17	17.5	18	99.51744	305.50229
-35.0338	-72.5907	31.747	30	17	17.5	18	128.0149	380.69861
-34.7763	-72.4906	31.747	30	17	17.5	18	113.328	604.11792
-34.5188	-72.3904	31.747	30	17	17.5	18	110.6046	687.97778
-34.2613	-72.2902	31.747	30	17	17.5	18	82.3396	365.06619
-34.0039	-72.1901	31.747	30	17	17.5	18	83.40627	273.9993
-33.7464	-72.0899	31.747	30	17	17.5	18	82.08871	269.4855
-33.4889	-71.9898	31.747	30	17	17.5	18	82.8644	191.14349
-33.2314	-71.8896	31.747	30	17	17.5	18	94.68501	77.3707
-38.1673	-73.6214	37	30	17	17.5	18	97.66632	50.26099
-37.9099	-73.5213	37	30	17	17.5	18	138.0516	0.37141
-37.6524	-73.4211	37	30	17	17.5	18	106.7835	24.88621
-37.3949	-73.321	37	30	17	17.5	18	151.8055	24.46956
-37.1374	-73.2208	37	30	17	17.5	18	99.1538	189.2065
-36.8799	-73.1206	37	30	17	17.5	18	122.7257	430.5972
-36.6224	-73.0205	37	30	17	17.5	18	130.2726	774.62433
-36.365	-72.9203	37	30	17	17.5	18	119.5019	1074.621
-36.1075	-72.8202	37	30	17	17.5	18	109.7316	1047.103
-35.85	-72.72	37	30	17	17.5	18	90.9534	801.40802
-35.5925	-72.6198	37	30	17	17.5	18	82.05587	589.60242
-35.335	-72.5197	37	30	17	17.5	18	82.63213	497.3382
-35.0775	-72.4195	37	30	17	17.5	18	114.0364	587.45001
-34.8201	-72.3194	37	30	17	17.5	18	95.06599	766.09229
-34.5626	-72.2192	37	30	17	17.5	18	98.66142	780.90839
-34.3051	-72.119	37	30	17	17.5	18	82.42822	344.5332
-34.0476	-72.0189	37	30	17	17.5	18	89.05041	181.65109
-33.7901	-71.9187	37	30	17	17.5	18	85.46042	242.2776
-33.5327	-71.8186	37	30	17	17.5	18	83.9471	186.9469
-33.2752	-71.7184	37	30	17	17.5	18	130.8895	101.6325
-38.2111	-73.4502	42.253	30	17	17.5	18	124.9387	72.17995
-37.9536	-73.3501	42.253	30	17	17.5	18	96.45799	0.93198
-37.6961	-73.2499	42.253	30	17	17.5	18	119.2375	18.37632
-37.4386	-73.1498	42.253	30	17	17.5	18	135.9315	12.85191
-37.1812	-73.0496	42.253	30	17	17.5	18	98.54649	110.725
-36.9237	-72.9494	42.253	30	17	17.5	18	128.583	341.34399
-36.6662	-72.8493	42.253	30	17	17.5	18	123.7675	740.95258
-36.4087	-72.7491	42.253	30	17	17.5	18	106.2797	1164.642
-36.1512	-72.649	42.253	30	17	17.5	18	101.8632	1289.689

-35.8938	-72.5488	42.253	30	17	17.5	18	100.7863	985.66559
-35.6363	-72.4486	42.253	30	17	17.5	18	82.73689	700.78387
-35.3788	-72.3485	42.253	30	17	17.5	18	94.46326	571.79053
-35.1213	-72.2483	42.253	30	17	17.5	18	113.2795	891.45319
-34.8638	-72.1482	42.253	30	17	17.5	18	100.7007	901.91528
-34.6063	-72.048	42.253	30	17	17.5	18	107.2735	735.11572
-34.3489	-71.9478	42.253	30	17	17.5	18	82.23347	294.32751
-34.0914	-71.8477	42.253	30	17	17.5	18	82.78474	85.72894
-33.8339	-71.7475	42.253	30	17	17.5	18	83.03049	181.1073
-33.5764	-71.6474	42.253	30	17	17.5	18	83.39211	173.06461
-33.3189	-71.5472	42.253	30	17	17.5	18	150.4897	184.9304
-38.2549	-73.279	47.507	30	17	17.5	18	130.7242	59.63332
-37.9974	-73.1789	47.507	30	17	17.5	18	86.59027	70.61333
-37.7399	-73.0787	47.507	30	17	17.5	18	82.64906	86.50245
-37.4824	-72.9786	47.507	30	17	17.5	18	123.6855	96.04082
-37.2249	-72.8784	47.507	30	17	17.5	18	151.5508	181.76849
-36.9674	-72.7782	47.507	30	17	17.5	18	117.4429	357.6763
-36.71	-72.6781	47.507	30	17	17.5	18	118.7272	691.35962
-36.4525	-72.5779	47.507	30	17	17.5	18	91.70148	1162.509
-36.195	-72.4778	47.507	30	17	17.5	18	99.30206	1097.269
-35.9375	-72.3776	47.507	30	17	17.5	18	119.3744	939.56702
-35.68	-72.2774	47.507	30	17	17.5	18	84.33289	589.10028
-35.4225	-72.1773	47.507	30	17	17.5	18	82.09238	679.34271
-35.1651	-72.0771	47.507	30	17	17.5	18	93.39726	766.17609
-34.9076	-71.977	47.507	30	17	17.5	18	93.85228	770.12488
-34.6501	-71.8768	47.507	30	17	17.5	18	105.312	523.99933
-34.3926	-71.7766	47.507	30	17	17.5	18	82.03445	126.4463
-34.1351	-71.6765	47.507	30	17	17.5	18	108.9306	26.73383
-33.8776	-71.5763	47.507	30	17	17.5	18	82.31315	211.5453
-33.6202	-71.4762	47.507	30	17	17.5	18	90.53333	147.3766
-33.3627	-71.376	47.507	30	17	17.5	18	149.4796	243.3096
-38.2986	-73.1078	52.76	30	17	17.5	18	106.6447	68.08176
-38.0411	-73.0077	52.76	30	17	17.5	18	85.02983	97.19032
-37.7836	-72.9075	52.76	30	17	17.5	18	107.0156	181.90559
-37.5262	-72.8074	52.76	30	17	17.5	18	134.8109	262.8685
-37.2687	-72.7072	52.76	30	17	17.5	18	151.9057	299.85971
-37.0112	-72.607	52.76	30	17	17.5	18	112.5971	331.59161
-36.7537	-72.5069	52.76	30	17	17.5	18	102.3431	522.80713

-36.4962	-72.4067	52.76	30	17	17.5	18	85.62786	879.65863
-36.2387	-72.3066	52.76	30	17	17.5	18	90.10095	676.81378
-35.9813	-72.2064	52.76	30	17	17.5	18	117.3298	619.45563
-35.7238	-72.1062	52.76	30	17	17.5	18	85.08347	416.74179
-35.4663	-72.0061	52.76	30	17	17.5	18	82.1633	530.13507
-35.2088	-71.9059	52.76	30	17	17.5	18	82.00436	549.09747
-34.9513	-71.8058	52.76	30	17	17.5	18	82.59761	508.1301
-34.6938	-71.7056	52.76	30	17	17.5	18	96.03195	312.10291
-34.4364	-71.6055	52.76	30	17	17.5	18	125.0335	0.84617
-34.1789	-71.5053	52.76	30	17	17.5	18	135.374	3.78169
-33.9214	-71.4051	52.76	30	17	17.5	18	82.04563	156.8725
-33.6639	-71.305	52.76	30	17	17.5	18	85.12779	134.9239
-33.4064	-71.2048	52.76	30	17	17.5	18	150.4734	239.2301
-38.3424	-72.9366	58.013	30	17	17.5	18	90.78945	99.83096
-38.0849	-72.8365	58.013	30	17	17.5	18	82.6241	118.3917
-37.8274	-72.7363	58.013	30	17	17.5	18	102.296	199.0593
-37.5699	-72.6362	58.013	30	17	17.5	18	131.011	332.45941
-37.3124	-72.536	58.013	30	17	17.5	18	144.9318	380.01599
-37.0549	-72.4358	58.013	30	17	17.5	18	123.6472	427.6861
-36.7975	-72.3357	58.013	30	17	17.5	18	113.5915	341.11789
-36.54	-72.2355	58.013	30	17	17.5	18	89.93624	401.7457
-36.2825	-72.1354	58.013	30	17	17.5	18	83.85087	293.55411
-36.025	-72.0352	58.013	30	17	17.5	18	82.29785	260.55151
-35.7675	-71.935	58.013	30	17	17.5	18	82.33324	255.7804
-35.51	-71.8349	58.013	30	17	17.5	18	82.30177	316.63101
-35.2526	-71.7347	58.013	30	17	17.5	18	82.39796	287.5307
-34.9951	-71.6346	58.013	30	17	17.5	18	82.27495	282.6969
-34.7376	-71.5344	58.013	30	17	17.5	18	82.30084	183.5377
-34.4801	-71.4342	58.013	30	17	17.5	18	108.0739	3.29879
-34.2226	-71.3341	58.013	30	17	17.5	18	118.1502	8.80795
-33.9651	-71.2339	58.013	30	17	17.5	18	83.68701	151.9599
-33.7077	-71.1338	58.013	30	17	17.5	18	83.00256	135.3936
-33.4502	-71.0336	58.013	30	17	17.5	18	150.5854	220.81551

Table D7: Sladen (2010) parameters.

Latitude	Longitude	Depth (km)	Length (km)	Width (km)	Strike	Dip	Rake	Slip (cm)
-37.7125	-74.3183	11.309	30	15	18	18	90	200
-37.4557	-74.2154	11.309	30	15	18	18	90	200
-37.1989	-74.1125	11.309	30	15	18	18	90	200
-36.9422	-74.0095	11.309	30	15	18	18	118	200
-36.6854	-73.9066	11.309	30	15	18	18	110	200
-36.4286	-73.8037	11.309	30	15	18	18	90	200
-36.1719	-73.7008	11.309	30	15	18	18	116	200
-35.9151	-73.5979	11.309	30	15	18	18	120	100
-35.6583	-73.4949	11.309	30	15	18	18	90	100
-35.4016	-73.392	11.309	30	15	18	18	130	100
-35.1448	-73.2891	11.309	30	15	18	18	130	100
-34.888	-73.1862	11.309	30	15	18	18	128	200
-34.6313	-73.0833	11.309	30	15	18	18	112	200
-34.3745	-72.9803	11.309	30	15	18	18	106	200
-34.1177	-72.8774	11.309	30	15	18	18	106	200
-33.861	-72.7745	11.309	30	15	18	18	90	100
-33.6042	-72.6716	11.309	30	15	18	18	90	100
-33.3475	-72.5686	11.309	30	15	18	18	98	200
-33.0907	-72.4657	11.309	30	15	18	18	102	200
-37.7521	-74.1677	15.944	30	15	18	18	90	200
-37.4954	-74.0648	15.944	30	15	18	18	90	225
-37.2386	-73.9618	15.944	30	15	18	18	122	225
-36.9818	-73.8589	15.944	30	15	18	18	118	225
-36.7251	-73.756	15.944	30	15	18	18	90	225
-36.4683	-73.6531	15.944	30	15	18	18	90	300
-36.2115	-73.5502	15.944	30	15	18	18	120	225
-35.9548	-73.4472	15.944	30	15	18	18	90	0
-35.698	-73.3443	15.944	30	15	18	18	126	0
-35.4412	-73.2414	15.944	30	15	18	18	90	0
-35.1845	-73.1385	15.944	30	15	18	18	126	75
-34.9277	-73.0355	15.944	30	15	18	18	116	225
-34.6709	-72.9326	15.944	30	15	18	18	120	300
-34.4142	-72.8297	15.944	30	15	18	18	106	450
-34.1574	-72.7268	15.944	30	15	18	18	102	375
-33.9007	-72.6239	15.944	30	15	18	18	128	150

-33.6439	-72.5209	15.944	30	15	18	18	90	150
-33.3871	-72.418	15.944	30	15	18	18	116	225
-33.1304	-72.3151	15.944	30	15	18	18	102	200
-37.7918	-74.0171	20.579	30	15	18	18	90	100
-37.535	-73.9141	20.579	30	15	18	18	90	150
-37.2783	-73.8112	20.579	30	15	18	18	126	225
-37.0215	-73.7083	20.579	30	15	18	18	120	300
-36.7647	-73.6054	20.579	30	15	18	18	96	300
-36.508	-73.5024	20.579	30	15	18	18	90	300
-36.2512	-73.3995	20.579	30	15	18	18	122	225
-35.9944	-73.2966	20.579	30	15	18	18	124	75
-35.7377	-73.1937	20.579	30	15	18	18	130	150
-35.4809	-73.0908	20.579	30	15	18	18	90	0
-35.2242	-72.9878	20.579	30	15	18	18	130	75
-34.9674	-72.8849	20.579	30	15	18	18	118	225
-34.7106	-72.782	20.579	30	15	18	18	118	375
-34.4539	-72.6791	20.579	30	15	18	18	98	525
-34.1971	-72.5761	20.579	30	15	18	18	92	450
-33.9403	-72.4732	20.579	30	15	18	18	130	150
-33.6836	-72.3703	20.579	30	15	18	18	90	75
-33.4268	-72.2674	20.579	30	15	18	18	90	150
-33.17	-72.1645	20.579	30	15	18	18	90	200
-37.8315	-73.8664	25.215	30	15	18	18	122	100
-37.5747	-73.7635	25.215	30	15	18	18	90	150
-37.3179	-73.6606	25.215	30	15	18	18	130	150
-37.0612	-73.5577	25.215	30	15	18	18	112	225
-36.8044	-73.4547	25.215	30	15	18	18	90	300
-36.5476	-73.3518	25.215	30	15	18	18	92	300
-36.2909	-73.2489	25.215	30	15	18	18	126	225
-36.0341	-73.146	25.215	30	15	18	18	124	300
-35.7774	-73.0431	25.215	30	15	18	18	106	150
-35.5206	-72.9401	25.215	30	15	18	18	90	0
-35.2638	-72.8372	25.215	30	15	18	18	130	150
-35.0071	-72.7343	25.215	30	15	18	18	128	375
-34.7503	-72.6314	25.215	30	15	18	18	102	525
-34.4935	-72.5284	25.215	30	15	18	18	90	750
-34.2368	-72.4255	25.215	30	15	18	18	90	675
-33.98	-72.3226	25.215	30	15	18	18	104	225
-33.7232	-72.2197	25.215	30	15	18	18	126	0

-33.4665	-72.1168	25.215	30	15	18	18	90	75
-33.2097	-72.0138	25.215	30	15	18	18	90	100
-37.8711	-73.7158	29.85	30	15	18	18	128	100
-37.6144	-73.6129	29.85	30	15	18	18	116	0
-37.3576	-73.51	29.85	30	15	18	18	116	75
-37.1008	-73.407	29.85	30	15	18	18	90	225
-36.8441	-73.3041	29.85	30	15	18	18	90	375
-36.5873	-73.2012	29.85	30	15	18	18	108	375
-36.3306	-73.0983	29.85	30	15	18	18	106	300
-36.0738	-72.9953	29.85	30	15	18	18	112	375
-35.817	-72.8924	29.85	30	15	18	18	90	300
-35.5603	-72.7895	29.85	30	15	18	18	130	75
-35.3035	-72.6866	29.85	30	15	18	18	130	300
-35.0467	-72.5837	29.85	30	15	18	18	120	525
-34.79	-72.4807	29.85	30	15	18	18	112	525
-34.5332	-72.3778	29.85	30	15	18	18	98	675
-34.2764	-72.2749	29.85	30	15	18	18	96	825
-34.0197	-72.172	29.85	30	15	18	18	98	375
-33.7629	-72.069	29.85	30	15	18	18	90	75
-33.5061	-71.9661	29.85	30	15	18	18	128	75
-33.2494	-71.8632	29.85	30	15	18	18	130	100
-37.9108	-73.5652	34.485	30	15	18	18	90	0
-37.654	-73.4622	34.485	30	15	18	18	114	0
-37.3973	-73.3593	34.485	30	15	18	18	90	150
-37.1405	-73.2564	34.485	30	15	18	18	102	300
-36.8838	-73.1535	34.485	30	15	18	18	108	450
-36.627	-73.0506	34.485	30	15	18	18	120	375
-36.3702	-72.9476	34.485	30	15	18	18	114	300
-36.1135	-72.8447	34.485	30	15	18	18	108	450
-35.8567	-72.7418	34.485	30	15	18	18	90	375
-35.5999	-72.6389	34.485	30	15	18	18	90	75
-35.3432	-72.5359	34.485	30	15	18	18	130	225
-35.0864	-72.433	34.485	30	15	18	18	114	450
-34.8296	-72.3301	34.485	30	15	18	18	106	525
-34.5729	-72.2272	34.485	30	15	18	18	104	675
-34.3161	-72.1243	34.485	30	15	18	18	106	675
-34.0593	-72.0213	34.485	30	15	18	18	114	375
-33.8026	-71.9184	34.485	30	15	18	18	106	225

-33.5458	-71.8155	34.485	30	15	18	18	116	225
-33.289	-71.7126	34.485	30	15	18	18	124	200
-37.9505	-73.4145	39.12	30	15	18	18	90	0
-37.6937	-73.3116	39.12	30	15	18	18	90	75
-37.437	-73.2087	39.12	30	15	18	18	96	225
-37.1802	-73.1058	39.12	30	15	18	18	114	375
-36.9234	-73.0029	39.12	30	15	18	18	118	375
-36.6667	-72.8999	39.12	30	15	18	18	90	150
-36.4099	-72.797	39.12	30	15	18	18	90	225
-36.1531	-72.6941	39.12	30	15	18	18	90	375
-35.8964	-72.5912	39.12	30	15	18	18	112	225
-35.6396	-72.4882	39.12	30	15	18	18	90	75
-35.3828	-72.3853	39.12	30	15	18	18	130	75
-35.1261	-72.2824	39.12	30	15	18	18	104	225
-34.8693	-72.1795	39.12	30	15	18	18	106	300
-34.6125	-72.0766	39.12	30	15	18	18	124	375
-34.3558	-71.9736	39.12	30	15	18	18	124	450
-34.099	-71.8707	39.12	30	15	18	18	118	375
-33.8423	-71.7678	39.12	30	15	18	18	90	225
-33.5855	-71.6649	39.12	30	15	18	18	98	225
-33.3287	-71.5619	39.12	30	15	18	18	90	100
-37.9902	-73.2639	43.756	30	15	18	18	130	200
-37.7334	-73.161	43.756	30	15	18	18	94	225
-37.4766	-73.0581	43.756	30	15	18	18	90	225
-37.2199	-72.9551	43.756	30	15	18	18	118	225
-36.9631	-72.8522	43.756	30	15	18	18	130	225
-36.7063	-72.7493	43.756	30	15	18	18	90	0
-36.4496	-72.6464	43.756	30	15	18	18	90	225
-36.1928	-72.5435	43.756	30	15	18	18	90	525
-35.936	-72.4405	43.756	30	15	18	18	118	525
-35.6793	-72.3376	43.756	30	15	18	18	130	375
-35.4225	-72.2347	43.756	30	15	18	18	130	150
-35.1657	-72.1318	43.756	30	15	18	18	94	150
-34.909	-72.0288	43.756	30	15	18	18	90	150
-34.6522	-71.9259	43.756	30	15	18	18	130	300
-34.3955	-71.823	43.756	30	15	18	18	128	450
-34.1387	-71.7201	43.756	30	15	18	18	106	375
-33.8819	-71.6172	43.756	30	15	18	18	90	225

-33.6252	-71.5142	43.756	30	15	18	18	130	150
-33.3684	-71.4113	43.756	30	15	18	18	90	0
-38.0298	-73.1133	48.391	30	15	18	18	130	200
-37.7731	-73.0104	48.391	30	15	18	18	112	225
-37.5163	-72.9074	48.391	30	15	18	18	90	225
-37.2595	-72.8045	48.391	30	15	18	18	90	75
-37.0028	-72.7016	48.391	30	15	18	18	116	75
-36.746	-72.5987	48.391	30	15	18	18	90	0
-36.4892	-72.4958	48.391	30	15	18	18	90	300
-36.2325	-72.3928	48.391	30	15	18	18	90	375
-35.9757	-72.2899	48.391	30	15	18	18	112	450
-35.7189	-72.187	48.391	30	15	18	18	128	450
-35.4622	-72.0841	48.391	30	15	18	18	118	300
-35.2054	-71.9811	48.391	30	15	18	18	90	225
-34.9487	-71.8782	48.391	30	15	18	18	90	150
-34.6919	-71.7753	48.391	30	15	18	18	110	375
-34.4351	-71.6724	48.391	30	15	18	18	104	600
-34.1784	-71.5695	48.391	30	15	18	18	102	375
-33.9216	-71.4665	48.391	30	15	18	18	124	300
-33.6648	-71.3636	48.391	30	15	18	18	130	225
-33.4081	-71.2607	48.391	30	15	18	18	130	100
-38.0695	-72.9627	53.026	30	15	18	18	130	100
-37.8127	-72.8597	53.026	30	15	18	18	130	300
-37.556	-72.7568	53.026	30	15	18	18	116	300
-37.2992	-72.6539	53.026	30	15	18	18	118	150
-37.0424	-72.551	53.026	30	15	18	18	130	150
-36.7857	-72.448	53.026	30	15	18	18	128	75
-36.5289	-72.3451	53.026	30	15	18	18	108	225
-36.2722	-72.2422	53.026	30	15	18	18	90	225
-36.0154	-72.1393	53.026	30	15	18	18	112	375
-35.7586	-72.0364	53.026	30	15	18	18	128	525
-35.5019	-71.9334	53.026	30	15	18	18	122	225
-35.2451	-71.8305	53.026	30	15	18	18	90	150
-34.9883	-71.7276	53.026	30	15	18	18	128	225
-34.7316	-71.6247	53.026	30	15	18	18	124	450
-34.4748	-71.5217	53.026	30	15	18	18	102	525
-34.218	-71.4188	53.026	30	15	18	18	90	225
-33.9613	-71.3159	53.026	30	15	18	18	130	225

-33.7045	-71.213	53.026	30	15	18	18	130	150
-33.4477	-71.1101	53.026	30	15	18	18	130	100
-38.1092	-72.812	57.661	30	15	18	18	100	100
-37.8524	-72.7091	57.661	30	15	18	18	130	150
-37.5956	-72.6062	57.661	30	15	18	18	108	225
-37.3389	-72.5033	57.661	30	15	18	18	90	150
-37.0821	-72.4003	57.661	30	15	18	18	130	150
-36.8254	-72.2974	57.661	30	15	18	18	114	75
-36.5686	-72.1945	57.661	30	15	18	18	122	225
-36.3118	-72.0916	57.661	30	15	18	18	128	150
-36.0551	-71.9886	57.661	30	15	18	18	130	150
-35.7983	-71.8857	57.661	30	15	18	18	128	300
-35.5415	-71.7828	57.661	30	15	18	18	116	75
-35.2848	-71.6799	57.661	30	15	18	18	90	75
-35.028	-71.577	57.661	30	15	18	18	124	225
-34.7712	-71.474	57.661	30	15	18	18	130	450
-34.5145	-71.3711	57.661	30	15	18	18	128	450
-34.2577	-71.2682	57.661	30	15	18	18	116	225
-34.0009	-71.1653	57.661	30	15	18	18	130	150
-33.7442	-71.0623	57.661	30	15	18	18	130	150
-33.4874	-70.9594	57.661	30	15	18	18	90	200
-38.1488	-72.6614	62.297	30	15	18	18	90	100
-37.8921	-72.5585	62.297	30	15	18	18	90	0
-37.6353	-72.4556	62.297	30	15	18	18	90	100
-37.3786	-72.3526	62.297	30	15	18	18	90	100
-37.1218	-72.2497	62.297	30	15	18	18	108	0
-36.865	-72.1468	62.297	30	15	18	18	90	0
-36.6083	-72.0439	62.297	30	15	18	18	108	200
-36.3515	-71.9409	62.297	30	15	18	18	130	100
-36.0947	-71.838	62.297	30	15	18	18	90	0
-35.838	-71.7351	62.297	30	15	18	18	112	100
-35.5812	-71.6322	62.297	30	15	18	18	122	100
-35.3244	-71.5293	62.297	30	15	18	18	130	200
-35.0677	-71.4263	62.297	30	15	18	18	130	200
-34.8109	-71.3234	62.297	30	15	18	18	130	200
-34.5541	-71.2205	62.297	30	15	18	18	102	200
-34.2974	-71.1176	62.297	30	15	18	18	90	200
-34.0406	-71.0146	62.297	30	15	18	18	92	0

-33.7838	-70.9117	62.297	30	15	18	18	92	200
-33.5271	-70.8088	62.297	30	15	18	18	90	200

Table D8: Vigny et al. (2011) parameters.

Latitude	Longitude	Depth (km)	Length (km)	Width (km)	Strike	Dip	Rake	Slip (m)
-39.2626	-74.72995	5.0007	55.7765	19.312	3.7035	15.0042	0	0
-38.89245	-74.69095	5.0007	28.0355	19.2522	6.9416	15.0519	0	0
-38.6457	-74.6526	5.0007	28.0355	19.117	6.9416	15.1609	0	0
-38.39575	-74.61385	5.0007	28.0355	19.0541	6.9416	15.2122	0	0
-38.1445	-74.5749	5.0007	28.0355	18.9919	6.9416	15.2631	0	0
-37.8919	-74.54085	5.0007	27.9429	18.9055	5.1517	15.3346	0	0
-37.64065	-74.51215	5.0007	27.9429	18.874	5.1517	15.3609	0	0
-37.27525	-74.4712	5.0007	55.8858	18.814	5.1517	15.411	90	0.000001
-36.79375	-74.34615	5.0007	58.346	19.147	17.4529	15.1365	90	0.000001
-36.42775	-74.19715	5.0007	29.173	18.5099	17.4529	15.6707	0	0
-36.18055	-74.097	5.0007	29.173	18.4497	17.4529	15.7232	0	0
-35.9359	-73.98655	5.0007	29.8242	18.5669	21.071	15.6213	0	0
-35.6886	-73.86345	5.0007	29.8242	18.2888	21.071	15.8651	0	0
-35.4388	-73.73915	5.0007	29.8242	18.2284	21.071	15.919	0	0
-35.18965	-73.61515	5.0007	29.8242	18.1688	21.071	15.9727	0	0
-34.94115	-73.4884	5.0007	30.0211	18.1585	22.0259	15.982	0	0
-34.692	-73.3582	5.0007	30.0211	18.0371	22.0259	16.0925	0	0
-34.4422	-73.2276	5.0007	30.0211	17.979	22.0259	16.1458	0	0
-34.1896	-73.0956	5.0007	30.0211	17.9217	22.0259	16.1989	0	0
-33.9341	-72.97475	5.0007	29.2844	17.7018	18.1333	16.4058	0	0
-33.68135	-72.8678	5.0007	29.2844	17.8741	18.1333	16.2433	0	0
-33.4315	-72.7622	5.0007	29.2844	17.821	18.1333	16.293	0	0
-33.17285	-72.6534	5.0007	29.2844	17.7685	18.1333	16.3425	0	0
-32.90455	-72.5779	5.0007	27.9961	17.519	-6.2446	16.5819	0	0
-32.63545	-72.5389	5.0007	27.9961	17.8099	-6.2446	16.3034	0	0
-39.27525	-74.51385	10.0003	55.405	19.3092	3.5633	15.0064	0	0
-38.90995	-74.47655	10.0003	27.3061	19.2481	6.8342	15.0552	0	0
-38.66645	-74.43945	10.0003	28.0199	19.1121	6.8122	15.1648	76.1877951	0.385804126
-38.41655	-74.40145	10.0003	28.02	19.0493	6.8138	15.2161	76.18620041	1.907178709
-38.164	-74.363	10.0003	28.32	18.9871	6.8126	15.2671	76.18737376	0.977078457
-37.90875	-74.32935	10.0003	28.2325	18.9022	5.0324	15.3373	0	0
-37.65625	-74.3012	10.0003	27.9259	18.8706	5.0273	15.3637	77.9726753	1.071575874
-37.3005	-74.2631	10.0003	53.7276	18.8072	4.8962	15.4168	78.1038007	15.38625276
-36.8375	-74.14425	10.0003	56.2583	19.1465	17.4483	15.1369	65.55170035	19.12724566
-36.4805	-73.9993	10.0003	29.1398	18.5003	17.3505	15.6791	65.6495041	5.060368096
-36.23605	-73.901	10.0003	28.5184	18.4379	17.3267	15.7335	65.67330282	5.798980149
-35.9968	-73.79365	10.0003	29.1797	18.5577	20.9913	15.6293	62.00869575	7.372574342
-35.75225	-73.67245	10.0003	29.7855	18.2784	20.979	15.8744	62.02100308	7.49434933
-35.50255	-73.5488	10.0003	29.7859	18.2181	20.9801	15.9283	62.01989603	8.14740565
-35.25425	-73.42585	10.0003	29.6233	18.1584	20.9786	15.9821	62.02140365	10.39084583
-35.0073	-73.30045	10.0003	29.8206	18.1482	21.939	15.9913	61.06099902	10.33018028
-34.759	-73.1712	10.0003	29.9826	18.027	21.9402	16.1017	61.0598019	7.422790087
-34.50935	-73.04125	10.0003	29.983	17.9691	21.9413	16.155	61.05870121	4.560091724

-34.25415	-72.9085	10.0003	30.6418	17.9102	21.9268	16.2096	61.07320036	2.252378375
-33.9932	-72.7856	10.0003	29.9308	17.6961	18.0717	16.4112	64.92839411	0.397682035
-33.73775	-72.678	10.0003	29.2527	17.8658	18.0453	16.251	0	0
-33.48805	-72.573	10.0003	29.2531	17.8128	18.0464	16.3007	64.95351076	0.23040084
-33.2207	-72.46165	10.0003	31.287	17.7442	17.8711	16.3655	65.12892752	0.24874113
-32.93415	-72.38155	10.0003	30.1372	17.5231	6.3758	16.5779	0	0
-32.64605	-72.33905	10.0003	27.991	17.8069	6.1481	16.3062	0	0
-39.2878	-74.2978	15	55.0339	19.3065	3.4212	15.0086	0	0
-38.92735	-74.26225	15	26.5768	19.2439	6.7208	15.0585	0	0
-38.6871	-74.2263	15	28.0044	19.1074	6.6827	15.1687	76.3172727	0.809764739
-38.43735	-74.18905	15	28.0047	19.0446	6.6859	15.2199	76.31409501	3.549150782
-38.18355	-74.15115	15	28.6047	18.9825	6.686	15.2709	76.31401898	1.438226508
-37.92565	-74.11785	15	28.5222	18.8991	4.9155	15.3399	0	0
-37.67185	-74.09025	15	27.909	18.8673	4.9028	15.3665	0	0
-37.3257	-74.05505	15	51.5706	18.8002	4.6193	15.4227	78.38069969	14.78492772
-36.8812	-73.9424	15	54.1706	19.1461	17.4433	15.1373	65.55669932	17.69572453
-36.53325	-73.80145	15	29.1066	18.4907	17.2478	15.6874	65.75220238	5.692951536
-36.29165	-73.705	15	27.864	18.4256	17.1946	15.7442	65.80540278	8.870589528
-36.0577	-73.6007	15	28.5352	18.5481	20.908	15.6376	62.09200134	12.12332737
-35.81585	-73.4814	15	29.7468	18.2679	20.8866	15.8837	62.11339781	11.56054613
-35.56635	-73.35845	15	29.7476	18.2079	20.889	15.9375	62.11100108	12.09454543
-35.3189	-73.2365	15	29.4226	18.1479	20.8849	15.9916	62.11509942	16.70905896
-35.0735	-73.11245	15	29.6202	18.1379	21.851	16.0006	61.14899976	17.60059342
-34.82605	-72.98425	15	29.9442	18.017	21.8542	16.1109	61.1457989	12.82284967
-34.57655	-72.85495	15	29.945	17.9593	21.8564	16.1641	61.14359705	8.636336561
-34.31875	-72.72145	15	31.2625	17.8992	21.8317	16.2199	61.16830484	4.852952801
-34.0523	-72.5965	15	30.5772	17.6906	18.0127	16.4165	64.9872988	1.253339609
-33.7941	-72.4882	15	29.2211	17.8576	17.9571	16.2587	65.04278839	0.19602963
-33.54455	-72.3838	15	29.2218	17.8047	17.9593	16.3083	65.04066523	0.514525851
-33.26855	-72.26995	15	33.2901	17.7231	17.6404	16.3855	65.3596476	0.465522192
-32.9637	-72.18525	15	32.2785	17.5267	6.4896	16.5744	0	0
-32.6565	-72.13915	15	27.986	17.804	6.0516	16.309	0	0
-39.2991	-74.08145	20	54.6631	19.3221	3.2772	14.9972	0	0
-38.9436	-74.04755	20	25.8477	19.2631	6.6011	15.0441	0	0
-38.7067	-74.01275	20	27.9891	19.1337	6.553	15.1484	76.44699208	1.033212316
-38.45695	-73.97625	20	27.9895	19.0716	6.5578	15.1988	76.44220007	3.554594595
-38.2019	-73.93895	20	28.8895	19.0094	6.562	15.2498	76.43801817	0.704371111
-37.94145	-73.90605	20	28.8121	18.9228	4.8009	15.3213	0	0
-37.68595	-73.879	20	27.8923	18.8868	4.7781	15.3512	0	0
-37.34935	-73.8465	20	49.4149	18.824	4.3183	15.4037	78.68170159	4.291332711
-36.92415	-73.7399	20	52.0829	19.199	17.438	15.0956	65.56199348	2.774983332
-36.58525	-73.60285	20	29.0736	18.5333	17.145	15.6514	65.85498883	2.700273522
-36.3461	-73.50805	20	27.2097	18.4885	17.0561	15.6904	65.94389856	8.476458906
-36.11765	-73.4068	20	27.8908	18.6196	20.8208	15.5771	62.1792006	12.98685801
-35.8786	-73.28945	20	29.7083	18.3383	20.7941	15.8222	62.20589668	10.82068113
-35.62925	-73.16715	20	29.7094	18.2794	20.7976	15.8745	62.20239797	10.32846134
-35.38265	-73.04625	20	29.2219	18.219	20.79	15.9286	62.21000033	16.68127027

-35.13875	-72.9236	20	29.4198	18.2105	21.7617	15.9362	61.23829957	19.83977331
-34.89215	-72.79635	20	29.9059	18.0897	21.7681	16.0455	61.23189999	14.76087096
-34.6428	-72.6677	20	29.907	18.0311	21.7714	16.099	61.22859977	11.40482086
-34.3825	-72.53355	20	31.8833	17.9712	21.7402	16.1542	61.25980155	7.472639778
-34.1107	-72.40665	20	31.2236	17.7548	17.9562	16.3566	65.04380947	2.712791545
-33.8497	-72.29765	20	29.1896	17.9106	17.8687	16.2104	65.13131125	0.827222015
-33.59985	-72.19365	20	29.1905	17.8623	17.872	16.2554	65.12800713	0.66343807
-33.3152	-72.0774	20	35.2938	17.7942	17.4359	16.3193	65.56411282	0.40438049
-32.993	-71.9886	20	34.4198	17.5707	6.5893	16.5328	76.40983034	0.031433085
-32.6678	-71.9394	20	27.981	17.8112	5.9551	16.3033	0	0
-39.3104	-73.8651	25	54.2992	19.3196	3.1366	14.9991	0	0
-38.95985	-73.8329	25	25.0947	19.2594	6.4979	15.0471	0	0
-38.7263	-73.79925	25	27.9812	19.1291	6.4229	15.1521	76.57708026	1.346980333
-38.4766	-73.7635	25	27.9731	19.0671	6.4293	15.2025	76.5706939	2.152856082
-38.22035	-73.72675	25	29.1689	19.0049	6.4324	15.2535	76.567632	0.142859963
-37.9573	-73.6943	25	29.101	18.9198	4.6807	15.3238	78.3193043	1.604723084
-37.7	-73.66775	25	27.9812	18.8836	4.6533	15.3539	78.34669356	3.048568869
-37.37295	-73.6379	25	47.1701	18.8174	4.0227	15.4092	78.97729755	6.361475673
-36.96705	-73.5374	25	49.9129	19.2012	17.4606	15.0938	65.53940093	3.468565862
-36.6372	-73.40425	25	29.1198	18.5238	17.0421	15.6597	0	0
-36.40055	-73.31115	25	26.548	18.4765	16.9247	15.7008	66.07530146	5.740005738
-36.17755	-73.21295	25	27.2291	18.6106	20.7422	15.5848	62.25780184	10.05007134
-35.9413	-73.0975	25	29.6734	18.3279	20.7006	15.8315	62.29939755	6.711427134
-35.6921	-72.9759	25	29.6723	18.2691	20.7053	15.8837	62.29470001	5.289785627
-35.44635	-72.856	25	29.0204	18.2086	20.696	15.9379	62.30399852	11.10216697
-35.20405	-72.7347	25	29.2158	18.2002	21.6735	15.9455	61.32649961	16.8834788
-34.9583	-72.6085	25	29.8659	18.0796	21.681	16.0547	61.31899899	13.2684919
-34.7091	-72.4805	25	29.8725	18.0212	21.6854	16.1082	61.31459824	11.81559593
-34.44625	-72.34565	25	32.4894	17.9599	21.6417	16.1646	61.35829916	9.256589679
-34.169	-72.2168	25	31.8632	17.7487	17.8906	16.3623	65.10939756	4.847519229
-33.90525	-72.10715	25	29.1733	17.9023	17.7796	16.218	65.2204093	1.937851085
-33.6552	-72.0036	25	29.238	17.8542	17.7842	16.263	65.21576311	0.539789474
-33.36195	-71.8849	25	37.2018	17.7753	17.224	16.3372	65.77654222	0.042042773
-33.0223	-71.79195	25	36.4522	17.5726	6.6471	16.531	76.35304301	0.127045761
-32.6789	-71.73965	25	28.101	17.8084	5.8596	16.306	0	0
-39.32175	-73.6488	30	53.9356	19.3172	2.9941	15.0011	80.00601744	0.172387815
-38.9761	-73.61825	30	24.3419	19.2555	6.3884	15.0502	76.61166465	0.259525104
-38.7459	-73.5857	30	27.9735	19.1246	6.2928	15.1558	76.70721271	1.701529681
-38.49625	-73.5507	30	27.9569	19.0627	6.3006	15.2062	76.69939452	2.236685874
-38.23875	-73.51455	30	29.4483	19.0005	6.3053	15.2571	76.69469485	1.558760935
-37.97305	-73.4825	30	29.39	18.9169	4.5628	15.3262	78.43720257	5.796015634
-37.714	-73.4565	30	28.0702	18.8806	4.5294	15.3564	78.47060173	9.659959961
-37.3965	-73.4294	30	44.9266	18.8107	3.6976	15.4148	79.30239869	6.809237679
-37.0099	-73.33495	30	47.7428	19.2036	17.4853	15.0919	65.51469746	9.714459485
-36.68915	-73.2057	30	29.1661	18.5144	16.9395	15.6678	66.06049229	0.501979062
-36.45505	-73.1143	30	25.8865	18.464	16.7867	15.7117	66.2132996	3.5468294

-36.23755	-73.0191	30	26.5675	18.6012	20.6596	15.5929	62.34040245	5.357261455
-36.00405	-72.90555	30	29.6387	18.3174	20.6069	15.8407	62.39309957	3.687513629
-35.755	-72.7846	30	29.6353	18.2588	20.6128	15.8929	62.38720169	2.777032849
-35.5101	-72.6657	30	28.819	18.198	20.6007	15.9474	62.39929638	5.524329337
-35.2693	-72.54575	30	29.0119	18.1898	21.584	15.9548	61.41599874	11.15142445
-35.02445	-72.42055	30	29.8259	18.0695	21.5937	16.0639	61.40629776	10.5060047
-34.77545	-72.2932	30	29.8381	18.0112	21.5993	16.1173	61.40069732	8.992127221
-34.51	-72.15765	30	33.0955	17.949	21.5467	16.1747	61.45330075	9.321050604
-34.22735	-72.02685	30	32.5028	17.743	17.8276	16.3678	65.17240311	7.463036611
-33.96085	-71.91655	30	29.157	17.8941	17.6904	16.2257	65.30960008	3.294422062
-33.7105	-71.8135	30	29.2855	17.8461	17.6967	16.2705	65.30324444	0.51496159
-33.4086	-71.69245	30	39.1103	17.7585	17.0328	16.3531	0	0
-33.05155	-71.59535	30	38.4847	17.5743	6.6987	16.5293	76.30133345	0.148605127
-32.69005	-71.53985	30	28.2212	17.8056	5.765	16.3086	0	0
-39.33175	-73.43225	35	53.5723	19.3298	2.8497	14.991	80.1502323	0.140010804
-38.9911	-73.4033	35	23.5891	19.2719	6.2719	15.0372	76.72798557	0.196149945
-38.7643	-73.37185	35	27.9659	19.1482	6.1625	15.1366	76.83748895	1.297808898
-38.5147	-73.3376	35	27.9408	19.087	6.1718	15.1863	76.82821034	2.287684188
-38.256	-73.30205	35	29.7279	19.0248	6.1806	15.2372	76.81939348	2.077086477
-37.98775	-73.27045	35	29.6791	18.9381	4.4473	15.3087	78.55270504	3.811929099
-37.72645	-73.24495	35	28.1594	18.8976	4.4062	15.3423	78.59380219	5.543650269
-37.41845	-73.22035	35	42.6848	18.8308	3.3383	15.398	79.66170152	5.584580994
-37.05205	-73.1319	35	45.5728	19.2573	17.5124	15.0488	65.48759748	11.69522421
-36.74035	-73.0064	35	29.2125	18.5522	16.8372	15.6351	66.16280193	5.903784702
-36.50835	-72.91645	35	25.2251	18.5243	16.6414	15.6593	66.35860985	3.531896485
-36.2965	-72.82435	35	25.9059	18.6713	20.5729	15.5329	62.42711063	3.204017685
-36.0659	-72.71275	35	29.604	18.386	20.513	15.7801	62.48700014	5.604229482
-35.81695	-72.59245	35	29.5984	18.3287	20.52	15.8307	62.48000091	5.216414339
-35.5729	-72.47455	35	28.6177	18.2676	20.5041	15.8851	62.49590302	6.400679831
-35.3337	-72.35595	35	28.8081	18.2609	21.4932	15.8911	61.50679802	6.853303109
-35.0897	-72.2318	35	29.786	18.1408	21.5061	15.9991	61.49390205	9.174174954
-34.84085	-72.1051	35	29.8037	18.0816	21.5129	16.0528	61.48709891	4.46309085
-34.57295	-71.9689	35	33.7018	18.0195	21.4552	16.1097	61.54480059	7.468201898
-34.28495	-71.83625	35	33.1424	17.8057	17.767	16.3085	65.23299763	8.568213745
-34.0156	-71.7253	35	29.1408	17.9459	17.6012	16.1776	65.39880501	3.984357372
-33.76465	-71.62255	35	29.3331	17.902	17.6095	16.2184	65.39049161	1.156261704
-33.45415	-71.4992	35	41.0192	17.8253	16.8595	16.29	66.14052183	0.724288509
-33.0804	-71.39835	35	40.5172	17.6152	6.7452	16.4898	0	0
-32.7016	-71.34005	35	28.3413	17.8144	5.6711	16.3003	0	0
-39.3417	-73.2157	40	53.2173	19.3277	2.7088	14.9927	0	0
-39.0061	-73.18835	40	22.81	19.2685	6.1749	15.0398	0	0
-38.78275	-73.158	40	27.967	19.1438	6.0318	15.1401	76.96818311	0.585528283
-38.53315	-73.12445	40	27.9235	19.0827	6.0426	15.1898	76.95739617	1.698128422
-38.2732	-73.0895	40	30.0023	19.0204	6.0505	15.2407	76.94947663	1.187032477
-38.0024	-73.05835	40	29.9666	18.9352	4.3262	15.311	78.67380563	0.689596918

-37.73885	-73.03335	40	28.3718	18.8946	4.2797	15.3447	78.72032795	0.643144912
-37.4403	-73.01135	40	40.339	18.8248	2.979	15.403	80.02099976	5.488206253
-37.09415	-72.92885	40	43.3061	19.2637	17.5776	15.0437	65.42240151	6.169538621
-36.7916	-72.8071	40	29.3515	18.5429	16.7344	15.6432	66.26560334	5.350998427
-36.56175	-72.7187	40	24.5577	18.512	16.5039	15.6699	66.49610717	2.775926335
-36.35545	-72.6296	40	25.2251	18.6626	20.4961	15.5403	62.50389884	3.951560359
-36.1277	-72.5199	40	29.5738	18.3755	20.4181	15.7894	62.58189999	7.43806965
-35.8789	-72.40025	40	29.5626	18.3184	20.4263	15.8399	62.57370064	5.948655788
-35.6357	-72.28335	40	28.4156	18.2571	20.4086	15.8945	62.59140086	6.255030246
-35.39805	-72.16615	40	28.6007	18.2505	21.4036	15.9003	61.59639505	3.876027431
-35.15495	-72.043	40	29.7444	18.1306	21.4176	16.0083	61.582398	7.131365308
-34.90625	-71.91695	40	29.7723	18.0716	21.4257	16.062	61.57431333	2.279833553
-34.6358	-71.78015	40	34.2944	18.0083	21.3568	16.12	61.64320345	4.819680043
-34.3425	-71.64565	40	33.7749	17.7994	17.698	16.3144	65.30199989	6.067325143
-34.07035	-71.53405	40	29.1386	17.9377	17.511	16.1852	65.48899284	3.135085973
-33.81885	-71.4316	40	29.4454	17.8938	17.5203	16.2259	65.47968049	1.422834549
-33.4998	-71.306	40	42.8479	17.8095	16.6767	16.3049	66.32329872	1.005572057
-33.10935	-71.20145	40	42.461	17.6158	6.7622	16.4893	0	0
-32.71325	-71.14035	40	28.5622	17.8117	5.5774	16.3028	0	0
-39.35175	-72.9992	45	52.8627	19.3256	2.566	14.9944	0	0
-39.02115	-72.9734	45	22.031	19.265	6.0711	15.0426	0	0
-38.8012	-72.9441	45	27.9683	19.1396	5.9012	15.1436	77.09889749	0.167712586
-38.5516	-72.91135	45	27.9063	19.0785	5.9132	15.1932	77.08678519	0.65407784
-38.29045	-72.877	45	30.2768	19.0163	5.9228	15.2441	0	0
-38.0171	-72.8463	45	30.2542	18.9325	4.2074	15.3133	0	0
-37.75125	-72.8218	45	28.5844	18.8918	4.1551	15.3471	0	0
-37.4622	-72.8023	45	37.9949	18.8188	2.5753	15.408	80.42469767	5.566828996
-37.1363	-72.7258	45	41.0394	19.271	17.65	15.0379	65.35000217	1.290823513
-36.84285	-72.60785	45	29.4905	18.5337	16.6325	15.6511	66.36752963	0.397808971
-36.6151	-72.5209	45	23.8904	18.4992	16.3589	15.681	66.6411187	0.927490689
-36.4144	-72.4348	45	24.5444	18.6534	20.4151	15.5481	62.58489517	3.092005691
-36.1895	-72.327	45	29.5436	18.365	20.323	15.7986	62.67699803	4.934804137
-35.94085	-72.20805	45	29.5269	18.308	20.3323	15.8491	62.66770813	3.196778879
-35.6985	-72.0922	45	28.2137	18.2465	20.3117	15.904	62.68829804	2.465944795
-35.4624	-71.9763	45	28.3933	18.24	21.3127	15.9097	61.68731496	1.891928978
-35.22025	-71.8542	45	29.7029	18.1205	21.3288	16.0175	61.67120352	3.976642848
-34.9717	-71.7288	45	29.7409	18.0617	21.3382	16.0711	61.66178937	0.857238631
-34.6987	-71.59135	45	34.887	17.9976	21.2618	16.1298	61.73820265	1.768933832
-34.40005	-71.45505	45	34.4074	17.7933	17.6314	16.3201	65.36860718	2.182144978
-34.1251	-71.3428	45	29.1365	17.9295	17.4209	16.1928	65.57909665	1.273530058
-33.873	-71.24065	45	29.5577	17.8858	17.4318	16.2334	65.56821255	0.735398774
-33.54535	-71.11275	45	44.677	17.7952	16.5089	16.3184	66.49110186	0.2551521
-33.1382	-71.00445	45	44.4048	17.6163	6.7777	16.4888	0	0
-32.7248	-70.94055	45	28.7832	17.8092	5.4851	16.3052	0	0
-39.3604	-72.7825	50	52.5084	19.3366	2.4213	14.9857	0	0

-39.03495	-72.7582	50	21.252	19.2797	5.9597	15.0309	0	0
-38.81855	-72.72995	50	27.9697	19.1618	5.7705	15.1256	0	0
-38.5689	-72.6979	50	27.8893	19.1015	5.7837	15.1745	0	0
-38.30655	-72.66415	50	30.5515	19.0392	5.7974	15.2254	0	0
-38.03065	-72.634	50	30.5419	18.9524	4.0909	15.2968	0	0
-37.7619	-72.61	50	28.7971	18.9076	4.0323	15.3339	0	0
-37.48225	-72.59285	50	35.653	18.8365	2.1186	15.3932	80.88138998	2.691716885
-37.17765	-72.5222	50	38.7729	19.329	17.7309	14.9917	65.26910943	2.309055178
-36.8934	-72.40785	50	29.6297	18.5669	16.5316	15.6224	0	0
-36.66735	-72.32225	50	23.2233	18.5578	16.2054	15.6302	0	0
-36.4724	-72.23915	50	23.8637	18.7235	20.3294	15.4885	62.67058769	1.283253624
-36.25045	-72.13325	50	29.5135	18.4329	20.2277	15.7389	62.77231951	1.932583014
-36.00185	-72.01495	50	29.4912	18.3775	20.2381	15.7876	62.76189606	0.956847753
-35.76035	-71.90005	50	28.0118	18.3156	20.2135	15.8424	62.7864927	0.1794394
-35.5259	-71.78555	50	28.1859	18.3108	21.2204	15.8466	61.77958529	1.304709231
-35.2846	-71.6645	50	29.6614	18.1914	21.2398	15.9534	61.76018808	1.440632437
-35.0362	-71.53975	50	29.7096	18.1318	21.2505	16.0072	0	0
-34.76075	-71.40175	50	35.4798	18.0677	21.1699	16.0655	0	0
-34.4568	-71.2637	50	35.04	17.8558	17.5673	16.2614	0	0
-34.179	-71.15085	50	29.1344	17.9812	17.3308	16.1449	0	0
-33.926	-71.0489	50	29.67	17.9412	17.3439	16.182	0	0
-33.5898	-70.91885	50	46.5065	17.8592	16.3543	16.2583	0	0
-33.16655	-70.8072	50	46.3486	17.6559	6.7919	16.4508	0	0
-32.73645	-70.7408	50	29.0042	17.8199	5.3942	16.2951	0	0
-39.3691	-72.56575	55	52.1643	19.3348	2.2803	14.9871	80.71960676	0.124415479
-39.04875	-72.54295	55	20.4434	19.2768	5.8717	15.0332	0	0
-38.83585	-72.51575	55	27.9816	19.1577	5.6392	15.1289	0	0
-38.5862	-72.48445	55	27.8711	19.0975	5.6539	15.1778	0	0
-38.3227	-72.45135	55	30.8211	19.0351	5.6669	15.2287	0	0
-38.04425	-72.4217	55	30.828	18.9497	3.969	15.299	0	0
-37.77255	-72.3982	55	29.1547	18.9048	3.902	15.3362	0	0
-37.5023	-72.38345	55	33.1883	18.8318	1.6469	15.3972	0	0
-37.21905	-72.31865	55	36.3907	19.3429	17.8683	14.9806	65.13169217	2.045456329
-36.94395	-72.20795	55	29.8777	18.5578	16.4298	15.6302	0	0
-36.7196	-72.12365	55	22.5524	18.5453	16.0608	15.6411	0	0
-36.5304	-72.0435	55	23.1614	18.7152	20.2556	15.4955	0	0
-36.31135	-71.9395	55	29.4887	18.4223	20.1314	15.7482	62.86854328	0.307356748
-36.06285	-71.8219	55	29.4568	18.3671	20.143	15.7967	62.85705426	0.27344522
-35.8222	-71.708	55	27.8094	18.305	20.1164	15.8517	0	0
-35.5893	-71.5948	55	27.9748	18.3004	21.1294	15.8559	61.87057738	0.466461113
-35.34895	-71.47475	55	29.6182	18.1812	21.1499	15.9626	0	0
-35.1007	-71.3507	55	29.6807	18.1217	21.1619	16.0164	0	0
-34.82275	-71.2121	55	36.0599	18.0567	21.0714	16.0756	0	0
-34.5136	-71.0723	55	35.6653	17.8493	17.495	16.2676	0	0
-34.23295	-70.95885	55	29.1455	17.973	17.2396	16.1525	0	0

-33.97905	-70.8571	55	29.8362	17.933	17.2531	16.1895	0	0
-33.63435	-70.72495	55	48.2678	17.8454	16.1898	16.2712	0	0
-33.19495	-70.60995	55	48.2187	17.6556	6.7835	16.4511	0	0
-32.74805	-70.54105	55	29.3063	17.8175	5.3024	16.2974	77.6977042	0.079537415
-39.3778	-72.349	60	51.8205	19.333	2.1373	14.9885	80.86265618	0.537551249
-39.06255	-72.32775	60	19.6349	19.2738	5.7765	15.0356	0	0
-38.8532	-72.3016	60	27.9935	19.1537	5.5081	15.1321	0	0
-38.6035	-72.27105	60	27.853	19.0935	5.5239	15.181	0	0
-38.3388	-72.23855	60	31.0909	19.0312	5.5387	15.2319	0	0
-38.05785	-72.2094	60	31.1141	18.9472	3.8494	15.3011	0	0
-37.7832	-72.1864	60	29.5125	18.9022	3.7749	15.3384	0	0
-37.52235	-72.174	60	30.7262	18.8278	1.0996	15.4005	0	0
-37.26045	-72.1151	60	34.0088	19.3589	18.025	14.968	64.97517062	0.166615063
-36.9945	-72.008	60	30.1259	18.549	16.3297	15.6379	66.67031419	0.363553668
-36.7718	-71.92495	60	21.8818	18.5321	15.9072	15.6525	67.0927046	0.193419895
-36.58835	-71.84785	60	22.4591	18.7064	20.1772	15.5029	0	0
-36.3723	-71.74575	60	29.464	18.4118	20.035	15.7574	0	0
-36.1239	-71.62875	60	29.4225	18.3568	20.0476	15.8059	0	0
-35.8841	-71.5159	60	27.607	18.2944	20.0179	15.8612	0	0
-35.6528	-71.4041	60	27.7638	18.2898	21.037	15.8653	0	0
-35.41335	-71.2851	60	29.575	18.171	21.0597	15.9718	0	0
-35.16525	-71.16165	60	29.652	18.1117	21.073	16.0255	0	0
-34.8848	-71.02245	60	36.6401	18.046	20.976	16.0854	0	0
-34.57035	-70.8809	60	36.2906	17.843	17.4253	16.2735	0	0
-34.28685	-70.76685	60	29.1566	17.9648	17.1485	16.16	65.85153677	0.191316391
-34.0321	-70.66535	60	30.0025	17.925	17.1632	16.197	65.83680527	0.61124204
-33.67885	-70.53105	60	50.0295	17.8327	16.0369	16.2831	66.96303299	0.197597928
-33.22335	-70.4127	60	50.0889	17.6553	6.7757	16.4513	76.22437044	0.07635634
-32.75985	-70.3413	60	29.6085	17.8151	5.2125	16.2996	77.78737259	0.116516858
-39.3852	-72.1321	65	51.477	19.3423	1.9924	14.9811	81.00760171	0.522163871
-39.0752	-72.11225	65	18.8265	19.2867	5.673	15.0253	0	0
-38.8694	-72.0871	65	28.0056	19.1745	5.3771	15.1153	77.62308837	0.100810975
-38.6196	-72.0573	65	27.8351	19.115	5.3937	15.1635	77.60649368	0.116160944
-38.35375	-72.02545	65	31.3609	19.0527	5.4126	15.2143	0	0
-38.07025	-71.99685	65	31.4004	18.9658	3.732	15.2857	0	0
-37.79195	-71.97435	65	29.8704	18.9167	3.6509	15.3263	0	0
-37.5404	-71.96415	65	28.2674	18.8442	0.4571	15.3867	0	0
-37.30115	-71.911	65	31.6271	19.4267	18.2053	14.9145	0	0
-37.0445	-71.8074	65	30.3741	18.5761	16.2313	15.6145	66.76868768	2.274570367
-36.82295	-71.72545	65	21.2113	18.5886	15.744	15.6037	67.25599703	1.953667355
-36.64535	-71.6513	65	21.7569	18.7766	20.0937	15.4435	62.90630231	0.957391342
-36.4323	-71.5511	65	29.4394	18.479	19.9384	15.6986	63.06160149	0.361760099
-36.18395	-71.4348	65	29.3883	18.4258	19.952	15.7451	0	0
-35.945	-71.32295	65	27.4047	18.363	19.918	15.8004	0	0
-35.71535	-71.21245	65	27.5529	18.3602	20.9431	15.8029	62.05689044	0.275327525
-35.47685	-71.09445	65	29.5319	18.2416	20.9693	15.9083	62.0306873	1.723484912
-35.2289	-70.9717	65	29.6233	18.1815	20.9841	15.9623	62.01591998	1.220509394

-34.946	-70.832	65	37.2203	18.1158	20.8836	16.0218	62.11636382	0.108792944
-34.62635	-70.6888	65	36.916	17.9052	17.3579	16.2154	0	0
-34.33995	-70.57415	65	29.1678	18.0165	17.0575	16.1125	65.94248477	0.597384815
-34.084	-70.4728	65	30.1688	17.9798	17.0744	16.1462	65.92558734	1.047813553
-33.72225	-70.3365	65	51.7915	17.8942	15.8945	16.2256	67.10556299	0.167854004
-33.25115	-70.2151	65	51.959	17.6938	6.7684	16.4146	76.23185153	0.06987164
-32.77145	-70.1415	65	29.9108	17.8274	5.1244	16.2881	77.8756813	0.127246334
-39.39255	-71.91525	70	51.1459	19.3408	1.8513	14.9823	81.14890226	0.10598107
-39.08775	-71.8968	70	17.9845	19.2844	5.5988	15.0271	0	0
-38.8856	-71.8726	70	28.0301	19.1707	5.2453	15.1184	77.754797	0.234337442
-38.63575	-71.8435	70	27.8161	19.1112	5.2632	15.1666	77.7368652	0.308938216
-38.36875	-71.8123	70	31.626	19.0489	5.2817	15.2174	77.71796539	0.078270428
-38.08275	-71.7843	70	31.6861	18.9633	3.6094	15.2877	0	0
-37.8007	-71.76235	70	30.4001	18.9141	3.514	15.3285	79.48621766	0.098036938
-37.55845	-71.7543	70	25.6632	18.8438	-0.246	15.3871	83.24606603	0.341123264
-37.34185	-71.70695	70	29.104	19.4557	18.4814	14.8918	64.51856879	0.870183288
-37.09445	-71.60685	70	30.7521	18.5674	16.1319	15.622	66.86810143	3.429553025
-36.87405	-71.5259	70	20.5412	18.5757	15.5905	15.6149	67.40950037	2.7556069
-36.7023	-71.45475	70	21.0297	18.769	20.0245	15.45	62.97550612	1.589092226
-36.4923	-71.3565	70	29.4211	18.4684	19.8407	15.7078	63.15927373	0.781509885
-36.24405	-71.2408	70	29.3554	18.4154	19.8554	15.7543	63.14490903	0.061841488
-36.0059	-71.1299	70	27.2019	18.3524	19.8194	15.8097	0	0
-35.7778	-71.0208	70	27.3381	18.3497	20.8507	15.8121	62.14932291	1.311870419
-35.54025	-70.90385	70	29.4871	18.2313	20.8779	15.9175	62.12210651	2.933235388
-35.29245	-70.7817	70	29.5967	18.1714	20.894	15.9714	62.10599929	1.930932075
-35.00715	-70.6415	70	37.7887	18.1048	20.7848	16.0318	62.21519611	0.427358446
-34.6823	-70.4967	70	37.5342	17.8984	17.2828	16.2217	65.71722394	0.104440138
-34.39305	-70.3815	70	29.1914	18.0083	16.9654	16.12	66.03455856	0.589146998
-34.136	-70.2803	70	30.3804	17.9716	16.9817	16.1538	66.01833584	0.808526593
-33.7657	-70.14195	70	53.4949	17.8817	15.7423	16.2372	0	0
-33.279	-70.0175	70	53.767	17.6929	6.7427	16.4154	0	0
-32.7832	-69.9417	70	30.2783	17.8251	5.0344	16.2903	77.9658311	0.084078762
-39.3999	-71.69835	75	50.8151	19.3394	1.7082	14.9834	0	0
-39.1003	-71.6813	75	17.1425	19.2819	5.5172	15.0291	0	0
-38.9018	-71.6581	75	28.0547	19.167	5.1138	15.1214	0	0
-38.6519	-71.6298	75	27.7973	19.1075	5.1326	15.1696	0	0
-38.3837	-71.59925	75	31.8914	19.0453	5.1529	15.2204	0	0
-38.09515	-71.57175	75	31.9718	18.961	3.4891	15.2896	0	0
-37.80945	-71.5503	75	30.9299	18.9117	3.3819	15.3305	0	0
-37.5765	-71.54445	75	23.0638	18.847	-1.1077	15.3845	0	0
-37.38255	-71.50285	75	26.5817	19.4909	18.8099	14.8643	0	0
-37.14445	-71.4063	75	31.1302	18.559	16.035	15.6292	0	0
-36.92515	-71.32645	75	19.8713	18.562	15.4267	15.6266	0	0
-36.75925	-71.2582	75	20.3025	18.7608	19.9504	15.4569	0	0
-36.5523	-71.1618	75	29.4028	18.4579	19.7429	15.717	0	0
-36.3041	-71.0468	75	29.3227	18.405	19.7586	15.7634	0	0

-36.0668	-70.93695	75	26.9992	18.3418	19.7193	15.8191	0	0
-35.84035	-70.82915	75	27.1233	18.3391	20.7569	15.8215	0	0
-35.60375	-70.71325	75	29.4423	18.2211	20.7863	15.9267	0	0
-35.3561	-70.5918	75	29.5702	18.1614	20.8038	15.9805	0	0
-35.06835	-70.45105	75	38.3572	18.0942	20.6889	16.0414	0	0
-34.73825	-70.3046	75	38.1523	17.8919	17.2101	16.2277	0	0
-34.4461	-70.1888	75	29.2151	18.0002	16.8734	16.1275	0	0
-34.18795	-70.0877	75	30.592	17.9635	16.8903	16.1613	0	0
-33.80915	-69.94735	75	55.1986	17.8702	15.5995	16.248	0	0
-33.30685	-69.8199	75	55.5749	17.6921	6.7186	16.4162	0	0
-32.79495	-69.7419	75	30.6459	17.8229	4.9466	16.2923	0	0

Table D9: Yue et al. (2014) parameters.

Latitude	Longitude	Depth (km)	Length (km)	Width (km)	Strike	Dip	Rake	Slip (m)
-38.533	-74.513	7.856	37.85	40.84	16	15.562	89	1.411
-38.65	-74.078	16.201	39.18	43.81	16	17.153	0	0
-38.757	-73.607	26	39.36	42.9	16	18.752	91.42	1.319
-38.86	-73.15	37.753	39.5	48.31	16	20.231	116.661	1.591
-38.966	-72.643	54.054	40.03	44.51	16	22.275	0	0
-39.063	-72.191	72.18	39.9	44.51	16	25.015	101.175	1.412
-38.196	-74.454	7.856	38.76	40.12	16	15.225	117.362	7.557
-38.3	-74.025	16.201	39.4	45.36	16	16.761	0	0
-38.407	-73.537	26	39.21	39.94	16	18.408	119	2.177
-38.505	-73.118	37.753	39.44	45.36	16	19.767	94.153	1.66
-38.606	-72.649	54.054	39.83	46.1	16	21.699	0	0
-38.705	-72.178	72.18	40.08	46.1	16	24.55	0	0
-37.849	-74.405	7.856	39.29	37.05	16	14.833	102.796	7.969
-37.945	-74.013	16.201	39.3	47.03	16	16.24	111.996	2.513
-38.055	-73.507	26	39.28	39.42	16	17.94	108.438	6.295
-38.151	-73.096	37.753	39.29	43.22	16	19.351	107.057	2.258
-38.248	-72.655	54.054	39.48	45.22	16	21.298	119	0.452
-38.345	-72.197	72.18	39.9	45.22	16	23.946	0	0
-37.499	-74.345	7.856	39.23	35.25	16	14.439	0	0
-37.593	-73.976	16.201	39.35	46.97	16	15.761	95.314	4.114
-37.703	-73.474	26	39.29	39.99	16	17.474	102.692	7.672
-37.799	-73.057	37.753	39.35	42.05	16	18.862	111.141	2.407
-37.893	-72.632	54.054	39.47	43.05	16	20.843	119	0.396
-37.986	-72.204	72.18	39.57	43.05	16	23.341	0	0
-37.152	-74.265	7.856	39.36	34.85	16	14.029	89	6.432
-37.244	-73.901	16.201	39.49	46.38	16	15.353	109.756	6.964
-37.354	-73.408	26	39.61	39.96	16	17.071	101.648	7.105
-37.449	-72.993	37.753	39.59	40.75	16	18.433	109.547	3.557
-37.54	-72.587	54.054	39.61	42.23	16	20.373	89	0.483
-37.631	-72.17	72.18	39.51	42.23	16	22.961	0	0
-36.806	-74.172	7.856	39.48	34.43	16	13.608	119	12.69
-36.896	-73.815	16.201	39.61	43.19	16	14.933	89	6.368
-36.999	-73.36	26	39.94	40.68	16	16.517	106.093	8.445
-37.095	-72.939	37.753	39.97	40.83	16	17.93	99.991	4.941
-37.186	-72.533	54.054	39.75	43.21	16	20.098	89	0.724

-37.279	-72.106	72.18	39.61	43.21	16	22.695	89	0.168
-36.461	-74.069	7.856	39.67	33.35	16	13.219	119	0.684
-36.547	-73.725	16.201	39.72	38.82	16	14.49	89	1.949
-36.642	-73.321	26	39.77	40.8	16	15.904	119	7.418
-36.737	-72.9	37.753	40.11	42.94	16	17.339	89	2.839
-36.832	-72.471	54.054	39.93	44.56	16	19.703	0	0
-36.928	-72.03	72.18	39.68	44.56	16	22.432	89	0.178
-36.12	-73.937	7.856	39.81	31.92	16	12.944	89	2.775
-36.202	-73.609	16.201	39.86	35.92	16	14.143	89	0.238
-36.29	-73.24	26	39.91	37.66	16	15.41	89	9.77
-36.378	-72.856	37.753	39.84	44.42	16	16.813	115.857	7.178
-36.476	-72.412	54.054	39.88	46.85	16	19.28	89	0.402
-36.578	-71.946	72.18	39.81	46.85	16	22.211	89	0.152
-35.783	-73.788	7.856	39.78	30.99	16	12.759	119	3.52
-35.862	-73.472	16.201	40.12	36	16	13.858	0	0
-35.949	-73.103	26	40.57	34.73	16	15.117	89	10.74
-36.03	-72.754	37.753	40.43	42.92	16	16.614	119	8.279
-36.124	-72.329	54.054	40.04	46.85	16	18.978	89.033	4.271
-36.226	-71.865	72.18	39.79	46.85	16	21.846	89	1.402
-35.446	-73.641	7.856	40.01	32.81	16	12.562	89	7.247
-35.527	-73.305	16.201	40.62	38.5	16	13.694	89	7.847
-35.619	-72.91	26	40.69	33.99	16	15.072	96.318	5.618
-35.698	-72.571	37.753	40.77	40.91	16	16.656	119	8.148
-35.787	-72.171	54.054	40.45	42.02	16	19.076	0	0
-35.877	-71.766	72.18	39.96	42.02	16	21.564	92.457	0.332
-35.112	-73.476	7.856	40.27	36.09	16	12.438	119	7.775
-35.2	-73.106	16.201	40.38	38.97	16	13.633	89	17.21
-35.293	-72.707	26	40.33	34.57	16	15.208	99.993	12.6
-35.373	-72.363	37.753	40.65	40.02	16	17.067	119	7.1
-35.461	-71.975	54.054	40.87	39.67	16	19.364	103.954	0.262
-35.544	-71.599	72.18	40.35	39.67	16	21.638	119	0.836
-34.782	-73.297	7.856	40.71	36.87	16	12.367	111.258	6.95
-34.871	-72.92	16.201	40.1	39.12	16	13.491	119	15.93
-34.964	-72.521	26	40.46	36.71	16	15.345	109.791	9.822
-35.05	-72.154	37.753	40.9	41.69	16	17.343	119	5.25
-35.143	-71.748	54.054	40.51	38.27	16	19.722	0	0
-35.223	-71.391	72.18	40.29	38.27	16	21.907	119	1.493
-34.451	-73.107	7.856	40.81	34.16	16	12.322	89	16.34
-34.535	-72.761	16.201	40.06	42.66	16	13.363	89	15.89

-34.637	-72.325	26	40.24	39.57	16	15.441	105.143	10.53
-34.732	-71.929	37.753	40.37	41.37	16	17.629	90.652	5.969
-34.826	-71.529	54.054	40.08	38.11	16	19.961	0	0
-34.907	-71.176	72.18	39.74	38.11	16	22.095	0	0
-34.113	-72.933	7.856	40.84	32.79	16	12.134	106.065	9.147
-34.198	-72.605	16.201	40.55	45.23	16	13.232	89	2.077
-34.308	-72.144	26	39.83	41.94	16	15.457	92.053	8.841
-34.41	-71.724	37.753	39.6	41.63	16	17.685	117.972	6.049
-34.508	-71.324	54.054	39.45	37.59	16	20.035	0	0
-34.589	-70.978	72.18	39.23	37.59	16	22.113	89	0.215
-33.772	-72.77	7.856	40.84	34.17	16	11.781	0	0
-33.864	-72.429	16.201	40.55	42.16	16	13.195	119	3.06
-33.969	-72.004	26	39.83	41.89	16	15.124	118.391	3.139
-34.073	-71.587	37.753	39.6	40.16	16	17.311	117.862	2.718
-34.167	-71.205	54.054	39.45	38.15	16	19.479	0	0
-34.251	-70.855	72.18	39.23	38.15	16	21.574	91.067	1.103

Table D10: Method 1 parameters.

Latitude	Longitude	Depth (km)	Length (km)	Width (km)	Strike	Dip	Rake	Slip (m)
-38.21598991	-74.77933821	0	50	50	16	14	104	0
-37.78385308	-74.62158757	0	50	50	16	14	104	0
-37.35059348	-74.47012233	0	50	50	16	14	104	0
-36.91732388	-74.31863746	0	50	50	16	14	104	5
-36.48406428	-74.16715313	0	50	50	16	14	104	5
-36.05079467	-74.01564959	0	50	50	16	14	104	5
-35.61753505	-73.86414701	0	50	50	16	14	104	5
-35.18426543	-73.71262561	0	50	50	16	14	104	5
-34.75100581	-73.56110555	0	50	50	16	14	104	5
-34.31773619	-73.40956703	0	50	50	16	14	104	15
-33.88447656	-73.25803022	0	50	50	16	14	104	10
-33.45120692	-73.10647529	0	50	50	16	14	104	0
-38.34022932	-74.24965616	12.1	50	50	16	14	104	0
-37.90809296	-74.09163535	12.1	50	50	16	14	104	5
-37.47482337	-73.94016293	12.1	50	50	16	14	104	10
-37.04156377	-73.78869079	12.1	50	50	16	14	104	5
-36.60829417	-73.63719916	12.1	50	50	16	14	104	5
-36.17503456	-73.48570824	12.1	50	50	16	14	104	10
-35.74176494	-73.33419824	12.1	50	50	16	14	104	10
-35.30850533	-73.18268933	12.1	50	50	16	14	104	10
-34.8752357	-73.03116174	12.1	50	50	16	14	104	15
-34.44197608	-72.87963563	12.1	50	50	16	14	104	15
-34.00870645	-72.72809118	12.1	50	50	16	14	104	5
-33.57544682	-72.57654856	12.1	50	50	16	14	104	0
-38.46445873	-73.71996495	24.2	50	50	16	14	104	5
-38.03232285	-73.56167233	24.2	50	50	16	14	104	10
-37.59906325	-73.41021272	24.2	50	50	16	14	104	10
-37.16579366	-73.25873336	24.2	50	50	16	14	104	0
-36.73253405	-73.10725442	24.2	50	50	16	14	104	5
-36.29926444	-72.95575614	24.2	50	50	16	14	104	5
-35.86600483	-72.80425872	24.2	50	50	16	14	104	5
-35.43273522	-72.65274236	24.2	50	50	16	14	104	10
-34.9994756	-72.50122723	24.2	50	50	16	14	104	10
-34.56621597	-72.34969354	24.2	50	50	16	14	104	10
-34.13294634	-72.19816147	24.2	50	50	16	14	104	10
-33.69968671	-72.04662117	24.2	50	50	16	14	104	0

Table D11: Method 1 Increase 2.5 m parameters.

Latitude	Longitude	Depth (km)	Length (km)	Width (km)	Strike	Dip	Rake	Slip (m)
-38.21598991	-74.77933821	0	50	50	16	14	104	2.5
-37.78385308	-74.62158757	0	50	50	16	14	104	2.5
-37.35059348	-74.47012233	0	50	50	16	14	104	2.5
-36.91732388	-74.31863746	0	50	50	16	14	104	7.5
-36.48406428	-74.16715313	0	50	50	16	14	104	7.5
-36.05079467	-74.01564959	0	50	50	16	14	104	7.5
-35.61753505	-73.86414701	0	50	50	16	14	104	7.5
-35.18426543	-73.71262561	0	50	50	16	14	104	7.5
-34.75100581	-73.56110555	0	50	50	16	14	104	7.5
-34.31773619	-73.40956703	0	50	50	16	14	104	17.5
-33.88447656	-73.25803022	0	50	50	16	14	104	12.5
-33.45120692	-73.10647529	0	50	50	16	14	104	2.5
-38.34022932	-74.24965616	12.1	50	50	16	14	104	2.5
-37.90809296	-74.09163535	12.1	50	50	16	14	104	7.5
-37.47482337	-73.94016293	12.1	50	50	16	14	104	12.5
-37.04156377	-73.78869079	12.1	50	50	16	14	104	7.5
-36.60829417	-73.63719916	12.1	50	50	16	14	104	7.5
-36.17503456	-73.48570824	12.1	50	50	16	14	104	12.5
-35.74176494	-73.33419824	12.1	50	50	16	14	104	12.5
-35.30850533	-73.18268933	12.1	50	50	16	14	104	12.5
-34.8752357	-73.03116174	12.1	50	50	16	14	104	17.5
-34.44197608	-72.87963563	12.1	50	50	16	14	104	17.5
-34.00870645	-72.72809118	12.1	50	50	16	14	104	7.5
-33.57544682	-72.57654856	12.1	50	50	16	14	104	2.5
-38.46445873	-73.71996495	24.2	50	50	16	14	104	7.5
-38.03232285	-73.56167233	24.2	50	50	16	14	104	12.5
-37.59906325	-73.41021272	24.2	50	50	16	14	104	12.5
-37.16579366	-73.25873336	24.2	50	50	16	14	104	2.5
-36.73253405	-73.10725442	24.2	50	50	16	14	104	7.5
-36.29926444	-72.95575614	24.2	50	50	16	14	104	7.5
-35.86600483	-72.80425872	24.2	50	50	16	14	104	7.5
-35.43273522	-72.65274236	24.2	50	50	16	14	104	12.5
-34.9994756	-72.50122723	24.2	50	50	16	14	104	12.5
-34.56621597	-72.34969354	24.2	50	50	16	14	104	12.5
-34.13294634	-72.19816147	24.2	50	50	16	14	104	12.5
-33.69968671	-72.04662117	24.2	50	50	16	14	104	2.5

Table D12: Method 1 Increase 5 m parameters.

Latitude	Longitude	Depth (km)	Length (km)	Width (km)	Strike	Dip	Rake	Slip (m)
-38.21598991	-74.77933821	0	50	50	16	14	104	5
-37.78385308	-74.62158757	0	50	50	16	14	104	5
-37.35059348	-74.47012233	0	50	50	16	14	104	5
-36.91732388	-74.31863746	0	50	50	16	14	104	10
-36.48406428	-74.16715313	0	50	50	16	14	104	10
-36.05079467	-74.01564959	0	50	50	16	14	104	10
-35.61753505	-73.86414701	0	50	50	16	14	104	10
-35.18426543	-73.71262561	0	50	50	16	14	104	10
-34.75100581	-73.56110555	0	50	50	16	14	104	10
-34.31773619	-73.40956703	0	50	50	16	14	104	20
-33.88447656	-73.25803022	0	50	50	16	14	104	15
-33.45120692	-73.10647529	0	50	50	16	14	104	5
-38.34022932	-74.24965616	12.1	50	50	16	14	104	5
-37.90809296	-74.09163535	12.1	50	50	16	14	104	10
-37.47482337	-73.94016293	12.1	50	50	16	14	104	15
-37.04156377	-73.78869079	12.1	50	50	16	14	104	10
-36.60829417	-73.63719916	12.1	50	50	16	14	104	10
-36.17503456	-73.48570824	12.1	50	50	16	14	104	15
-35.74176494	-73.33419824	12.1	50	50	16	14	104	15
-35.30850533	-73.18268933	12.1	50	50	16	14	104	15
-34.8752357	-73.03116174	12.1	50	50	16	14	104	20
-34.44197608	-72.87963563	12.1	50	50	16	14	104	20
-34.00870645	-72.72809118	12.1	50	50	16	14	104	10
-33.57544682	-72.57654856	12.1	50	50	16	14	104	5
-38.46445873	-73.71996495	24.2	50	50	16	14	104	10
-38.03232285	-73.56167233	24.2	50	50	16	14	104	15
-37.59906325	-73.41021272	24.2	50	50	16	14	104	15
-37.16579366	-73.25873336	24.2	50	50	16	14	104	5
-36.73253405	-73.10725442	24.2	50	50	16	14	104	10
-36.29926444	-72.95575614	24.2	50	50	16	14	104	10
-35.86600483	-72.80425872	24.2	50	50	16	14	104	10
-35.43273522	-72.65274236	24.2	50	50	16	14	104	15
-34.9994756	-72.50122723	24.2	50	50	16	14	104	15
-34.56621597	-72.34969354	24.2	50	50	16	14	104	15
-34.13294634	-72.19816147	24.2	50	50	16	14	104	15
-33.69968671	-72.04662117	24.2	50	50	16	14	104	5

Table D13: Method 1 Reduce 2.5 m parameters.

Latitude	Longitude	Depth (km)	Length (km)	Width (km)	Strike	Dip	Rake	Slip (m)
-38.21598991	-74.77933821	0	50	50	16	14	104	0
-37.78385308	-74.62158757	0	50	50	16	14	104	0
-37.35059348	-74.47012233	0	50	50	16	14	104	0
-36.91732388	-74.31863746	0	50	50	16	14	104	2.5
-36.48406428	-74.16715313	0	50	50	16	14	104	2.5
-36.05079467	-74.01564959	0	50	50	16	14	104	2.5
-35.61753505	-73.86414701	0	50	50	16	14	104	2.5
-35.18426543	-73.71262561	0	50	50	16	14	104	2.5
-34.75100581	-73.56110555	0	50	50	16	14	104	2.5
-34.31773619	-73.40956703	0	50	50	16	14	104	12.5
-33.88447656	-73.25803022	0	50	50	16	14	104	7.5
-33.45120692	-73.10647529	0	50	50	16	14	104	0
-38.34022932	-74.24965616	12.1	50	50	16	14	104	0
-37.90809296	-74.09163535	12.1	50	50	16	14	104	2.5
-37.47482337	-73.94016293	12.1	50	50	16	14	104	7.5
-37.04156377	-73.78869079	12.1	50	50	16	14	104	2.5
-36.60829417	-73.63719916	12.1	50	50	16	14	104	2.5
-36.17503456	-73.48570824	12.1	50	50	16	14	104	7.5
-35.74176494	-73.33419824	12.1	50	50	16	14	104	7.5
-35.30850533	-73.18268933	12.1	50	50	16	14	104	7.5
-34.8752357	-73.03116174	12.1	50	50	16	14	104	12.5
-34.44197608	-72.87963563	12.1	50	50	16	14	104	12.5
-34.00870645	-72.72809118	12.1	50	50	16	14	104	2.5
-33.57544682	-72.57654856	12.1	50	50	16	14	104	0
-38.46445873	-73.71996495	24.2	50	50	16	14	104	2.5
-38.03232285	-73.56167233	24.2	50	50	16	14	104	7.5
-37.59906325	-73.41021272	24.2	50	50	16	14	104	7.5
-37.16579366	-73.25873336	24.2	50	50	16	14	104	0
-36.73253405	-73.10725442	24.2	50	50	16	14	104	2.5
-36.29926444	-72.95575614	24.2	50	50	16	14	104	2.5
-35.86600483	-72.80425872	24.2	50	50	16	14	104	2.5
-35.43273522	-72.65274236	24.2	50	50	16	14	104	7.5
-34.9994756	-72.50122723	24.2	50	50	16	14	104	7.5
-34.56621597	-72.34969354	24.2	50	50	16	14	104	7.5
-34.13294634	-72.19816147	24.2	50	50	16	14	104	7.5
-33.69968671	-72.04662117	24.2	50	50	16	14	104	0

Table D14: Method 1 Reduce 5 m parameters.

Latitude	Longitude	Depth (km)	Length (km)	Width (km)	Strike	Dip	Rake	Slip (m)
-38.21598991	-74.77933821	0	50	50	16	14	104	0
-37.78385308	-74.62158757	0	50	50	16	14	104	0
-37.35059348	-74.47012233	0	50	50	16	14	104	0
-36.91732388	-74.31863746	0	50	50	16	14	104	0
-36.48406428	-74.16715313	0	50	50	16	14	104	0
-36.05079467	-74.01564959	0	50	50	16	14	104	0
-35.61753505	-73.86414701	0	50	50	16	14	104	0
-35.18426543	-73.71262561	0	50	50	16	14	104	0
-34.75100581	-73.56110555	0	50	50	16	14	104	0
-34.31773619	-73.40956703	0	50	50	16	14	104	10
-33.88447656	-73.25803022	0	50	50	16	14	104	5
-33.45120692	-73.10647529	0	50	50	16	14	104	0
-38.34022932	-74.24965616	12.1	50	50	16	14	104	0
-37.90809296	-74.09163535	12.1	50	50	16	14	104	0
-37.47482337	-73.94016293	12.1	50	50	16	14	104	5
-37.04156377	-73.78869079	12.1	50	50	16	14	104	0
-36.60829417	-73.63719916	12.1	50	50	16	14	104	0
-36.17503456	-73.48570824	12.1	50	50	16	14	104	5
-35.74176494	-73.33419824	12.1	50	50	16	14	104	5
-35.30850533	-73.18268933	12.1	50	50	16	14	104	5
-34.8752357	-73.03116174	12.1	50	50	16	14	104	10
-34.44197608	-72.87963563	12.1	50	50	16	14	104	10
-34.00870645	-72.72809118	12.1	50	50	16	14	104	0
-33.57544682	-72.57654856	12.1	50	50	16	14	104	0
-38.46445873	-73.71996495	24.2	50	50	16	14	104	0
-38.03232285	-73.56167233	24.2	50	50	16	14	104	5
-37.59906325	-73.41021272	24.2	50	50	16	14	104	5
-37.16579366	-73.25873336	24.2	50	50	16	14	104	0
-36.73253405	-73.10725442	24.2	50	50	16	14	104	0
-36.29926444	-72.95575614	24.2	50	50	16	14	104	0
-35.86600483	-72.80425872	24.2	50	50	16	14	104	0
-35.43273522	-72.65274236	24.2	50	50	16	14	104	5
-34.9994756	-72.50122723	24.2	50	50	16	14	104	5
-34.56621597	-72.34969354	24.2	50	50	16	14	104	5
-34.13294634	-72.19816147	24.2	50	50	16	14	104	5
-33.69968671	-72.04662117	24.2	50	50	16	14	104	0

Table D15: Method 1 Composite parameters.

Latitude	Longitude	Depth (km)	Length (km)	Width (km)	Strike	Dip	Rake	Slip (m)
-38.2159899	-74.7793382	0	50	50	16	14	104	5
-37.7838531	-74.6215876	0	50	50	16	14	104	5
-37.3505935	-74.4701223	0	50	50	16	14	104	5
-36.9173239	-74.3186375	0	50	50	16	14	104	0
-36.4840643	-74.1671531	0	50	50	16	14	104	10
-36.0507947	-74.0156496	0	50	50	16	14	104	10
-35.6175351	-73.864147	0	50	50	16	14	104	10
-35.1842654	-73.7126256	0	50	50	16	14	104	7.5
-34.7510058	-73.5611056	0	50	50	16	14	104	10
-34.3177362	-73.409567	0	50	50	16	14	104	20
-33.8844766	-73.2580302	0	50	50	16	14	104	15
-33.4512069	-73.1064753	0	50	50	16	14	104	5
-38.3402293	-74.2496562	12.1	50	50	16	14	104	5
-37.908093	-74.0916354	12.1	50	50	16	14	104	10
-37.4748234	-73.9401629	12.1	50	50	16	14	104	15
-37.0415638	-73.7886908	12.1	50	50	16	14	104	0
-36.6082942	-73.6371992	12.1	50	50	16	14	104	10
-36.1750346	-73.4857082	12.1	50	50	16	14	104	15
-35.7417649	-73.3341982	12.1	50	50	16	14	104	15
-35.3085053	-73.1826893	12.1	50	50	16	14	104	13
-34.8752357	-73.0311617	12.1	50	50	16	14	104	20
-34.4419761	-72.8796356	12.1	50	50	16	14	104	20
-34.0087065	-72.7280912	12.1	50	50	16	14	104	10
-33.5754468	-72.5765486	12.1	50	50	16	14	104	5
-38.4644587	-73.719965	24.2	50	50	16	14	104	10
-38.0323229	-73.5616723	24.2	50	50	16	14	104	15
-37.5990633	-73.4102127	24.2	50	50	16	14	104	15
-37.1657937	-73.2587334	24.2	50	50	16	14	104	0
-36.7325341	-73.1072544	24.2	50	50	16	14	104	10
-36.2992644	-72.9557561	24.2	50	50	16	14	104	10
-35.8660048	-72.8042587	24.2	50	50	16	14	104	10
-35.4327352	-72.6527424	24.2	50	50	16	14	104	13
-34.9994756	-72.5012272	24.2	50	50	16	14	104	15
-34.566216	-72.3496935	24.2	50	50	16	14	104	15
-34.1329463	-72.1981615	24.2	50	50	16	14	104	15
-33.6996867	-72.0466212	24.2	50	50	16	14	104	5

Table D16: Method 2 parameters.

Latitude	Longitude	Depth (km)	Length (km)	Width (km)	Strike	Dip	Rake	Slip (m)
-38.21598991	-74.77933821	0	50	50	16	14	104	0
-37.78385308	-74.62158757	0	50	50	16	14	104	0
-37.35059348	-74.47012233	0	50	50	16	14	104	0
-36.91732388	-74.31863746	0	50	50	16	14	104	10
-36.48406428	-74.16715313	0	50	50	16	14	104	0
-36.05079467	-74.01564959	0	50	50	16	14	104	0
-35.61753505	-73.86414701	0	50	50	16	14	104	0
-35.18426543	-73.71262561	0	50	50	16	14	104	5
-34.75100581	-73.56110555	0	50	50	16	14	104	5
-34.31773619	-73.40956703	0	50	50	16	14	104	15
-33.88447656	-73.25803022	0	50	50	16	14	104	10
-33.45120692	-73.10647529	0	50	50	16	14	104	0
-38.34022932	-74.24965616	12.1	50	50	16	14	104	0
-37.90809296	-74.09163535	12.1	50	50	16	14	104	5
-37.47482337	-73.94016293	12.1	50	50	16	14	104	10
-37.04156377	-73.78869079	12.1	50	50	16	14	104	5
-36.60829417	-73.63719916	12.1	50	50	16	14	104	10
-36.17503456	-73.48570824	12.1	50	50	16	14	104	0
-35.74176494	-73.33419824	12.1	50	50	16	14	104	0
-35.30850533	-73.18268933	12.1	50	50	16	14	104	10
-34.8752357	-73.03116174	12.1	50	50	16	14	104	15
-34.44197608	-72.87963563	12.1	50	50	16	14	104	15
-34.00870645	-72.72809118	12.1	50	50	16	14	104	5
-33.57544682	-72.57654856	12.1	50	50	16	14	104	0
-38.46445873	-73.71996495	24.2	50	50	16	14	104	5
-38.03232285	-73.56167233	24.2	50	50	16	14	104	10
-37.59906325	-73.41021272	24.2	50	50	16	14	104	10
-37.16579366	-73.25873336	24.2	50	50	16	14	104	10
-36.73253405	-73.10725442	24.2	50	50	16	14	104	10
-36.29926444	-72.95575614	24.2	50	50	16	14	104	10
-35.86600483	-72.80425872	24.2	50	50	16	14	104	10
-35.43273522	-72.65274236	24.2	50	50	16	14	104	10
-34.9994756	-72.50122723	24.2	50	50	16	14	104	10
-34.56621597	-72.34969354	24.2	50	50	16	14	104	10
-34.13294634	-72.19816147	24.2	50	50	16	14	104	10
-33.69968671	-72.04662117	24.2	50	50	16	14	104	0

Table D17: Method 2 Increase 2.5 m parameters.

Latitude	Longitude	Depth (km)	Length (km)	Width (km)	Strike	Dip	Rake	Slip (m)
-38.2159899	-74.7793382	0	50	50	16	14	104	2.5
-37.7838531	-74.6215876	0	50	50	16	14	104	2.5
-37.3505935	-74.4701223	0	50	50	16	14	104	2.5
-36.9173239	-74.3186375	0	50	50	16	14	104	12.5
-36.4840643	-74.1671531	0	50	50	16	14	104	2.5
-36.0507947	-74.0156496	0	50	50	16	14	104	2.5
-35.6175351	-73.864147	0	50	50	16	14	104	2.5
-35.1842654	-73.7126256	0	50	50	16	14	104	7.5
-34.7510058	-73.5611056	0	50	50	16	14	104	7.5
-34.3177362	-73.409567	0	50	50	16	14	104	17.5
-33.8844766	-73.2580302	0	50	50	16	14	104	12.5
-33.4512069	-73.1064753	0	50	50	16	14	104	2.5
-38.3402293	-74.2496562	12.1	50	50	16	14	104	2.5
-37.908093	-74.0916354	12.1	50	50	16	14	104	7.5
-37.4748234	-73.9401629	12.1	50	50	16	14	104	12.5
-37.0415638	-73.7886908	12.1	50	50	16	14	104	7.5
-36.6082942	-73.6371992	12.1	50	50	16	14	104	12.5
-36.1750346	-73.4857082	12.1	50	50	16	14	104	2.5
-35.7417649	-73.3341982	12.1	50	50	16	14	104	2.5
-35.3085053	-73.1826893	12.1	50	50	16	14	104	12.5
-34.8752357	-73.0311617	12.1	50	50	16	14	104	17.5
-34.4419761	-72.8796356	12.1	50	50	16	14	104	17.5
-34.0087065	-72.7280912	12.1	50	50	16	14	104	7.5
-33.5754468	-72.5765486	12.1	50	50	16	14	104	2.5
-38.4644587	-73.719965	24.2	50	50	16	14	104	7.5
-38.0323229	-73.5616723	24.2	50	50	16	14	104	12.5
-37.5990633	-73.4102127	24.2	50	50	16	14	104	12.5
-37.1657937	-73.2587334	24.2	50	50	16	14	104	12.5
-36.7325341	-73.1072544	24.2	50	50	16	14	104	12.5
-36.2992644	-72.9557561	24.2	50	50	16	14	104	12.5
-35.8660048	-72.8042587	24.2	50	50	16	14	104	12.5
-35.4327352	-72.6527424	24.2	50	50	16	14	104	12.5
-34.9994756	-72.5012272	24.2	50	50	16	14	104	12.5
-34.566216	-72.3496935	24.2	50	50	16	14	104	12.5
-34.1329463	-72.1981615	24.2	50	50	16	14	104	12.5
-33.6996867	-72.0466212	24.2	50	50	16	14	104	2.5

Table D18: Method 2 Increase 5 m parameters.

Latitude	Longitude	Depth (km)	Length (km)	Width (km)	Strike	Dip	Rake	Slip (m)
-38.2159899	-74.7793382	0	50	50	16	14	104	5
-37.7838531	-74.6215876	0	50	50	16	14	104	5
-37.3505935	-74.4701223	0	50	50	16	14	104	5
-36.9173239	-74.3186375	0	50	50	16	14	104	15
-36.4840643	-74.1671531	0	50	50	16	14	104	5
-36.0507947	-74.0156496	0	50	50	16	14	104	5
-35.6175351	-73.864147	0	50	50	16	14	104	5
-35.1842654	-73.7126256	0	50	50	16	14	104	10
-34.7510058	-73.5611056	0	50	50	16	14	104	10
-34.3177362	-73.409567	0	50	50	16	14	104	20
-33.8844766	-73.2580302	0	50	50	16	14	104	15
-33.4512069	-73.1064753	0	50	50	16	14	104	5
-38.3402293	-74.2496562	12.1	50	50	16	14	104	5
-37.908093	-74.0916354	12.1	50	50	16	14	104	10
-37.4748234	-73.9401629	12.1	50	50	16	14	104	15
-37.0415638	-73.7886908	12.1	50	50	16	14	104	10
-36.6082942	-73.6371992	12.1	50	50	16	14	104	15
-36.1750346	-73.4857082	12.1	50	50	16	14	104	5
-35.7417649	-73.3341982	12.1	50	50	16	14	104	5
-35.3085053	-73.1826893	12.1	50	50	16	14	104	15
-34.8752357	-73.0311617	12.1	50	50	16	14	104	20
-34.4419761	-72.8796356	12.1	50	50	16	14	104	20
-34.0087065	-72.7280912	12.1	50	50	16	14	104	10
-33.5754468	-72.5765486	12.1	50	50	16	14	104	5
-38.4644587	-73.719965	24.2	50	50	16	14	104	10
-38.0323229	-73.5616723	24.2	50	50	16	14	104	15
-37.5990633	-73.4102127	24.2	50	50	16	14	104	15
-37.1657937	-73.2587334	24.2	50	50	16	14	104	15
-36.7325341	-73.1072544	24.2	50	50	16	14	104	15
-36.2992644	-72.9557561	24.2	50	50	16	14	104	15
-35.8660048	-72.8042587	24.2	50	50	16	14	104	15
-35.4327352	-72.6527424	24.2	50	50	16	14	104	15
-34.9994756	-72.5012272	24.2	50	50	16	14	104	15
-34.566216	-72.3496935	24.2	50	50	16	14	104	15
-34.1329463	-72.1981615	24.2	50	50	16	14	104	15
-33.6996867	-72.0466212	24.2	50	50	16	14	104	5

Table D19: Method 2 Increase 5 m & 2.5 m parameters.

Latitude	Longitude	Depth (km)	Length (km)	Width (km)	Strike	Dip	Rake	Slip (m)
-38.2159899	-74.7793382	0	50	50	16	14	104	5
-37.7838531	-74.6215876	0	50	50	16	14	104	5
-37.3505935	-74.4701223	0	50	50	16	14	104	5
-36.9173239	-74.3186375	0	50	50	16	14	104	15
-36.4840643	-74.1671531	0	50	50	16	14	104	5
-36.0507947	-74.0156496	0	50	50	16	14	104	5
-35.6175351	-73.864147	0	50	50	16	14	104	5
-35.1842654	-73.7126256	0	50	50	16	14	104	10
-34.7510058	-73.5611056	0	50	50	16	14	104	10
-34.3177362	-73.409567	0	50	50	16	14	104	20
-33.8844766	-73.2580302	0	50	50	16	14	104	15
-33.4512069	-73.1064753	0	50	50	16	14	104	5
-38.3402293	-74.2496562	12.1	50	50	16	14	104	2.5
-37.908093	-74.0916354	12.1	50	50	16	14	104	7.5
-37.4748234	-73.9401629	12.1	50	50	16	14	104	12.5
-37.0415638	-73.7886908	12.1	50	50	16	14	104	7.5
-36.6082942	-73.6371992	12.1	50	50	16	14	104	12.5
-36.1750346	-73.4857082	12.1	50	50	16	14	104	2.5
-35.7417649	-73.3341982	12.1	50	50	16	14	104	2.5
-35.3085053	-73.1826893	12.1	50	50	16	14	104	12.5
-34.8752357	-73.0311617	12.1	50	50	16	14	104	17.5
-34.4419761	-72.8796356	12.1	50	50	16	14	104	17.5
-34.0087065	-72.7280912	12.1	50	50	16	14	104	7.5
-33.5754468	-72.5765486	12.1	50	50	16	14	104	2.5
-38.4644587	-73.719965	24.2	50	50	16	14	104	7.5
-38.0323229	-73.5616723	24.2	50	50	16	14	104	12.5
-37.5990633	-73.4102127	24.2	50	50	16	14	104	12.5
-37.1657937	-73.2587334	24.2	50	50	16	14	104	12.5
-36.7325341	-73.1072544	24.2	50	50	16	14	104	12.5
-36.2992644	-72.9557561	24.2	50	50	16	14	104	12.5
-35.8660048	-72.8042587	24.2	50	50	16	14	104	12.5
-35.4327352	-72.6527424	24.2	50	50	16	14	104	12.5
-34.9994756	-72.5012272	24.2	50	50	16	14	104	12.5
-34.566216	-72.3496935	24.2	50	50	16	14	104	12.5
-34.1329463	-72.1981615	24.2	50	50	16	14	104	12.5
-33.6996867	-72.0466212	24.2	50	50	16	14	104	2.5

Table D20: Method 2 Increase 5 m shallow parameters.

Latitude	Longitude	Depth (km)	Length (km)	Width (km)	Strike	Dip	Rake	Slip (m)
-38.2159899	-74.7793382	0	50	50	16	14	104	5
-37.7838531	-74.6215876	0	50	50	16	14	104	5
-37.3505935	-74.4701223	0	50	50	16	14	104	5
-36.9173239	-74.3186375	0	50	50	16	14	104	15
-36.4840643	-74.1671531	0	50	50	16	14	104	5
-36.0507947	-74.0156496	0	50	50	16	14	104	5
-35.6175351	-73.864147	0	50	50	16	14	104	5
-35.1842654	-73.7126256	0	50	50	16	14	104	10
-34.7510058	-73.5611056	0	50	50	16	14	104	10
-34.3177362	-73.409567	0	50	50	16	14	104	20
-33.8844766	-73.2580302	0	50	50	16	14	104	15
-33.4512069	-73.1064753	0	50	50	16	14	104	5
-38.3402293	-74.2496562	12.1	50	50	16	14	104	0
-37.908093	-74.0916354	12.1	50	50	16	14	104	5
-37.4748234	-73.9401629	12.1	50	50	16	14	104	10
-37.0415638	-73.7886908	12.1	50	50	16	14	104	5
-36.6082942	-73.6371992	12.1	50	50	16	14	104	10
-36.1750346	-73.4857082	12.1	50	50	16	14	104	0
-35.7417649	-73.3341982	12.1	50	50	16	14	104	0
-35.3085053	-73.1826893	12.1	50	50	16	14	104	10
-34.8752357	-73.0311617	12.1	50	50	16	14	104	15
-34.4419761	-72.8796356	12.1	50	50	16	14	104	15
-34.0087065	-72.7280912	12.1	50	50	16	14	104	5
-33.5754468	-72.5765486	12.1	50	50	16	14	104	0
-38.4644587	-73.719965	24.2	50	50	16	14	104	5
-38.0323229	-73.5616723	24.2	50	50	16	14	104	10
-37.5990633	-73.4102127	24.2	50	50	16	14	104	10
-37.1657937	-73.2587334	24.2	50	50	16	14	104	10
-36.7325341	-73.1072544	24.2	50	50	16	14	104	10
-36.2992644	-72.9557561	24.2	50	50	16	14	104	10
-35.8660048	-72.8042587	24.2	50	50	16	14	104	10
-35.4327352	-72.6527424	24.2	50	50	16	14	104	10
-34.9994756	-72.5012272	24.2	50	50	16	14	104	10
-34.566216	-72.3496935	24.2	50	50	16	14	104	10
-34.1329463	-72.1981615	24.2	50	50	16	14	104	10
-33.6996867	-72.0466212	24.2	50	50	16	14	104	0